Dynamics and stability of lean-premixed swirl-stabilized combustion

Ying Huang, Vigor Yang*

The Pennsylvania State University, University Park, PA 16802, USA

ARTICLE INFO

ABSTRACT

Combustion instability remains a critical issue limiting the development of low-emission, lean-premixed (LPM) gas turbine combustion systems. The present work provides a comprehensive review of the advances made over the past two decades in this area. Recent developments in industrial dry-low-emission (DLE) swirl-stabilized combustors are first summarized. Various swirl injector configurations and related flow characteristics, including vortex breakdown, precessing vortex core, large-scale coherent structures, and liquid fuel atomization and spray formation, are discussed. Nonlinear behaviors of combustion processes observed in combustors are described. The influence of fuel preparation, combustor geometry, and operating conditions on combustion characteristics in swirl-stabilized combustors is examined. The mechanisms driving combustion instabilities, including hydrodynamic instabilities, equivalence ratio fluctuations, flame surface variations, and oscillatory liquid fuel atomization and evaporation are investigated. Instability stabilization methods, including both passive and active control techniques, are also reviewed. Finally, recent progress in both analytical modeling and numerical simulation of swirl-stabilized combustion are surveyed.

Contents

* Correspondence to: Prof. Vigor Yang, Daniel Guggenheim School of Aerospace Engineering, Williams R. T. Oakes Professor and Chair, Georgia Institute of Technology, 313 Montgomery Knight Building, 270 Ferst Drive, Atlanta, GA 30332-0150, USA.
E-mail address: vigor.yang@aerospace.gatech.edu (V. Yang).

1. Introduction

Gas turbine engines for power generation and propulsion applications have traditionally used diffusion-flame combustors because of their reliable performance and reasonable stability characteristics. Unfortunately, this type of combustor usually produces unacceptably high levels of thermal NO_x. The increasingly strict regulation for pollutant emissions has recently led engine manufacturers to develop combustors that meet various regulatory requirements (Bahr [1]; Correa [2]). New concepts for combustion technology have been introduced to the gas turbine industry, including lean-premixed (LPM) combustion (or lean-premixed prevaporized (LPP) combustion when liquid fuels are employed), rich-burn quick-quench lean-burn (RQL) combustion, and catalytic combustion (Lefebvre [3]; Correa [4]). Among these three methods, RQL techniques are hampered by soot formation and incomplete mixing between fuel-rich combustion products and air. Catalytic combustion suffers from challenges associated with cost, durability and safety. Lean-premixed (prevaporized) combustion appears to

be the most promising technology for practical systems at the present time (note that for aero-engine gas turbines using liquid fuels, lean direct injection (LDI) combustion is often adopted for pollution control because of its superior stability behavior). In LPM combustion, the fuel and air are premixed upstream of the combustor to avoid the formation of stoichiometric regions. The combustion zone is operated with excess air to reduce the flame temperature; consequently, thermal NO_x is virtually eliminated (Zeldovich [5]). Unsteady flow oscillations, also referred to as combustion instability, however, have emerged as a common problem, and hindered the development of LPM combustors (Lieuwen and Yang [6]). These oscillations may reach sufficient amplitudes to interfere with engine operation, and in extreme cases, lead to failure of the system due to excessive structural vibration and heat transfer to the chamber. Fig. 1 shows a burner assembly damaged by combustion oscillations. Also shown for comparison is a new burner assembly [7].

Combustion oscillations are not limited to gas turbine engines. They have been observed in the development of virtually all

Fig. 1. Burner assembly (left) damaged by combustion instability and new burner assembly (right) (Goy et al. [7]).

propulsion systems, including liquid rocket engines (Harrje and Reardon [8]; Yang and Anderson [9]), solid rocket motors (DeLuca et al. [10]), ramjet engines (Culick [11]), scramjet engines (Ma et al. [12]), and even industrial boilers and furnaces (Putnam [13]). The phenomenon may be defined as the unsteady motions in a dynamic system capable of sustaining large oscillations over a broad range of frequencies. Instabilities in different combustion systems are distinguished primarily by the geometry of the systems and the manner in which the reactants are introduced. The prevalence of instabilities in combustion systems can be primarily attributed to two fundamental causes (Culick and Yang [14,15]):

a) combustion chambers are almost entirely closed and the internal processes tending to attenuate unsteady motions are weak; and

b) the energy required to drive unsteady motions represents an exceedingly small fraction of the heat released by combustion.

These underlying issues are present in any combustion chamber, but are especially consequential for systems such as gas turbine engines, in which energy intensity is quite high, typically on the order of 100 MW/m^3/bar. In general, less than 0.1% of the energy released in chemical reactions is sufficient to generate pressure fluctuations having peak amplitudes equal to the mean chamber pressure.

Although combustion instability is not considered to be an issue of heightened concern for diffusion-flame type gas turbine combustors, there is some literature on the topic. Putnam [13] presented an overview of combustion-driven oscillations in combustors with so-called diffusion burners and film-cooled liners. Potential instability problems, however, can be largely eliminated before their appearance during the development phase, and design guidelines based on empirical data have been developed (Mongia et al. [16]).

In contrast, combustion instability in lean-premixed combustion systems remains a substantial challenge for designers. LPM combustors have several features that can render them more prone to flow oscillations [17–19]. First, the system usually operates near the lean blowout limit. A small perturbation in the equivalence ratio may produce a significant variation in heat release, which, if it resonates with the chamber acoustic wave, can result in large excursions of combustion oscillations. Second, as opposed to conventional diffusion-flame type combustors, limited dilution or film cooling air is supplied along the

combustor liner. The liner cooling system in general acts as an efficient acoustic attenuator to suppress resonant amplifications of combustion oscillations. Third, in premixed combustors, especially those for power-generation applications, the flame is short relative to the longitudinal acoustic wave length, and typically situated at the acoustic pressure anti-node point. Such an acoustically compact configuration facilitates the interactions between oscillatory heat release and flow motion. In addition, since the flame is primarily anchored by an aerodynamically induced recirculating flow, a strong flow oscillation may cause flow reversal and even flame flashback, driving the flame upstream toward the fuel injectors.

The above observations suggest that the possibility of instabilities occurring during the development of a new LPM gas turbine combustor must be anticipated and recognized from the beginning of a project. Stable combustion may become unstable (oscillatory) due to small changes in operating parameters, geometric configurations, and the manner in which the reactants are introduced. Clearly, a comprehensive understanding of combustion instability is required if LPM combustor designs are to be improved. Over the past decade, extensive efforts have been made worldwide in the industrial, government, and academic communities to understand the unique stability characteristics of low-emission lean-premixed gas turbine engines. The purpose of this review is to compile and analyze these results, and thus to achieve an improved understanding of the dynamics and stability of LPM swirl-stabilized combustion. Recent advances in experimental diagnostics, analytical modeling, numerical simulation, and technology implementation will be discussed systematically.

The present review is organized into eight sections. Section 2 provides an overview of the effort to mitigate combustion oscillations in industrial dry-low-emission combustors. Section 3 discusses the flow characteristics of swirl injectors. Various injector configurations and their intrinsic flow characteristics will be described in depth. Section 4 examines the influence of fuel preparation, combustor geometry, and operating conditions on the dynamics of LPM swirl-stabilized combustors. Section 5 deals with underlying mechanisms driving combustion instabilities, including hydrodynamic instability, equivalence ratio fluctuation, flame surface variation, and oscillatory liquid fuel atomization and evaporation. Section 6 summarizes commonly used methods for suppressing instabilities. Both passive and active control techniques are discussed. Section 7 provides a survey of recent progress in analytical modeling and numerical simulation of lean-premixed swirl-stabilized combustion.
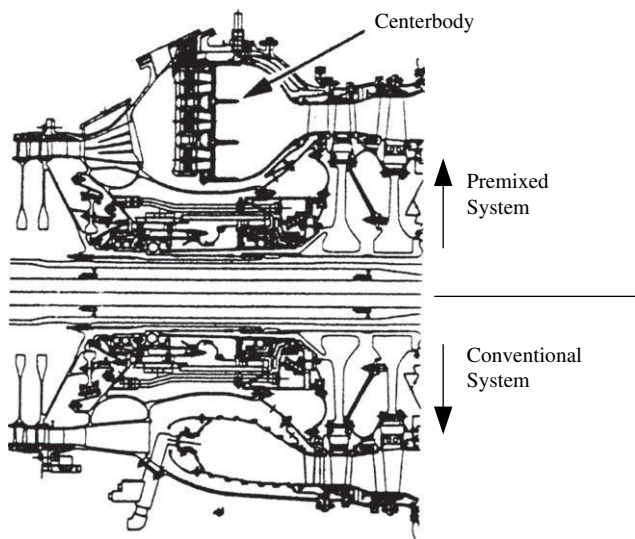
Fig. 2. General electrical (GE) aero-derivative LM6000 lean-premixed (top) and conventional (bottom) combustion systems (Joshi et al. [22,23]).

2. Recent development of industrial dry-low-emission (DLE) gas turbine combustors

Reduction of pollutant emissions has always been a major thrust in the development of modern combustion devices. Among the various techniques considered [20], fuel diluents, such as water and steam, have commonly been employed to reduce the flame temperature and consequently pollutant emissions, especially in some stationary systems for industrial processes and power generation. In spite of its effectiveness, this approach suffers reduced thermodynamic cycle efficiency, and undesirable side effects, such as quenching of CO burnout and mechanical corrosion of turbine hardware due to water impurities. Since no water or steam injection is needed in lean-premixed combustors, they are often termed dry-low-emission (DLE) combustors.

The major differences in design between lean-premixed and conventional diffusion-flame type combustion systems may be illustrated by considering the General Electric (GE) aero-derivative

LM6000 combustor [21–23]. Fig. 2 shows a comparison between the LM6000 premixed combustor and a conventional single annular combustor (SAC). The former employs a triple annular design for fuel staging to achieve an ultra-lean flame with a reduced temperature. Double annular counter-rotating swirler (DACRS) premix injectors are adopted. There is no dilution and liner cooling air ingested into the front end of the combustor. Instead, turbine nozzle cooling air is utilized to cool the liners convectively on the backside. In addition, a thermal barrier coating is applied to maintain acceptable liner metal temperatures. A short annular liner is applied in the premixed design to minimize the amount of air required for convective cooling. The combustor volume, however, is approximately twice that of a conventional combustor, to increase the residence time for complete reactions of CO and unburned hydrocarbons (UHCs). A more detailed description of these two combustion systems can be found in Refs. [21–23].

In the last decade, a variety of DLE gas turbine combustors have been developed by industry vendors. A comprehensive review of the underlying technologies can be found in Refs. [24,25]. Figs. 3–8 summarize specifications of selected industrial DLE combustors. The configurations, fuel preparation and combustion strategies, achieved emission level, and liner cooling approach are briefly described. Since combustion instabilities were encountered in virtually all the development programs, the techniques employed to mitigate instabilities are also presented in these figures. The instability control approaches will be classified and further elaborated in Section 6. More detailed information in this subject area can be also found in a recent overview by Lieuwen and Yang [6].

3. Flow dynamics of swirl injectors

Fuel injection and mixing are critical to achieving efficient and clean combustion in modern gas turbine engines, whether they are powered by gaseous or liquid fuels. For gaseous fuels, the major concern is to obtain an optimal level of mixing among the air, fuel, and combustion products in the combustion zone. When liquid fuels are employed, they must be atomized into small droplets and then distributed in an air stream before entering the combustion zone. In addition to its primary function of preparing a combustible mixture, the fuel injector acts as a sensitive element capable of modulating the flowfield and combustion processes in a combustor.

Specifications:
- NO_x < 25 ppm and CO < 10 ppm for gaseous fuels
- Eight can combustors per engine
- Three-stage serial premixed combustion technology
- Injection system consists of double mixed flow swirlers

Instability control strategies:
- Adaptive fuel staging
- Equivalence-ratio oscillation damping
- Acoustic dampers and air-flow damping

(a) Original (left) and modified (right) mixing ducts (or premixers)

(b) Trent 60 DLE three-stage combustor

Fig. 3. Rolls-Royce Trent aero-derivative combustion system [26–28].

Specifications:

- NO_x < 25 ppm and CO < 20 ppm for gaseous fuel
- Triple dome annular combustor
- 75 double annular counter-rotating swirler (DACRS) premixers
- Backside convective cooling, thermal barrier coating

Instability control strategies:

- Spatial and temporal fuel staging
- Acoustic dampers (quarter wave tubes)
- Injection of a small amount of fuel through a separate circuit into combustor
- Adjustment of dome flame temperature

(a) DACRS premixer with ELBO fuel injection

(b) Dry-low- emissions annular combustor

Fig. 4. GE LM6000 aero-derivative DLE combustion system [16,18,21–23,29].

The vast majority of gas turbine systems employ swirl injectors that produce central toroidal recirculation zones (CTRZs) to provide the dominant flame stabilization mechanism. The flow in this region is generally associated with high shear stresses and strong turbulence intensity resulting from vortex breakdown. In the past decades, considerable efforts have been devoted to the development of swirl injectors. Overviews of this subject were published by Bazarov et al. [79] for liquid-propellant rocket engines, and by Beer and Chigier [80], Winterfeld et al. [81] and Lefebrve [24] for gas turbine engines. More recent advances in gas turbine fuel injection technologies can be found in the works of Mansour [82] and Huang et al. [83]. Figs. 3–8 present the swirl injectors adopted in several industrial DLE gas turbine combustion systems.

3.1. Configurations of swirl injectors

In a typical swirl injector, the flow is deflected by an array of vanes positioned either axially or radially [81], as illustrated in Fig. 9. Both single and multiple swirlers have been employed to provide the desired fuel/air distribution for efficient combustion. Multiple swirlers mounted concentrically may be arranged into either a co-rotating or a counter-rotating orientation. Fig. 5a shows the single axial-entry swirl for the gaseous fuel injector in a Solar turbine engine. The fuel is delivered into the airflow immediately downstream of the swirler vanes through injection spokes extending radially towards the injector centerbody. The fuel and air are mixed in the premixing duct before entering into the combustion chamber. Fig. 10 shows a typical radial-entry swirl injector [84,85], which consists of a mixing duct and a fuel nozzle located coaxially at the head end. Three radial-entry swirlers, counter-rotating with each other, are located at the entrance. Liquid fuel injected from the centerbody is dispersed into swirling airflows.

When liquid fuels are used as energy sources, they usually need to be atomized, vaporized, and mixed with air before burning in the flame zone. Two types of atomization systems are commonly used: pressure and airblast atomizers. The former makes use of pressure and exposes the liquid fuel to an axial or a rotating motion. In the

Specifications:

- NO_x < 25 ppm and CO < 50 ppm for gaseous fuel
- Annular combustion chamber
- Lean premixed gaseous fuel swirl injector
- Effusion cooling or convective backside cooling

Instability control strategies:

- Fuel injector modifications
- Pilot fuel

(a) Gaseous fuel injector

(b) Annular combustor
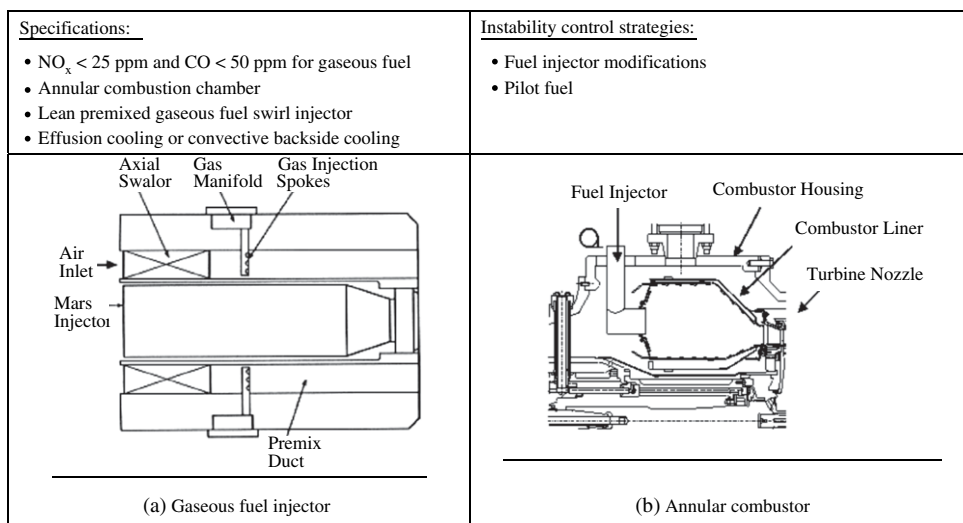
Fig. 5. Solar turbines SoLoNO$_x$ combustion system [30–36].

Specifications:	Instability control strategies:
• NO_x < 25 ppm and CO < 10 ppm for gaseous fuel, NO_x< 42 ppm for liquid fuel • Annular or can combustion chamber • Dual fuel premix swirl injector • Film cooling	• Helmholtz resonator • Fuel injector modification with cylindrical burner outlet (CBO) • Active control by modulating pilot gas fuel flow rate based on phase-shift algorithm

(a) Standard hybrid burner

(b) Annular combustor

Fig. 6. Siemens Vx4.3A land-based combustion system [37–50].

Specifications:	Instability control strategies:
• NO_x < 23.5 ppm and CO < 16 ppm for gaseous fuel • Annular combustion chamber • Tangential entry fuel nozzle • Thermal barrier coating, and film cooling	• Helmoltz resonators • Re-schedules pilot fuel flow or reduces output power • Active control through modulation of fuel flow rate based on phase-shift or adaptive control algorithm

(a) Fuel nozzle with tangential entry

(b) Annular combustor

Fig. 7. Pratt & Whitney FT8 combustion system [51–63].

Specifications:	Instability control strategies:
• $NO_x < 15$ ppm for gaseous fuel; $NO_x < 35$ ppm for liquid fuel • Annular or silo-type combustor • Double conical EV burner • Convective and effusion cooling	• Helmholtz resonators • Vortex generator • Extended burner fuel lance • Elliptically shaped burner

(a) EV premix injector

(b) Sequential combustor equipped with EV injector
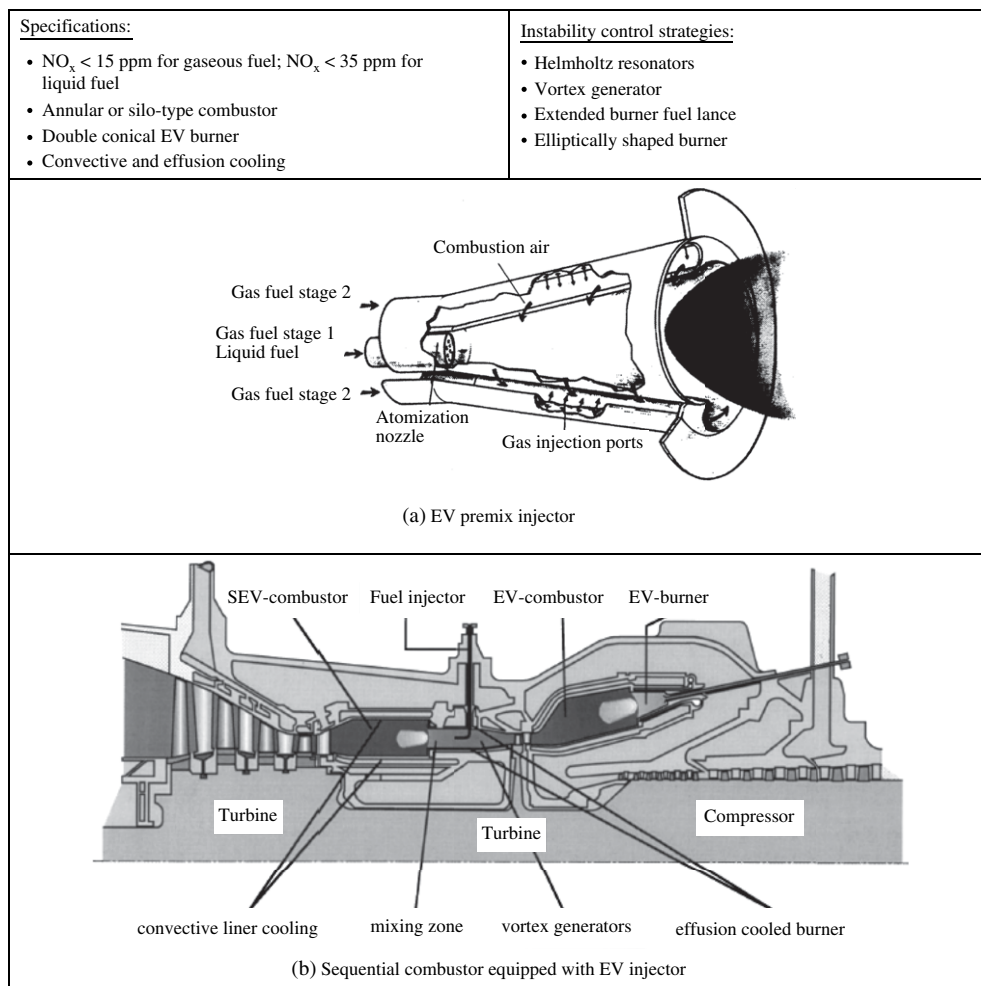
Fig. 8. ABB ALSTOM gas turbine combustion system [64–78].

latter, atomization of a liquid is achieved by injecting it into a high-velocity gas stream, either within the atomizer body or externally. Pressure atomizers feature good mechanical reliability and are capable of sustaining combustion at very weak mixture strengths, while airblast atomizers have the advantages of low fuel injection pressures and finer sprays over a wide range of fuel flow rates, except in start-up operations. Fig. 11 shows two specific designs of airblast atomizers: plain-jet and prefilming configurations. The former has discrete jets of fuel directly delivered into a high-velocity swirling air stream. In the latter design, the liquid first
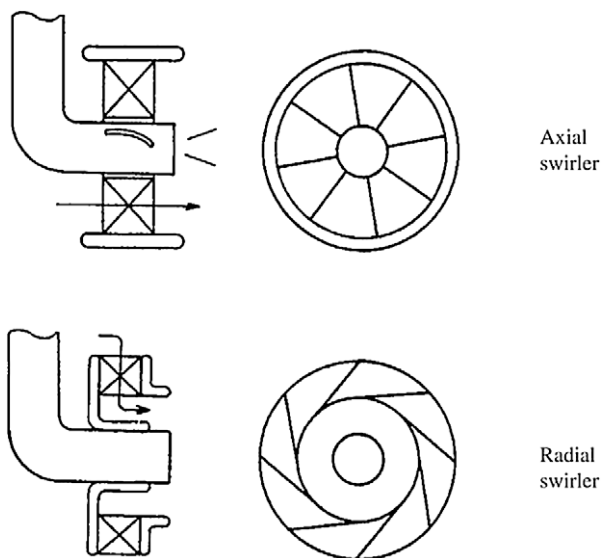
Fig. 9. Schematics of axial and radial swirlers (Winterfeld et al. [81]).
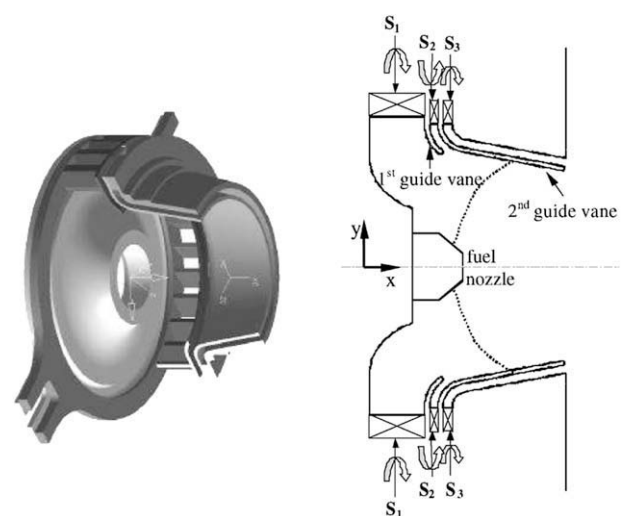
Fig. 10. Schematic of gas turbine swirl injector with radial-entry (Wang et al. [85]).
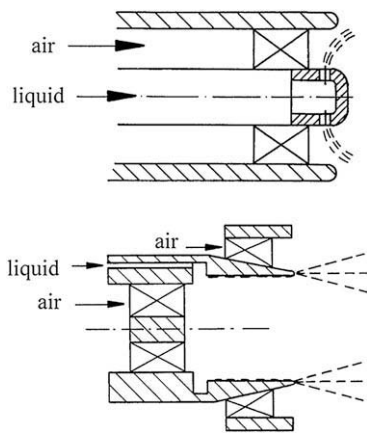
Fig. 11. Schematics of plain-jet airblast atomizer (top) and prefilming airblast atomizer (bottom) (Winterfeld et al. [81]).

forms a thin film and then disintegrates into droplets in the shear layer between the two counter-rotating swirling airflows. A liquid fuel atomizer, when connected directly with a combustor, can be regarded as a direct injection system. When a section of the mixing tube is inserted between the fuel atomizers and combustor, a pre-mixed fuel delivery system is obtained.

Swirling flows can also be produced by means other than swirler assemblies. Fig. 7a shows the tangential-entry swirl injector developed by Pratt & Whitney. Air is delivered into the premixing chamber through two tangentially oriented air slots that span the entire axial length of the premixing chamber. In the gaseous fuel version of injector, fuel is injected through a row of orifices in the inlet section into each of these air slots to achieve premixing for low-emission combustion. For liquid fuels, a series of six axial spokes is used to inject and atomize fuel in the interior of the premixing chamber. Fig. 8a shows another type of fuel injector without swirler vanes. The EV burner, developed by ABB ALSTOM, consists of two half cones shifted perpendicular to their centerlines forming two inlet slots of a constant slot width. Air entering through these slots is mixed with gaseous fuel emerging from a large number of holes along each of the slots. With a carefully selected ratio of the slot width to the burner length, a center recirculation zone is formed along the centerline at the end of the burner and serves as an aerodynamic flame holder.

The swirl intensity is usually characterized by the swirl number S. Following common practice (Beer and Chigier [80], Gupta [86]), it is defined as the ratio of the axial flux of the tangential momentum to the product of the axial momentum flux and a characteristic radius. The exact expression of swirl number depends on the injector geometry and flow profiles. For a typical single-element injector (Fig. 12) with a flat vane swirler (Fig. 13),

$$S = \int_{R_h}^{R_n} \overline{u}\,\overline{w}r^2 \mathrm{d}r \bigg/ \int_{R_h}^{R_n} R_n \overline{u}^2 r \mathrm{d}r \qquad (3.1)$$
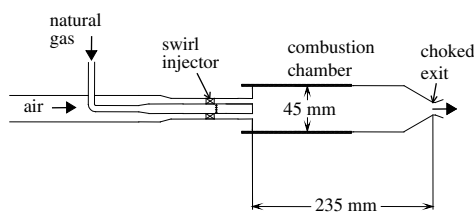
Fig. 12. Schematic of a model combustor with a single-element swirl injector (Seo [196]).
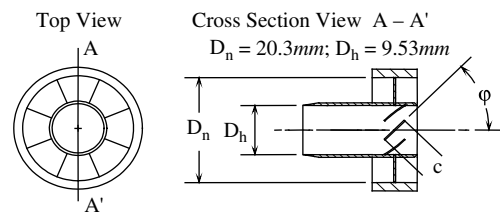
Fig. 13. Schematic of top and cross-section views of a flat vane swirler (Seo [196]).

where R_n and R_h are the radii of the centerbody and the inlet duct, respectively. If the axial and azimuthal velocities are assumed to be uniform and the vanes are very thin, the swirl number can be written as

$$S = \frac{2}{3}\left[\frac{1-(R_h/R_n)^3}{1-(R_h/R_n)^2}\right]\tan\varphi \qquad (3.2)$$

where φ is the swirler vane angle. In the case of a hubless swirler ($R_h = 0$), the above expression simplifies to:

$$S = \frac{2}{3}\tan\varphi \qquad (3.3)$$

3.2. Flow characteristics of swirl injectors

The flow structures of a typical gas turbine swirl injector are shown in Fig. 14. The flowfield features three salient structures: vortex breakdown-induced center recirculation zone downstream of the injector, precessing vortex layer surrounding the center recirculation zone, and shear layers originating from the outer edge of the inlet annulus.

3.2.1. Vortex breakdown
One of the most important flow characteristics of a swirl injector is vortex breakdown, a phenomenon that manifests itself as an abrupt change in the core of a slender vortex, and usually develops downstream into a recirculating bubble or a spiral pattern. The flow region of vortex breakdown provides the dominant flame stabilization mechanism, and is characterized by the existence of internal stagnation points and reversed flows. Because of the widespread occurrence of vortex breakdown in high swirl flows, considerable effort has been devoted to achieving a better understanding of this phenomenon. Reviews on this subject have been given by Hall [87], Leibovich [88,89], and recently by Lucca-Negro and O'Doherty [90].

Sarpkaya [91,92] observed three types of vortex breakdown in laminar swirling pipe flows: axisymmetric (bubble), spiral, and double helix. The bubble mode usually prevails at high swirl numbers, while the spiral mode occurs at low swirl numbers. The
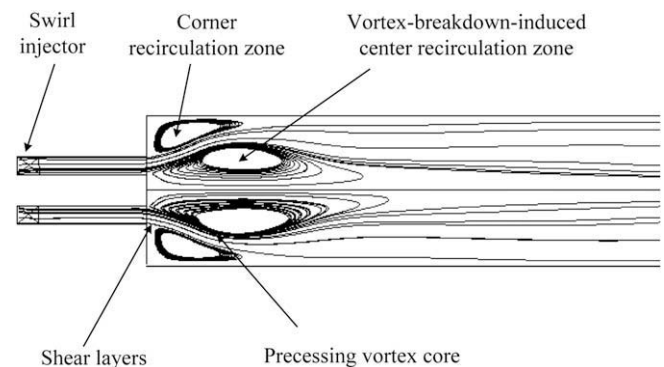
Fig. 14. Flow structures of a typical gas turbine combustor with a coaxial injector.

double helix mode takes place when the vortex core expands and spirals. It occurs only in a diverging tube. Later, Faler and Leibovich [89,93,94] revealed seven different types of vortex breakdown, using a liquid dye tracer in their water pipe flow visualizations, over a wide range of Reynolds and swirl numbers. At higher Reynolds numbers, the only characteristic geometric forms are the bubble and spiral modes. Many other investigations of vortex breakdown in laminar flows with low Reynolds numbers have also been reported [95–97]. In practical applications such as swirl injectors, vortex breakdown often occurs in the turbulent flow regime. Sarpkaya [98] and Sarpkaya and Novak [99] investigated turbulent vortex breakdown in non-cavitating swirling flows at high Reynolds numbers in a slightly diverging pipe. A "conical" breakdown fundamentally distinct from the various forms of laminar cases was observed. It was suggested that this type of vortex breakdown results from rapid precessing, in which the vortex core deviates slightly from the tube centerline.

Several theories based on the wave propagation [100,101], hydrodynamic instability [102–105], and flow-stagnation [106] concepts, have been proposed to explain the onset, internal structure, and mode selection of vortex breakdown. In the wave theories introduced by Squire [100] and Benjamin [101], the abruptness of vortex breakdown represents the existence of a critical state, which separates a supercritical from a subcritical flow state. In supercritical flows, disturbances propagate downstream, whereas in subcritical flows, standing waves exist with disturbances propagating both upstream and downstream. The idea that vortex breakdown is induced by hydrodynamic instability was examined by Ludwieg [102], Jones [103], Lessen et al. [104] and Leibovich and Stewartson [105]. The theory suggests that vortex breakdown, with a local stagnation point, results from the response of the flow to spiral disturbances. In the flow-stagnation concept [106], vortex breakdown is considered to be analogous to boundary layer separation or flow-stagnation phenomena. Although the above theories improve our understanding of vortex breakdown, none of them is able to completely and accurately describe all of the features of vortex breakdown [90].

In an effort to study the vortex breakdown in a coaxial swirl injector, shown in Fig. 15, Lu et al. [107] conducted a large-eddy simulation (LES) analysis with emphasis placed on flow development and its interaction with acoustic waves. Fig. 16 shows the streamlines of the time-mean flowfield based on the axial and radial velocities at two different swirl numbers. The Reynolds number based on the inlet diameter was 1.25×10^5. For the low swirl number case with $S = 0.3$, no vortex breakdown was observed. A vortex breakdown-induced toroidal recirculation zone, however, was found in the central region for $S = 0.5$. The situation can be explained based on the momentum balance in the radial direction as follows

$$\frac{\partial p}{\partial r} \sim f_c \sim \frac{\rho U_\theta^2}{r} \tag{3.4}$$

where f_c denotes the centrifugal force and U_θ the azimuthal velocity. A radial pressure gradient is produced by the centrifugal force arising from the azimuthal flow. As the flow expands and the azimuthal velocity decays with the axial distance, the pressure is recovered in the downstream region. A positive pressure gradient is generated along the axial axis, which consequently leads to the formation of a recirculation zone, providing the swirl strength is high enough.

Wang et al. [85,108] performed an LES study of unsteady flow evolution in the radial-entry swirl injector shown in Fig. 10. The Reynolds number based on the inlet diameter and centerline velocity was 2×10^5. Two swirl numbers, $S = 0.35$ and 0.49, were investigated. Fig. 17 shows the instantaneous iso-surfaces of the
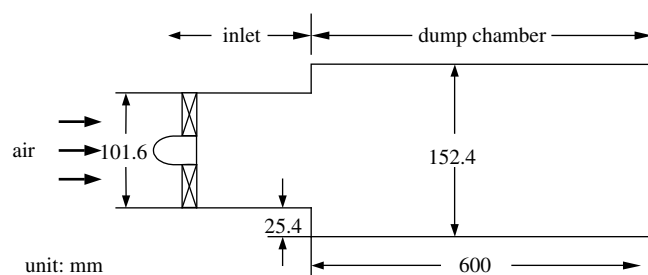
Fig. 15. Schematic of a dump chamber with a coaxial swirler (Lu et al. [107]).

azimuthal velocities. In the low swirl number case, a stable bubble type of vortex breakdown was observed immediately downstream of the centerbody, whereas a much more complex structure prevailed at the higher swirl number. The streamlines of the mean flowfields given in Fig. 18 show the formation of central toroidal recirculation zones. The local flow development is also revealed quantitatively with respect to the swirl intensity in this region. As the swirl number increases, the size of the recirculation zone also increases. The stagnation point of the vortex breakdown moves upstream for an equilibrium position and eventually reaches the centerbody.

3.2.2. Precessing vortex core

The precessing vortex core (PVC), a three-dimensional unsteady asymmetric flow structure, has often been reported in turbulent swirl combustion devices [109–115]. The PVC develops when a central vortex core starts to precess around the axis of symmetry at a well-defined frequency. This phenomenon is usually linked to vortex breakdown and the associated recirculation zone in a high Reynolds number flow. Syred and Beer [109] observed that the PVC is usually situated on the boundary of the reverse flow zone between the zero velocity and zero streamline. The frequency of precession depends on the swirl number and chamber configurations, and increases linearly with flow rate.

The existence of PVC structures in gas turbine swirl combustors was demonstrated in several recent studies [116–120]. Wang et al. [116] performed an LES study of the CFM56 gas turbine swirl injector with axial jet entry (shown in Fig. 19). A snapshot of an isobaric surface with $p = 99.5$ kPa is shown in Fig. 20. The low-pressure core was found to align initially with the axial axis in the region downstream of the fuel nozzle. It was then driven away from the centerline at the stagnation point of the recirculating flow, and extended downstream spirally against the direction of the main flow rotation, although the structure as a whole was found to follow the main flow. Fig. 21 shows snapshots of the instantaneous
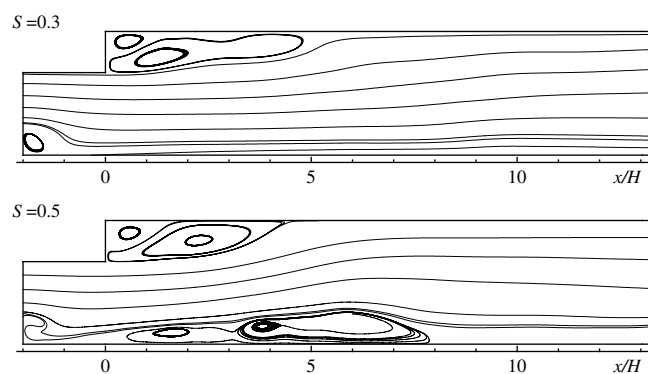
Fig. 16. Streamlines based on mean axial and radial velocity components; swirl numbers $S = 0.3$ and 0.5 (Lu et al. [107]).
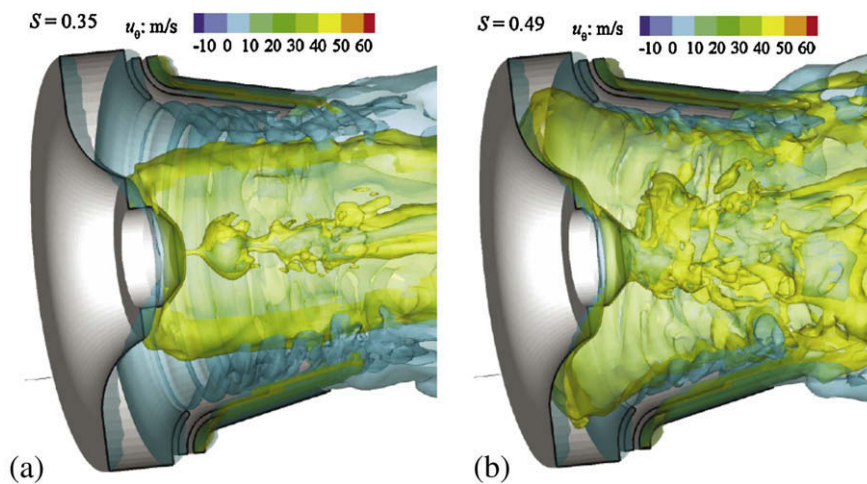
Fig. 17. Instantaneous iso-surfaces of azimuthal velocities at $u_\theta = 10$ and 50 m/s. (a) low swirl number and (b) high swirl number (Wang et al. [85]).
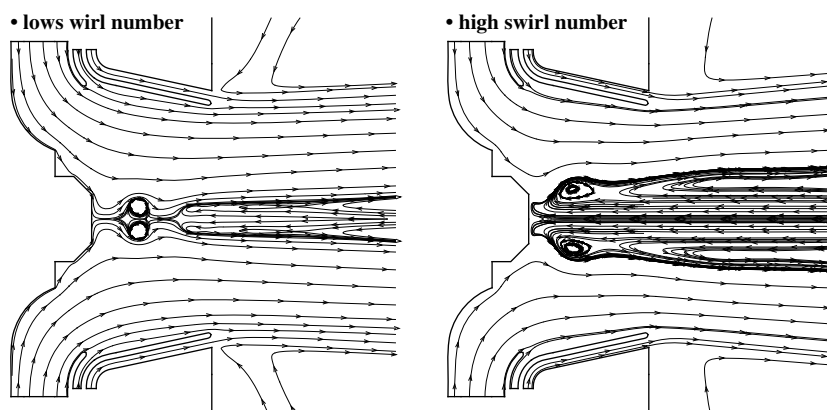
Fig. 18. Streamlines of mean flowfields for swirl numbers of $S = 0.35$ and 0.49 (Wang et al. [85]).

streamlines and pressure fields on a longitudinal plane at various times. The clustered streamlines indicate that large vortices around the low-pressure core are pushed outward. Furthermore, the induced low-pressure core is located outside the region defined by zero axial velocity. This is consistent with the observations of Syred and Beer [109]. When the vortex core rotates in the injector, large structures are peeled off from the spiral core periodically and are convected downstream by the local flow. Selle et al. [117] and Roux et al. [118] investigated a Siemens premixed swirl injector under both non-reacting and reacting conditions. A strong PVC was observed for non-reacting flows. For the operating conditions considered, this vortex disappeared, however, when combustion occurred, possibly due to volume dilatation and increased viscosity in the burnt gases.

The PVC strongly affects the flow and flame evolution in combustion systems. The displacement of the vortex core squeezes the flowfield at one side against the chamber wall, and causes a considerable increase in the tangential velocity in the squeezed flow region due to the conservation of angular momentum. The presence of a PVC also helps explain the occurrence of instantaneous negative azimuthal velocity in the region near the centerline of the chamber. The PVC may improve combustion efficiency through its enhancement of turbulence intensity and mixing, but it also represents a largely undesired characteristic because of the possible resonant coupling with low-frequency acoustic oscillation in gas turbine combustors. Several techniques, including the modulation of swirl strength and use of multi-annular swirl

injector configurations, have been proposed to suppress PVC oscillations in swirl combustors [110]. A recent review on PVC oscillation mechanisms in swirl combustion systems can be found in Ref. [121]

3.2.3. Shear layers and coherent structures

As the flow expands from the injector exit and evolves downstream, strong shear layers develop, due to the velocity difference
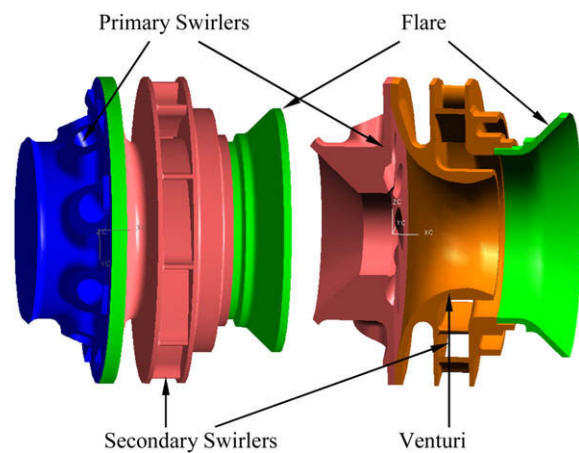
Fig. 19. Schematic of CFM56 gas turbine swirl cup assembly (Wang et al. [116]).
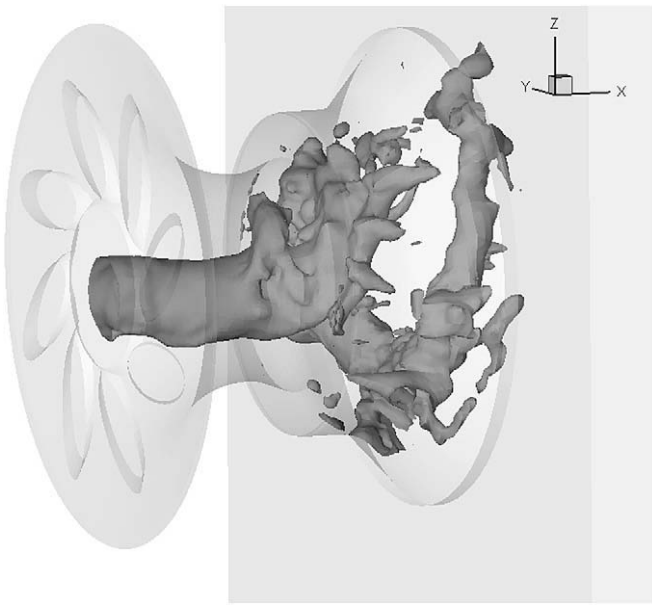
Fig. 20. Isobaric surface at $p = 99{,}500$ Pa (Wang et al. [116]).

between the jet flow and the ambient fluid. Large-scale coherent structures are generated in the shear layer regions, and shed downstream sequentially due to Kelvin–Helmholtz (K–H) instabilities. These vortex structures exert a significant influence on the combustion process by modulating the mixing processes among fuel, air, and hot combustion products.

The origin and characteristics of the large-scale vortex structures in shear layers have been the subject of intensive research in the past decades. Comprehensive reviews of coherent structures in non-swirling flows were given by Hussain [122], Ho and Huerre [123], Huerre and Monkewitz [124], Holmes et al. [125], Coats [126], and Ferziger [127]. Instability waves usually develop and grow in a shear layer in its initial region. For an axisymmetric jet without swirl, when the amplified waves reach a certain energy level, they roll up into coherent vortex rings. As vortices move downstream, they merge and increase the shear layer spread. Streamwise braid structures may form between two neighboring ring structures through a secondary three-dimensional instability, and these braids propagate into the cores of the rings. Eventually, these large-scale structures breakdown into smaller, less-organized turbulence structures further downstream.

Two distinct instability length scales exist in a jet flow: the initial momentum thickness θ_0 and the jet diameter D. The former describes the near field flow dynamics and the latter governs the flow evolution in the far field. The two corresponding instability modes are the high-frequency shear layer mode (associated with the most amplified wave of the initial velocity profile) and the low-frequency preferred mode (or jet-column mode).

Unlike large-scale structures in non-swirling flows, which are usually predominantly axisymmetric, swirl enhances asymmetric flow structures. The presence of swirl produces an azimuthal shear layer and centrifugal instabilities when the circulation decreases in the outward direction. In a high swirl number flow where the azimuthal velocity is comparable to the axial velocity, vortex breakdown may take place. Several important studies on swirling flow instabilities and coherent vortex motions, including experimental investigations [128–133], theoretical analyses [134–138],
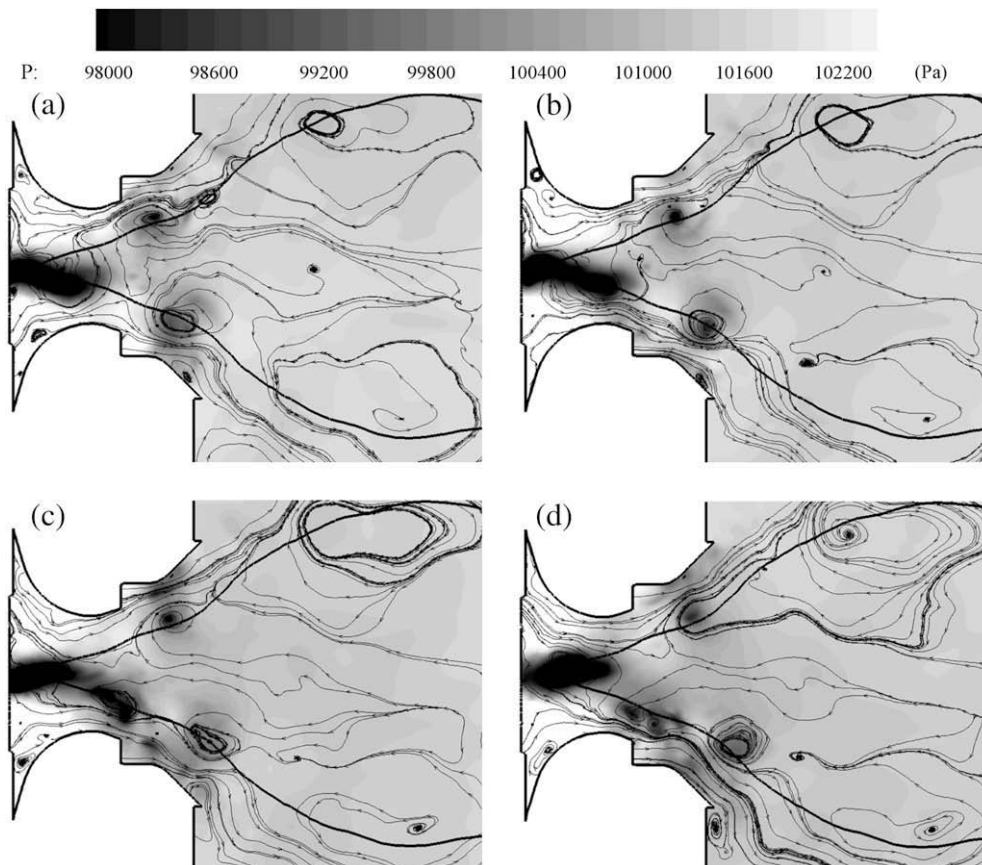
Fig. 21. Time evolution of streamlines and pressure field (time increment of 0.1 ms). Thick dark line indicates the contour of zero axial velocity (Wang et al. [116]).

and numerical simulations [139–144], have been recently reported. Liang and Maxworthy [133] performed a notable experimental study of swirling jets, in which swirl is generated using a long rotating tube. Their research focused on the dominant role of the underlying vortical flow structures and their dynamic evolution. Fig. 22 shows instantaneous photographs of slices of jets under different swirl numbers. The Kelvin–Helmholtz (K–H) instability in the axial shear layer, generated by the axial velocity, leading to vortex ring formation, dominated non-swirling and weakly swirling jets, as expected. After the introduction of swirl motion, the combined axial and azimuthal shear layers became unstable and evolved to a modified form of the K–H instability. For weak swirl, tilted vortex rings evolved downstream. For strongly swirling jets, vorticity in the azimuthal shear layer, formed by the azimuthal or swirl velocity, grew and became comparable with vorticity in the axial shear layer. The flow lost its axisymmetry, and strong helical waves with $m = +2$ or $+3$ replaced vortex rings as the dominant vortex structure prior to vortex breakdown. After breakdown, strong helical waves with $m = +1$ and $+2$ co-existed, with $m = +1$ being dominant. Here, m is the azimuthal wave number, and the positive sign represents the counter-winding direction for helical waves.

The prevalence of large-scale structures in swirl injectors was illustrated by Wang et al. [85] in the radial-entry swirl injector (shown in Fig. 10). Fig. 23 shows snapshots of the vorticity magnitude fields on two cross sections at two different swirl numbers. Because of the opposition of the swirler vane angles, two counter-rotating flows with different velocities merged at the trailing edges of the guide vanes. Vortices were generated in the shear layer regions and shed downstream sequentially. In comparison with the vortex breakdown-induced recirculating flow in the central region, the flow structures associated with the periodic vortex shedding in the outer region were small and well organized. The shear layer instability, along with the helical and centrifugal instabilities, induced large asymmetric structures on the transverse plane. For the high swirl number case, the center recirculating flow was found to intersect with the outer shear layer, causing a complex flowfield near the injector exit.

3.3. Atomization and spray formation of liquid fuel

In premixed systems, liquid fuels are usually injected into a premixing chamber, and undergo atomization, droplet dispersion and evaporation, and fuel/air mixing before entering the combustion zone. To achieve low-emission combustion, complete evaporation of liquid fuel droplets and thorough mixing of fuel and air within a short distance are desirable. The evaporation rate of a liquid fuel droplet strongly depends on the size of the contact area between liquid and air, which is a function of the mean droplet size and size
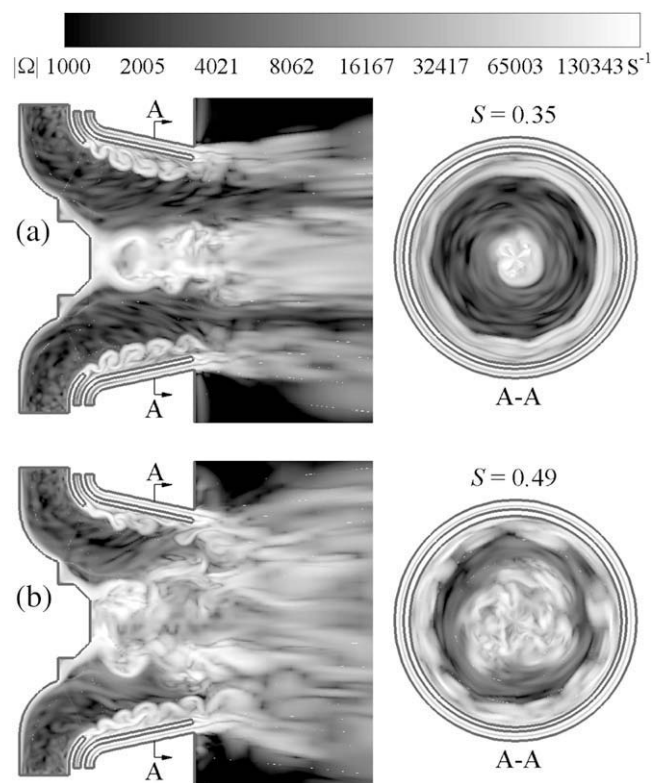
Fig. 23. Snapshots of vorticity magnitude contours. (a) Low swirl number and (b) high swirl number (Wang et al. [85]).

distribution of the fuel spray. At the same time, the fuel/air mixing process depends on the droplet spatial distribution. Thus the main tasks of a fuel atomizer are to produce a large number of droplets with sufficiently large total surface area, and to distribute the fuel droplets uniformly in the air stream to enhance the mixing process.

In most modern gas turbine combustors, fuel atomization is usually accomplished either by fuel pressure, via a pressure atomizer, or by airblast forces, such as an airblast atomizer. The combined effect of fuel pressure and airblast atomization can also be implemented through a so-called hybrid atomizer. A number of experimental and theoretical studies [145–165] have been conducted on the atomization performance of liquid fuel injectors in various configurations. Several reviews on this subject are available (see, for example, Winterfeld et al. [81], Lefebvre [24], Bachalo [166], Benjamin [167]). Presser et al. [145,146] investigated the aerodynamic characteristics of a swirling spray flame using a pressure-jet atomizer. The effects of swirl on droplet transport, as well
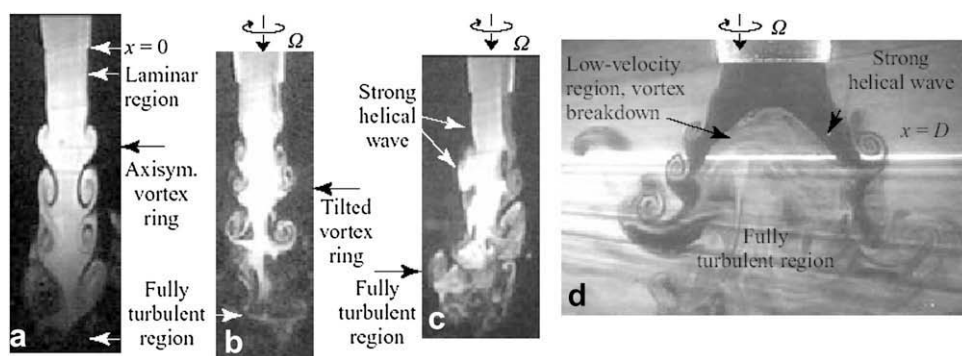
Fig. 22. Instantaneous photographs of slices of jets (Re = 1000) at different swirl numbers: (a) $S = 0$, (b) $S = 0.44$, (c) $S = 0.80$, and (d) $S = 1.03$ (Liang et al. [133]).

as the interactions between droplets and air flowfield, were studied under both non-reacting and reacting conditions. Cohen and Rosfjord [147,148] examined the airflow and spray field in 21 different fuel atomizer/swirler configurations. Three types of fuel atomizer, including radial jet nozzle, duplex nozzle, and airblast nozzle, were used to span a range of fuel injection techniques. Seven compound radial-entry double swirler assemblies were evaluated with each fuel nozzle. One important observation was that spray distribution is more dependent on injector type than on swirler type. The radial jet fuel nozzle was able to deliver liquid fuel to the filming lip, and always produced well-defined, hollow cone sprays. The duplex injector often did not create a spray cone wide enough to reach the filming lip of the swirler. The airblast fuel nozzle was found to have poor performance, due to the counter-rotation of the injector and the swirler airflow.

Chin et al. [149,150] reported experimental studies of a hybrid atomizer, where the atomization was accomplished through the combined effects of liquid pressure and airblast. Several fuel injection configurations were adopted to evaluate the effects of air/liquid relative velocity, liquid pressure, air/liquid mass flow rate ratio, and some other key parameters on the atomization and mixing performance of injectors. Two types of pressure swirl atomizers with different flow capacities and two air nozzle configurations with different flow areas were employed in the experiments. At a low air-pressure drop, increasing the air/liquid mass ratio was most beneficial for atomization over a range of low air/liquid mass ratios. At a higher air-pressure drop, the influences of both liquid pressure and relative velocity were significantly reduced. Improved atomization could be obtained under high liquid pressures for the same level of relative velocity. Wang et al. [153–155] and McDonell et al. [156] conducted experimental studies of a 3× scale model of the CFM56 hybrid swirl cup, which consists of a simplex atomizer and two counter-rotating swirlers. Both the time-averaged structure of the two-phase flowfield and the transient behavior of droplets downstream of the swirl cup were investigated. Jeng and colleagues [157–159] examined the counter-rotating flow structures produced by the actual-size CFM56 swirl cup. The effects of air temperature, fluid properties, and equivalence ratio on spray characteristics were studied under both non-reacting and reacting conditions. Ibrahim et al. [160] considered the influence of the liquid swirl velocity profile on the instability of an annular liquid sheet.

Due to manufacturing variations and provisions for thermal expansion, misalignment of fuel injector hardware may occur, and consequently modify the spray behavior by changing the fuel flow rate and interaction between the spray liquid and the swirling air. Several studies were performed on the effects of misalignment of the fuel nozzle on the structure of fuel spray. McDonell et al. [156] examined the influence of a radial shift of the CFM56 hybrid swirl cup on its atomization performance. The gas-phase structure was found to remain similar, with slight flow asymmetries. The liquid fuel distribution was dramatically impacted, while the overall droplet size remained similar. Han et al. [165] investigated the effects of axial displacement of a fuel nozzle on the spray characteristics. Nozzle displacement was found to significantly alter the flow swirl strength and the axial pressure gradient at the exit of the prefilmer lip, leading to a much different recirculation flow pattern. A nozzle shift in the upstream direction increased the amount of fuel subject to the prefilming atomization and made the spray more divergent. An opposite trend was observed when the nozzle was shifted in the downstream direction. The effects of manufacturing and assembly defects on the spray mass-flux distribution were also examined by Cohen and Rosfjord [148]. They found that radial translation of the fuel injector was the most significant alteration, causing a large deviation in the spray pattern from the baseline case.

3.4. Effect of swirler configurations on flow development

As stated earlier, both axial and radial swirlers are commonly used in gas turbine combustors. For multiple swirler systems, swirlers can be arranged into either a co-rotating or a counter-rotating orientation. The differences in swirler configuration obviously impose substantial influence on the flow and flame characteristics of swirl injectors.

Both axial and radial swirler configurations in a can combustor were evaluated by Smith et al. [35] using natural gas and by Cowell and Smith [36] using liquid fuel. There appeared to be no fundamental hurdle to achieving ultra-low-emissions with each swirler configuration. The radial swirler performed better than the axial swirler, however, in emissions performance, despite an increased premixing length. One possible factor contributing to this change in emissions performance is the characteristics of the recirculation zone generated with each swirler type. Although both swirlers had the same swirl number, the radial swirler produced a stronger central recirculation zone than its axial counterpart, due to differences in the expansion ratio, channel height, and exit velocity of the swirlers. It should be noted that the axial swirler was later adopted for the product design of Solar annular combustors because of its more compact size and its use as standard engine hardware. The effect of radial and axial configurations on the flowfield in a gas turbine combustor was numerically investigated by Etemad and Forbes [168]. The radial swirler provides a widely dispersed, flat swirling mechanism attached to the swirler face, with the possibility of fuel impingement on the swirler and liner wall. In contrast, the axial swirler provides a narrower, centralized fuel pattern, influenced partially by primary air jets, with less chance of fuel impingement on the wall.

The flow dynamics of a swirl injector with axial jet entry (shown in Fig. 19) with co- and counter-rotating swirler arrangements was explored by Wang et al. [116] by reversing the orientation of the secondary swirl vanes. Fig. 24 shows the radial distributions of three mean flow velocity components downstream of the injector. The mean velocity field in the co-rotating case bears a close resemblance to its counterpart in the counter-rotating case, except that the former possesses a much larger recirculation zone, due to the stronger swirling motion. Since a large recirculation zone tends to reduce the effective flow passage in the injector, the influence of the secondary swirling flow on the flow development within the Venturi is reduced, and the injector flow evolution is mainly driven by the flow through the primary swirlers. Another major difference between the two configurations lies in the distributions of turbulent kinetic energy and shear stress near the exit of the Venturi. At that location, in the counter-rotating case, strong shear stress was observed not only near the boundary of the central recirculation zone, as in the co-rotating case, but also near the tip of the prefilming surface. The co-rotating configuration also appeared to exhibit PVC, with rotation and twist in the same direction as in the counter-rotating case, but at a slightly lower frequency. This common characteristic indicates that the key mechanism dictating the flow evolution in the two configurations is identical. The observation is further corroborated by the fact that the origin of PVC was located within the Venturi, in which the flow motion is mainly controlled by the swirling flow through the primary swirler.

Wang et al. [116] further conclude that the counter-rotating arrangement appears to be more desirable than its co-rotating counterpart for this particular injector design for several reasons. First, the co-rotating configuration produces a large recirculation zone, which is more susceptible to flame oscillation. Second, the strong shear layer and high intensity turbulence near the trailing edge of the Venturi in the counter-rotating case promote the development of the Kelvin–Helmholtz instability in the liquid film
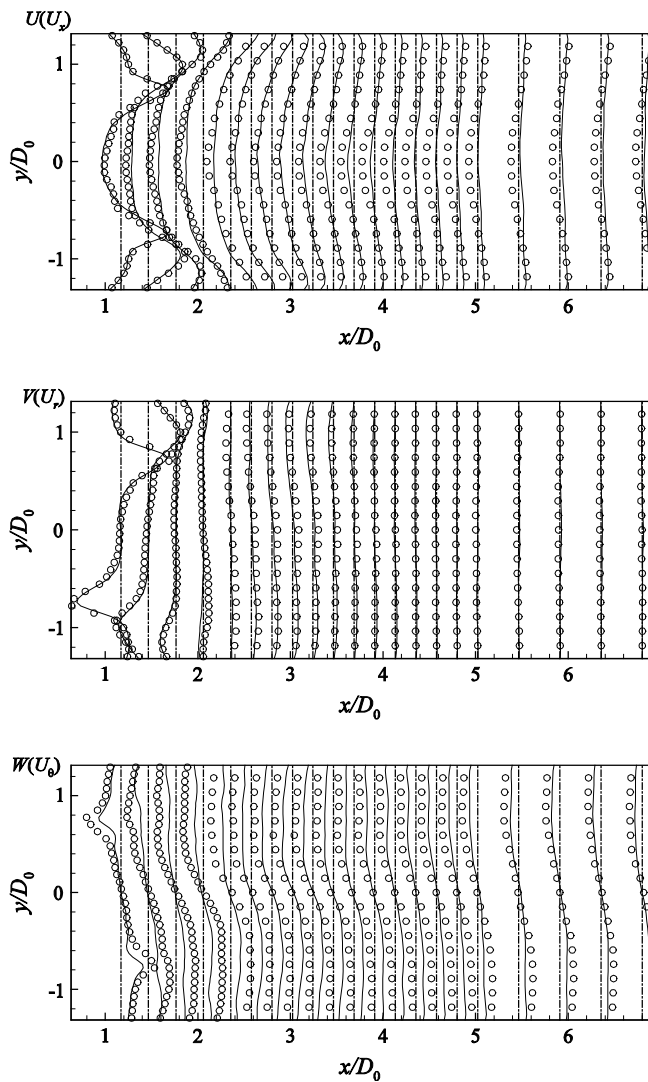
Fig. 24. Radial distributions of mean flow axial, radial, and azimuthal velocity components (symbol: co-rotation; line: counter-rotation (Wang et al. [116])).

and subsequently the formation of fine droplets. Third, the counter-rotating flow accelerates the pressure recovery in the downstream region, and leads to a higher adverse pressure gradient along the centerline. The process further enhances turbulent motion downstream of the fuel nozzle, and facilitates the breakup of the liquid fuel. Therefore, the counter-rotating design is expected to produce finer droplets and a much more stable flame.

Additional investigations of the effects of swirler orientations on injector dynamics were performed by Ateshkadi et al. [169], Merkle et al. [170], Li and Gutmark [171], Mehta et al. [172], Durbin et al. [173,174] and Gupta et al. [175]. Ateshkadi et al. [169] found that the swirl direction and the presence of a Venturi impose the greatest effects on the gas and droplet behavior in a liquid double swirler airblast fuel injector. The co-swirl configuration enhances the radial dispersion of the continuous phase, while the counter-swirl arrangement increases the level of mixing that occurs in the downstream region of the fuel injector. A large population of droplets exists in the center recirculation zone near the counter-swirl injector exit, which helps promote stability. Merkle et al. [170] measured the isothermal flow and mixture fields in a double swirler airblast fuel nozzle. The counter-swirl configuration exhibited a considerable attenuation of the turbulent exchange of momentum

perpendicular to the main flow direction. As a result, the mixture field with counter-rotating airflows featured a reduction in the turbulent mass transfer rate in the radial direction. Li and Gutmark [171] investigated the effects of swirler configurations on the flow structures and combustion characteristics in a triple annular research swirler (TARS) fuel injector. The co-swirling configuration was shown to have lower NO_x emission levels than the counter-swirling configuration for both gaseous and liquid fuels.

3.5. Dynamic response of swirl injector flow to external excitations

In gas turbine engines, the injector is an active element that can generate and modify flow oscillations in the chamber because of its intrinsic unsteadiness. The injector flow may interact resonantly with the acoustic wave traveling upstream from the combustion chamber. The coupling often leads to large flame oscillations in the combustor. In addition, acoustic forcing can be utilized to modulate the fuel distribution and the mixing between fuel and air, thus having the potential to control the combustion process.

Although considerable efforts have been devoted to studying forced shear layers and jets in the past few decades (Ho and Huerre [123], Panda and McLaughlin [128], Longmire and Eaton [176], Swanson and Richards [177], Cerecedo et al. [178], Gallaire et al. [132]), relatively limited investigations have been conducted to examine the response of a swirl injector to externally imposed excitations [179–186]. Cohen and Hibshman [179] studied the response of a two-passage swirl injector over a frequency range from 300 to 600 Hz. An electro-pneumatic actuator (Ling driver) was employed to generate a sinusoidally oscillating airflow entering the swirler. The acoustic impedance, defined as a transfer function of the fluctuations between the outlet flow velocity and the inlet pressure, was measured as a function of excitation frequency to characterize the injector response. It was found that the velocity near the wall between the two passages was highly sensitive to external forcing for frequencies between 400 and 600 Hz. This phenomenon was attributed to periodic vortex shedding or other velocity-sensitive mechanisms. Anderson et al. [180] later measured the acoustic coupling of airflow with fuel spray in four different aero-engine fuel injectors. Strong interactions between the pulsed airflow and the fuel spray mass flow rate were observed in the range of 350–650 Hz. Haile et al. [181,182] also performed a study to characterize the spray field of a liquid fuel injector under continuous and modulated flow conditions. The results indicate that strong modulation of the flow rate is observed at low forcing frequencies, but the time-averaged flow rate is reduced. Higher frequency forcing leads to a relatively unchanged time-averaged fuel flow rate.

Motivated by the experiments of Cohen and Hibshman [179], Wang et al. [108] performed a comprehensive study of the dynamic response of a radial-entry swirl injector to external excitation. The swirl injector geometry is shown in Fig. 10. Periodic oscillations of the mass flow rate, $\dot{m}$, were enforced at the injector entrance,

$$\dot{m} = \dot{m}_0[1 + \alpha \sin(2\pi f_F t)] \tag{3.5}$$

where $\dot{m}_0$ and f_F denote the mean mass flow rate and the forcing frequency, respectively. The amplitude of the oscillation, α, is fixed at 10%. The forcing frequency covers a range from 400 through 13,000 Hz, commensurate with the broadband nature of the injector flow dynamics.

3.5.1. Flow structure

Fig. 25 shows snapshots of the fluctuating vorticity magnitude fields, $|\varOmega'|$, obtained by subtracting the long-time-averaged quantity from its instantaneous value, at various forcing frequencies.

When the frequency is higher than f_v (characteristic frequency of convective motions, estimated by the mean flow residence time, with a value of 1.7 kHz), well-defined vortical structures are observed in the forward section of the injector (see Fig. 25c and d). These waves, generated by the flow oscillations at the entrance, are convected downstream with the local flow velocity. The wavelength is inversely proportional to the forcing frequency, and shortens in the middle region of the injector due to the flow turning effect, i.e., the flow direction turns in this region and the velocity component perpendicular to the wave front decreases. The intensive turbulent fluctuations downstream of the centerbody overshadow the organized vortical waves, which are eventually damped out by turbulent diffusion and viscous dissipation. When the forcing frequency is less than f_v, it is difficult to clearly observe organized vortical waves inside the injector, because of the long vortical wavelengths associated with the low-frequency oscillations (see Fig. 25a and b).

Fig. 26 shows snapshots of the fluctuating velocity and pressure fields under external forcing with a frequency of 13 kHz. This case was chosen because of the presence of a well-established vortical wave, which helps identify the disturbance propagation mechanisms. The vortical wave is mainly aligned with the fluctuating azimuthal velocity (see Fig. 26c), whereas the acoustic wave is most closely related to the pressure oscillation (see Fig. 26d). The imposed excitation at the injector entrance can be decomposed into two components in the azimuthal and radial directions. The former generates a vortical wave due to the shear stress resulting from the flow oscillation in the azimuthal direction, and its dynamics are governed by the conservation of angular momentum. The latter produces an irrotational, traveling acoustic wave, and can be characterized by the pressure and streamwise-velocity fluctuations through mass conservation.

To further clarify the wave propagation mechanisms, the fluctuating velocity components in various regions of the injector were investigated. Fig. 27 shows the temporal variations of the velocity fluctuations in the streamwise and azimuthal directions at three different locations along the streamline originating from the middle point of the entrance. These measurement points are all in the forward section of the injector, and the corresponding distances from the entrance are 0, 5.9, and 12.2 mm. Both the streamwise and azimuthal velocity fluctuations increase when the fluid particles travel downstream, due to the conservation of mass and angular momentum, respectively. Of particular interest is the propagation of the streamwise disturbance in the form of an acoustic wave with its phase speed equal to the local acoustic wave propagation speed. The flow disturbance in the azimuthal direction, on the other hand, travels in the form of a convective/vortical wave, with its phase speed equal to the local flow velocity. The large disparity between the two-phase speeds indicates that the streamwise disturbance arrives in the downstream region much earlier than its azimuthal counterpart. This phenomenon of decomposed oscillations is analogous to the wave propagation during an earthquake; the vertical oscillation is always detected earlier than the horizontal counterpart at the surface because of the higher propagation speed of the former.

3.5.2. Acoustic admittance at injector exit

The global response of the injector is described by the acoustic admittance at the exit. The admittance function, the reciprocal of the impedance function, measures the velocity fluctuation in response to incident pressure fluctuation. Following common practice, the acoustic admittance function, A_d, was defined as

$$A_d(f) = \frac{\hat{u}^a/\bar{a}}{\hat{p}^a/\gamma\bar{p}}, \tag{3.6}$$
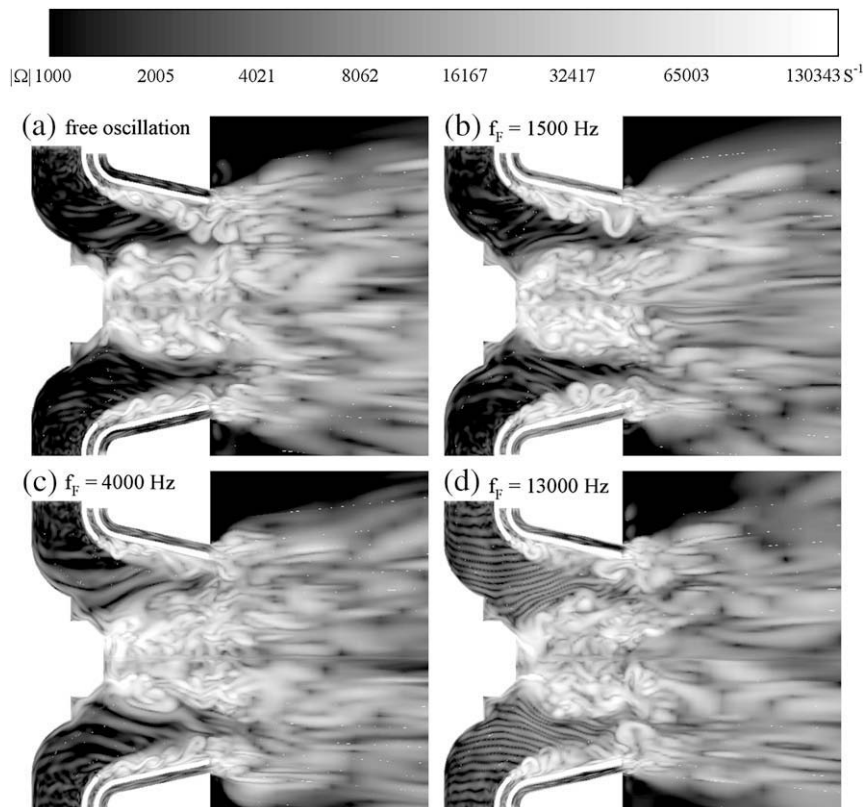
Fig. 25. Snapshots of fluctuating vorticity magnitude field on a longitudinal cross section under conditions with and without forcing. Contour levels between 10^3 and 10^5 1/s with exponential distribution (Wang et al. [108]).
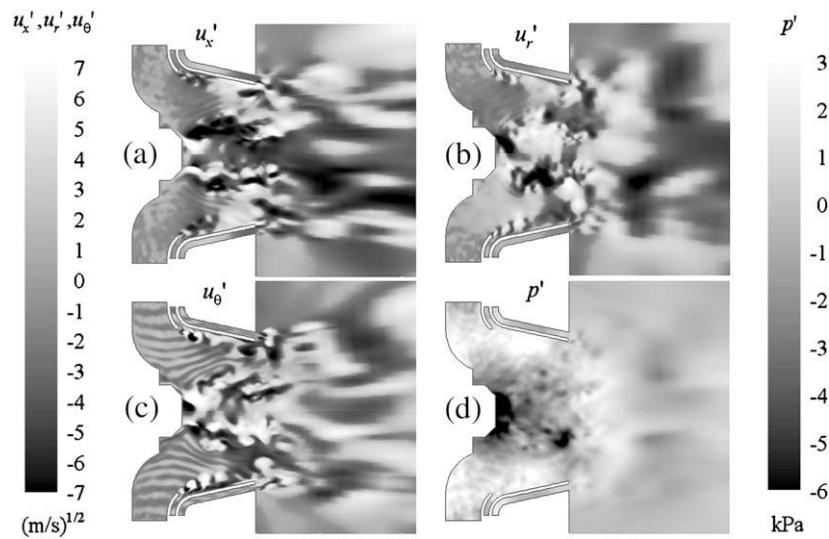
Fig. 26. Snapshots of velocity and pressure fluctuations at forcing frequency of $f_F = 13$ kHz. Velocity contour levels between -49 and 49 m/s with increment of $0.2 \sqrt{m/s}$ in square root of velocity magnitude; pressure contour levels between -6 and 3 kPa with increment of 0.1 kPa (Wang et al. [108]).

where $\bar{p}$ and $\bar{a}$ denote the mean pressure and the speed of sound, respectively. The overhat $()^a$ represents the Fourier component of the oscillation at the forcing frequency.

Fig. 28 shows the radial distributions of the admittance functions at the injector exit for four different forcing frequencies of 500, 900, 1500, and 4000 Hz. The maximum response occurs at 500 Hz, especially near the rim of the second guide vane. Excitations at 500, 900, and 1500 Hz exhibit the same trend and the admittances achieve their maxima when the outer boundary $r = R_0$ is approached. This may be attributed to the relatively low-pressure oscillation and high-velocity fluctuations near the upper boundary. In this region, the pressure response at the 500 Hz forcing is less than 300 Pa, which is smaller than its counterparts at other excitation frequencies ($>$1000 Pa). When the oscillation is impressed at 4000 Hz, the velocity response in the outer region ($0.8 < r/R_0 < 1.0$) becomes very small. Since the liquid film breaks up at the trailing edge of the second guide vane, the flow response in this region plays an important role in dictating the dynamic behavior of the

liquid fuel. A small pressure oscillation at 500 Hz may result in a large velocity fluctuation, which consequently exerts a strong influence on spray formation at that location.

The phase distribution of the admittance function indicates a lag of around 90° between the velocity and pressure fluctuations in the main flow passage ($0.3 < r/R_0 < 0.8$). The situation is consistent with the behavior of a simple traveling acoustic wave without much influence from shear layers. The phase behavior for the 4000 Hz case exhibits a trend distinct from the other cases, especially in the central recirculation zone. A major factor contributing to this phenomenon is the proximity of the forcing frequency to the characteristic frequency of the central recirculating flow. The imposed axisymmetric excitation in the streamwise and azimuthal directions does not promote the evolution of the precessing vortex along the boundary of the central recirculation zone. The pressure and velocity coupling at 4000 Hz is different from that at other frequencies because of the phase difference between the oscillations induced by external forcing and the intrinsic flow instabilities.

4. Combustion instability phenomena

Flow oscillations always exist in a practical combustion device, even under stable operating conditions. Combustion with small-amplitude pressure fluctuations (e.g., less than about 5% of the mean chamber pressure for certain combustors) is defined as stable combustion. Combustion with large-amplitude periodic pressure oscillations is termed unstable (oscillatory) combustion, and is referred to as "combustion instability" (Crocco and Cheng [187], Weiss [188], Sutton and Biblarz [189]).

Combustion instability may either develop spontaneously within the system or be initiated by any natural or artificial perturbation external to it. The first case is referred to as self-excited instability. Generally, a small perturbation grows out of system noise for some time and eventually displays periodic behavior. Because the oscillations arise from causes internal to the system, they are true instabilities and an external observer perceives the result as the dynamic behavior of a self-excited system. For the latter case, the instabilities are initiated by a finite-amplitude perturbation external to the system, which is otherwise stable to small disturbances (Wicker et al. [190]; Wang [191]). For both types of instability, the pressure amplitude of oscillations grows with time only if the energy

Fig. 27. Fluctuations of streamwise and azimuthal velocities at three different locations along the streamline originating from the middle point of the entrance (Wang et al. [108]).
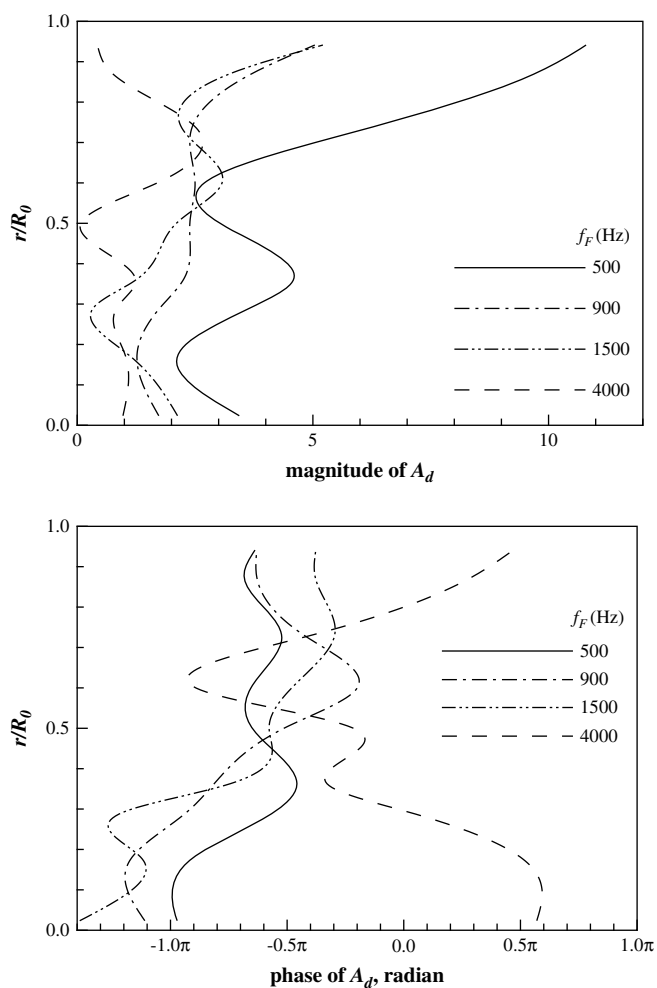
Fig. 28. Radial distributions of acoustic admittance function at injector exit for different forcing frequencies (Wang et al. [108]).

gain from combustion to the oscillation field is greater than the energy lost. Whether or not a pressure perturbation leads to instability depends on the excitation mechanism and the nature of the driving and damping processes.

Combustion instability in a specific gas turbine engine can generally be classified by the oscillation frequencies and grouped into the following categories: low-frequency, intermediate-frequency, and high-frequency instabilities [44,192–194], but there is no universally accepted criterion with well-defined frequency boundaries currently available to define these three types of instabilities. According to Mongia et al. [193], low-frequency instabilities occur at frequencies below than 30 Hz, and are often related to incipient blowout phenomena. Intermediate-frequency instabilities are observed in the range of 100–1000 Hz, and are usually associated with the coupling between the fuel–air ratio and acoustic oscillations. High-frequency oscillations take place above 1000 Hz, and are caused by interactions between acoustic disturbances and flame evolution. In the instabilities classification proposed by Krebs et al. [44], low-frequency dynamics (<50 Hz) are referred to as the "bulk" or "Helmholtz" mode of oscillations. Intermediate-frequency instabilities (50–1000 Hz) usually correspond to the longitudinal acoustic modes of the combustor. High-frequency dynamics take place at frequencies above 1000 Hz, and are related to tangential acoustic modes. Sewell and Sobieski [194] term low-frequency oscillations (10–50 Hz) "rumble instabilities". These are often observed at very lean conditions near blowout, and

sound like a freight train running through the plant. They are also referred to as "cold tones," because their amplitude increases as the flame temperature decreases. Intermediate-frequency dynamics (50–250 Hz) are referred to as "hot tones," as their amplitude often increases with flame temperature. High-frequency (>250 Hz) or screech instabilities are very destructive and can cause the engine hardware to fail in a few minutes. These three types of instabilities are all observed in many industrial gas turbine engines [194].

4.1. Flame evolution

Unstable combustion is characterized by large-amplitude flow oscillations with well-defined frequencies, while stable combustion is usually accompanied by turbulent flow noise, whose spectrum is white with no dominant characteristic frequency. In some cases, low amplitude oscillation with a distinct frequency may appear in a stable flame due to the evolution of coherent structures. In addition to the magnitude of pressure fluctuation, stable combustion may distinguish itself from the unstable state by the overall flame structure (position and shape) in certain circumstances (Broda et al. [195], Seo [196], Lee et al. [197], Huang and colleagues [198,199], Venkataraman [200]).

Broda et al. [195] and Seo [196] performed experimental studies of combustion dynamics in a swirl-stabilized combustor. The system consisted of a single-element swirl injector, an axisymmetric chamber, and a choked nozzle, as shown schematically in Fig. 12. Natural gas was injected radially from the centerbody through ten holes immediately downstream of the swirler vanes. The fuel and air streams were well mixed before entering the combustor. A broad range of equivalence ratio and inlet air temperature was considered systematically. Fig. 29 shows stability maps as a function of inlet air temperature and equivalence ratio. Instabilities occur only when the inlet air temperature is greater than a threshold value T_{in}^* around 660 K and the equivalence ratio falls into the range between 0.5 and 0.7. Fig. 30 shows typical photographic images of stable and unstable flames with an equivalence ratio 0.6 and a chamber pressure 0.48 MPa. Significant differences in overall flame structure are observed between the stable and unstable combustion modes. The shape of the combusting flow shifts from a blue, conical flame (stable state) to a white, deflected flame with intense emissions of light (unstable state). The corner recirculation zone (CRZ) behind the backward-facing step of the dump plane is filled with a reacting flow under unstable operating conditions, as compared to stable combustion, where no chemical reaction appears in the CRZ.

Fig. 31 shows the calculated mean temperature contours and pseudo-streamlines on the $x - r$ plane based on the mean axial and radial velocity components (Huang and Yang [198]), corresponding to the stable and unstable flames shown in Fig. 30. In both cases, a central toroidal recirculation zone (CRTZ) is established in the wake of the centerbody under the effects of the swirling flow. The CTRZ, a form of vortex breakdown, serves as a flame stabilization region, where hot products are mixed with the incoming mixture of air and fuel. In addition, as a result of the sudden increase in the combustor area, a CRZ is formed downstream of the backward-facing step. Under stable operation conditions, the flame spreads from the corner of the centerbody to the chamber wall. For unstable combustion, the flame is anchored by both the corner and the center recirculating flows, and it forms a compact enveloped configuration.

Fig. 32 presents the stable flame evolution and vortex shedding process in the upstream region of the chamber over one cycle of oscillation. The pressure and velocity are measured at the middle point of the inlet annulus exit. The phase angle θ is referenced with respect to the acoustic velocity at the interface between the inlet and
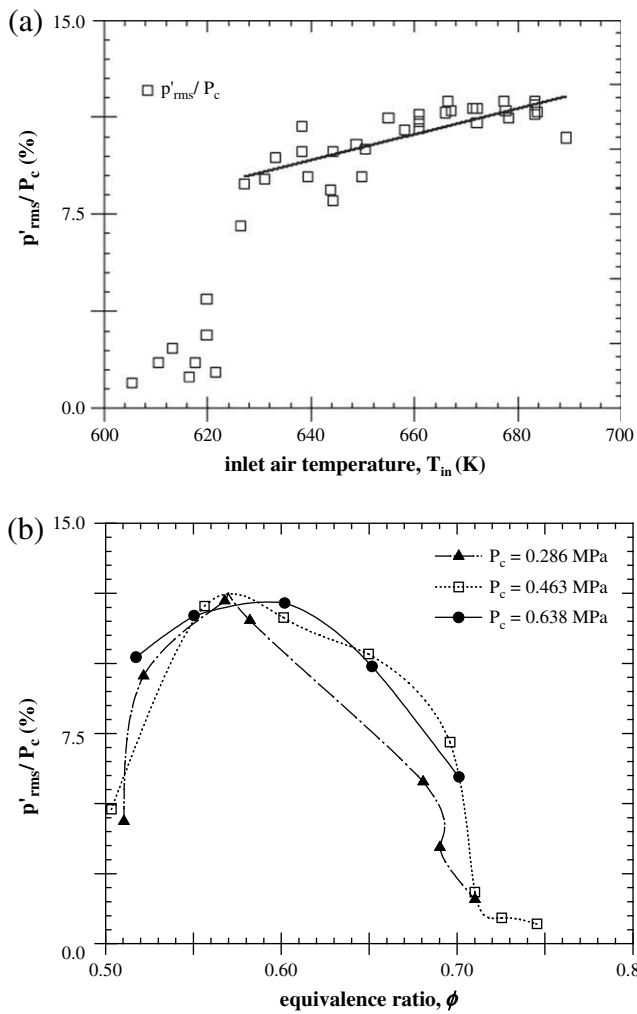
Fig. 29. Stability maps as function of inlet air temperature and equivalence ratio; (a) $p_c = 0.45$ MPa, $\phi = 0.573$; and (b) $T_{in} = 669$ K (Seo [196]).

Fig. 30. Top: photographic images of stable and unstable flames; and bottom: pressure–time trace, $p_c = 0.483$ MPa, $\phi = 0.573$ (Seo [196]).

the combustor. The entire process is dictated by the temporal evolution and spatial distribution of the flame front, which moves back and forth under the influence of the vortical motion (indicated by the concentrated streamlines) in the chamber. A new vortex with a higher local flow velocity begins to shed from the centerbody at $\theta = 90°$. As the vortex moves downstream ($\theta = 180° - 270°$), it distorts the flame front or even produces a separated flame pocket. At the same time, the higher-speed mixture pushes the flame downstream. When the vortex moves away from the flame ($\theta = 360°$) and dissipates into small-scale structures, the flame front propagates upstream (since the higher-speed mixture is convected downstream) and interacts with another incoming vortex. During this process, a new vortex appears at the corner of the centerbody and another cycle repeats. Under stable operating conditions, the calculated pressure and velocity fields exhibit small-amplitude fluctuations ($p'/p = 2\%$) with a harmonic mode at 3214 Hz, corresponding to the frequency of the vortex shedding from the centerbody.

Under unstable operating conditions, the dominant acoustic motion is found to correspond to the first longitudinal mode of the combustion chamber. Fig. 33 shows experimentally observed OH• PLIF images of an unstable flame with $x_{inj} = 36.8$ mm, $\phi_0 = 0.57$, and $\varphi = 45°$ for one cycle of 1L acoustic oscillations (Seo [196]). The images are phase-locked to dynamic pressure, providing two-dimensional information on flame structures on the center plane of the combustion chamber. The flame structures are coupled to the pressure oscillations, and change significantly in the near field over the cycle of oscillations. The OH• intensity barely varies further downstream of the combustor. Around the maximum dynamic pressure (images 3 and 4), coherent reaction zones are attached at the tip of the centerbody. These reaction zones are then pushed by
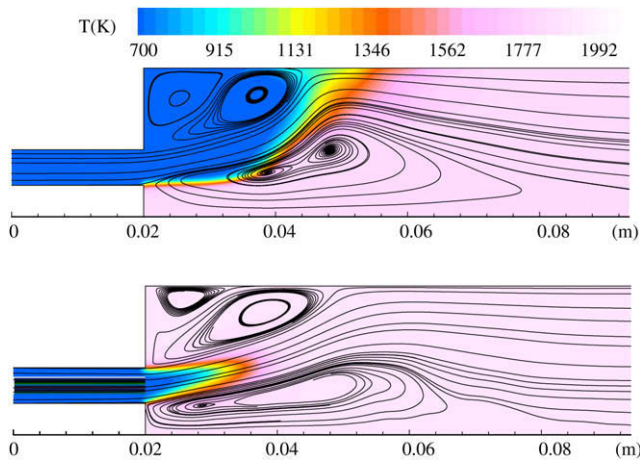
Fig. 31. Mean temperature contours and streamlines of stable (top) and unstable (bottom) flames (Huang and Yang [198]).

Fig. 32. Stable flame evolution over one cycle of oscillation (3214 Hz): temperature contours and streamlines (Huang and Yang [198]).

the incoming flow with the increasing velocity on the negative gradient of the pressure wave. The flame structure becomes more stretched by the incoming flow until the minimum dynamic pressure is reached (image 12). On the positive gradient of the pressure wave, the flame begins to retreat towards the dump plane with decreasing inlet flow velocity.

4.2. Nonlinear combustion dynamics

The flow and flame characteristics in a combustion chamber can change dramatically as the governing parameters pass through the critical values at which bifurcation points are located. Combustion processes alone may or may not exhibit bifurcation phenomena, but when they take place in the presence of the nonlinear behavior of the chamber dynamics, they become dominant in many combustion devices (Knoop et al. [201], Broda, et al. [195], and Lieuwen [202]). Sometimes, when bifurcation takes place, arising from disturbances of the governing parameters, transition from a stable operation (characterized by a limit cycle with small oscillation or no oscillation) to an unstable operation (characterized by a limit cycle with large oscillation) is observed. The reverse transition, from an unstable to a stable operation, may not occur at the same critical parameter value, due to the hysteresis behavior of the system. Phenomena of this kind may be explained using dynamical systems theory.

4.2.1. Limit cycles, bifurcation, and hysteresis: an overview

Dynamical systems theory has been often employed to study nonlinear flow and flame dynamics in combustion systems (Knoop et al. [201], Lieuwen [202], Sterling [203] Jahnke and Culick [204], Ananthkrishnan et al. [205], Di Benedetto et al. [206,207]). Some important concepts of dynamical systems theory, including limit cycle, bifurcation and hysteresis, will be briefly reviewed here, following the discussions given by Ananthkrishnan et al. [208,209]. More information can be found in the text books of Drazin [210], Strogatz [211], and Kuznetsv [212].

Consider a one-parameter autonomous (time-invariant) nonlinear dynamical system as follows

$$\dot{\mathbf{x}} = f(\mathbf{x}, \mu) \tag{4.1}$$

where $\mathbf{x}$ is the state vector variable, and μ is a scalar parameter. The equilibrium point $\mathbf{x}_0$ of the autonomous system of Eq. (4.1) for a given μ is the real root of the equation
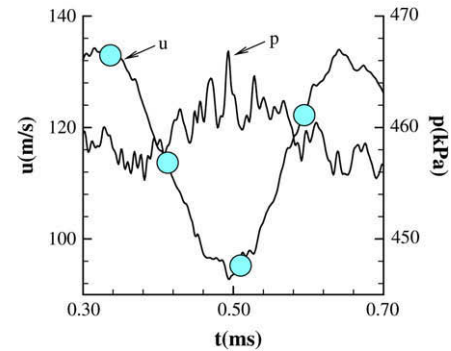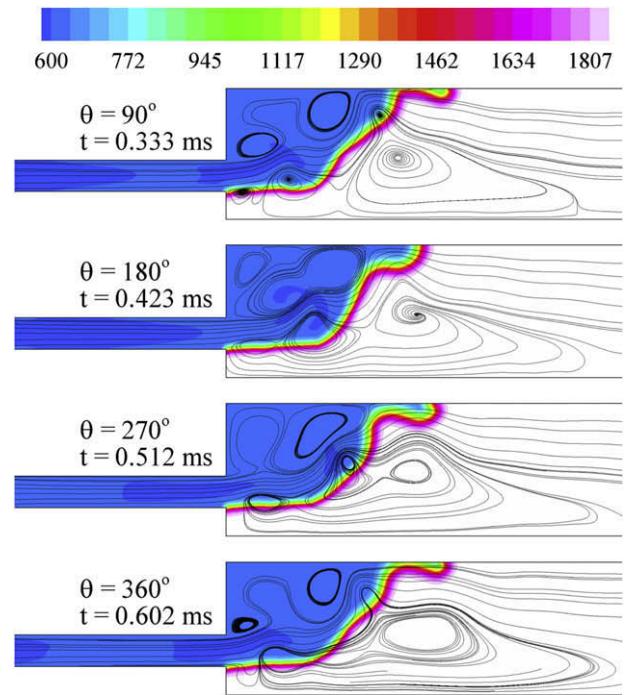
$$\dot{\mathbf{x}} = f(\mathbf{x}_0, \mu) = 0 \tag{4.2}$$

The equilibrium solution $\mathbf{x}_0$ has the property that whenever the state of the system starts at $\mathbf{x}_0$, it will remain there for all future time. The stability of an equilibrium point is determined by the eigenvalues of the Jacobian matrix $\mathbf{A} = \partial f/\partial \mathbf{x}|_{\mathbf{x}_0, \mu}$ evaluated at that point. For an equilibrium solution to be stable (which means that a small perturbation of the solution decays with time), all eigenvalues must have negative real parts. Dynamical systems of Eq. (4.1) may have not only equilibrium solutions but also periodic solutions called limit cycles. Limit cycles are presented by isolated periodic orbits in the phase portrait of the elements of the state vector $\mathbf{x}$. Limit cycles are self-excited oscillations, which distinguish themselves from forced oscillations. The qualitative behavior of an autonomous dynamical system is thus determined by the pattern of its equilibrium points and periodic orbits, as well as by their stability properties, which further depend on the parameter μ. Bifurcation is defined as the change in the equilibrium points, or periodic orbits, or in the stability properties as the parameter μ is varied [213]. Several types of bifurcations, including saddle-node, transcritical, pitchfork, and Hopf bifurcations, are commonly observed in dynamical systems [210,211,212]. In particular, when
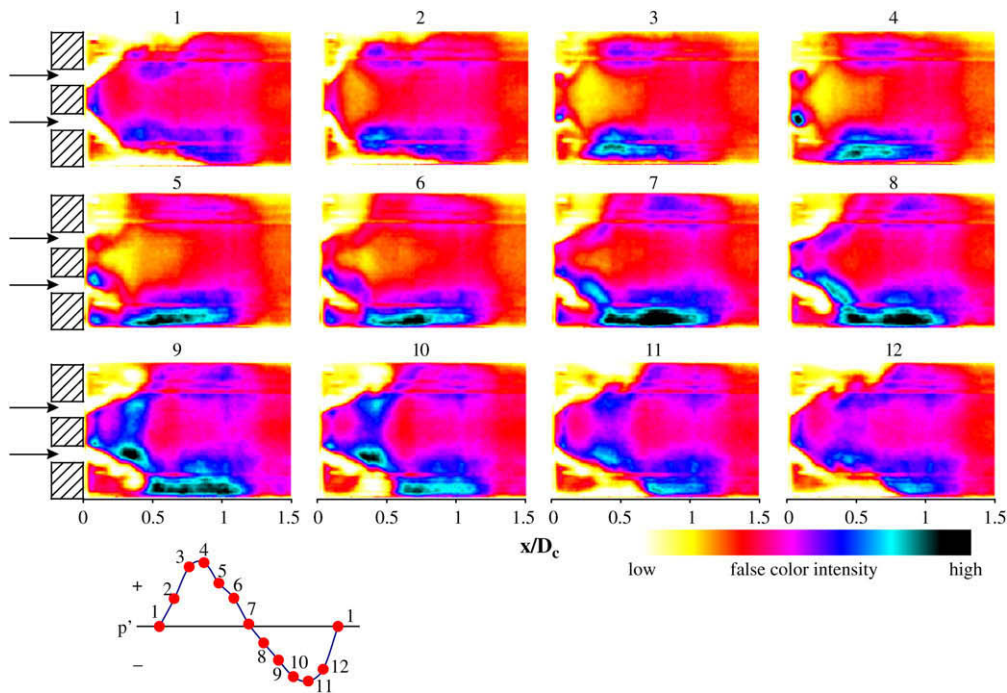
Fig. 33. Background-corrected, average OH• PLIF images phased-locked to the pressure oscillations at $x/L_c = 0.08$. $x_{inj} = 36.8$ mm, $\varphi = 45°$, $T_o = 660$ K, $p_c = 0.467$ MPa, $\phi_o = 0.57$, and $p'_{rms}/p_c = 12\%$ (Seo [196]).

a pair of complex-conjugate eigenvalues passes through the imaginary axis with varying values of parameter μ, Hopf bifurcation takes place. For a Hopf bifurcation, the associated equilibrium solution loses its stability and a limit cycle usually arises with varying values of the parameter μ. The critical value of μ for which the eigenvalues lie precisely on the imaginary axis corresponds to the onset of instability, and is called a Hopf bifurcation point.

There are two types of Hopf bifurcations: supercritical and subcritical. For supercritical Hopf bifurcations, steady limit cycles are created about equilibrium solutions at the bifurcation point as the parameter μ increases (see Fig. 34a). For subcritical Hopf bifurcation, unsteady limit cycles are created about the stable equilibrium solutions as the parameter μ varies, as shown in Fig. 34b. Here, limit cycles are represented by the maximum amplitude of oscillations. In both types of bifurcations shown in Fig. 34, the amplitude of the limit cycle builds up gradually, as the parameter μ moves away from the Hopf bifurcation point.

In the subcritical Hopf bifurcation shown in Fig. 34b, when the parameter μ crosses the bifurcation point, the solution loses its stability and will diverge to infinity. In practical physical systems, such a blowup will not usually happen, and the solution will eventually approach a steady large-amplitude limit cycle. As shown in Fig. 35a, the system jumps at the Hopf bifurcation point from a stable equilibrium solution to a steady large-amplitude limit cycle, as indicated by the upward arrow. This steady limit cycle in fact originates from the unstable solution branches due to a saddle-node bifurcation. The existence of several different stable states allows for the occurrence of hysteresis as the parameter μ varies. For decreasing values of μ, the reverse jump from a steady limit cycle to the stable equilibrium solution occurs at the saddle-node bifurcation point, as shown by the downward arrow. With hysteresis, the system does not return to the stable equilibrium state at the value of the parameter where the large-amplitude limit cycle originates.

Hysteresis can also occur in systems with supercritical Hopf bifurcations [208,209]. In Fig. 35b, the stable solution branch arising from a supercritical Hopf bifurcation first undergoes

a saddle-node bifurcation and loses its stability. The resultant unstable solution branch goes through a second saddle-node bifurcation and regains stability. Thus, the system jumps at the first saddle-node bifurcation point to a steady large-amplitude limit cycle with increasing values of μ. The system switches off the large-amplitude limit cycle to the stable equilibrium or small-amplitude periodic solutions at the second saddle-node bifurcation point with decreasing value of μ.

In the dynamical systems shown in Fig. 35, limit cycles with a large-amplitude are built up abruptly with varying values of the parameter μ. Such limit cycles are called large-amplitude limit cycles [208,209]. The occurrence of a large-amplitude limit cycle in a practical dynamical system could be catastrophic because of its unpredictable nature. In the next subsection, bifurcation and hysteresis phenomena observed in combustion systems are discussed.

4.2.2. Bifurcation and hysteresis in combustion chambers

Bifurcation- and hysteresis-related combustion dynamics have been reported in several experimental studies [195,196,201, 202,214]. Broda et al. [195] and Seo [196] noted the presence of hysteresis phenomena under certain operating conditions in their study of a model combustor with a single-element gaseous fuel
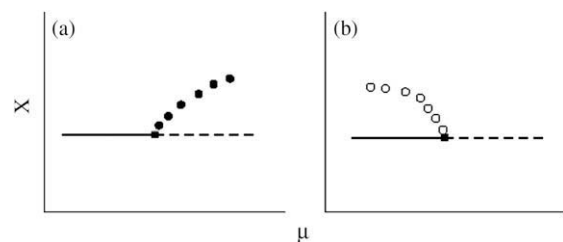
Fig. 34. Supercritical Hopf bifurcation (a); subcritical Hopf bifurcation (b) (Ananthkrishnan et al. [208,209]).
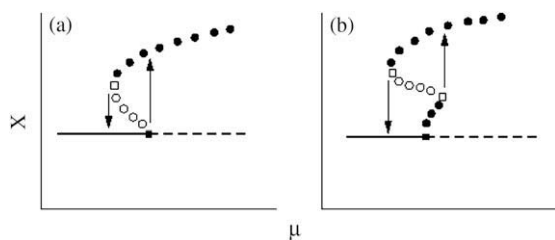
Fig. 35. Hysteresis due to subcritical Hopf bifurcation (a) and supcritical Hopf bifurcation (b) (Ananthkrishnan et al. [208,209]).

swirl injector (Fig. 12). Fig. 36 shows the stability map as a function of the overall equivalence ratio for two different swirl angles. Gaseous methane fuel is injected at $x_{inj} = 5.08$ mm, and chamber pressure is $p_c = 0.46$ MPa. The dominant acoustic motion in the chamber is the second longitudinal mode. Strong hysteresis exists for both cases, a situation not found when the first longitudinal mode prevails. The amplitude of pressure oscillations initially remains almost unchanged at a low level, then grows rapidly once the equivalence ratio exceeds a critical value, and finally levels off a high level. When the equivalence ratio is reduced from a value at which instability already exists, the pressure oscillation is able to maintain its amplitude for a certain range of equivalence ratio, and then it abruptly decreases. Hysteresis with respect to equivalence ratio was also observed by Mordaunt [215] in a similar experimental configuration using liquid fuels (kerosene and n-heptane).

Lieuwen [202] studied the limit cycle oscillations in a lean-premixed gas turbine combustor. The facility consists of inlet, mixing, combustor, and exhaust sections. Four pressure transducers were mounted along the inlet section and combustor to measure the pressure oscillations. A wide range of operating conditions (equivalence ratio of 0.65–1, combustor pressure of 1–10 atm, reactant mass flow rate of 6.1–21.1 g/s) was considered. Both super- and subcritical Hopf bifurcations were observed in the same combustor under different operating conditions. Generally, the supercritical Hopf bifurcation (Fig. 37) occurred under high inlet-velocity and low combustor pressure operating conditions, where the excited instability frequencies were in the range of 400–700 Hz. On the other hand, subcritical Hopf bifurcations (Fig. 38) appeared under low velocity, high-pressure conditions where the excited instabilities were in the range of 100–200 Hz. Fig. 38 shows that the changes in system stability characteristics depend upon whether the mean velocity is increasing or decreasing, a demonstration of hysteresis behavior. The bifurcation points marked by the vertical arrows (see Fig. 38) varied from test to test, which may be attributed to the effects of background disturbances. It should be noted that the nonlinearities that describe the combustion dynamics under certain operating conditions may not work at others.
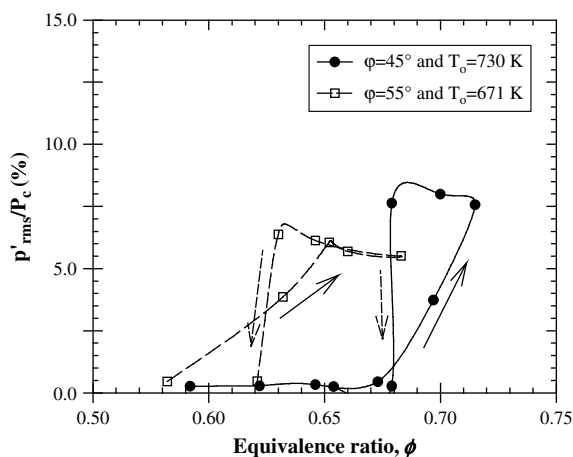
Culick and colleagues [201,214] investigated the flame dynamics in a dump combustor. At any operating point within the hysteresis region, for a given pair of flow velocity and equivalence ratio, the combustion may be either stable or unstable, depending on the history of the process. The authors attempted to take advantage of a hysteresis loop for exercising active control of the combustion dynamics. It was shown that the oscillating combustion could be stabilized by injecting short pulses of secondary fuel either in the boundary layer upstream of the dump plane or in the combustor recirculation zone. More importantly, when the control pulses were removed, stable combustion was maintained and there was no spontaneous transition from a stable to an unstable state. The results suggested the possibilities of active control with little external power input.

4.2.3. Transition of flame structure

In the experimental studies of Broda et al. [195] and Seo [196], as the inlet temperature increased from 600 to 660 K, flame bifurcation took place. The flame originally anchored in the center recirculation zone penetrated into the corner recirculation zone and flashed back. Consequently, the flame was stabilized by both the corner- and center-recirculating flows and formed a compact enveloped configuration. The flame flapped dynamically and drove flow oscillations through its influence on unsteady heat release. This kind of bifurcation phenomenon in flame structure, as the inlet temperature varies, was also investigated numerically by Huang and Yang [198]. They suggested that the inlet temperature exerts its influence on the flame dynamics through flow velocity and flame speed. When the inlet temperature increases, for a fixed mass flow rate, the flow velocity also increases and pushes the flame downstream. On the other hand, the increased inlet temperature leads to an increase in the flame speed, and consequently causes the flame to propagate upstream. In addition, flashback may occur near the wall, due to the small local flow velocity. The combined effects of flow acceleration, flame-speed enhancement, and flashback determine the final form of the flame structure.

According to Huang and Yang [198], the entire bifurcation process can be divided into three stages: high temperature mixture filling, flame trapping, and vortex flashback processes, as shown in Fig. 39, where $t = 0$ ms denotes the time at which the inlet mixture temperature starts to increase from 600 to 660 K. Fig. 39a–c shows the high temperature mixture filling process. As the inlet mixture

Fig. 36. Stability maps as a function of the overall equivalence ratio for two different swirl angles at $x_{inj} = 5.08$ mm and $p_c = 0.465$ MPa. Normalized rms pressures were taken at $x/L_c = 0.51$. Arrows indicate the chronological order of measurements (Seo [196]).
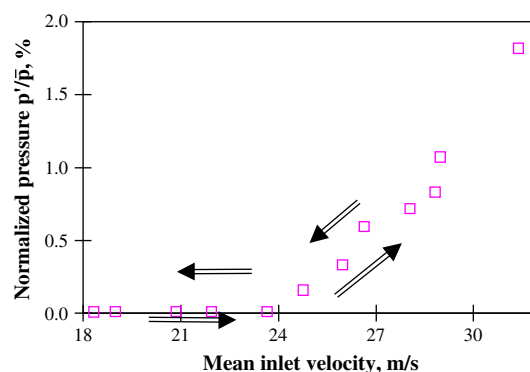
Fig. 37. Dependence of the pressure oscillation amplitude upon the mean inlet velocity, experimentally observed supcritical bifurcation (Lieuwen [202]).
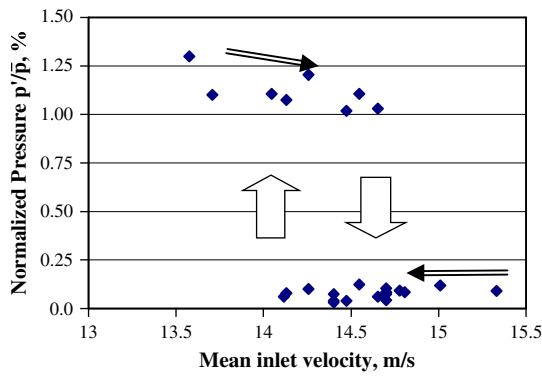
Fig. 38. Dependence of the pressure oscillation amplitude on the mean inlet velocity, experimental observed subcritical bifurcation (Lieuwen [202]).

temperature increases, the flow speed increases due to the decreased density for a fixed mass flow rate. As a result, the original low-temperature mixture is pushed downstream toward the flame. Although flashback is observed near the wall, the high temperature mixture has not reached the flame front near the wall and the flame speed remains unchanged at this stage.

Fig. 39d–e shows the flame trapping process. Once the high temperature mixture reaches the flame front, with the help of the increased flame speed, the near-wall flashback overshadows the flow acceleration effects. Consequently, the flame front penetrates into the corner recirculation zone and is trapped by the local vortical motion.

In the vortex flashback process, as shown in Fig. 39f–h, the flame propagates upstream under the influence of the vortical motion. A counter-clockwise rotating vortex originally shed from the edge of the backward-facing step approaches the flame front in the corner recirculation zone and then pushes it toward the dump plane. At the same time, a small flame pocket is produced and separates from the main stream. After this vortex is convected downstream and passes through the flame, another vortex approaches and interacts with the flame. This process continues and eventually the fresh reactants in the corner recirculation zone are completely burnt. The flame is stabilized by both the corner- and center-recirculating flows and its overall length is substantially reduced. This situation renders the combustor more prone to instabilities, according to the Rayleigh criterion, since considerable heat is released within a short distance close to the chamber head-end (i.e., the acoustic anti-node point).

Once the flame becomes unstable when the inlet flow temperature exceeds the critical value T_{in}^*, it becomes rather difficult to re-establish stable operation unless the inlet temperature is reduced to a level significantly lower than T_{in}^*, a typical hysteresis phenomenon. The occurrence of hysteresis under the current circumstance may be explained as follows. During unstable combustion, the corner recirculation zone is filled with high temperature products and the chamber wall in this region is heated to reach the local flame temperature. To recover stable operation, the cold flow needs not only to extinguish the flame stabilized by the corner recirculating flow through entrainment or flame liftoff, but also to offset the effect of the high temperature wall, which tends to increase the local gas temperature and inhibit extinction and near-wall flashback. Consequently, a much lower inlet temperature is required to regain stable operation.

4.3. Influence of combustor geometry

The geometry of a combustor includes chamber dimensions (diameter and length), inlet and exit configurations, fuel injector
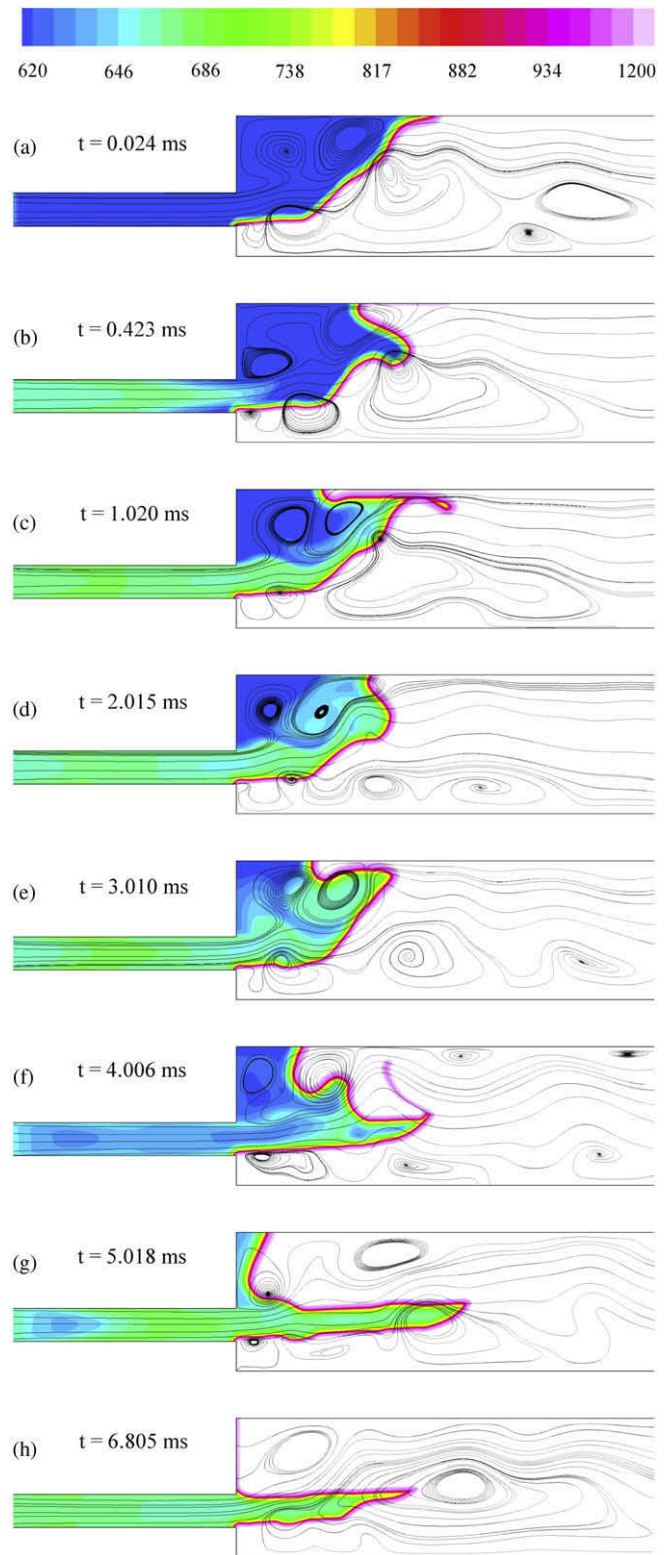
Fig. 39. Transition from stable to unstable flame with increased inlet temperature from 600 K to 660 K (Huang and Yang [198]).

arrangement, flame stabilization setup, and other factors. Combustor geometry is of crucial importance to the instability characteristics, because it not only determines the acoustic properties, but also exerts considerable influence on the flow and flame

structures in the system. The overall effects of combustor geometry on combustion instabilities have been given substantial attention [216–223].

Katsuki and Whitelaw [216] studied the influence of duct geometry on bluff-body-stabilized premixed combustors. Several duct configurations were considered, including a straight pipe with a baffle, a sudden contraction, a smooth contraction, and a sudden expansion with or without a central baffle. Methane and air were premixed in a swirl register. Except for the smooth contraction, almost all of the tested geometries gave rise to combustion oscillations in a certain range of equivalence ratio. The dominant instability oscillations were generally found to be associated with the quarter-wave of the upstream cold-gas duct. Attempts to attenuate the oscillations by using a baffle or a central pilot flame were also made and were unsuccessful. In a subsequent study, the influence of swirl intensity on combustion oscillations was examined for various combustor geometries by Sivasegaram and Whitelaw [217].

Straub and Richards [220] investigated the effect of fuel nozzle configurations on combustion dynamics in a lean-premixed combustor fueled by natural gas. The fuel nozzle geometry was varied by changing the axial location of the fuel injection point in the premixer, and by employing two injection ports along the axial direction. The former results in significant changes in the root-mean-square (rms) pressure amplitude and the dominant oscillation frequencies in the combustor. A time lag (the averaged time for a fuel/air mixture traveling from the injection port to the flame front) model was used to interpret the experimental data. Moving the fuel injection location along the axis of the premix nozzle causes the time lag to vary at a given nozzle velocity, and thus alters the interactions between heat release and pressure oscillations. Stable combustion could not be achieved by simply relocating the point of fuel injection, due to the existence of multiple acoustic modes and the transitions between different modes of instabilities in the combustor. Reduced rms pressure could be obtained, however, with dual-port fuel injection at most operating conditions. Two mechanisms, including cancellation of fuel/air variations, and competition from different acoustic feedback modes, were proposed to explain the reduction in pressure oscillations. Straub and Richards [221] also reported the influence of the swirler vane location on the flame dynamics. Four different swirler vane locations were examined. Moving the vanes upstream produced the same trend as increasing the nozzle velocity at a fixed vane position, which further confirmed the importance of the convective fuel time lag on combustion oscillations.

Venkataraman et al. [222] examined the effect of a centerbody recess on combustion stability in a coaxial, bluff-body-stabilized dump combustor. Fig. 40 shows a stability map for various centerbody recess configurations as a function of equivalence ratio. The baseline case with no centerbody recess is most susceptible to combustion instabilities. As the centerbody is recessed, instability oscillation is gradually attenuated and the flame becomes more stable over a wider range of equivalence ratios. At a centerbody recess of $D/2$, no high-amplitude flow oscillations are observed. Here D is the diameter of the centerbody. The authors suggest that recessing the centerbody alters the flame–vortex interaction and causes the combustion to stabilize. One explanation is that with a recessed centerbody, the flame is partially confined by the mixing tube and locates upstream of the dump plane where the vortex is formed. Therefore, the flame interacts less with the vortex that is shed at the dump plane.

4.4. Influence of fuel/air mixedness

For premixed gas turbine systems, full mixing of the fuel and air streams before the mixture enters the combustion zone is desired.

It is usually very difficult to obtain complete fuel–air mixing in operational engines, however, because of practical constraints, including avoiding flashback and auto-ignition, and reducing the mixing zone length. Studies have shown that incomplete fuel–air mixing has significant effects on pollutant emissions. The effect of fuel–air mixedness on combustion instabilities has been a subject of extensive research [195,196,215,222,224].

Shih et al. [224] investigated the effect of incomplete fuel–air mixing on combustion stability and NO_x emissions in a laboratory-scale premixed dump combustor. Fuel (natural gas) was injected into the mixing section at two different locations (5.5 and 6 mixing tube diameters upstream of the mixing section exit). The degree of fuel–air mixing at the entrance to the combustion zone was varied by changing the fuel split ratio. The fuel distribution at the combustor inlet was quantified using two-dimensional acetone fluorescence. Incomplete fuel–air mixing significantly reduced the stable operating range of the combustor, in terms of combustion-induced pressure oscillation level and lean blowout limit. Under unstable combustion modes, the flame moved in a well-defined periodic manner. Depending on the overall equivalence ratio and the degree of fuel–air mixing, the details of the flame behavior were found to vary significantly, and instabilities were found to originate from different combustor regions according to the Rayleigh index.

Venkataraman et al. [222] studied the influence of fuel/air mixedness and inlet fuel distribution on combustion stability in a coaxial, bluff-body-stabilized dump combustor. In this type of combustor, fuel (natural gas) injected from the centerbody generally reaches the outer wall layer of the mixing tube, and as a result, whenever incomplete fuel–air mixing occurs, there always exists a gradient in the mean fuel distribution at the mixing tube exit. Fig. 41 shows a typical inlet fuel distribution for a 50% partially premixed condition. The equivalence ratio increases from a minimum along the centerbody to a maximum along the wall of the mixing tube. A sufficiently large value of the equivalence ratio is thus required at the centerbody to anchor the flame and avoid lean blowout. Fig. 42 shows the stability map as a function of the equivalence ratio under 50%, 75% and 100% premixed conditions. As the degree of mixedness decreases, there is a significant increase in the strength of the instability, both in the midrange of the equivalence ratios and at near stoichiometric conditions. It was suggested that the reaction zone or the flame moves radially outward as the mixedness decreases, which makes the system more susceptible to flame–vortex interactions.
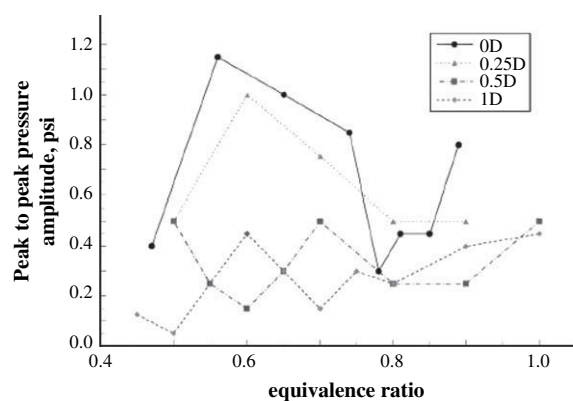
Fig. 40. Stability map as function of equivalence ratio for different centerbody recess (Venkataraman et al. [200]).
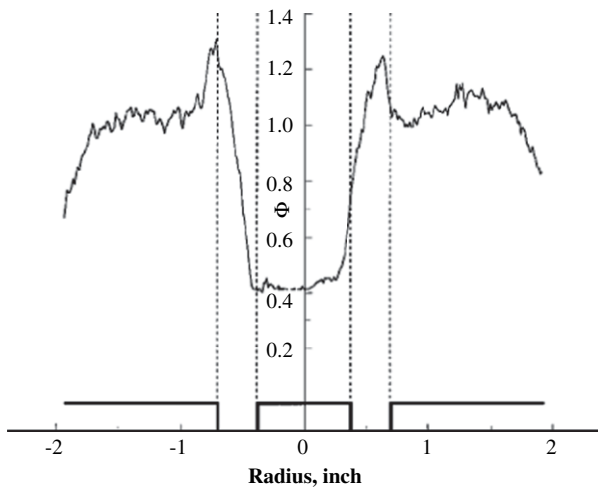
Fig. 41. Inlet fuel distribution under partially premixed conditions (Venkataraman et al. [200]).

Fig. 42. Stability map as function of equivalence ratio under different mixedness conditions (Venkataraman et al. [200]).

4.5. Influence of fuel variability (fuel type and composition)

Although natural gas is the primary fuel for gas turbine engines, there is growing interest, due to ever-increasing natural gas prices, in burning alternative fuels. These alternative fuels, including coal-derived syngas (synthetic fuel gas), biomass and landfill gases, and liquefied natural gas (LNG) are usually significantly different from natural gas in terms of physical and chemical properties. For example, syngas obtained from gasification of coal is typically a mixture of methane (CH_4), hydrogen (H_2), and carbon monoxide (CO). Advanced power systems based on the integrated gasification combined cycle (IGCC) technology have been developed utilizing syngas as the primary fuel. The composition of syngas, however, can vary widely depending on the source and processing technique. The change in fuel type and composition usually leads to significant changes in the characteristic time scale of chemical reactions in the combustion system, which consequently has a major impact on combustion operability, including flashback, auto-ignition, lean blowout, and combustion dynamics. Motivated by developing fuel-flexible combustion systems capable of burning a variety of fuels without significantly altering combustor operability and performance, a number of researchers [215,225–229,231,232] have studied the influence of fuel type and fuel composition on gas turbine combustion.

Lieuwen et al. [227] investigated the effect of fuel composition on the operability of lean-premixed combustors. The basic combustion properties, such as laminar and turbulent flame speeds, auto-ignition and chemical kinetic time scale, were first studied. One notable observation is that the combustion behavior of fuel mixtures, such as turbulent flame speed and ignition delay time, can be markedly different from that of the individual constituents, and exhibit a highly nonlinear dependence on fuel composition. Fig. 43 shows the effect of turbulence intensity on the turbulent flame speed for several fuel blends with the same laminar flame speed [230]. The graph indicates that fuels with similar laminar flame speed have substantial variation in the turbulent flame speed, due to the different diffusion properties of the reactants. Because of those complex fuel variability effects, it is apparent that combustor operability is strongly affected by fuel composition. Lieuwen et al. [227] and Figura et al. [229] explored the effect of fuel composition on the flame structure and combustion dynamics in a lean-premixed combustor. A spatially distributed flame was approximated as a point source, referred to as the "center of heat release" in the flame. Variation in fuel composition produces changes in the location of the "center of heat release", due to the changing flame speed. As a result, the convective time scale from the fuel injection point to the flame was changed, which resulted in the modification of the phase relationship between the heat release and pressure oscillations. Fuel composition was thus shown to exert a significant impact on the stability characteristics of the system.
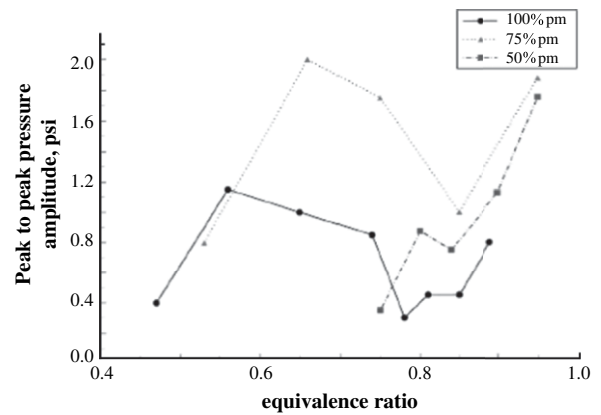
Ferguson et al. [228] studied the influence of fuel composition and heat content on combustion instabilities in both laboratory-scale and atmospheric-pressure combustors. The effect of fuel Wobbe index (a parameter characterizing fuel interchangeability in terms of heating value) was examined by blending natural gas with various amounts of ethane, propane, and nitrogen. It was found that a constant Wobbe index would not necessarily produce a constant dynamic response. Results also suggested that a modest variation in fuel composition did not significantly change the dynamic properties of the system. Different dynamic responses of flames were observed, however, for fuels with high concentrations of heavier hydrocarbons (such as propane).
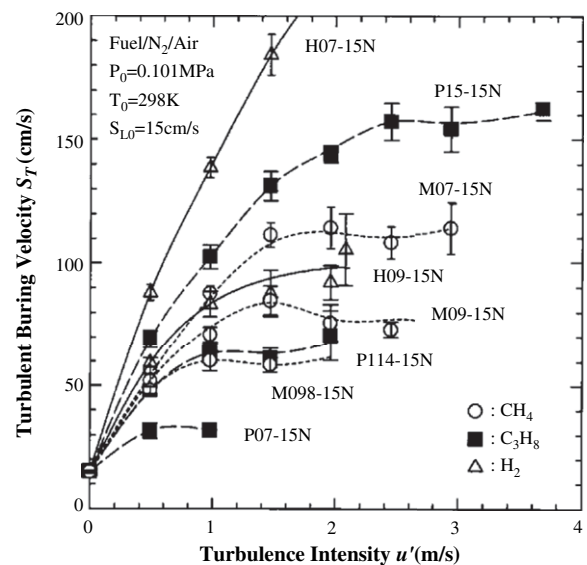
Fig. 43. Dependence of turbulent burning velocity on turbulence intensity, fuel type, and equivalence ratio (Kido et al. [230]).

Mordaunt et al. [215,231] conducted a series of studies to examine the combustion dynamics of a model lean-premixed combustor using various gaseous and liquid fuels, including natural gas, ethylene, and three different liquid hydrocarbon fuels: n-heptane, JP-8, and a coal-derived fuel. The general trends of the stability maps as a function of inlet equivalence ratio and temperature for these liquid fuels were found to bear a close resemblance to those of natural gas. Gaseous ethylene, however, exhibits a considerable difference in the stability domain because of its much lower auto-ignition temperature.

4.6. Influence of operating conditions

Broda et al. [195] and Seo [196] investigated the influence of operating conditions, including inlet air temperature, chamber pressure, equivalence ratio, and swirl strength, on the lean-premixed combustion dynamics of a gaseous-fueled, single-element swirl injector. Instabilities were found to appear only if the inlet air temperature is greater than a threshold value, which lies between 650 and 670 K, and the equivalence ratio falls in the range between 0.5 and 0.7. In addition, with an increase in the swirler angle, the intensity of instability tends to decrease, and the equivalence ratio at which the maximum rms pressure occurs shifts towards a leaner condition. The changes in instability characteristics with swirl strength were attributed to the modification of flow structures and acoustic boundary conditions at the surfaces of different swirlers.

Venkataraman et al. [222] also performed a parametric study on the effects of equivalence ratio, inlet velocity, and inlet swirl on combustion instability in a coaxial, bluff-body-stabilized dump combustor using natural gas as the fuel. Fig. 44 shows stability maps as function of equivalence ratio for different inlet velocities. Combustion tends to become unstable as the inlet velocity increases. For the case with an inlet velocity of 6 m/s, as the equivalence ratio increases from the lean blowout limit, combustion first becomes unstable around an equivalence ratio of $\phi = 0.55$. It regains a stable state at about $\phi = 0.8$, and then it loses its stability again as ϕ approaches stoichiometry. Increasing swirl strength, however, tends to stabilize the combustion process at higher equivalence ratios, and to establish an unstable region of combustion at equivalence ratios close to lean blowout, as shown in Fig. 45. The authors attributed the stabilization of combustion at higher equivalence ratios with swirl to the disruption of the vortex and flame interactions.

Bernier et al. [233] studied the instability characteristics in premixed prevaporized swirl-stabilized combustors using co- and counter-rotating swirl injectors. Liquid heptane was used as fuel. These two swirl configurations have distinct domains of instability. In the co-swirl configuration, instabilities are observed when the fuel injection velocity is lower than a critical value u_c, which depends on the equivalence ratio, injection temperature, and swirl geometry. In the counter-swirl geometry, instabilities occur when the injection velocity exceeds the critical velocity. In both swirl configurations, instabilities take place when the equivalence ratio is increased beyond a critical value for a fixed injection velocity. This observation differs from the experimental results obtained by Venkataraman et al. [222], in which unstable combustion was found to arise near lean blowout and not at higher equivalence ratios. Additional studies on the influence of operating conditions on lean-premixed gas turbine combustion can be found in the literature [202,215,220,221,223,231,234–238].

5. Driving mechanisms of combustion instability

Heat release from chemical reactions is the major energy source driving unsteady flow oscillations in combustion systems. Although the energy needed to drive unsteady motions is only an exceedingly
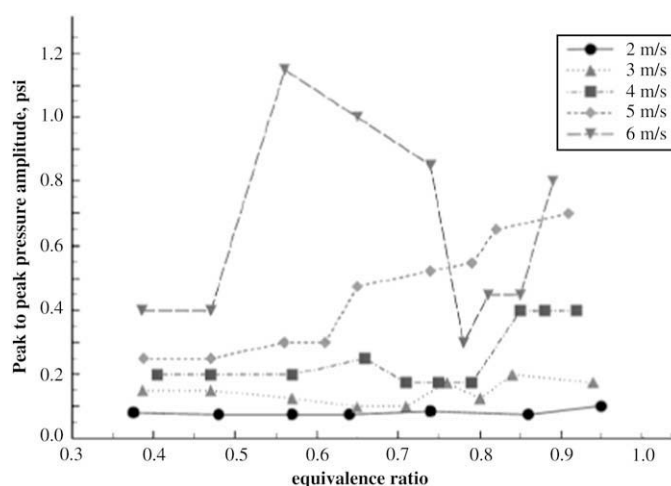
Fig. 44. Stability map as function of equivalence ratio for different inlet velocities (Venkataraman et al. [200]).

small fraction of the heat release from combustion (Culick and Yang [14,15]), instabilities usually cannot be sustained unless a certain dynamic relation between heat release fluctuations and acoustic pressure oscillations is satisfied in the combustion chamber. The dependence of instability on the relationship between heat release and acoustic oscillations was first identified by Lord Rayleigh [239]. In his monograph "The Theory of Sound", he explained the excitation of tones in a Rijke tube as follows:

> If heat be given to the air at the moment of greatest condensation, or be taken from it at the moment of greatest rarefaction, the vibration is encouraged. On the other hand, if heat be given at the moment of greatest rarefaction, or abstracted at the moment of greatest condensation, the vibration is discouraged.

This paragraph gives the so-called Rayleigh criterion for the occurrence of combustion instability. The criterion states that if heat is released when a pressure oscillation is near its maximum, the pressure fluctuation increases in amplitude. On the other hand, if heat release occurs when the pressure oscillation is at a minimum point, the pressure fluctuation is attenuated. The Rayleigh criterion can be explained mathematically by analyzing the energy balance equations for periodic motions, as in the following section.
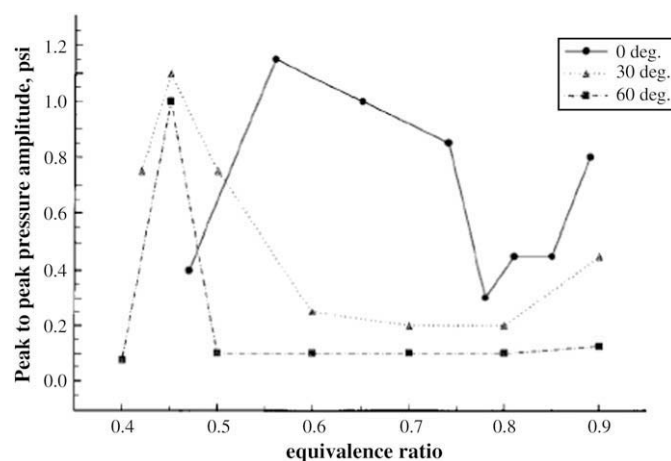
Fig. 45. Stability map as function of equivalence ratio with different swirler vane angles (Venkataraman et al. [200]).

5.1. Energy transfer mechanisms

In many practical turbulent flows, especially in gas turbine combustors, random and periodic (coherent) motions co-exist. It is instructive to consider the energy exchanges between the mean, periodic, and turbulent flowfields. This may enable us to understand why and how periodic flow motions are amplified, and provides some indications as to the mechanisms of instabilities. Chu [240], Pierce [241], Culick [11], Candel et al. [242], and Dowling [243] analyzed the energy fluxes to small disturbances (including both periodic and turbulent motions) by means of a Reynolds decomposition technique. Their work, however, did not distinguish periodic motions from background turbulent fluctuations. Recently, Huang et al. [244] studied the energy transfer mechanisms between mean, periodic, and turbulent motions using a triple decomposition technique. The influence of heat release on flow dynamics in a turbulent reacting environment was also explored. Almost all pathways through which oscillatory motions acquire energy were identified.

When the triple decomposition technique is applied to compressible flows (Apte and Yang [245], Huang et al. [244]), each flow variable $\Im$ can be expressed as the sum of density-weighted long-time-averaged, $\overleftrightarrow{\Im}$, periodic (coherent), $\Im^a$, and turbulent (stochastic), $\Im^t$, quantities as follows:

$$\Im(\mathbf{x}, t) = \overleftrightarrow{\Im}(\mathbf{x}) + \Im^a(\mathbf{x}, t) + \Im^t(\mathbf{x}, t) \tag{5.1}$$

The decomposition is achieved using the density-weighted long-time and ensemble-phase averaging techniques (see Refs. [244–246] for detail), respectively. The averaged kinetic energy per unit volume is defined as follows:

$$\kappa = \overline{\rho u_i u_i}/2 = \overline{\rho}\,\overleftrightarrow{u}_i\overleftrightarrow{u}/2 + \overline{\rho u_i^a u_i^a}/2 + \overline{\rho u_i^t u_i^t}/2 \tag{5.2}$$

The energy associated with periodic motion, ε, contains both kinetic (ε_k) and potential (ε_p) energies, in accordance with acoustic theories.

$$\varepsilon = \varepsilon_k + \varepsilon_p = \overline{\rho u_i^a u_i^a}/2 + \overline{(p^a)^2}/\left(2\overline{\rho}\cdot\overline{c}^2\right) \tag{5.3}$$

When the triple decomposition technique is applied to the balance equations of mass, momentum and energy for an ideal gas mixture, the equations for the three components of kinetic energy can be derived as follows (see Ref. [244] for detailed derivation)

time-mean

$$\frac{\partial\left(\overleftrightarrow{u}_j\overline{\rho}\,\overleftrightarrow{u}_i\overleftrightarrow{u}_i/2\right)}{\partial x_j} = \overline{\rho u_i^a u_j^a}\frac{\partial\overleftrightarrow{u}_i}{\partial x_j} + \overline{\rho u_i^t u_j^t}\frac{\partial\overleftrightarrow{u}_i}{\partial x_j} - \frac{\partial\left(\overleftrightarrow{u}_i\overline{\rho u_i^a u_j^a} + \overleftrightarrow{u}_i\overline{\rho u_i^t u_j^t}\right)}{\partial x_j}$$
$$+ \overline{p}\frac{\partial\overleftrightarrow{u}_i}{\partial x_i} + \frac{\partial\left[\overleftrightarrow{u}_i(\overline{\sigma}_{ij} - \overline{p})\right]}{\partial x_j} - \overline{\sigma}_{ij}\frac{\partial\overleftrightarrow{u}_i}{\partial x_j} \tag{5.4}$$

periodic (acoustic or coherent)

$$\frac{\partial(\overline{\rho u_i^a u_i^a}/2)}{\partial t} + \frac{\partial(\overline{\rho}\,\overleftrightarrow{u}_j\overline{u_i^a u_i^a}/2)}{\partial x_j} + \frac{\partial\left(\overline{\rho u_j^a u_i^a u_i^a/2}\right)}{\partial x_j} = -\overline{\rho u_i^a u_j^a}\frac{\partial\overleftrightarrow{u}_i}{\partial x_j}$$
$$+ \overline{\left(\rho u_i^t u_j^t\right)^a\frac{\partial u_i^a}{\partial x_j}} - \frac{\partial\overline{u_i^a p^a}}{\partial x_i} + \overline{p^a\frac{\partial u_i^a}{\partial x_i}} - \overline{\rho u_i^a u_j^a}\frac{\partial u_i^a}{\partial x_j}$$
$$- \frac{\partial\left\{\overline{u_i^a\left[\left(\rho u_i^t u_j^t\right)^a - \overline{\rho u_i^a u_j^a}\right]}\right\}}{\partial x_j} + \frac{\partial\overline{u_i^a\sigma_{ij}^a}}{\partial x_j} - \overline{\sigma_{ij}^a\frac{\partial u_i^a}{\partial x_j}} - \frac{\overline{u_i^a\rho^a\aleph_{\overleftrightarrow{u},i}}}{\overline{\rho}} \tag{5.5}$$

stochastic (turbulent)

$$\frac{\partial}{\partial t}\left(\frac{\overline{\rho u_i^t u_i^t}}{2}\right) + \frac{\partial}{\partial x_j}\left(\frac{\overline{\rho}\,\overleftrightarrow{u}_j\overline{u_i^t u_i^t}}{2}\right) + \frac{\partial}{\partial x_j}\left(\frac{\overline{\rho u_j^a u_i^t u_i^t}}{2}\right) = -\overline{\rho u_i^t u_j^t}\frac{\partial\overleftrightarrow{u}_i}{\partial x_j}$$
$$- \overline{\left(\rho u_i^t u_j^t\right)^a\frac{\partial u_i^a}{\partial x_j}} - \overline{\rho u_i^t u_j^t}\frac{\partial\overline{u_i^a}}{\partial x_j} - \overline{\left(\rho u_i^t u_j^t\right)^t\frac{\partial u_i^a}{\partial x_j}} - \frac{\partial\left(\overline{\rho u_j^t u_i^t u_i^t/2}\right)}{\partial x_j}$$
$$+ \frac{\partial\left(\overline{u_i^t < \rho u_i^t u_j^t >}\right)}{\partial x_j} - \overline{< \rho u_i^t u_j^t >\frac{\partial u_i^t}{\partial x_j}} - \overline{< \rho u_i^t u_j^t >\frac{\partial u_i^t}{\partial x_j}} - \overline{u_i^t\frac{\partial p^t}{\partial x_i}}$$
$$+ \frac{\overline{\partial u_i^t\sigma_{ij}^t}}{\partial x_j} - \overline{\sigma_{ij}^t\frac{\partial u_i^t}{\partial x_j}} - \frac{\overline{u_i^t\rho^t\aleph_{<u>,i}}}{< \rho >} \tag{5.6}$$

where $\aleph_{\overleftrightarrow{u},i} = -\partial(\overline{\rho u_i^a u_j^a})/\partial x_j - \partial(\overline{\rho u_i^t u_j^t})/\partial x_j - \partial\overline{p}/\partial x_i + \partial\overline{\sigma}_{ij}/\partial x_j$ and $\aleph_{<u>,i} = -\partial < \rho u_i^t u_j^t >/\partial x_j - \partial < p >/\partial x_i + \partial < \sigma_{ij} >/\partial x_j$.

Each kinetic energy equation contains convection, production, pressure work, and dissipation terms. The production terms are of particular interest in understanding the energy exchange among the three constituent flowfields. The term $\overline{\rho u_i^t u_j^t}\partial\overleftrightarrow{u}_i/\partial x_j$ serves as a pathway for exchanging the kinetic energy between the mean and turbulent fields. The term $\overline{\rho u_i^a u_j^a}\partial\overleftrightarrow{u}_i/\partial x_j$ characterizes the energy transfer between the mean and deterministic fields. The energy exchange between the deterministic and turbulent fields is characterized by the term $\overline{(\rho u_i^t u_j^t)^a}\partial u_i^a/\partial x_j$. Thus, the introduction of organized flow oscillations provides an additional pathway to transfer energy from the mean flowfield to turbulent motion, in comparison with stationary flow conditions. The viscous dissipation terms in these three energy equations, $\overline{\sigma}_{ij}\partial\overleftrightarrow{u}_i/\partial x_j$, $\overline{\sigma_{ij}^a\partial u_i^a/\partial x_j}$, and $\overline{\sigma_{ij}^t\partial u_i^t/\partial x_j}$, account for the transfer between kinetic and internal energy.

Similarly, an equation for the potential energy of periodic motions, $\varepsilon_p = \overline{(p^a)^2}/(2\overline{\rho}\cdot\overline{c}^2)$, can be derived,

$$\frac{\partial\left[\overline{(p^a)^2}/(2\overline{\rho}\cdot\overline{c}^2)\right]}{\partial t} + \overleftrightarrow{u}_j\frac{\partial\left[\overline{(p^a)^2}/(2\overline{\rho}\cdot\overline{c}^2)\right]}{\partial x_j} + \overline{u_j^a\frac{\partial\left[(p^a)^2/(2\overline{\rho}\cdot\overline{c}^2)\right]}{\partial x_j}}$$
$$= -\overline{p^a\frac{\partial u_j^a}{\partial x_j}} - \frac{\overline{p^a u_j^a}}{\gamma\overline{p}}\cdot\frac{\partial\overline{p}}{\partial x_j} - \frac{\overline{(p^a)^2}}{\overline{p}}\cdot\frac{\partial\left(\overleftrightarrow{u}_j + u_j^a\right)}{\partial x_j} + \frac{(\gamma-1)}{\gamma\overline{p}}\cdot\left\{\overline{p^a\left(\rho R T^t\frac{\partial u_j^t}{\partial x_j}\right)^a}\right.$$
$$\left. + \overline{p^a\left[-\left(\frac{\partial\dot{q}_i''}{\partial x_i}\right)^a + \Phi^a\right]} + \overline{p^a\dot{q}^a}\right\} - \frac{\overline{p^a}}{\gamma\overline{p}}\cdot\frac{\partial\left[R\left(\rho u_j^t T^t\right)^a\right]}{\partial x_j} - \overline{\left(\frac{p^a}{\overline{p}}\right)^2}\frac{\aleph_{\overline{p}}}{2\gamma} \tag{5.7}$$

where $\aleph_{\overline{p}} = \partial\overline{p}/\partial t + (\overleftrightarrow{u}_j + u_j^a)\partial\overline{p}/\partial x_j$

Combining Eqs. (5.5) and (5.7), we obtain the equation for the total energy of periodic motions, ε, based on the definition given in Eq. (5.3),

$$\frac{\partial\overline{\varepsilon}}{\partial t} + \overleftrightarrow{u}_j\frac{\partial\overline{\varepsilon}}{\partial x_j} + \overline{u_j^a\frac{\partial\varepsilon}{\partial x_j}} + \frac{\partial\overline{u_j^a p^a}}{\partial x_j} = \frac{\overline{p^a u_j^a}}{\gamma\overline{p}}\cdot\frac{\partial\overline{p}}{\partial x_j} - \frac{\overline{(p^a)^2}}{\overline{p}}\cdot\frac{\partial\left(\overleftrightarrow{u}_j + u_j^a\right)}{\partial x_j}$$
$$- \overline{\rho u_i^a u_j^a}\frac{\partial\overleftrightarrow{u}_i}{\partial x_j} + \overline{\left(\rho u_i^t u_j^t\right)^a\frac{\partial u_i^a}{\partial x_j}} + \frac{(\gamma-1)}{\gamma\overline{p}}\cdot\overline{p^a\left(-\left(\frac{\partial\dot{q}_i''}{\partial x_i}\right)^a + \Phi^a\right)}$$
$$+ \frac{(\gamma-1)}{\gamma\overline{p}}\cdot\overline{p^a\dot{q}^a} + \frac{\partial\overline{u_i^a\sigma_{ij}^a}}{\partial x_j} - \overline{\sigma_{ij}^a\frac{\partial u_i^a}{\partial x_j}} - \frac{\overline{p^a}}{\gamma\overline{p}}\cdot\frac{\partial\left[R\left(\rho u_j^t T^t\right)^a\right]}{\partial x_j}$$
$$+ \frac{(\gamma-1)}{\gamma\overline{p}}\cdot\overline{p^a\left(\rho R T^t\frac{\partial u_i^t}{\partial x_j}\right)^a} - (\overline{\rho u_i^a u_i^a}/2)\cdot\frac{\partial\overleftrightarrow{u}_j}{\partial x_j} - \overline{\left(\rho u_i^a u_i^a/2\right)\frac{\partial u_j^a}{\partial x_j}}$$
$$- \overline{\rho u_i^a u_j^a}\frac{\partial\overline{u_i^a}}{\partial x_j} - \frac{\partial\left\{\overline{u_i^a\left[\left(\rho u_i^t u_j^t\right)^a - \overline{\rho u_i^a u_j^a}\right]}\right\}}{\partial x_j} - \overline{\left(\frac{p^a}{\overline{p}}\right)^2}\frac{\aleph_{\overline{p}}}{2\gamma} - \frac{\overline{u_i^a\rho^a\aleph_{\overleftrightarrow{u},i}}}{\overline{\rho}} \tag{5.8}$$

The term, $\overline{p^a \partial u_j^a / \partial x_j}$, appears in both Eqs. (5.5) and (5.7), but with opposite signs. It facilitates the exchange between the kinetic (ε_k) and potential (ε_p) energies. When p^a and $\partial u_j^a / \partial x_j$ are in phase, energy flows from its potential to its kinetic component, and vice versa. The convection of the energy flux, $\partial \overline{u_j^a p^a} / \partial x_j$, on the left hand side of Eq. (5.8), represents the transport of acoustic energy within the flowfield. This term vanishes upon integration over the entire flowfield for a closed system without energy flow across the boundary.

The source term, $(\gamma - 1)\overline{p^a \dot{q}^a}/\gamma \overline{p}$, on the right hand side of Eq. (5.8) represents the contribution of energy from unsteady heat release. Let θ be the phase difference between pressure and heat release oscillations, then

$$(\gamma - 1)\overline{p^a \dot{q}^a}/\gamma \overline{p} = (\gamma - 1)\left| p^a \dot{q}^a \right| \cos \theta / \gamma \overline{p} \tag{5.9}$$

If the oscillations of pressure and heat release are in phase ($-\pi/2 < \theta < \pi/2$), this term is positive, and energy is supplied to the oscillatory flowfield. Otherwise, energy is subtracted from the system for $\pi/2 < \theta < 3\pi/4$. This result is closely related to the Rayleigh criterion. The unsteady heat flux, $-(\partial \dot{q}_i'' / \partial x_i)^a$, plays a role in driving flow oscillations similar to that of unsteady heat release, as shown in Eq. (5.8), but its effect is not as significant as the heat release term in a combustion system. Nonetheless, self-excited acoustic oscillations are often observed in many heat transfer devices [247,248].

The energy exchange mechanisms in a turbulent reacting flow are summarized in the schematic diagram shown in Fig. 46. The oscillatory motions can acquire energy through several different pathways. They may extract energy from the mean flowfield and chemical reactions, exchange energy with background turbulent motion, or be dissipated into thermal energy through viscous damping. When there are no chemical reactions, the primary energy provider for periodic motions is the mean flowfield and/or boundary effects. With combustion, heat release from chemical reactions is the major source for driving periodic motions. The transfer of energy from chemical reactions to the periodic flowfield only takes place when heat release is in phase with pressure oscillation.

The above analysis suggests that the dominant physical processes or mechanisms responsible for driving unsteady flow oscillations in a combustion system arise from either heat release or gasdynamic fluctuations, or both. The latter include acoustic motions in the chamber, evolution of large-scale coherent structures, and other flow phenomena. Heat release is largely related to local equivalence ratio and mass flow rate, together with instantaneous pressure and temperature. In a gaseous premixed flame, heat release fluctuations may result from flame surface variations, equivalence ratio fluctuations, mass flow rate oscillations, and vortex shedding processes due to hydrodynamic instabilities. In systems using liquid fuel, atomization and droplet vaporization are additional sources of periodic exothermicity of the combustion process. Many of these mechanisms capable of driving combustion instabilities in gas turbines have been identified and summarized by Zinn and Lieuwen [249] and Ducruix et al. [250]. Some specific discussions of sources of gasdynamic and heat release fluctuations are presented in the following.

5.2. Acoustic motion in combustor chamber

The most problematic type of instability involves the coupling between acoustic motion and transient combustion response. A major reason for the prevalence of acoustically coupled instabilities in gas turbine combustors and many other propulsion systems is the relatively closed acoustic environment within which combustion occurs, and the relatively large amount of energy available from chemical reactions to drive the acoustic field (Culick and Yang [14,15]). In addition, acoustic waves can propagate throughout the entire chamber and affect the flame dynamics, thereby providing a pathway for energy feedback between the flow motion and combustion process. Thus a prerequisite of any instability research is the identification of acoustic modes in the combustion chamber.

With the expression of a flow variable as the sum of a mean and a fluctuating part, one can derive a wave equation from the linearized conservation equations of mass, momentum and energy as follows, neglecting all source terms,

$$\nabla^2 p' - \frac{1}{\overline{c}^2} \frac{\partial^2 p'}{\partial t^2} = 0 \tag{5.10}$$
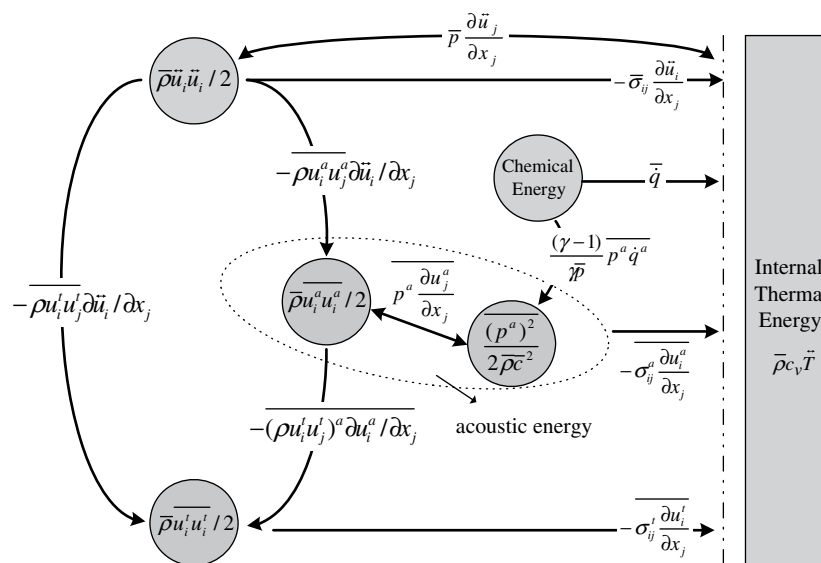
Fig. 46. Diagram of energy exchange among mean, periodic, and stochastic motion in turbulent reacting flows (Huang et al. [244]).

where $\bar{c}$ is the mean sound speed in the chamber. If we consider a cylindrical combustion chamber with a closed boundary, by using the method of separation of variables, a general solution to Eq. (5.10) can be written as:

$$p' = \sum_{l,m,n} A_{lmn} J_m(k_{rmn}r)\cos(m\theta + \gamma_{lmn})\cos(k_{zl}z)e^{j\omega_{lmn}t} \qquad (5.11)$$

where l, m, and n are integers; J_m is the Bessel function of the first kind of order m; $k_{zl}L = l\pi$, where L is chamber length; $k_{rmn}R = j'_{mn}$, j'_{mn} is the nth extremum of the mth Bessel function of the first kind; and R is the chamber radius. The permitted radian frequencies are determined from:

$$\omega_{lmn} = \bar{c}\left(k_{rmn}^2 + k_{zl}^2\right)^{1/2} \qquad (5.12)$$

The terms in Eq. (5.12) with $m = n = 0$, $l \neq 0$ describe longitudinal modes; those with $l = m = 0$, $n \neq 0$ correspond to radial modes; and those with $l = n = 0$, $m \neq 0$ represent tangential (azimuthal) modes.

The estimated frequencies of oscillations obtained from the above classical acoustics analysis commonly lie within 10–15% or less of the frequencies observed in experiments for combustion instabilities (Culick [251]). It is precisely the departure, however, from classical acoustics that defines the class of problems we call combustion instabilities. According to Culick, there are three main reasons that the classical view of acoustics is a good first approximation to wave propagation in the combustion chamber. First, the Mach number of the mean flow is usually so low that convective and refractive effects are small. Second, if the exhaust nozzle is choked, the incident waves are efficiently reflected, and the exit plane can be regarded as a rigid surface, acoustically. Third, in the limit of small-amplitude disturbances, the unsteady motion in the compressible flow can be decomposed into three independent modes of propagation: acoustic, vortical and entropy waves. Even in the highly turbulent non-uniform flow usually present in a combustion chamber, acoustic waves behave according to their own simple classical laws. The role of the classical linear acoustic analysis should not, however, be exaggerated. It cannot decide which modes of acoustic oscillations will be excited, nor is it able to predict the amplitude of the excited modes. These are determined by the flow and combustion conditions in the chamber, and can be approached using the framework discussed in Section 7.2.

5.3. Flame surface variation

For a gas-fueled premixed flame, the heat release per unit volume can be expressed as:

$$\dot{Q} = q\rho S_L A \qquad (5.13)$$

where S_L is the flame speed, A the flame surface area per unit volume, ρ the density of unburnt gas, and q the heat of reaction per unit mass. Assuming that all properties except the flame surface area are constant, the fluctuation of the heat release rate is proportional to the variation in the flame surface area

$$\dot{Q}' \sim A' \qquad (5.14)$$

Usually, an idealized planar configuration does not exist for practical flames. Depending on flow conditions, a laminar flame may become unstable and wrinkle under intrinsic flame instabilities, resulting in an enhanced flame front area and ultimately leading to transition to turbulent of combustion. These intrinsic instabilities, including the Darrieus–Landau instability (Landau [252]) and thermal-diffusive instabilities (Sivashinsky [253]), have been extensively studied in the past (Clavin [254], Buckmaster [255], Law and Sung [256]). In a turbulent flow, one complicating

feature of the topology of a flame surface is that it becomes wrinkled over a wide range of length scales. Wrinkling, whether it is caused by small-scale turbulent eddies or large-scale coherent structures, may make significant contributions to the overall flame surface area and reaction rate.

The interactions between flame and acoustic motions have been investigated theoretically by a number of researchers. Marble and Candel [257] studied the flame response to acoustic waves in a two-dimensional duct. The work was based on an integral formulation within which the conservation equations are integrated with respect to the vertical coordinate. The flowfield was decomposed into a flow of reactants and a region of combustion products, separated by an infinitesimally thin flame sheet anchored by a point flame holder. The oscillatory flow properties in the unburnt and burnt regions were matched at the flame sheet by taking into account the kinematic and conservation relations, to determine the system dynamics under the effects of longitudinal flow oscillations. Results indicate that the flame acts as a damper for disturbances arising downstream. The trend, however, is reversed for disturbances arising upstream in a certain frequency range. The frequency spectrum of the acoustic reflection coefficient at the flame front can be expressed with a Strouhal number, defined as $\omega L/u_0$, with ω being the radian frequency of oscillation, L the flame length, and u_0 the flow velocity upstream of the flame zone. The same approach was followed in similar studies by Subbaiah [258] and Poinsot and Candel [259]. It was also extended by Yang and Culick [260] to investigate the combustion instability in a ramjet engine with a coaxial dump combustor. The model accommodates gas-compressibility effects, mean flow gradients, and the recirculating flow behind the dump plane.

Fleifil et al. [261] proposed an analytical model to examine a conical laminar flame stabilized on the rim of a cylindrical duct with a uniform distribution of acoustic velocity along the flame axis. The formulation was derived based on a linearized equation for flame surface evolution. The flame dynamics were found to be governed by two parameters: a reduced frequency normalized by the flame speed and the duct radius, $\omega R/S_L$, and the ratio of the flame speed to the mean flow velocity, $S_L/\bar{u}$. The flame was found to behave like a high-pass filter, in the sense that high-frequency oscillations pass through the flame without significantly affecting the heat release rate, although the flame surface becomes wrinkled when the reduced frequency exceeds a critical value. Low-frequency oscillations, on the other hand, exert a strong influence on the heat release fluctuation. The transfer function between the heat release and impressed velocity fluctuations is unity in the limit of zero frequency, and decreases with increasing frequency. The approach of Fleifil et al. [261] was later extended by Dowling [262] to model the unsteady behavior of a ducted flame stabilized by a centerbody. Turbulent flames were modeled by simply replacing the laminar flame speed in the formulation with its turbulent counterpart. This analysis took account of the effect of mixture-composition variation, which dominates the overall flame response at fuel-lean conditions through the influence on the flame speed. For linear fluctuations, the modeled transfer function between heat release and velocity was found to agree with the experimental data from Bloxsidge et al. [263]. Similar studies were also reported by Ducruix et al. [264], Schuller et al. [265], Mehta et al. [266], and You et al. [267]. Lieuwen [268] recently reviewed the literature on the interactions between acoustic waves and premixed combustion processes.

The influence of flame surface area variations on instabilities was demonstrated experimentally by Santavicca and his co-workers [222,200,269] in a lean-premixed dump combustor operating with natural gas. OH PLIF images were used to characterize the flame area changes during unstable combustion. To determine

the flame shape, the images were corrected for shot-to-shot laser energy variations, background noise, and laser sheet non-uniformity. Since there is a significant increase in OH concentration at the leading edge of the flame front, the flame front location can be identified by applying a threshold to corrected images. Fig. 47 shows a sequence of flame fronts obtained from single-shot images over one period of a 378-Hz instability. The interactions between the flame front and turbulence and the resultant wrinkling and elongations of the flame surface are clearly observed. An average flame area at several phase angles of instability was calculated using five single-shot OH PLIF images. The resulting flame surface-area versus phase angle over one period of the instability is plotted in Fig. 48. The measured overall heat release fluctuation (characterized by the overall CO_2^* chemiluminescence intensity fluctuation) is also plotted for comparison. The flame surface-area fluctuation is almost in phase with the pressure oscillation, demonstrating the significance role of the flame surface-area change in this kind of instability. Measurements of flame surface area were also performed by Reuter et al. [270] using a phase-locked shadow photography technique. A cyclic variation in the flame surface area and heat release was observed due to periodic vortex shedding.

5.4. Equivalence ratio fluctuation

The influence of equivalence ratio oscillations on combustion instability has been widely recognized. Equivalence ratio oscillation is one of the major sources of heat release fluctuations, especially at lean conditions. One explanation for the susceptibility of lean-premixed combustion to instabilities can be given in terms of the relationship between equivalence ratio and chemical reaction time. The experimental data obtained by Zukoski [271], shown in Fig. 49, indicates that the gradient of chemical reaction time with respect to equivalence ratio, $\partial\tau_{chem}/\partial\phi$, increases significantly as the flame gets leaner. Since the chemical reaction time is inversely proportional to the reaction rate, a small variation in ϕ can create large fluctuations in the reaction rate at lean conditions, as compared to the stoichiometric condition. Consequently, pressure oscillations tend to grow strongly in amplitude when the fluctuations in the chemical heat release are coupled with the acoustics of the
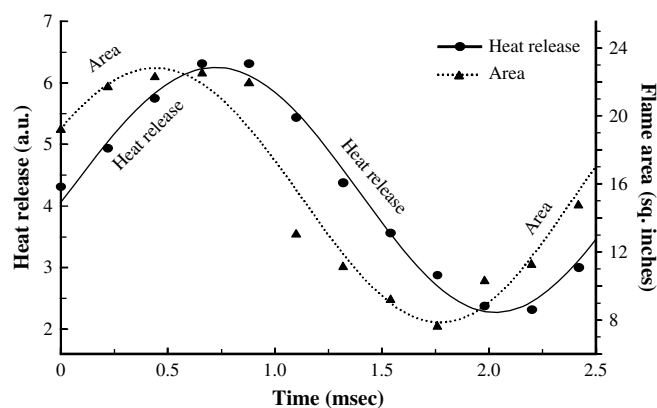
Fig. 48. Temporal variation of flame surface area and heat release during one period of instability oscillation (Lee and Santavicca [269]).

combustion system. The high sensitivity of the reaction rate to equivalence ratio oscillations at lean conditions was demonstrated by Lieuwen et al. [272] in an unsteady well-stirred reactor (WSR) model. Fig. 50 shows the response of the WSR reaction rate to the inlet equivalence ratio fluctuation. The magnitudes of the reaction rate fluctuation and consequently the heat release oscillation increase significantly as the equivalence ratio decreases under lean conditions.

Fluctuations in equivalence ratio may arise either from the unmixedness of fuel and air, or from the fluctuations of fuel and air mass flow rates at the fuel injection point. The former is due to the limited space and time available for proper mixing in the injection system. Although incomplete mixing may broaden the range of unstable combustion (Shih et al. [224], Seo [196]), variations in the fuel/air mixture entering the flame zone are regarded as one of the major root causes of combustion instability (Richards and Janus [273], Richards et al. [274], Lieuwen and Zinn [235] and Liewwen et al. [236]). This mechanism is illustrated in Fig. 51. Acoustic waves, originating from the combustion chamber, travel upstream and modulate the fuel and air mass flows in the injectors, which in turn produce a local equivalence ratio oscillation. The resultant disturbance is convected downstream into the combustion zone, leading
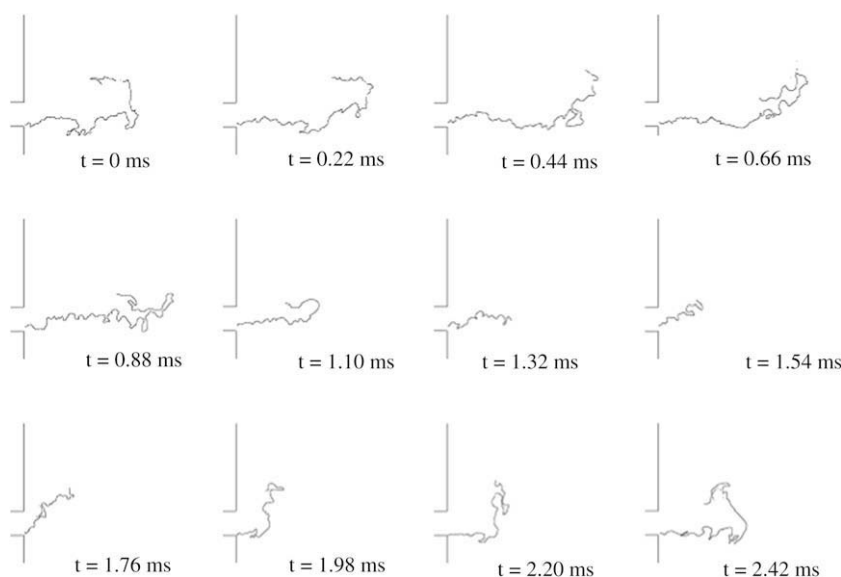
Fig. 47. Evolution of flame surface over one period of instability oscillations (Lee and Santavicca [269]).
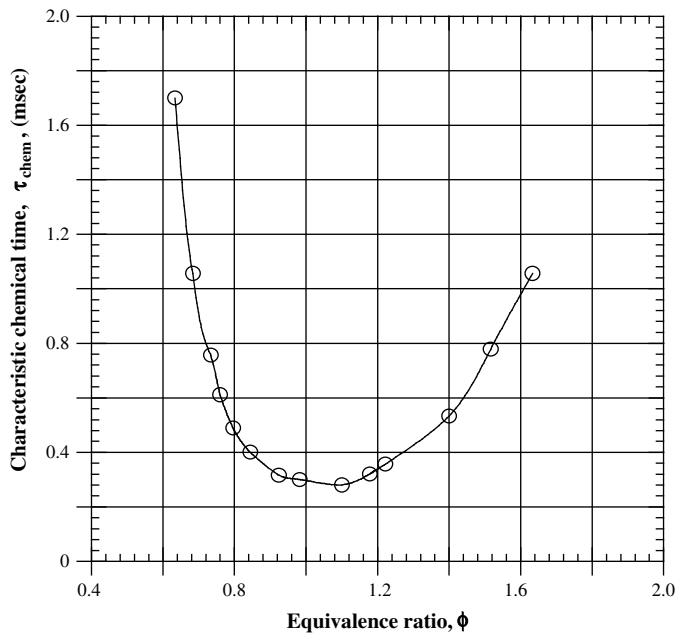
Fig. 49. Experimentally obtained chemical reaction time as a function of the equivalence ratio of a hydrocarbon fuel with a molecular weight of about 100 (Zukoski [271]).

to pulsating heat release. A feedback loop between heat release and acoustic waves thus forms and drives oscillatory combustion.

Following the approaches of You et al. [267], a simple theoretical analysis is used here to demonstrate how the fuel or air mass flow rate produces equivalence ratio oscillations, and how combustion instabilities are excited by this mechanism in lean-premixed combustion systems. This model extends the basic idea of the time lag theory first developed by Crocco and Cheng [187] through careful consideration of acoustic boundary conditions and effects of fuel feedline. Similar analyses were also given by Richards and his colleagues [273,274] and Lieuwen and his colleagues [235,236]. Consider a typical mixer in which fuel is injected from the center-body spokes and mixed with the incoming air in an inlet annulus, as
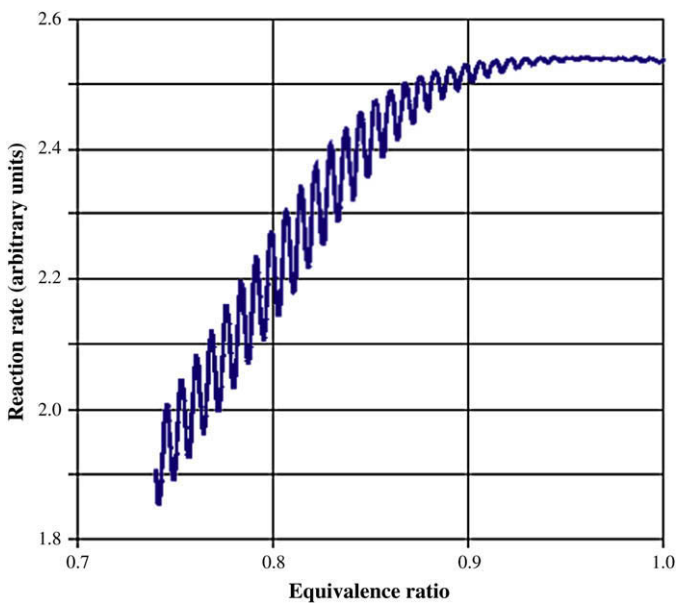
Fig. 50. Response of reaction rate to inlet equivalence ratio perturbations in a well-stirred reactor (Lieuwen et al. [272]).

shown in Fig. 52. A linear expression for the equivalence ratio ϕ fluctuation can be derived from its definition,

$$\frac{\phi'}{\overline{\phi}} = \frac{\dot{m}'_{fuel}}{\overline{\dot{m}}_{fuel}} - \frac{\dot{m}'_{air}}{\overline{\dot{m}}_{air}} \tag{5.15}$$

For a choked fuel injector, $\dot{m}'_{fuel} = 0$. Substitution of the air mass flow rate $\dot{m}_{air} = \rho u A_{in}$ into Eq. (5.15) yields

$$\frac{\phi'}{\overline{\phi}} = -\left(\frac{u'}{\overline{u}} + \frac{\rho'}{\overline{\rho}}\right) \tag{5.16}$$

Since the mixture convected from the fuel injector plane will burn in the flame zone after a time delay τ_{conv} from its injection, a relationship can be established between the flame location and such a time lag (Fung et al. [275]).

$$\xi + L_{in} = \int_{t}^{t+\tau_{conv}} u(t,\tau)\mathrm{d}\tau \tag{5.17}$$

where L_{in} measures the distance from the injector to the base of the flame holder. The integral is evaluated following the motion of the mixture element injected at t, and $u(t,\tau)$ is the velocity of the mixture element injected at t after an interval τ. Accordingly, the equivalence ratio oscillation at the flame front for a time-harmonic disturbance becomes

$$\left[\frac{\phi'}{\overline{\phi}}\right]_f = -\left[\frac{u'}{\overline{u}} + \frac{\rho'}{\overline{\rho}}\right]_{in} \exp(-i\Omega\tau_{conv}) \tag{5.18}$$

where the subscripts f and in represent variables evaluated at the flame front and injector, respectively. Although turbulent diffusion tends to homogenize the mixture as it flows downstream, this process is neglected here to simplify the formulation. In the limiting case with a constant flow velocity (i.e., $u(t,\tau) = \overline{u}$), a simple expression for the convective time delay is obtained as $\tau_{conv} = (L_{in} + \overline{\xi})/\overline{u}$.
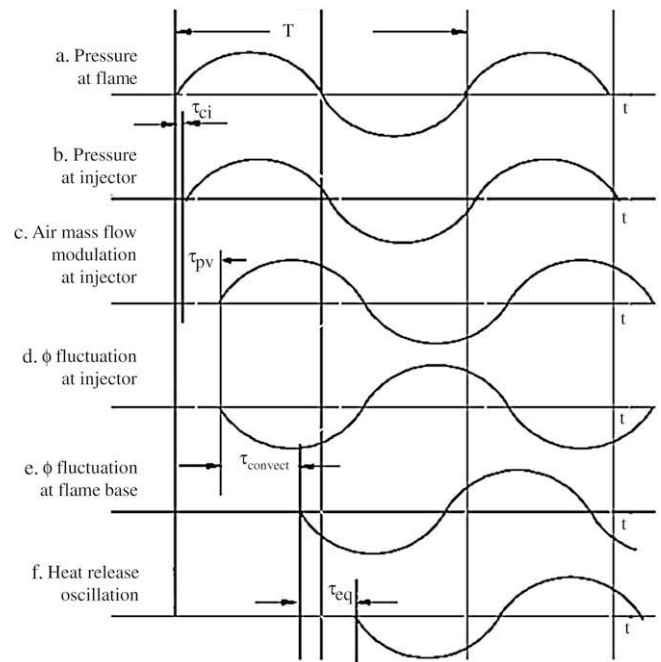
Fig. 51. Schematic drawing of the time evolutions of perturbations responsible for driving combustion instabilities (Lieuwen et al. [272]).
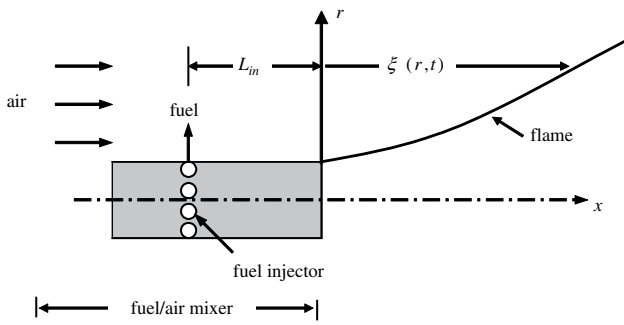
Fig. 52. Schematic of fuel/air mixer and flame displacement (You et al. [267]).

For longitudinal acoustic waves, a flow disturbance of frequency $\Omega = 2\pi/T$ at the flame front can be related to that at the injector plane with a phase difference. If the mean flow Mach number is small, the relationship becomes

$$\left.\frac{u'}{\overline{a}}\right|_f = \left.\frac{u'}{\overline{a}}\right|_{in} \exp[-i\Omega(L_{in} + \overline{\xi})/\overline{a}] \qquad (5.19)$$

where $\overline{a}$ is the speed of sound. Since the acoustic phase difference $\Omega(L_{in} + \overline{\xi})/\overline{a}$ is much smaller than that associated with flow convection, $\Omega\tau_{conv}$, the equivalence ratio fluctuation can be derived by substituting Eq. (5.19) into (5.18).

$$\left.\frac{\phi'}{\overline{\phi}}\right|_f = \left[-\left.\frac{u'}{\overline{u}}\right|_f \left(\frac{\overline{M}_f}{\overline{M}_{in}}\right) - \left.\frac{p'}{\gamma\overline{p}}\right|_f\right] \exp(-i\Omega\tau_{conv}) \qquad (5.20)$$

On the conditions that the mean flow Mach number is small (which means that the second term on the right hand side of Eq. (5.20) is small compared to the first term and can be ignored), and the difference between the Mach number at the flame front $\overline{M}_f$ and the fuel injector $\overline{M}_{in}$ is also insignificant, we have

$$\left.\frac{\phi'}{\overline{\phi}}\right|_f = -\left.\frac{u'}{\overline{u}}\right|_f \exp(-i\Omega\tau_{conv}) \qquad (5.21)$$

If we further assume that the upstream boundary is a pressure node, that is, the velocity leads the pressure by 90 degrees, and the total heat release lags the equivalence ratio oscillation at the flame by a time of chemical reaction delay, τ_{chem}, then the following expression can be used to describe the relations between the heat release and pressure oscillations:

$$\left.\frac{q'}{\overline{q}}\right|_f \sim \frac{1}{\overline{M}_f} \frac{p'}{\gamma\overline{p}} \exp(-i\Omega(\tau_{conv} + \tau_{chem} + T/4)) \qquad (5.22)$$

It follows from Rayleigh's criterion that an instability may occur if

$$(\tau_{conv} + \tau_{chem}) \cdot f = n - 1/4 \quad n = 1, 2\dots \qquad (5.23)$$

Similar results can be obtained using different upstream inlet boundary conditions or employing fuel flow modulation at the injectors, but the corresponding instability conditions change accordingly (Lieuwen et al. [236]). The equivalence ratio time lag type theories have been incorporated into stability analysis of LPM gas turbine combustors by a number of researchers [196,235–238,273,274,276,277]. Lieuwen et al. [236] analyzed the experimental data for several combustors. Fig. 53 shows the measured pressure amplitudes and predicted instability regions as a function of convective time lag τ_{conv} and instability frequency for a typical setup. Most of the large-amplitude pressure oscillations fall in the predicted region.

5.5. Vortex shedding due to hydrodynamic instability

In gas turbine and many other types of combustors, strong shear layers are often formed downstream of fuel injectors and flame holders. Such transitional shear layers are usually characterized by large-scale coherent structures or vortices. The recognition of vortex shedding as a possible mechanism for driving combustion instabilities was first independently reported by Kaskan and Noreen [278] and by Rogers and Marble [279], as pointed out by Culick [11]. In particular, Rogers and Marble [279] provided an explanation of how this mechanism generates self-excited combustion oscillations through a closed-loop process in ramjet combustors. Fresh mixture is entrained by vortical structures, and ignition takes place after a certain characteristic time. Delayed periodic combustion in shed vortices causes periodic acoustic oscillations. The fluctuating velocity of the acoustic field interacts with shear layers and closes the loop. Since those seminal studies, a great deal of attention, both experimental and numerical, has been given to the influence of hydrodynamic instabilities on combustion instabilities [76,222,280–293].

Zukoski and his colleagues [280,281] investigated the excitation of longitudinal combustion instabilities in a two-dimensional dump combustor. The oscillatory combustion was observed to be associated with the shedding of large-scale vortical structures from the flame holder. Poinsot et al. [282] investigated low-frequency combustion instabilities in a multiple inlet dump combustor. Vortex motions and flame evolution were examined using spark-schlieren and phase-averaged images of C_2 emission. Results indicated that certain longitudinal instabilities are vortex driven and the occurrence of vortex shedding is in phase with the acoustic velocity fluctuation. Hegde et al. [283] studied interactions between wedge-shaped flame and longitudinal acoustic motions in a coaxial, dump-type combustor. In the flame region, burning vortical structures appear at the first natural frequency of the setup. Kailasanath et al. [285,286] and Najm and Ghoniem [287,288] also numerically examined the interactions between vorticity and pressure oscillations in dump combustors.

In a review, Schadow and Gutmark [284] summarized experimental results in a variety of dump combustors and bluff-body flame holder geometries, with emphasis placed on combustion instabilities associated with vortex shedding. The authors consistently interpreted distinct frequencies found in the experiments in terms of vortex shedding dynamics, and carefully examined the interactions between acoustic waves and shear layer instabilities. The shear layer is usually characterized by several instability frequencies associated with different sizes of vortices. When acoustic waves
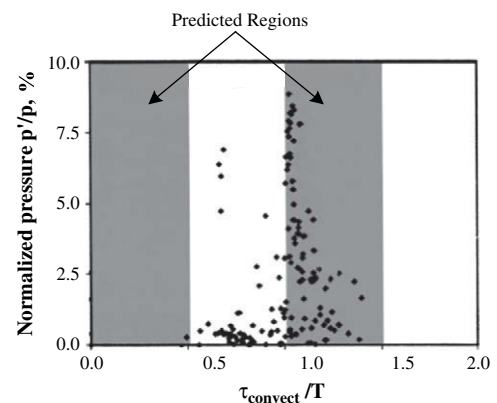
Fig. 53. Pressure amplitudes measured in a lean-premixed combustor and predicted instability regions as function of convective time lag and instability frequency (Liuwen et al. [236]).

interact with the shear layer, the stabilization of the vortex size depends on the match between acoustic and shear layer instability frequencies. The vortices are smallest when the acoustic frequency equals the initial vortex shedding frequency (most amplified mode). The vortices attain their largest size when the acoustic frequency is near the preferred-mode frequency (jet-column mode). In non-reacting flow tests, the acoustic emission of vortices is low. There is no obvious feedback between the flow and acoustic pressure in the chamber. In reacting flows, however, the periodic heat release from the combustion inside the vortices provides the missing link for the necessary feedback loop. Thus, the evolution of coherent flow structures leads to periodic heat release, which, when in phase with the pressure oscillation, can drive the instabilities as stated by the Rayleigh criterion. Recent overviews on shear-flow-instability driven combustion oscillations can be found in Refs. [250,289].

Most of the studies cited above have focused on flow-instability-driven combustion dynamics in dump combustors without swirl, but similar mechanisms can be found in swirl combustors [222,291–294]. Paschereit et al. [293,294] investigated the coupling between coherent structures and acoustic motions in a premixed swirl-stabilized combustor. Both axisymmetric and helical unstable acoustic modes were identified. These unstable modes were associated with hydrodynamic instabilities in the recirculation wake-like region near the combustor axis, and in the shear layer region behind the sudden expansion after the dump plane. The axisymmetric mode induces a large variation in heat release over one cycle, while the helical mode gives rise to variation in the radial location of the maximal heat release. Venkataraman et al. [222] conducted a study of unstable combustion in a lean-premixed swirl combustor. Periodic shedding of vortices from the dump plane and their interaction with the flames were observed.

5.6. Oscillatory liquid fuel atomization and droplet evaporation

Interactions between the liquid fuel spray and oscillatory flowfield in a fuel injection system may result in periodic atomization, vaporization, and mixing, which leads to periodic variation of equivalence ratio. The process in turn produces heat release fluctuation. A number of studies [11,295–307] dealing with the role of atomization and spray vaporization on combustion instability have been conducted on liquid-fueled propulsion systems.

Sirignano [295] and Tong and Sirignano [296] considered the effect of droplet thermal inertia on combustion instability using a one-dimensional droplet vaporization model in a liquid fuel combustor. The responses of the vaporizing droplet to the oscillating ambient pressure and velocity were examined in both standing and traveling waves. Droplets were continuously injected through the oscillation cycle, and the behavior of each droplet was calculated. Individual droplet vaporization rates were combined to give the total vaporization rate of a spray. To determine whether vaporization is capable of driving instability, a response factor

$$G = \int_0^{2\pi} \dot{m}' p' \mathrm{d}\theta / \int_0^{2\pi} (p')^2 \mathrm{d}\theta \qquad (5.24)$$

was introduced, as suggested by the Rayleigh criterion. Here $\dot{m}'$ is the total vaporization rate oscillation, p' pressure fluctuation, and θ phase angle between $\dot{m}'$ and p'. It was assumed that vaporization is the rate-controlling process, and mixing and chemical reactions are very rapid, so that the combustion response can be approximated by the vaporization response. The results indicated that the gain or response function associated with the oscillatory vaporization rate that is in phase with the pressure oscillation is sufficiently large to sustain instability in certain frequency domains. This work was later extended by Sirignano, Chiang, and their colleagues [297–301]

using more advanced vaporization models. Duvvur et al. [301] employed an axisymmetric convective droplet model in their study of combustion instabilities. Similarly, droplet vaporization as a rate-controlling factor can allow the chemical energy conversion to be in phase with the pressure fluctuation, and consequently to drive acoustic oscillations. The frequency of the oscillation is a key parameter determining the fraction of the total energy that is in phase with the pressure oscillation.

In the analysis mentioned above, atomization was assumed to occur instantaneously, and the vaporization process was taken to be the rate-limiting step in spray combustion. Anderson et al. [303], on the other hand, studied the effect of periodic atomization on combustion instability, both theoretically and experimentally, in a liquid-propellant rocket engine. An atomization model was developed and incorporated into the calculation of the combustion response factor G in Eq. (5.24). The analysis indicated that when atomization occurred continuously, a wider distribution of droplet sizes reduced the response magnitude, and a mono-dispersed size distribution gave the highest magnitude. In both cases, the calculated response factor was lower than the theoretical limit for driving instabilities. When atomization occurred periodically, a large increase in the response factor was observed about an order of magnitude greater then its counterpart for the continuous atomization case. The resultant response factor far exceeded the theoretical limit for driving instabilities. Experiments were also conducted to determine the conditions under which periodic atomization could cause longitudinal mode combustion instabilities in a model combustor using gaseous oxygen and liquid ethanol as propellants. An electromechanical modulation technique was used to control the atomization frequency. Pressure oscillations at frequencies corresponding to the first- through third-longitudinal modes were observed under certain forced atomization frequencies, which further demonstrated that atomization is a key mechanism in driving combustion instabilities.

Conrad et al. [306,307] recently developed a "smart" liquid fuel injector for instability abatement by modulation of spray properties. The underlying concept is that instabilities usually depend on the relative magnitudes of the acoustic and combustion time scales. The injector attempts to modify the liquid fuel burning time by controlling the spray characteristics, thus reducing the coupling between acoustics and combustion. The onset of detrimental combustion instabilities could be effectively prevented using fuel sprays with desired properties in a specific combustor.

6. Instability suppression methods

The essential reason for the presence of instabilities in a combustion system is the existence of an internal feedback loop, such that energy may be transferred to a fluctuation at a rate dependent on the fluctuation itself. To eliminate combustion oscillations, the coupling between acoustic waves and unsteady heat release must be interrupted. Two types of instability mitigation approaches have been proposed: passive and active control techniques. Passive control involves changes of fuel or hardware designs (for example, in the composition or types of reactants, fuel injection devices and chamber geometry, or the installation of acoustic dampers), either to reduce the rate at which energy is transferred to unsteady motions, or to increase losses of energy, such as by the use of suitable resonators to introduce a dissipative process.

In contrast to passive control, the term 'active control' implies control of a system involving expenditure of energy from a source external to the system. Generally, the purpose is to minimize the difference or 'error' between the instantaneous desired and actual behavior of the system. Active control may involve sensing the

instabilities and then using a feedback control loop to modify one or more input parameters, which consequently interrupts the coupling between unsteady heat release and acoustic waves. The field of active control of combustion is concerned both with control of dynamics, notably combustion instabilities, and with various issues associated with steady-state operation, for example, optimization of combustion distribution and emission characteristics. Both passive and active control techniques have been successfully applied in instability control in many combustion systems. What may be possible, or what actually happens in a particular case, can be established only by understanding the system in question (Schadow et al. [308], Yang et al. [309])

6.1. Passive control of combustion instability

6.1.1. Acoustic dampers: Helmholtz resonators and quarter-wave tubes

Suppression of combustion instabilities by means of acoustic damping has been commonly employed in various propulsion systems, including rockets, gas turbines, and afterburners. Perhaps the simplest acoustic damper is a hole (Putnam [13], Richards et al. [310]). The usage of holes to eliminate combustion oscillation in industrial burners is described by Putnam [13] in a humorous manner: "*To solve an oscillating combustion problem, drill a hole. If that doesn't work, drill two holes.*" As stated in the Introduction (Section 1), in a conventional diffusion system, numerous dilution holes are utilized to provide cooling air for combustor liners, as well as acoustic damping. In a premixed gas turbine combustor, however, flow splits must be accurately controlled to meet performance targets, and drilling holes is not an acceptable control strategy. This substantially reduces acoustic damping in premixed systems. Two types of acoustic dampers with closed resonators have been employed in premixed gas turbine combustors: Helmholtz resonators and acoustic slots (also referred to as quarter-wave tubes). When pressure oscillations occur, flow enters and exits the resonator mouth. The energy may dissipate at the entrance, providing damping to the system. The installation of an acoustic damper also provides a jump in the acoustic impedance of the combustor liner and subsequently modifies the boundary conditions in such a way that certain discrete oscillations are attenuated and therefore become less destructive to the combustor.

6.1.1.1. Analytical model of acoustic resonator.
A Helmholtz resonator consists of a large cavity and a short neck through which the fluid inside the resonator interacts with the fluid in the combustion chamber, as shown in Fig. 54. The geometric parameters: cavity volume V, cross-sectional area of the neck S and neck length l, are selected to dissipate the acoustic energy of the combustor flow at desired frequencies.

At the open end of the resonator neck, there is a pressure disturbance p'_1, which generates a mass flow into the resonator at a volumetric rate:

$$Q = V\frac{d\rho_2}{dt} \tag{6.1}$$

Here the volume of the neck is neglected. The subscript 2 denotes the flow conditions in the cavity. The fluid density inside the resonator ρ_2 changes due to the mass flow through the neck. If we assume time-harmonic motion, and let $\rho'_2 = \hat{\rho}_2 e^{i\omega t}$, then we have

$$\rho'_2 = \frac{Q}{Vi\omega} \tag{6.2}$$

Also, $Q = \rho_1 u'S$, thus, $u' = Q/\rho_1 S$. Since u' is also a time harmonic function, its time derivative becomes
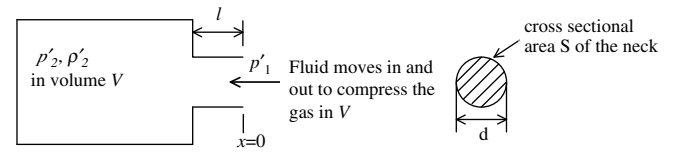
Fig. 54. Schematic diagram of a Helmholtz resonator.

$$\frac{du'}{dt} = \frac{Q}{\rho_1 S}i\omega \tag{6.3}$$

Note that $u' = u'_1 = u'_2$ for an acoustically compact neck.

For an isentropic process, the pressure fluctuation inside the resonator can be related to the density fluctuation as follows.

$$p'_2 = a_2^2\rho'_2 = a_2^2\frac{Q}{Vi\omega} \tag{6.4}$$

where a_2 is the speed of sound in the cavity. If convection and viscous force are neglected, the equation of motion for the fluid mass in the neck becomes

$$p'_1 - p'_2 = \rho_1 l\frac{du'}{dt} \tag{6.5}$$

Substitution of Eqs. (6.3) and (6.4) into Eq. (6.5) and rearrangement of the result yields

$$p'_1 = p'_2 + \rho_1 l\frac{du}{dt} = a_2^2\frac{Q}{Vi\omega} + \rho_1 l\frac{Q}{\rho_1 S}i\omega = \left(\omega^2 - \frac{a_2^2 S}{Vl}\right)\frac{ilQ}{\omega S} \tag{6.6}$$

Thus, the natural frequency of the resonator is

$$\omega_0 = a_2\sqrt{\frac{S}{Vl}} \tag{6.7}$$

At this particular frequency, a small pressure disturbance leads to a large mass fluctuation in the resonator.

The acoustic behavior of a Helmholtz resonator, especially its absorption effect, can be characterized by the impedance Z at the entrance, defined as follows

$$Z = \left.\frac{p'_1}{u'_1}\right|_{x=0} = R + i\chi \tag{6.8}$$

where p'_1 represents the acoustic pressure at the orifice, $x = 0$, as shown in Fig. 54. The impedance is usually a complex variable, and its real and imaginary parts are referred to as acoustic resistance R and reactance χ, respectively.

Consider the resonator as a mass-spring-damper system described by the following equation

$$m\frac{d^2x}{dt^2} + R_D\frac{dx}{dt} + kx = F_d \tag{6.9}$$

where m is the total effective mass of the neck-flow, x the displacement of the mass, R_D the mechanical resistance of the system, and k the stiffness coefficient. The second term on the left hand side of Eq. (6.9) represents the viscous damping of the fluid motion in the neck, yet to be determined. F_d is the specific driving force acting on the neck-flow mass: $F_d/m = p'_1 S/m$.

Equation (6.9) may be recast as follows.

$$\frac{d^2x}{dt^2} + 2\zeta\omega_0\frac{dx}{dt} + \omega_0^2 x = \frac{p'_1 S}{m} \tag{6.10}$$

Comparison of Eqs. (6.9) and (6.10) shows that the natural frequency $\omega_0 = \sqrt{k/m}$ and the damping coefficient $\zeta = R_D/2\omega_0 m$.

Now take the time derivative of Eq. (6.10) to obtain

$$\frac{d^2 u'}{dt^2} + 2\zeta\omega_0 \frac{du'}{dt} + \omega_0^2 u' = \frac{d}{dt}\left(\frac{p_1' S}{m}\right) \qquad (6.11)$$

Note that $dx/dt = u' = u_1' = u_2'$ for an acoustically compact neck. For harmonic oscillations,

$$p_1' = \hat{p}e^{i\omega t}; \quad u' = \hat{u}e^{i\omega t} \qquad (6.12)$$

Substitute Eq. (6.12) into Eq. (6.11) and combine the result with Eq. (6.8) to obtain an explicit expression of the acoustic impedance at the neck entrance, $x = 0$.

$$Z = 2\zeta\omega_0\rho l + i\frac{(\omega^2 - \omega_0^2)\rho l}{\omega} \qquad (6.13)$$

Thus, the acoustic resistance R and acoustic reactance χ are

$$R = R_D\rho l/m \quad and \quad \chi = 2\pi f\rho l\left[1 - \frac{f_0^2}{f^2}\right] \qquad (6.14)$$

Once the acoustic impedance is known, the absorption coefficient α which is defined as the fraction of the incident wave intensity absorbed by the resonator, can be evaluated. We consider a one-dimensional acoustic field in the combustion chamber. The acoustic pressure and velocity fields can be expressed as follows.

$$p_c' = P_i e^{i(\omega t - kx)} + P_r e^{i(\omega t + kx)} \qquad (6.15)$$

$$u_c'\rho_c a_c = P_i e^{i(\omega t - kx)} - P_r e^{i(\omega t + kx)} \qquad (6.16)$$

where the subscript c stands for the combustion chamber. The subscripts i and r denote the incident and reflected waves, respectively. The wave number k is defined as $k = \omega/a_c$. P_i and P_r are the amplitudes of the incident and reflective traveling waves, respectively, and can be expressed in terms of the acoustic fluctuations at the resonator/chamber interface, $x = 0$.

$$P_i = \left(\frac{p_c' + u_c'\rho_c a_c}{2}\right)_{x=0}, \quad P_r = \left(\frac{p_c' - u_c'\rho_c a_c}{2}\right)_{x=0} \qquad (6.17)$$

The acoustic intensities of the incident and reflective waves become

$$I_r = \frac{|P_r|^2}{\rho_c a_c} \quad and \quad I_i = \frac{|P_i|^2}{\rho_c a_c} \qquad (6.18)$$

The acoustic absorption coefficient α becomes

$$\alpha = 1 - \frac{I_r}{I_i} = 1 - \frac{|P_r|^2}{|P_i|^2} \qquad (6.19)$$

Substitution of Eq. (6.17) into Eq. (6.19) gives

$$\alpha = \frac{4R\rho_c a_c}{(R + \rho_c a_c)^2 + \chi^2} \qquad (6.20)$$

For a fixed acoustic resistance R, the fraction of the incident wave intensity absorbed by the resonator reaches its maximum when the acoustic reactance χ is set to zero, i.e., the frequency of the incident wave is equal to the natural frequency of the resonator. Thus, the dissipation of acoustic energy can be maximized by tuning the resonator geometric parameters in such a manner that the natural frequency matches the frequency that is to be damped in the combustor. The maximum value of absorption is determined by the acoustic resistance, which largely relies on the viscous damping of the fluid motion in the neck. Fig. 55 shows photographic images of typical Helmholtz resonators mounted in the

Siemens combustor rig. It should be noted that resonators in practical applications may require a cooling through-flow to avoid overheating, but the use of such cooling through-flow will affect resonator acoustic characteristics. The actual damping performance of a resonator depends not only on its geometry, but also on its location and system operating conditions. A good resonator design is system and configuration specific, and must be tested and finalized by experiments.

The acoustic behavior of acoustic slots (quarter-wave tubes) can be analyzed in a similar manner. A quarter-wave tube is a pipe that is open at the end that connects with the combustor and closed at the other end. The presence of a quarter-wave in the acoustic slot can counteract the acoustic wave in the combustor. In the quarter-wave design, the natural frequency can only be established by length. The damping effect of the acoustic slot depends directly on the slot area and the real part of the slot admittance function.

6.1.1.2. Application to gas turbine combustors. Helmholtz resonators have been employed to suppress combustion instabilities in both annular and can-annular gas turbine combustors (Krebs et al. [44], Lepers et al. [45]). Fig. 56 shows a setup involving fourteen resonators installed on the outer shell of an annular combustor rig to inhibit an observed 200 Hz instability mode. The arrangement of resonators on the circumference was asymmetric, and was carefully tuned to provide optimum damping effects. Two types of resonators, shown in Fig. 55, were examined. The larger resonator produced a substantial improvement of the stability limit of the combustor, while the effect of smaller one was less obvious. Fig. 57 shows the root-mean-square (rms) value of the dynamic pressure as a function of air/fuel ratio (AFR). For the baseline case without resonators, when the fuel mass flow increased up to an AFR of 35, there was a sudden excitation of the acoustic mode at 200 Hz. For the case with the larger resonator, the fuel could be increased up to an AFR of 30.5 before a sudden excitation occurred. In both cases, hysteresis phenomena were observed, and the excited acoustic mode could only be damped if the fuel mass flow was considerably reduced, towards an AFR of 38. This suggests that the installation of larger resonators resulted in a significantly wider stable operation envelope.

Various sizes of resonators were also mounted around the basket of a Siemens can-annular combustor to damp high-frequency instabilities (Krebs et al. [44]). Several resonator tubes were connected in parallel to one big volume in practical configurations, which resulted in a higher acoustic absorption area, and consequently in enhancement of acoustic damping performance.

Fig. 55. Helmholtz resonators mounted in the Siemens annular combustor rig (Krebs et al. [44]).
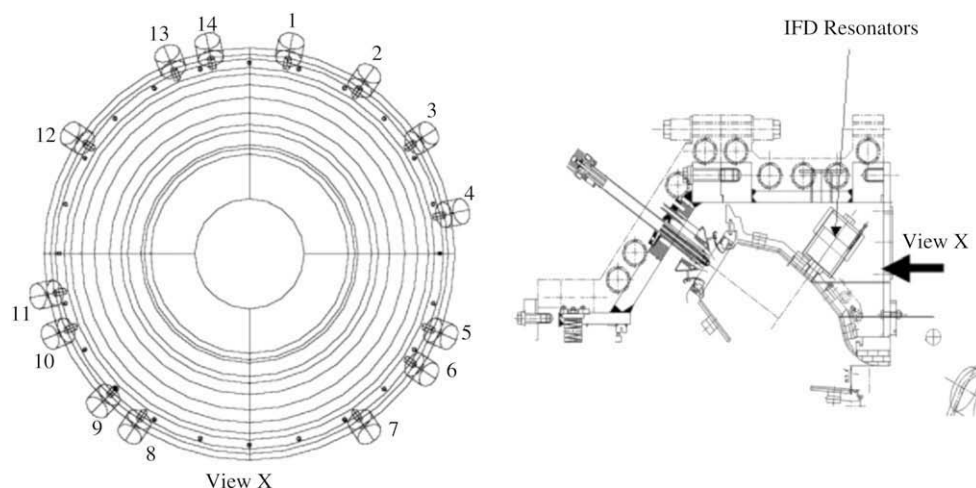
Fig. 56. Annular combustor test-rig (Siemens) with 14 Helmholtz resonators placed circumferentially (Krebs et al. [44]).

To maintain a relatively low resonator temperature, the resonators were purged with compressor discharge air through open holes located at the closed end of the cavity. The purging air requirement must, however, be balanced with the physical dimensions of the resonator and the need for acoustic damping, in practical applications.

Bellucci et al. [72,311] examined the implementation of Helmholtz resonators on an ALSTOM silo gas turbine combustor. Two-throat purged resonators were used. The purging air from the plenum chamber entered the resonator through an inlet tube on the head end of the resonator. The neck communicated directly with the combustion chamber on the other side. A nonlinear model, which accounting for the effects of purging air and the nonlinearity arising from the pressure loss, was established to predict the acoustic response of the resonator. The model parameters were calibrated with atmospheric experiments. A three-dimensional acoustic analysis was then performed to help identify the optimum location of the dampers, using the predicted damper impedance as a boundary condition. As determined by mechanical constraints, seven resonators were installed on the top of the silo combustor. The resonator arrangement so designed widened the low-pulsation operation regime of the gas turbine.

Gysling et al. [312] analytically and experimentally investigated the effects of Helmholtz resonators on acoustic oscillations in a UTRC sector rig combustor. Three resonator configurations were examined. A simplified model for bulk-mode combustor

instabilities coupled with Helmholtz resonators was developed, and was used to determine the influence of system parameters on damping augmentation achievable with resonators. Other applications of Helmholtz resonators to gas turbines have been reported in the literature (Schlein et al. [57], Dupere and Dowling [313], Mastrovito et al. [314]).

Mongia and his co-workers [16,18] reported the application of quarter-wave tubes to absorb combustion-generated noise in GE DLE aero-derivative combustors. A set of damper tubes was installed in the cold section of the combustor just upstream of the premixers, as shown in Fig. 4b. These acoustic dampers, of three different lengths, consisted of 1 inch diameter stainless steel tubes with perforated plates at the end facing the combustor. Each quarter-wave tube length was designed to detune the predominant oscillation frequencies in the combustor by providing a finite number of impedance discontinuities at locations where they are installed. With this approach, the oscillation amplitudes were reduced to a tolerable level for engine operation.

6.1.2. Fuel staging and pilot flame

Control of combustion dynamics can often be achieved by manipulating the way in which the reactive mixtures are introduced into combustor. Several instability abatement methods involving adjustment of fuel flow distribution were reported, including radial and axial fuel staging (Mongia et al. [16], Joshi et al. [22,23], Scarinci et al. [26–28]), asymmetric fuel distribution (James [315]), and pilot fuel (Steele et al. [33], Smith and Blust [34]).

In Trent DLE combustion systems, axial staging of fuel flow distribution is used to control the longitudinal instabilities of the combustor (Scarinci et al. [26,28]). The combustion chamber consists of three premixing channels, which are respectively referred to as the primary, secondary and tertiary premixers, shown in Fig. 3b. At a given power level, the total amount of fuel consumed in the combustor is predetermined. The primary and secondary premixer temperatures can be modulated independently, while the tertiary takes the balance of the total fuel. The ensemble of possible ways to allocate the total fuel among these three premix stages defines an operating envelope, whose coordinates are best defined in terms of premixer temperatures.

In order to characterize the dynamics and emission characteristics of the combustion system with different fuel flow axial distributions, measurements of pressure amplitude and emissions were conducted at a variety of power levels and ambient conditions. Detailed mappings describing the relation between observed
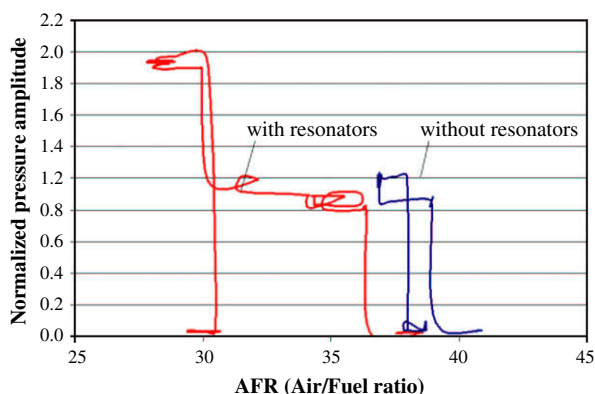
Fig. 57. Operation envelope of Siemens annular combustor test-rig (Krebs et al. [44]).

pressure amplitude and fuel flow distributions were obtained. Fig. 58 illustrates typical results of a measurement at 100% power. The amplitude of pressure fluctuation is strongly affected by the distribution of heat release inside the combustor. It is possible to find regions of high- and low-pressure oscillations in each contour map (Scarinci et al. [26–28]). Empirical correlations were developed based on these measurements to predict the amplitude of unstable modes under a particular condition. The correlations were able to reproduce pressure oscillation results within approximately 10% accuracy, and capture relatively well the effects of engine cycle, ambient conditions and variations in combustor fuel splits. The correlations were then used to design fuel schedules to minimize combustion oscillations for Trent three-stage premix combustors. A similar fuel staging technique was employed for GE radial-staged combustors for instability abatement (Mongia et al. [16], Pandalai and Mongia [18], Joshi et al. [22,23]).

The use of pilot fuel was adopted in the early testing of Solar annular lean-premixed combustors to suppress combustion instabilities (Steele et al. [33], Smith and Blust [34]). The pilot was originally designed to enhance engine light-off, part-load operation and off-load response. Later, it was found that the operation of the pilot injector, even with just a few percent of the total engine fuel flow, was extremely effective at reducing combustion oscillations. Fig. 59 shows the effect of pilot fuel on combustor pressure oscillation and NO$_x$ emissions. With injection of approximately 10% pilot fuel, combustor pressure oscillations could be reduced to well below 1 psi (rms) while NO$_x$ emissions were maintained below 42 ppm. In GE's DLE combustors, the so-called Enhanced Lean Blow-Out (ELBO) pilot fuel, which was originally introduced to enhance lean-blow-out performance of the combustors, was injected through equally spaced holes located at the exit of the premixer (see Fig. 4a) for combustion instability control (Joshi, et al. [23], Pandalai and Mongia [18]).

The strategies of modifying fuel distributions and using pilot fuel must be carefully employed. These strategies tend to deteriorate the emissions performance of the combustor, since they usually move the flame temperatures away from the ideal uniform distribution (Mongia et al. [16]). For example, an increase in pilot fuel flow may suppress pressure oscillation, but jeopardize NO$_x$ emissions, as shown in Fig. 59 for a Solar combustor design [33].

6.1.3. Fuel/air mixing

As suggested in Section 5.4, equivalence ratio fluctuation is one of the driving mechanisms for combustion dynamics. Acoustic
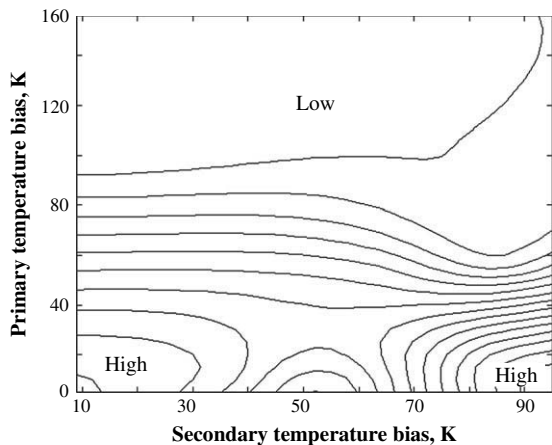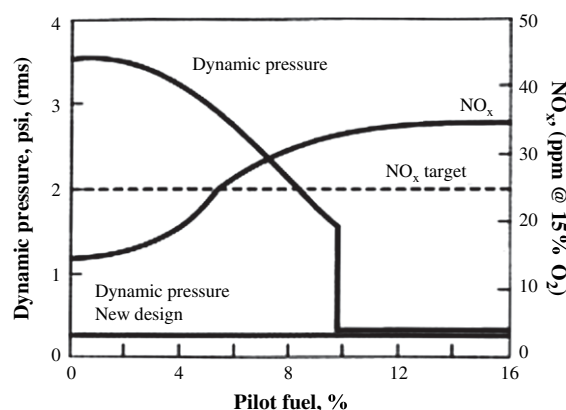
Fig. 59. Effect of pilot fuel on dynamic pressure oscillations and NO$_x$ emissions in a Solar gas turbine system (Steele et al. [33]).

waves from the combustion chamber travel upstream and cause the equivalence ratio of the fuel/air mixture to fluctuate. The resultant mixedness disturbances are convected downstream into the flame zone, which in turn generates heat release pulsations producing pressure oscillations. A feedback loop is then formed. All engine manufacturers have adopted injector modification of some sort to achieve improved fuel/air mixing. For example, Rolls-Royce developed the so-called "fuel–air-ratio (FAR) wave damping" technique for instability control (Scarinci and Halpin [27,28]), as will be discussed below.

To eliminate fuel–air ratio oscillations, several candidate injector configurations, as shown in Fig. 60, were examined in experimental tests (Scarinci and Halpin [27,28]). Configuration A, which has only one fuel injection location in the longitudinal direction, was treated as the baseline case. In design B, a second fuel injection point was added, and the fuel flow was equally divided between these two points. The latter geometrical arrangement was a first logical attempt to eliminate the equivalence ratio oscillation at a given frequency based on the "wave-cancellation" concept. In configuration C, fuel was split between more than two injection locations to widen the frequency range of configuration B. In this design, there are $N(N > 2)$ equally spread locations of fuel injection. Equivalence ratio oscillations could thus be damped over a much wider range of frequencies. Several practical limitations exist for configuration C. First, the fuel/air mixing process is incomplete in configuration C, since part of the fuel is from downstream injection points. Second, one cannot arbitrarily increase the number of fuel holes because, to achieve the same overall flow rate, the holes would have to decrease in size. Holes below a certain critical size are vulnerable to blockage from particulate matter in the fuel. Configuration C was thus abandoned. Configuration D is a much different design. A large number of air jets, instead of fuel jets, were equally spaced on the external walls of the premixer. All the fuel was now introduced at the head of the premixer and air was progressively introduced to dilute the fuel. In a volumetric sense, more air was flowing through the premixer than fuel; it is reasonable to supply the air through multiple small holes and provide the fuel from a single source. Unlike configuration C, there is little practical constraint to the number of air injection holes.

To quantify the response of equivalence ratio fluctuations with respect to velocity disturbance in a specific injector design, a parameter α, defined as the ratio between normalized fuel–air-ratio and velocity fluctuations, is introduced

$$\alpha = \left(FAR'/\overline{FAR}\right)/(u'/\overline{u}) \tag{6.22}$$

Fig. 58. Contour map of pressure oscillation amplitude near 100% power for Rolls-Royce Trent combustion systems (Scarinci and Halpin [26–28]).
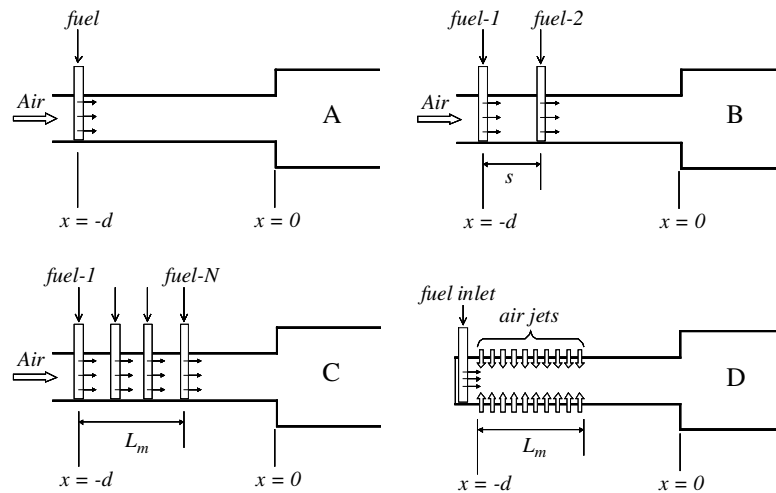
Fig. 60. Schematics of several premixer concepts (Scarinci and Halpin [26–28]).

In a "good premixer," α approaches zero, i.e., velocity fluctuations in the premixer will not produce in any FAR oscillations at the exit. In general, $0 < \alpha < 1$ and α is frequency dependent. Fig. 61 shows the value of parameter α as a function of non-dimensional frequency for configurations A, B and D. Configuration B shows some improvement over certain frequency ranges. Configuration D, which acts like a low-pass filter, damps out equivalence ratio oscillations over a wide frequency range. Fig. 62 shows a comparison between the pressure oscillation levels using the original premixer (analogous to configuration A in Fig. 60) and a modified premixer (design implementation of configuration D in Fig. 60). The pressure fluctuation level measured with modified premixers is considerably lower than that with original premixers, even though the fuel split between the primary, secondary and tertiary premixers was not purposefully chosen (Scarinci and Halpin [27,28]).

6.1.4. Fuel injector and burner geometries

Modification of fuel injector geometry has proved to be an effective strategy for reducing combustion oscillations (e.g., Steele et al. [33], Smith and Blust [34]). The injector design elements, including the inner diameter of the premixing barrel, and the length from the fuel injection spokes to the injector exit plane, were observed to have a strong influence on combustion dynamics by affecting the injector exit velocity, the overall fuel/air mixedness, and the fuel "transport time" from the spokes to the flame. As an

example, Fig. 63 shows a comparison of the old and new fuel injector designs for Solar Turbine's Centaur engine, representing the company's first effort to reduce combustion instabilities [33,34]. The cross-sectional area of the premixing channel of the original injector was increased by an added step in the outer wall just downstream of the fuel injection plane. The change exercised significant effects on the fuel/air residence time by reducing the injector axial velocity, and thus stabilized the oscillations in the modified Centaur combustor. Following this successful experience, a modified Mars injector was developed that included both a modification in flow cross-sectional area and a new spoke location. Subsequent tests on Solar Mars engines demonstrated that these modifications, along with the injection of pilot fuel, were effective in abating combustion oscillations without compromising NO_x emissions.

In Siemens gas turbine systems, passive suppression of combustion instabilities was achieved by modification of the hybrid burner exit (see Fig. 6a) (Berenbrink and Hoffmann [49]; Krebs et al. [44]). The basic idea was to decouple heat release oscillations from acoustic waves by changing the convective time lag. A cylindrical extension, which was also referred to as a cylindrical burner outlet (CBO) was welded onto the burner nozzle (see Fig. 64). The length of this extension was adjusted to increase the time lag by approximately one quarter of the instability oscillation period. In addition, the flow axis of the neighboring burners was inclined by
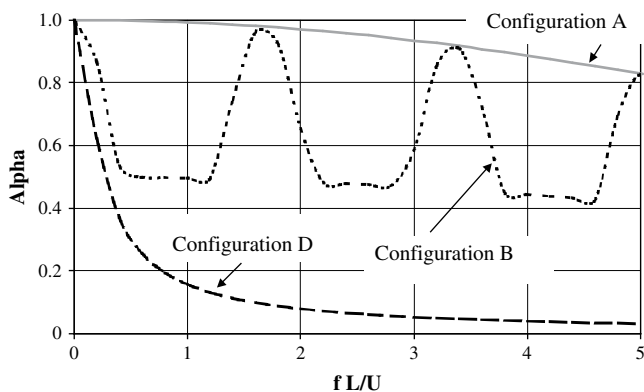
Fig. 61. Comparison of frequency responses for configurations A, B and D (configuration B result obtained using $d/U = 4$ ms, $s/d = 0.25$) (Scarinci and Halpin [26–28]).
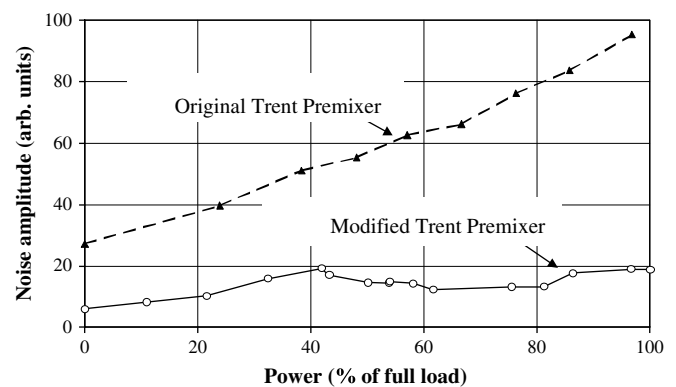
Fig. 62. Pressure fluctuation levels as a function of engine power, comparing original and modified Trent premixers (Scarinci and Halpin [26–28]).

OLD DESIGN   NEW DESIGN
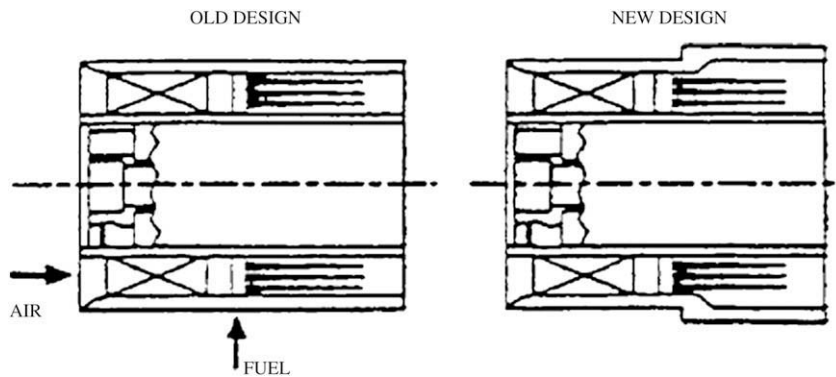
Fig. 63. Fuel injector modification to eliminate combustion oscillations in a Solar Turbine engine (Steele et al. [33]).

approximately 10°, so that they have a common intersection point. This is the so-called "asymmetric burner outlet" (ABO). ABOs can disrupt the formation of coherent structures and increase the time lag.

Abatement of combustion instabilities and pollutant emissions by burner geometry modifications was also reported in both laboratory devices and field gas turbines of ALSTOM (Eroglu et al. [73], Paschereit et al. [74–78]). Several passive methods were proposed and investigated for controlling combustion oscillations associated with hydrodynamic instabilities and equivalence ratio fluctuations. These methods, including miniature vortex generators (MVGs), an elliptically shaped burner, and an extended pilot fuel lance, are discussed below.

Miniature vortex generators, shown in Fig. 65, consist of small triangular ramps. Since coherent vortex motions produced at the burner exit by the Kelvin–Helmholtz instabilities might be one of the driving mechanisms of combustion dynamics, MVGs were installed around the circumference of the burner's exit to induce circumferential instabilities and interfere with the coherent structures. The height of each vortex generator was approximately equivalent to the burner exit shear layer thickness. The resultant circumferential instabilities disrupted the roll-up of the azimuthal vortices and eliminated the source of heat release pulsations that could otherwise have led to instabilities. Experimental results (Paschereit et al. [74], Paschereit and Gutmark [77]) indicated that suppression of both low and high-frequency instabilities over 10 dB could be achieved in some burner designs.
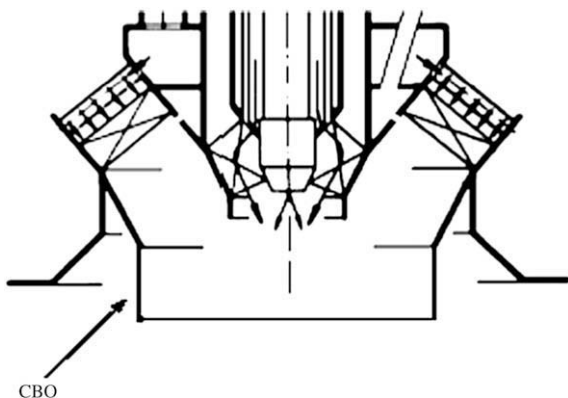
An elliptically shaped burner, as shown in Fig. 66, was also tested to abate the combustion dynamics driven by large-scale coherent structures. This geometry could generate axial vorticity, reduce the coherence of shear layer vortices, and enhance small-scale mixing, thereby decoupling hydrodynamics instabilities from chamber acoustics. Experiments indicated that the elliptic nozzle could result in suppression of instabilities and reduction of NO_x and CO emissions over a wide range of operating conditions (Paschereit and Gutmark [76]). An extended pilot fuel lance provided another passive means for instability control. Protruding into burner plenum, an extended pilot fuel lance was able to prevent the instability mechanism associated with large-amplitude movement of the vortex breakdown location and the resultant flame oscillation. The long fuel lance concept was successfully implemented in single burner tests and in full-scale field gas turbines [74,77].

6.1.5. Other passive control techniques

As stated in Section 5.5, flow oscillation induced by hydrodynamic instability is one of the driving mechanisms that lead to combustion instability. Large-scale eddies convected to the premixers can cause significant velocity fluctuations, which subsequently disturb the combustion process. A number of "air-flow-damping devices" were installed upstream of the premixers in Trent DLE combustion systems to damp out upstream velocity fluctuations (Scarinci [28]). Some of the "air-flow-damping" configurations tested included a number of reticulated materials such as honeycomb and metal foams. These devices could reduce aerodynamic plenum fluctuations by more than 20 dB over a wide frequency range. Thus, the premixer, and hence the flame, would experience a reduced level of velocity fluctuations, resulting in a quieter combustion process.

Fig. 64. Siemens hybrid burner with cylindrical burner outlet (CBO) extension (Berenbrink and Hoffmann [49]).
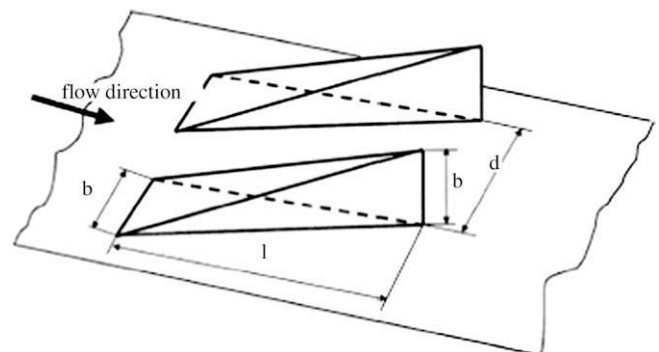
Fig. 65. Schematic drawing of miniature vortex generators in separating shear layers (Paschereit et al. [74,77]).
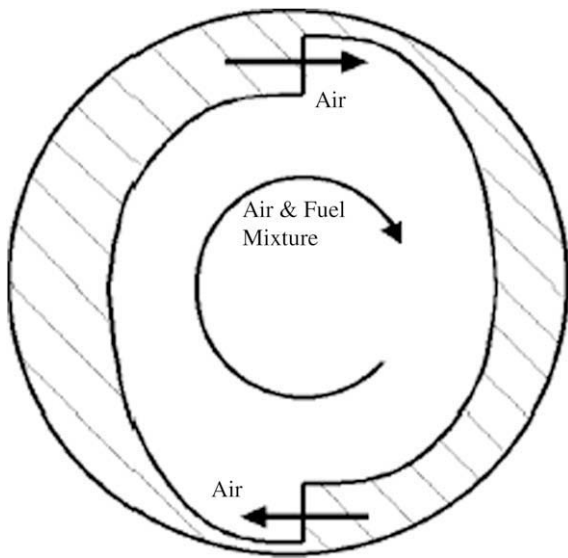
Fig. 66. Cross-section of an elliptic burner exit (Paschereit et al. [77]).

Baffles provide another means to stabilize pressure oscillations in combustors. A typical configuration consists of flat plates extending into a chamber perpendicularly from the injector face. Three mechanisms (Reardon [316], Combs et al. [317], Wicker et al. [318]) have been proposed for explaining successful elimination of instability by baffles: (1) modification of acoustic resonance properties (i.e., frequency and waveform); (2) restriction of unsteady motion between baffle blades, and subsequent shielding of the sensitive mechanisms for instabilities; and (3) damping of oscillations by vortex shedding, flow separation, and viscous dissipation. Baffles have been widely used in rocket engines since 1954 (Male et al. [319]), but their use in gas turbine engines is rare.

The passive control techniques previously mentioned can be implemented simultaneously in a gas turbine combustion system.

Since combustion instabilities are often driven by a collection of mechanisms, a combination of the methods described may, in fact, be more effective. For example, the two-stage Trent 60 DLE combustor incorporates several different means for equivalence ratio, acoustic, and air-flow damping, as shown in Fig. 67 (Scarinci [28]). A major problem with passive approaches is that they tend to be effective only over a limited range of operating conditions, and usually become less effective at low frequencies, at which some of the most damaging instabilities occur. Furthermore, the changes of design involved are normally costly and time-consuming.

6.2. Active control of combustion instability

Active control techniques utilize external excitations (such as acoustic forcing and fuel modulation) to attenuate combustion oscillations. Generally, the purpose is to minimize the difference between the instantaneous desired and actual behavior of a dynamic system. Fig. 68 shows a schematic of an active combustion control system, consisting of sensors, actuators, and a controller. Control may be exercised without feedback of information about the actual response of the system (open-loop control) or with feedback (close-loop control). Closed-loop operation can be further classified as fixed-parameter or adaptive feedback control. In open-loop control, the controller output is pre-defined, and the actuator is applied without any feedback. In fixed-parameter close-loop operation, a fast sensor provides real-time feedback, and control action is modified accordingly. In adaptive close-loop control, an additional sensor is employed to detect the overall combustor performance in a time-averaged manner. This sensor output is used by an adaptive filter to adjust the controller parameter to accommodate changes in operating conditions.

Active control is an attractive strategy because it relies on proper modulation of combustion system parameters, rather than spatial changes of the flowfield as required in passive approaches. Since adjustment of system timing parameters is much simpler and more practical than the potential geometry modification associated with passive control, active control provides flexibility for adaptation and eliminates costly design changes.
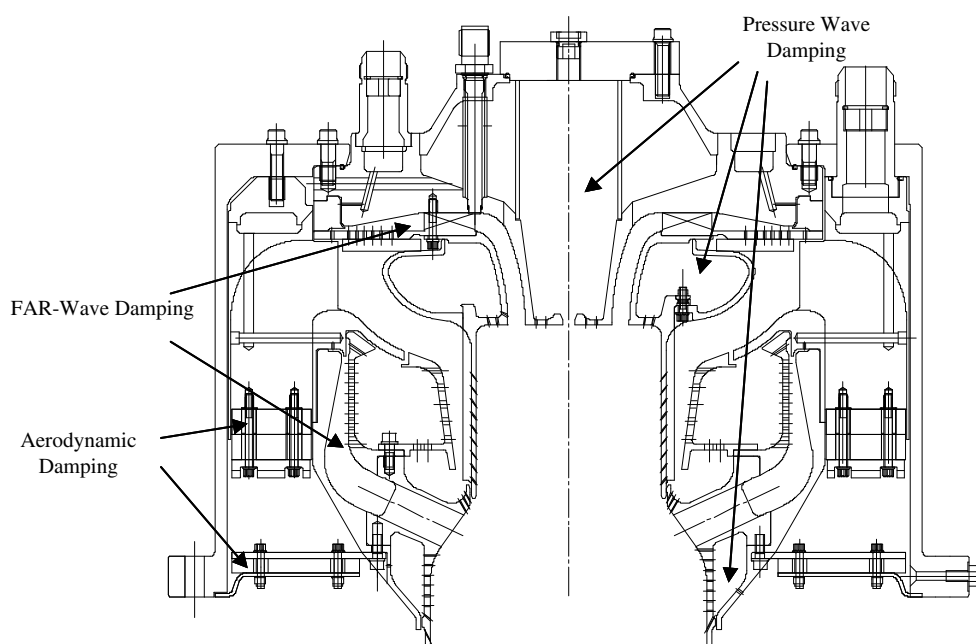
Fig. 67. Cross-section of a modified two-stage Trent 60 DLE combustion system implemented with various passive instability control devices (Scarinci [28]).

6.2.1. Sensors and actuators

Practical applications of active control require reliable sensing and actuation devices with proper time-response characteristics (Kurtz et al. [320], Yu [321]). Sensors must provide fast and accurate information on the dynamic quantities related to instabilities. Both fast and slow-response sensors may be used. For real-time feedback applications, fast-response sensors are required. For adaptive control applications, an additional slow-response sensor could be used. The most commonly used sensors are pressure transducers, since instabilities can be conveniently characterized by pressure oscillations. The placement of pressure sensors is important. The acoustic mode shapes should be anticipated accurately to avoid placing a pressure sensor at a pressure node point, and to maximize the signal to noise ratio. In addition, multiple pressure sensors may be required to properly identify the amplitude and phase information on azimuthal acoustic modes in annular combustors.

Photomultipliers have been widely used experimentally. Luminosity sensors, when combined with narrow-band interference filters, measure the chemiluminescence emissions from radical species such as C_2, OH, CH and CO_2 in the flame reaction zones. Their signals give a rough measure of unsteady heat release, which provides the energy source for driving combustion instability. Photomultiplier measurements, however, are independent of acoustic mode shapes. They are highly sensitive to fuel flow rate, equivalence ratio, and other parameters (Lee and Santivacca [269], Nori and Seitzman [322]). The signal may be misleading if the sensor is such positioned that its field of view does not completely cover the entire range of motion of a spatially varying reaction zone. Recent advances in machine vision using an array of optical sensors may provide the controller with information regarding the global distribution of unsteady heat release.

Other optical diagnostic sensors, such as infrared absorption, laser-induced fluorescence, and laser Doppler velocimeters (LDV), are also utilized to characterize unsteady combustion in experimental control systems. Infrared absorption is used to measure the magnitude and frequency of species concentrations and temperature (Hanson and colleagues [323–325], Lee and Santivacca [269]). Laser-induced fluorescence measurements can characterize fuel–air mixing and resultant fuel distribution (Lee and Santivacca [269]). LDV provides transient velocity measurements. Optical sensors may also play key roles in pattern factor control, since the information on the temperature distribution throughout the cross section of a chamber is desired. Sensor requirements for active gas turbine engine control were discussed by Kurz et al. [320]. A comprehensive review of various sensors used in combustion control was given by Docquier and Candel [326].

Actuators are essential in both open-loop and feedback control systems. Good actuators should have the ability to introduce an action that produces a fast system response over the desired range of frequencies. For the action triggered by the actuator to be truly effective, it must interfere with the root-cause mechanism of instabilities, i.e., the coupling between acoustic oscillations and unsteady heat release. Thus, most AIC actuators attack either acoustic waves or the temporal and spatial distributions of heat release. The former can be achieved directly with mechanical acoustic actuation using loudspeakers [327–331] or indirectly through modification of acoustic boundary conditions using, for example, an oscillating centerbody (Bloxsidge et al. [332]). The latter can be realized by modulation of the primary or secondary fuel flow, or indirectly by excitation of shear layers, which in turn affect fuel/oxidizer mixing and flame structures. Acoustic devices have also been used for fuel flow modulation, as well as excitation of coherent structures in shear layers [294,333–340]. It should be noted that, although acoustic devices have good high-frequency responses, they may not be robust and powerful enough for use in large-scale combustion systems.

In most active instability control (AIC) systems, modulation of fuel flow rate has demonstrated its effectiveness. This can usually be achieved via a high-speed valve, such as a solenoid valve, a direct-driven valve (DDV), or a spinning drum valve [59]. Recently, Zinn and his co-workers [306,307] have demonstrated the feasibility of using a "smart" liquid fuel injector that can modify the combustion time by modulating liquid fuel spray characteristics. It should be note that the efficiency of fuel modulation depends on the manner and location of fuel injection (Lee et al. [401]). All the actuators mentioned have demonstrated varying degrees of success in closed-loop control. Perhaps a combination of multiple actuators could accomplish more than a single actuator.

6.2.2. Active control algorithms

The control algorithm is a key element in the success of active instability control. The controller needs to be effective across all operating condition regimes, and must remain stable to avoid causing damage to the system. The simple phase-shift (also known as a time delay or phase delay) control strategy, which identifies the oscillation frequency and phase through a filter, adds an appropriate phase, amplifies the signal, and feeds it back as a control input to counteract the instability, was the first to be widely used. Without detailed information on the system dynamics, however, such a controller needs to be carefully tuned to obtain an optimal phase for each operating condition. In addition, a secondary mode of instability may appear as the control gain is increased (e.g., Langhorne et al. [341], Fleifil et al. [342]). Thus, more robust control algorithms were desired for performance improvement. Yang and his colleagues [275,343] made a first theoretical attempt. Since then, a variety of control techniques, summarized in Table 1, have been developed for suppressing combustion instabilities.

Among the various feedback control approaches shown in Table 1, the most primitive type is the proportional (P)-controller in a single-input and single-output (SISO) setting, in which stability and performance are achieved only by an operational amplifier between the sensor and the actuator. The P-controller can be extended to form a proportional-integral-derivative (PID) control system, in which the I-control is used for achieving zero steady error, since it integrates the error in time, and the D-control serves to enhance the transient response, since it regulates the tendency of motion (Fung et al. [275]). Conceptually, there are only three control parameters in a single PID controller module, so that the controller design is fairly simple. A low-order controller may not satisfy performance requirements for high-order plant dynamics, however. For linear systems, a PID controller can be extended to accommodate a filter with phase compensation in the frequency domain, or to form an integral state-feedback controller in the time domain. If all states cannot be measured, an observer is needed for output-feedback control (Yang et al. [344], Neumeier and Zinn [345]). It is not difficult to design an observer for a finite-dimensional linear time-invariant (FDLTI) system, but it may be much more challenging to design one for a time-varying or nonlinear system.
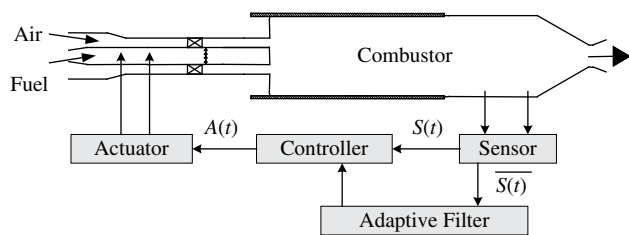
Fig. 68. Schematic of an active combustion control system.

Table 1
Survey of active combustion instability control techniques.

Control Technique	Application	References	Remarks
PID design	Nonlinear generic combustion instability; Premixed swirl-stabilized combustor.	Fung and Yang, 1992 [343]; Pascphereit and Gutmark, 2002 [340].	Easy to adjust control parameters; May not fulfill various performance requirements.
Bode–Nyquist frequency domain design and root locus	Generic combustion instability; Low-frequency combustion instability; Low-frequency combustion instability; Coaxial dump combustor; Premixed laminar combustors; Liquid-fueled combustion systems.	Bloxsidge et al., 1987 [346]; Langhorne et al., 1990 [341]; Fung et al., 1991 [275]; Schadow et al., 1992 [334]; Gulati and Mani, 1992 [329]; Annaswamy and Ghoniem, 1995 [388]; Hantschk et al., 1996 [46].	Easy to identify systems and design controller in frequency domain; Fails in time-varying and nonlinear systems; only for SISO, Can be more general in H_∞ and μ control; Controllability and observability cannot be predicted; Easy for filter design; Can serve as the basis of phase-lead and phase-lag compensator design.
Observer-based design: adaptive observer and model-based observer	Longitudinal combustion instability; Thermoacoustic instability in rocket motor; Subscale swirl combustor.	Yang et al., 1992 [344]; Neumeier and Zinn, 1996 [410,345]; Sattinger et al., 2000 [406].	Nominal model-based observer can be extended to optimal LQG regulator; Adaptive observer has no guarantee of convergence; its algorithm is one branch of the gradient iterative rules.
LQR and LQG control	Premixed laminar combustor; Generic combustion instability; Swirl-stabilized combustors.	Annaswamy et al., 1995 [388]; 2002 [389]; Hathout et al., 1998 [353]; Campos-Delgado et al., 2003 [357,358]; Murugappan et al. 2003 [356].	LQR control has optimal and robust properties of gain and phase margins, but requires measurements of all states; LQG control has no robust property and is used only for rejection of intensity-known noise.
LMS adaptive and neural network back-propagation	Generic combustion instability; Boiler combustion systems; Dump combustor; Large-scale solid rocket motor; Rijke tube burner; Premixed duct flame; Swirl-stabilized combustor.	Billoud et al., 1992 [363]; Allen et al., 1993 [360]; Kemal and Bowman, 1996 [364]; Koshigoe et al., 1999 [361]; Blonbou et al., 2000 [365]; Evesque and Dowling, 2001 [362]; Bernier et al., 2003 [404].	Sensitive to initial conditions and gradient dynamic parameters; Has similar algorithm in System ID; May be replaced by off-line ID plus Bode–Nyquist or observer-based controller.
Fuzzy logic control	Longitudinal combustion instability	Menon and Sun, 1996 [367]	Effective only when many states can be directly measured; Need experience to set up logic rules and scales.
H_∞ and μ control	Generic combustion instability; Premixed duct flame.	Hong et al., 2000 [349]; Chu et al., 2003 [350].	Observer-based controller with robust properties; valid for intensity-unknown disturbance; Can regulate frequency domain properties; Accommodate, model uncertainty.
LPV L_2 gain control	Generic combustion instability	Hong et al. 2002 [372]; 2003 [373].	Multiple-time scale, multiple-layer system for wide-range control; Observer-embedded LPV controller for robust state estimation.
Self-tuning control	Generic combustion instability; Rijke tube burner; Swirl-stabilized combustor.	Krstic et al., 1999 [368]; Annaswamy et al., 1998 [369]; Evesque et al., 2003 [370], 2004 [371].	Model-based adaptive controller; established based on a Lyapunov stability analysis.
Extremum-seeking and time-averaged gradient control algorithm	Swirl-stabilized combustor; Rijke tube burner; Industrial-scale gas turbine combustor.	Murugappan et al., 2000 [366]; Vaudrey et al., 2003 [331]; Banzszuk et al., 2004 [62].	Gradient-based adaptive algorithm; Require no detailed knowledge of the system dynamics.

In the frequency domain, the open-loop dynamics of an FDLTI system can be conveniently represented by the Bode plot, through either physics-based modeling or system identification, or a combination of the two (e.g., [275,329,334,341,346]). The representation of system dynamics in the frequency domain simplifies the filter design, and the stability analysis can be based on the Nyquist criterion. The robustness of a controller is traditionally predicted in terms of phase and gain margins for single-input single-output (SISO) systems. When uncertainties are simultaneously present in both phase and gain, the issue of robustness can be expressed by the H_∞-based structured singular value (μ) of the closed-loop system (Doyle et al. [347], Packard and Doyle [348], Hong et al. [349], and Chu et al. [350]).

Among the various time-domain tools for controller design, the linear quadratic regulator (LQR) controller appears to be quite robust, with its gain margin in the range of $[1/2, \infty)$ and at least $60°$ phase

margin (Safonov and Athans [351]). The LQR controller, however, can be applied only if all the states can be measured without any appreciable noise contamination. Otherwise, a state estimator is needed to meet this requirement. The resulting output-feedback control system is known as a linear quadratic Gaussian (LQG) controller, if a Kalman filter is used as the state estimator. The scheme may be further extended for nonlinear systems using an energy method in terms of the Lyapunov function. The major deficiency of the LQG technique lies in its failure to guarantee any gain and phase margin (Doyle [352]). Applications of LQR and LQG algorithms on combustion instabilities can be found in Refs. [353–358]

Non-model-based adaptive controllers, such as least mean square (LMS), artificial neural network back-propagation, extremum-seeking, and time-averaged gradient adaptive controllers, employ iterative approaches or gradient-based methods to update control parameters in real time [331,359–366]. Some of those methods, however, often encounter difficulties with numerical divergence and local optimization, and consequently may not guarantee stability and performance. In addition, most adaptive algorithms do not accommodate a physical model of plant dynamics. It is also often risky to establish general rules for performance improvement and fault diagnostics based on approximate reasoning, such as fuzzy logic (Menon and Sun [367]). Moreover, formulation of fuzzy logic rules requires extensive physical understanding and operations experience that are not usually available for combustion dynamics.

For model-based adaptive controllers, self-tuning regulators (STR) were examined by Kristic et al. [368] and Annaswamy et al. [369]. The algorithms are established based on a Lyapunov stability analysis, and do not require online system identification. STRs were originally designed for models of specific combustors. Later, Evesque and colleagues [370,371] showed that self-tuning regulators could be extended to achieve robust control over a variety of combustion systems and operating conditions. The only information required by the STR is the total time delay between actuation and response. Hong et al. [372,373] recently developed a linear parameter varying (LPV)-L_2 gain algorithm for wide-range robust control. The control law is synthesized based on a two-time-scale model of combustion dynamics. Control actions on the fast-time scale are provided by secondary fuel injection, and are gain-scheduled according to the variation of mean flow temperature and velocity on the slow-time scale. The LPV control law provides robust performance with model uncertainties and exogenous input for both narrow and wide-range conditions of the slowing varying mean flow variables.

6.2.3. Laboratory-scale experiments

Tsien [374] made the first attempt to apply control theories to suppress the chugging instability in a liquid-propellant rocket engine in 1952. His theoretical analysis was based on a pressure-dependent time lag model. Stabilization of the combustion conditions was achieved by modulating the propellant injection rate through a capacitor controlled by a servomechanism with pressure feedback. Similar approaches were used by Marble and Cox [375] and Lee et al. [376] to control the low-frequency instabilities in bipropellant liquid rocket engines. No experimental results based on this "servo-stabilization" concept were published, however, primarily due to the limitations in instrumentation, such as lack of fast-response sensors and actuators, at that time.

The first experimental applications of active combustion instability control were reported by Ffowcs-Williams and his colleagues at Cambridge University [377,378,379,380]. Ffowcs-Williams [377] described the concept of "anti-sound" — the elimination of unwanted oscillations in an acoustic field by means of acoustic interference. The basic idea is to first determine the characteristics of a given acoustic field, and then to use that information to manipulate a secondary source of sound (e.g., loudspeakers), which serves as an acoustic actuator. Control is achieved by producing waves out of phase with the unwanted oscillations. The principle of "anti-sound" was successfully tested on Rijke tube burners [378,379,380]. Since then, a large number of experimental studies have appeared.

Although applications of acoustic devices, such as loudspeakers and moving bodies, have demonstrated varying degrees of success in instability control (Gulati and Mani [329], Sivasegaram et al. [330], Paschereit et al. [293,294,338–340], Vaudrey et al. [331]), for practical systems containing high energy density, implementation of these means may not be feasible due to the relatively large amount of power required to drive the control actuators. Control methods based on the direct manipulation of energy sources of oscillatory flowfields appear to be much more feasible and effective. Langhorne et al. [341] first reported that pressure oscillations in a laboratory afterburner could be reduced significantly by a controlled secondary supply of fuel. It was found that just 3% fuel addition is sufficient in generating the energy necessary for instability control. They concluded that this method offers a promising solution to problems of low-frequency oscillations in full-scale combustors. The theoretical study of Yang et al. [344] and Fung et al. [275] and the numerical simulations of Menon [381], Shyy et al. [382], and Mohanraj et al. [383] have also demonstrated the viability of controlled fuel injection.

Table 2 summarizes the characteristics of published experimental studies on combustion instability controls. Most of the experimental studies have been performed at laboratory scales. The research studies on gas turbine combustors with swirl injectors are briefly reviewed in the following. There have also been several implementations of active instability control on full-scale gas turbine systems, and those will be discussed in detail in Section 6.2.4. Detailed reviews of active instability control on various combustion systems were also given by Culick [11], Candel [384,385], McManus et al. [386], Hendricks and Schadow [387], Annaswamy and Ghomiem [388,389], Zinn and his co-workers [390,391], Yang et al. [309], Schadow et al. [308], Yu [321], and more recently by Dowling and Morgans [392]. Applications of active control for gas turbine combustor emission performance were also reported by Samuelsen and his co-workers [393,394].

6.2.3.1. Open-loop active control. Richards and colleagues [274] investigated open-loop active control of combustion instability in a 30-kW atmospheric-pressure, swirl-stabilized combustor. Since the combustor exhibited unstable oscillations over a limited range of equivalence ratios, a control technique to periodically modulate the equivalence ratio was proposed to hop over the unstable operating regime. Under this control scheme, the combustor operated under unstable operating conditions in a time-average sense, but switched between stable conditions on an instantaneous basis. The fuel was natural gas. Fuel flow modulation was achieved using a solenoid valve. The rms pressure amplitude was reduced from 2.7 to 0.8 kPa for a 300-Hz oscillation. Control was accomplished by modulating the fuel flow at frequencies less than 20 Hz.

Zinn and his co-workers [395,396] reported a study of open-loop control of combustion instability in a liquid-fueled swirl combustor using harmonic fuel flow modulation at a non-resonant frequency. The dominant instability frequency in the combustor was around 400 Hz. The actuator was based on fuel injection using a fast-response actuating valve. Combustion instabilities were reduced by a factor of 10, when the control frequency was in the range of 250–330 Hz. The possibility of stabilizing combustion oscillation using relatively low-frequency modulation of the fuel

Table 2
Survey of experimental studies on active combustion instability control.

Physical model	Active control strategy	Sensor and actuator	References	Remarks
Rijke tube type burners	Anti-sound control using phase-shift algorithm	CH emission sensor or microphone; loudspeakers	Dine, 1983 [378]; Heckl, 1985 [379], 1986 [380]	Instabilities could be attenuated over a wide range of phase difference between self-excited and imposed oscillations
Laboratory reheat buzz rig with flame stabilized by a conical gutter	Modification of upstream acoustic boundary condition	Pressure transducers; Movable centerbody capable of flow rate modulation	Bloxsidge et al., 1987 [346], 1988 [332]	Reduction of peak pressure amplitude by up to 20 dB
	Secondary fuel supply modulation based on phase-shift algorithm	C_2 light emission sensor and pressure transducers; Solenoid valve based automotive fuel injector actuators	Langhorne, et al., 1990 [341]	Reduction of peak pressure amplitude by 12 dB
Laminar-premixed combustors with a multiple orifice plate flame-holder	Anti-sound control using phase-shift algorithm	Microphone; loudspeaker	Lang et al., 1987 [327]; Poinsot et al., 1989 [328]	Up to 66 dB reduction in pressure oscillation amplitude
Non-premixed combustor with flame stabilized by three backward-facing steps	a) Anti-sound control; b) Modulation of fuel flow and adaptive control based on Linear Mean Square (LMS) algorithms	Microphone and C_2 light emission sensor; loudspeaker to modulate fuel flow rate	Poinsot et al., 1989 [328], 1992 [333]; Billoud et al., 1992 [363]	More than 20 dB reduction in sound pressure level
Dump combustor	Open-loop control by direct shear layer excitation	Loudspeakers	McManus et al., 1990 [411,412]	Up to 30% reduction in rms pressure fluctuation level
Coaxial dump combustors	a) Open-loop control by shear layer excitation; b) Close-loop control of fuel flow based on phase-shift algorithm.	Pressure transducer and CH emission sensor; loudspeaker were used to modulate the fuel flow and modify the shear layer	Schadow et al., 1992 [334]; Gutmark et al., 1993 [335]; Wilson et al., 1995 [336]	Up to 50% reduction in pressure oscillations
Small-scale premixed combustor with perforated plate flame-holder	Anti-sound control using phase-shift algorithm	Kistler pressure transducer; loudspeaker	Gulati and Mani, 1992 [329]	Up to 33 dB reduction in amplitude of dominant pressure mode
Premixed sudden expansion combustions	a) Anti-sound control; b) Secondary fuel flow modulation based phase-shift algorithm	Pressure transducer; Loudspeakers; Secondary fuel flow modulation using a needle-valve	Sivasegaram et al., 1995 [330]; De Zilwa et al., 1999 [413]; Emiris and Whitelaw, 2003 [414]	Up to 16 dB reduction in pressure oscillations
Ducted orifice nozzle premixed flame	Direct excitation of shear layer or acoustic cancellation	Microphone and CH emission sensor; Loudspeakers	Parr et al., 1993 [415]	Up to 30 dB reduction in acoustic oscillations
Laboratory-scale premixed dump combustor	Spanwise forcing of shear layer and adaptive control using least mean-square (LMS) algorithm	Piezoelectric pressure transducer; Actuation of the inlet boundary layer using loud-speakers	Padmanabhan et al., 1995 [337]; Kemal and Bowman, 1996 [364]	Up to 15% reduction in pressure oscillations
Laboratory-scale liquid-fueled combustor with flame stabilized using a mixing pipe	Modulation of liquid fuel flow based on phase-shift control algorithm	Microphone for pressure level and photomultiplier for heat release level; Liquid-fuel modulations were achieved using piezo and direct-drive valve actuators	Hermann et al., 1996 [47]; Hantschk et al, 1996 [46]	Reduction of pressure amplitude up to 40 dB using piezo actuator and 153 dB using DDV actuator
Model ramjet dump combustors	Secondary fuel injection based on phase-shift control algorithm	Kristler pressure transducer; Liquid-fuel automotive injector actuator	Yu et al., 1996 [416], 1998 [417], 2002 [418]	Up to 15 dB reduction in the sound pressure level
Laboratory-scale gas-fueled combustor	Secondary fuel injection based on real time phase-shift control algorithm	Pressure transducers; Secondary fuel injector actuator;	Neumeier et al., 1996 [410,345], 1997 [419]; Zinn and Neumeier, 1997 [390];	Fundamental acoustic mode was reduced by 26 dB in 40 ms.
Subscale gas turbine swirl combustor fueled with natural gas			Sattinger et al., 2000 [406]	Four-fold overall reduction in pressure amplitudes
Full-scale gas turbine swirl combustor fueled with natural gas.			Johnson et al., 2001 [407]	10–15 dB reduction of dominant mode acoustic amplitude.
Full-scale gas turbine combustors with duel-fuel swirl burner	Modulation of pilot fuel flow based on phase-shift control algorithm	High temperature piezo pressure transducers; modulating pilot fuel flow rate through direct-drive-valve (DDV) actuator	Seume et al., 1998 [48]; Berenbrink et al., 2000 [49]; Hermann and Hoffmann 2005 [50];	Reduction of pressure amplitudes by 17 dB in 170-MW ring combustor
Full-scale liquid-fuelled combustor with single swirl injector	Portion fuel flow rate modulation based on phase-shift control algorithm and extremum-seeking adaptive control algorithm	Pressure transducers; modulation of a portion of fuel flow using solenoid valve or spinning valve actuators	Cohen et al., 1999 [58], 2001 [60], 2003 [61]; Barooah et al. 2003 [59]; Banaszuk et al. 2004 [62]	Suppression of instability by up to 15 dB

(continued on next page)

Table 2 (continued)

Physical model	Active control strategy	Sensor and actuator	References	Remarks
Full-scale liquid-fuelled sector combustor with three swirl injectors	Portion fuel flow modulation based on phase-shift control algorithm	Pressure transducers; modulation of a portion of fuel flow using solenoid valve	Hibshman et al., 1999 [63]	Reduction of 6.5 dB in the amplitude of dominant instability mode
Laboratory dump combustor	Nonlinear active control based on hysteresis: pulse injection of pilot fuel	Pressure transducers; Automotive fuel injector	Knoop et al., 1997 [201]; Isella et al., 1997 [214]	Only a single pulse of secondary fuel required to suppress instability
Laboratory-scale premixed combustor with swirl injector	Open-loop control with equivalence ratio modulation	Fuel flow rate modulation using solenoid valve	Richard et al., 1997 [397], 1999 [274]	Up to 10 dB reduction in pressure amplitude
Swirl-stabilized combustors using gaseous fuel	a) Anti-sound control; b) Modulation of air supply based on phase-shift and proportional control algorithm	Microphones and OH emission probe; loudspeakers to modulate air supply	Paschereit et al., 1998 [294,293], 1999 [338]; 2000 [339], 2002 [340]	Modification of shear layer evolution is more effective than anti-sound control; suppression of pressure oscillations up to 12 dB
Small-scale liquid-fueled combustors with swirl injector	Magnitude-based pulse-width fuel flow modulation	Pressure transducer and flame emission sensor; fuel flow modulation using solenoid valve	McManus et al., 1998 [399]; Magill et al., 2000 [400]	Up to 50% reduction in the magnitude of pressure oscillations
Laboratory-scale lean-premixed combustor with swirl injector;	Subharmonic fuel modulation and phase-shift control algorithm	Microphone-based sound level meter; secondary fuel injector actuator	Jones, et al., 1999 [420]; Lee et al., 2000 [401]	Noise level reduction of 22 dB; effective control depends on the secondary fuel injection location.
Rijke tube burner	Anti-sound control based on artificial neural networks algorithm	Microphone and OH emission sensor; loudspeakers	Blonbou et al., 2000 [365]	Reduction of pressure amplitude level up to 40 dB
Full-scale afterburner of a turbofan engine	Fuel flow modulation based on phase-shift control algorithm	Pressure transducer; high-response electro-hydraulic servo-valve actuator	Moran et al., 2000 [409]	12 dB reduction in dominant low-frequency "buzz" instability; modulation through spilling fuel from the engine rather than adding it
Swirl-stabilized spray combustor	Fuel flow modulation based on extremum-seeking adaptive control algorithm	Kistler pressure transducer; fuel stream modulation using high-frequency valve	Murugappan et al., 2000 [366]	43% Reduction in pressure oscillations
	Secondary fuel flow modulation based on LQG-LTR algorithm	Pressure sensor; secondary fuel stream modulation using automotive fuel injector	Murugappan et al., 2003 [356], Allgood, et al. 2003 [355]	The LQG-LTR controller yield an additional pressure reduction of 14 dB compared to the phase-shift controller
Swirl-stabilized spray combustors	Fuel flow modulation using LQG, LQG-LTR, and H_∞ loop-shaping control algorithms	Kistler pressure transducer; fuel flow modulation using loud-speakers	Campos-Delgado et al. 2003 [357,358]	Effectiveness of model-based controllers was demonstrated
Rijke tube combustors	Anti-sound control based on adaptive, time-averaged gradient algorithm	Pressure transducer; loudspeaker	Vaudrey et al. 2003 [331]	Effectiveness of the time-averaged gradient controller was demonstrated
Lean-premixed, prevaporized combustor with swirl injector	Secondary airflow modulation based on adaptive control with LMS algorithm	Microphone and CH* chemiluminescence; modulation of secondary airflow using direct-drive-valve (DDV)	Bernier et al. 2003 [404]	50% Reduction in mean pressure oscillation amplitude
Swirl-stabilized spray combustor	Both open-loop and close-loop modulation with high-momentum air jet	Pressure transducer; modulation of air jet using a proportional-drive valve	Uhm and Acharya, 2004 [421], 2005 [398]	Pressure oscillations were reduced by a factor of nearly 10
Subscale lean-premixed gas turbine combustor with gaseous fuel swirl injector	Fuel flow modulation based on adaptive control with self-tuning regulator algorithm	Kistler piezoelectric pressure transducer; modulation of fuel flow rate through direct-drive-valve (DDV) actuator	Riley et al. 2004 [405]; Evesque et al., 2004 [371]	Reduction of pressure amplitude up to 30 dB on the primary instability frequency
Premixed combustor with gas-fueled swirl injector	Secondary fuel flow modulation based on phase-shift control algorithm	Microphones; modulating secondary fuel flow rate through drive servo-valve (DDV) actuator	Auer et al., 2005 [402]	The effectiveness of secondary fuel modulation is investigated
Laboratory-scale liquid-fuelled swirl combustor	Open-loop control through fuel flow modulation at non-resonant frequency	Fast-response actuating valve	Lubarsky et al., 2003 [395], 2004 [396]	Nearly 10-fold reduction in amplitude of pressure oscillation
Laboratory-scale liquid-fueled swirl combustor	Combustion time control by modulating liquid fuel spray properties	Pressure transducer; Liquid fuel injector capable of modulating spray characteristics	Conrad, et al., 2004 [306,307]; Lee, et al., 2005 [422]; Zinn, 2005 [391]	Decouple characteristic combustion time from acoustic period of instability by changing the spray properties

flow was also demonstrated by Richards et al. [397] in a 20-kW gaseous-fueled swirl combustor.

Instead of fuel flow modulation, Uhm and Acharya [398] adopted an open-loop control strategy using a high-momentum air jet. Experiments were carried out in a 150-kW swirl-stabilized spray combustor. The dominant instability modes were a longitudinal acoustic mode (235 Hz) and a low-frequency (13 Hz) bulk mode. The control was achieved by means of a low-bandwidth modulation of a high-momentum air jet to penetrate directly into the region of a positive Rayleigh index from where the instability originates. The air jet was modulated using a proportional-drive valve. With a low-frequency modulation (1–7 Hz), the pressure oscillation was reduced by a factor of nearly 10. Both square-wave and sine-wave modulations were examined. The former was considerably more effective than the latter.

6.2.3.2. Closed-loop active control. Paschereit et al. [293,294, 338,339] investigated close-loop active control of combustion instability in a gaseous-fueled, swirl-stabilized combustor. Two control strategies were examined. The first approach was based on the principle of anti-sound. Loudspeakers were installed downstream of the swirl burner to excite the chamber flowfield. In the second approach, loudspeakers were placed upstream of the burner to interrupt the coherence of large-scale structures in the shear layer. Microphones or OH emission probes were used to monitor the combustion process, and to provide input to the control system. The sensor output was used by the controller to produce a phase-shifted sine-wave signal at the instability frequency, which was fed back for loudspeaker actuation. The direct excitation of the shear layer was found to be more effective in instability control than the noise cancellation technique. The former required less energy to obtain the same effect as the latter, mainly due to the inherent instability of the flow. In their experiments, up to 5 dB reduction in the pressure oscillation were achieved using less then 0.002% of the combustor power for actuation. In a subsequent study (Paschereit et al. [340]), a proportional close-loop active control system was tested. The controller utilized a time-shifted signal instead of a phase-shifted pure sine wave to drive the actuator. The control system can respond continuously to variations in the instability magnitude, frequency, and phase, and can thus modify the control signal accordingly. For example, the control actuation is proportionally reduced as the amplitude of the instability decreases. With this proportional controller, more than 12 dB reduction in pressure oscillation can be achieved.

McManus et al. [399] and Magill et al. [400] applied closed-loop active instability control to a liquid-fueled swirl combustor with a dual-stream injector. Control was exercised using fuel flow modulation. The injector had separate primary and secondary fuel nozzles. The primary section of the dual-stream injector was connected to a solenoid valve to provide modulation. The controller used an amplitude-based pulse-width modulation (PWM) control algorithm. The amplitude of the emission or pressure oscillation was detected using a sensor. The width of the control output pulse or the amount of fuel injected during the pulse event was proportional to the instantaneous magnitude of the signal envelope. The combustor exhibited a self-excited instability at 140 Hz. With control on, the energy of the dominant mode was reduced by more than 50%.

Lee et al. [401] demonstrated closed-loop active instability control in a laboratory-scale swirl-stabilized combustor using subharmonic modulation of secondary fuel injection. The pressure transducer placed at the dump plane was used as the sensor for the control system. Active control was exercised by modulating the injection rate of the secondary fuel stream on every fourth cycle of the instability. The injection of secondary fuel was phase-locked with the combustor pressure oscillation and the phase delay was adjusted for the maximum. Open-loop operation, in which secondary fuel was injected at a fixed frequency, was also investigated. Three fuel injection locations were examined. The effectiveness of both open- and closed-loop control was found to be strongly dependent on the injection location. Feedback active control of combustion instability in a swirl-stabilized combustor based on fuel flow modulation was also reported by Murugappan et al. [356], Campos-Delgado et al. [357,358], Uhm and Acharya [398], Auer et al. [402], and Choi et al. [403].

Zinn and his co-workers [306,307] recently proposed a 'combustion time control' technique to attenuate instability in a liquid-fueled swirl combustor. Since combustion instabilities usually result from the dynamic coupling between chamber acoustics and heat release, which requires the characteristic time scale of the combustion process be of the order of the acoustic period of the instability, one possible way to suppress instabilities is to modify the combustion time in such a manner that the condition for equality of the two time scales is avoided. They developed a "smart" liquid fuel injector with capabilities for modifying the liquid fuel burning time by changing the spray characteristics. In contrast to most of the active control techniques mentioned above, which require continuous operation of the actuator, this approach only requires a 'one-time' modulation of the combustion process to attain control.

6.2.3.3. Adaptive active control. Murugappan et al. [366] applied an extremum-seeking adaptive control algorithm to stabilize combustion instability in a swirl-stabilized spray combustor. A pressure transducer installed at the dump plane was utilized as a sensor. The sensor output was processed and used by the adaptive controller to modulate the fuel stream using a high-frequency valve. The extremum-seeking scheme was employed to determine the optimum phase delay required for instability suppression in real time. Control at the optimal phase was achieved within 1.75 s, with 43% and 79% reduction in pressure and heat flux oscillations, respectively.

Bernier et al. [404] reported an experimental study of adaptive control in a laboratory-scale premixed, prevaporized swirl combustor. The control scheme was based on a linear mean square (LMS) algorithm. The transfer function was identified through a finite impulse response (FIR) numerical filter. A direct measurement of the command and heat release signals was performed to validate the FIR identification technique. Two types of sensors, microphone and CH* chemiluminescence probe, were employed to obtain the flame response. Active control was exercised using secondary air modulation through a direct drive valve. The pressure oscillation amplitude was reduced by about 50%.

Riley et al. [405] demonstrated closed-loop active control in a gaseous lean-premixed swirl-stabilized combustor. An adaptive, model-based self-tuning regulator (STR) algorithm was adopted. A piezoelectric pressure transducer was used to measure the combustor pressure downstream of the swirler unit. Actuation was achieved using a direct drive valve (DDV), which modulated the fuel flow rate into the swirler and generated an equivalence ratio variation in the premixed duct. The STR controller required the total time delay between actuation and response as an input. This time delay was determined through open-loop forcing tests. A reduction of up to 30 dB in pressure magnitude at the primary instability frequency was obtained by adaptive control.

Sattinger et al. [406] applied an adaptive control technique to a subscale swirl combustor fueled by natural gas. A real-time observer was employed to identify the frequencies, amplitudes, and phases of the dominant instability modes. This observer could rapidly respond to changes in instability characteristics. A fast-response secondary fuel injector then introduced auxiliary fuel

flow for control action based on a phase-shift algorithm. The active control system resulted in a four-fold reduction in instability amplitudes. Other research studies on adaptive active instability control in swirl combustors were reported by Evesque et al. [371] and Banaszuk et al. [62].

6.2.4. Implementation in full-scale gas turbine systems

Although numerous active instability control techniques have been developed and applied to laboratory-scale research combustors, only a few full-scale implementations have been reported on gas turbine combustors in the past [48,63,407], and more recently by Richards et al. [408]. Practical full-scale implementations present several technological challenges. First, the active control hardware, i.e., sensors and actuators, must be sufficiently reliable for extended periods of use under the high-temperature and -pressure environment typical of industrial combustors. Second, the actuators must have sufficient power to damp instabilities without consuming too much energy. Third, designing actuators that can provide large modulation levels at relatively high frequencies, which might be in excess of 500 Hz or even 1000 Hz, still remains challenging. Thus, current full-scale implementations all have employed auxiliary fuel modulation and very simple controller algorithms, as discussed in detail in the following. Note that a full-scale AIC system was also demonstrated on the afterburner of a turbofan engine [409], but it will not be discussed here.

6.2.4.1. Annular combustors. The first full-scale demonstration of active instability control (AIC) on gas turbine systems was made in 1996 [48–50] in the Siemens test facility on the V84.3A heave-duty combustor with an electric power output of 160 MW. Later, a similar active instability control system was applied to the largest type of this family of gas turbines, the Siemens V94.3A, delivering 267 MW of electrical power.

Siemens Vx4.3A series gas turbine combustion systems, as shown in Fig. 6b, feature an annular combustor comprising 24 hybrid burners distributed peripherally. Fig. 6a shows a schematic drawing of a standard Siemens hybrid burner. This hybrid burner may be operated using either liquid and gaseous fuels. To stabilize premixed flames, the hybrid burner is equipped with an additional pilot fuel nozzle. During the development of this type of gas turbine systems, self-excited combustion instabilities were commonly

observed in various power ranges with different burner configurations. The instabilities were characterized by azimuthal, standing acoustic waves in the annular chambers.

An active control technique was developed to cure the instability problem. Fig. 69 provides a simplified schematic diagram of AIC design. The control system measured the acoustic pressures at the burner flanges as inputs. The wall temperatures were substantially lower around the burner flanges than in the combustor, so that the piezo pressure transducer could be used without requiring any additional cooling. Test result indicated that acoustic pressure signals measured at these two locations correlated sufficiently well in amplitude and phase. Active control was achieved by modulating the pilot gas supply using a Moog direct-drive-valve (DDV) actuator. These actuators allow the modulation of flow rate with frequencies of up to 400 Hz. Every burner was fitted with its own actuator, and 24 valves were installed around the annular combustor of the gas turbine.

According to Seume et al. [48], instabilities of azimuthal modes were excited within the annular combustion chamber. Since the burners and actuators for pilot gas supply were placed evenly along the circumference of the annular combustor, they were located at positions characterized by differing pressure amplitude and phase values. To obtain anti-phase and in-amplitude modulation of the unsteady flames, the AIC system required individual control of each pilot fuel actuator. The simplest case would therefore involve one sensor and one feedback loop for each burner, and result in a 24-channel AIC system.

To minimize the number of feedback loops, the AIC system took advantage of the spatial symmetry of azimuthal instability modes. This property is marked by a characteristic distribution of acoustic nodes and anti-nodes, i.e., regions of high and low amplitudes. These regions are related to each other by a constant phase-shift. Thus, the signal measured at a specific position by one sensor can be used to control not only the actuator for this position, but also the actuators located at several other locations. For Vx4.3A series combustors at lower part-load operation, where the dominant instability waves correspond to the second and forth harmonic azimuthal mode (Seume et al. [48]), an installation of the AIC system as shown in Fig. 70 was chosen. Here a total of four actuators were controlled by one input signal and one feedback loop. The combustor was fitted with six independent control loops, each consisting of a sensor and four valves.
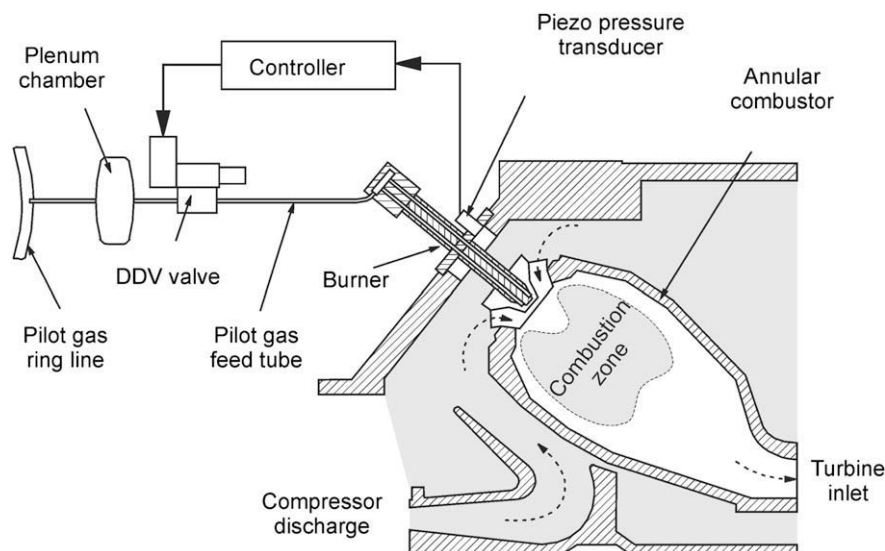
Fig. 69. Schematic of the Siemens model Vx4.3A heavy-duty gas turbine with active control setup (Hermann and Hoffmann [50]).

Fig. 71 shows the acoustic pressure spectrum with and without AIC during part-load operation. With the AIC activated, damping levels of 20 dB (second harmonic) and 14 dB (fourth harmonic) were achieved, respectively. Successful damping of combustion instabilities was also demonstrated under a wide range of operating conditions, irrespective of burner configurations.

6.2.4.2. Sector combustor. Hibshman et al. [63] designed and implemented active instability control systems on a full-scale three-nozzle sector combustor. Fig. 72 shows a cross section of the sector combustor test facility with the instrumentation and actuation systems. Three tangential-entry fuel nozzles (see Fig. 7a) were installed on a 67.5^0 sector rig cut from an aero-derivative annular combustor. In each fuel nozzle, air from the pre-diffuser entered tangentially, and liquid fuel was injected into the airflow through six axial spokes. The premixed and prevaporized fuel/air mixture left the fuel nozzle axially with streamwise swirl motions. No. 2 diesel was delivered to the sector combustor at a nominal flow rate of 460 kg/h. Experiments were operated over a wide range of equivalence ratios and inlet temperatures and pressures corresponding to realistic operating conditions (nominally 710 K and 1.5 MPa, respectively).

The control system was scaled up from a unit previously designed for use in a single-injector combustor (Cohen et al. [58], Banaszuk et al. [62]). Combustor pressure oscillations were measured using piezoelectric pressure transducers at two locations: downstream of the fuel nozzle exit and upstream of the diffuser. At each fuel nozzle, one of the six spokes was disconnected from the main fuel system, and was attached to a separately metered fuel system, in which fuel flow was modulated using a high-speed solenoid valve. The solenoid valves had a maximum operating frequency of approximately 250 Hz. An observer was used to identify the frequency and amplitude of the instability mode from measured pressure signal. Results were then fed back to the on/off control valve with a phase-shift. Active control through modulation of the fuel supply led to a 6.5-dB reduction in the amplitude of the dominant instability mode at approximately 200 Hz, retaining the same emissions characteristics.

6.2.4.3. Can combustor. Active instability control on a Siemens-Westinghouse dry-low-NO_x can-type combustor was reported by Johnson et al. [407]. The combustion system consisted of eight main premixing passages dumping into a common flame zone. The premixing passages were divided between two fuel stages, and each stage delivered fuel to four premixed passages. Natural gas was used as fuel. An additional central diffusion stage was employed for flame holding.

The active instability control system employed a pressure transducer installed near the upstream end of the flame zone in the combustor. The measured pressure was sent to a real-time observer that determined the characteristics of a specified number of the "most unstable" modes according to their relative amplitudes. The output from the real-time observer was transferred to the controller in order to determine the optimal phase and gain required to attenuate each unstable mode. Results were then used to generate a control signal that was amplified and sent to a fuel modulation system consisting of a fuel valve driven by a magneto-strictive actuator. The fuel valve actuator could provide up to 250 g/s mean flow and excite flow rate modulation with a peak-to-peak amplitude of 100 g/s in the frequency ranges of 0–1000 Hz.

Two control actuation configurations were investigated. In the first configuration, the actuator was mounted on one of two premixed fuel stages, and in the second configuration, it was attached to the stabilizing diffusion fuel stage. The former could provide larger flow rate modulation, but the latter might be more efficient, since the fuel injection location was very close to the heat release zone. In both configurations, the active control system attenuated the dominant acoustic modes by up to 15 dB and reduced the overall broadband noise by 30–40%. NO_x emissions were also reduced by approximately 10% when control was applied. Similar control systems were previously tested on a laboratory-scale gas rocket combustor (Neumeier and Zinn [410,345]) and a subscale lean-premixed combustor (Sattinger et al. [406]).

7. Modeling and simulation of combustion dynamics

7.1. Numerical simulation of lean-premixed gas turbine combustion dynamics

7.1.1. Turbulence modeling strategies: RANS and LES

Most flows occurring in engineering applications are turbulent, and turbulence continues to present engineering challenges due to its strong nonlinear behavior. One of the characteristics of a turbulent flow is that various length scales co-exist in the global
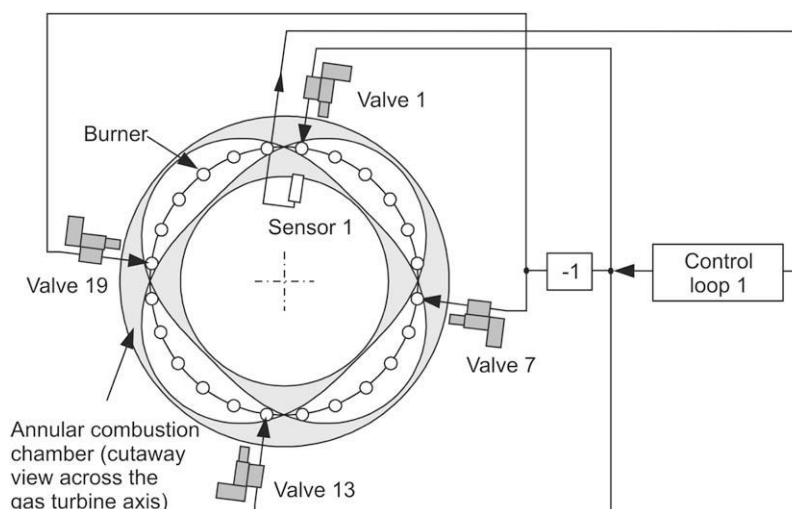
Fig. 70. Schematic of the Siemens active control system. To suppress the second, symmetric azimuthal mode, one sensor and one controller provide the input signals for four DDVs (Hermann and Hoffmann [50]).
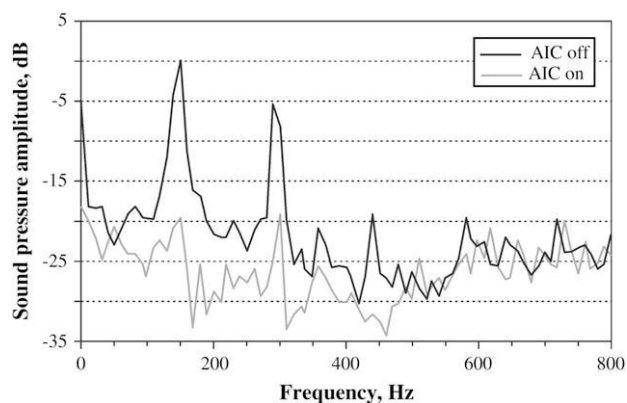
Fig. 71. Suppression of pressure oscillations by AIC during part-load operation of Siemens V94.3A gas turbine (Hermann and Hoffmann [50]).

structure, and each length scale functions differently. According to Kolmogorov's energy cascade hypothesis, large-scale eddies extract kinetic energy from the bulk flow, and transfer it (by inviscid processes) to successively smaller and smaller scale eddies, until the energy is dissipated into internal heat at the smallest scales. Large-scale eddies are anisotropic, and are strongly dependent on flowfield geometries. Small-scale eddies tend to be more homogeneous and universal, and less affected by flow boundary conditions (Tennekes and Lumley [423], Pope [424], Mathieu and Scott [425]).

Numerical simulation of turbulent flows may be classified into three categories: direct numerical simulation (DNS), large-eddy simulation (LES), and Reynolds-averaged Navier-Stokes simulation (RANS). DNS has been applied to turbulent premixed and non-premixed combustion with simple geometries and low Reynolds numbers (Givi [426], Poinsot et al. [427], Vervisch and Poinsot [428]). The main role of DNS is to provide fundamental insight into turbulent flows and their interactions with flames, and to help develop and validate turbulence sub-models. In most industrial applications, the Reynolds number is far too high to resolve all relevant spatial and temporal scales directly without turbulent modeling. RANS has been commonly used for engineering applications due to its reasonable computer resource requirements. These simulations have offered valuable information, which cannot be gathered by experimental investigations. In RANS, the effect of turbulent fluctuations (represented by the Reynolds stress tensor terms in Reynolds-averaged conservation equations) needs to be modeled to achieve closure of the system. A wide range of models
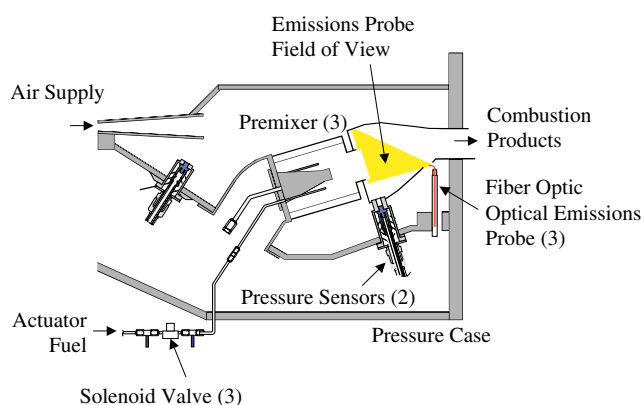
Fig. 72. Cross-section of three-premixer sector combustor test facility with instrumentation and actuation system (Cohen et al. [61]).

for the Reynolds stresses have been developed, ranging from simple algebraic models, to $k - \varepsilon$ two equation models, to full-Reynolds stress closure. RANS may be appropriate for time-mean turbulent flow properties, but its validity for unsteady flow evolution has yet to be established, especially for problems involving such complicated configurations as swirling flows with recirculation. Nevertheless, some research studies (Steele et al. [33], Brookes et al. [429], Zhu et al. [430–432]) have demonstrated that RANS was able to capture fully developed combustion-driven oscillations under certain conditions, and obtained good agreement with limited experimental data. Brewster et al. [433] conducted a comprehensive review of RANS-based numerical simulations for stationary gas turbine combustion.

LES computes the contributions of large energy-carrying structures to mass, momentum, and energy transfer, with the effects of small-scale turbulence modeled either analytically or empirically. LES is a particularly attractive approach for the study of gas turbine combustion dynamics, since the flowfield of concern is highly unsteady and dominated by turbulence motions that can be adequately resolved computationally. In LES, subgrid scale (SGS) turbulence models, as well as turbulent combustion models, are required for closure. Since small-scale turbulent motions tend to be more isotropic and universal, and less affected by boundary conditions, their behavior can be represented by simple models, which require limited adjustments when applied to various flows (Piomelli [434]). The main function of the SGS turbulence model is to mimic the drain of energy associated with the energy cascade, i.e., to remove energy from resolved large-scale motions. Eddy-viscosity type models based on Boussinesq's hypothesis are widely used. The Smagorinsky model [435,436] and Erlebacher's model (a compressible flow version of the Smagorinsky model [437]) are representatives of this class. In Smagorinsky-type models, the assumption of the equilibrium flow of kinetic energy cascade is adopted. The model coefficients are prescribed, and can be determined from isotropic turbulence decay. However, ad hoc modifications, such as wall functions or intermittency functions, are usually needed to tune the anisotropic flow properties near the boundary. In addition, the Smagorinsky model does not consider the kinetic energy backscatter phenomenon. The dynamic models proposed by Germano et al. [438] and Ghosal et al. [439] relax the equilibrium assumption, and are able to treat non-equilibrium flows by calculating model coefficients based on Germano's identity. This model makes use of the scale-invariance assumption and determines model parameters from the resolved scales during the simulation, thus avoiding the need to prescribe or tune the coefficients. The dynamic models have demonstrated the possibility of the application of LES to a variety of flows in complex engineering geometries (Moin [440]). They have the potential to properly treat the energy backscatter phenomenon by allowing negative coefficients, although this treatment may lead to numerical difficulties (Da Silva and Pereira [441]). Many other different types of SGS models have been proposed, including one equation models (Schumann [442]), two-point closure (Kraichnan [443], Chollet and Lesieur [444], Metais and Lesieur [445]), scale-similar and mixed models (Bardina et al. [446], Liu et al. [447]), the MILES model (Boris et al. [448]), and the deconvolution model (Domaradzki and Saiki [449], Domaradzki and Loh [450], Stolz and Adams [451]), to name only a few. More detailed reviews on SGS models can be found in Refs. [424,434,452,453].

Although the RANS approach currently remains the main workhorse for combustor design analysis [433], LES is considered to be the next-generation analytical design tool for gas turbine combustors. In an effort to identify and describe the flow and flame phenomena within the CFM56 aero-engine swirl cup, a series of numerical investigations have been performed using both RANS

and LES techniques [116,454–461]. The LES method was also implemented to facilitate industrial combustor designs [462,463,464,533].

7.1.2. Regime diagram of premixed turbulent combustion

Premixed turbulent combustion involves a wide range of length and time scales associated with chemical reactions and flow motions. According to the relative magnitudes of these scales, regime diagrams defining different modes of combustion have been proposed by various researchers (Borghi [465], Williams [466], Abdel-Gayed and Bradley [467], Peters [468], Poinsot and Veynante [469]). Peters [468] examined the problem of turbulence/chemistry interactions in terms of two non-dimensional parameters, the turbulent Reynolds number Re and turbulent Karlovitz number Ka, as defined below

$$Re \approx v'l/S_L l_F \tag{7.1}$$

$$Ka = t_F/t_\eta \approx l_F^2/\eta^2 \tag{7.2}$$

where v' is the turbulent velocity fluctuation, l the turbulent integral length scale, S_L and l_F the flame speed and thickness, respectively, t_F and t_η the flame and the Kolmogorov time scales, respectively, and η the Kolmogorov length scale. Another Karlovitz number, Ka_δ, defined as the square of ratio of the flame inner layer thickness l_δ to the Kolmogorov length scale η, is also introduced. Based on the relative scales of these parameters, premixed turbulent combustion can be classified into four different regimes, as shown in Fig. 73. Corrugated flamelets occur when $Re > 1$, $v'/S_L > 1$ and $Ka < 1$. In this regime, the turbulent velocity fluctuation v' is large enough to allow eddies to corrugate the flame front. The smallest eddies of size η, however, are still larger than the laminar flame thickness l_F, and thus cannot modify the flame structure. The interaction between eddies of all sizes and the laminar flame structure is purely kinematic. The chemical and transport processes within the flame remain essentially unchanged. A thin reaction zone exists when $Re > 1$, $v'/S_L > 1$, $Ka > 1$ and $Ka_\delta < 1$. In this regime, the smallest eddies of size η are smaller than the laminar flame thickness l_F, and can penetrate into the bulk of the flame structure. They cannot, however, enter into the inner layer because the smallest eddies are larger than the thickness of the inner layer. Although the local transport of chemical species and energy is enhanced in the preheat zone, the chemical reactions that sustain the flame are essentially uninfluenced by turbulence, since they do not penetrate into the inner layer. The wrinkled flamelet regime ($Re > 1$, $v'/S_L < 1$ and $Ka < 1$) and the broken reaction zone ($Re > 1$, $v'/S_L > 1$ and $Ka_\delta > 1$) are two extreme situations with very weak turbulence intensity or with very small turbulence eddies, which can alter the chemical reactions in the inner layer. In both the thin reaction zone and flamelet regimes, the inner layer of the laminar flame structure is not affected by turbulence. The premixed turbulent flame can be treated as a synthesis of thin reaction–diffusion layers, commonly referred to as flamelets, embedded in an otherwise inert turbulent flowfield. In practical systems, combustion may span several regimes in their operational envelopes. Although turbulence/chemistry interactions may occur in the broken reaction zone regime in certain circumstances, for example, near the lean blowout limit (Eggenspieler and Menon [470]), chemical reactions are often confined in thin, sheet-like flamelets under most conditions in many practical combustion devices (Poinsot et al. [471], Linan and Williams [472], Peters [468], Driscoll [473]).

7.1.3. LES of premixed turbulent combustion

Turbulent combustion modeling for both premixed and non-premixed flames has been the subject of extensive research studies
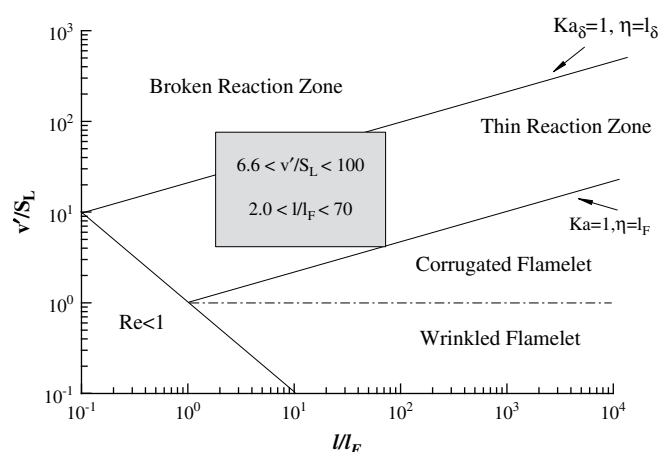
Fig. 73. Regime diagram of premixed turbulent combustion.

for several decades. A large number of models have been proposed and tested in the context of RANS. Detailed reviews on this topic are given by Borghi [465], Pope [474], Bray [475], Candel et al. [476], Peters [468], Veynante and Vervisch [477], and recently by Bilger et al. [478]. In the treatment of turbulent reacting flows within the context of LES, as with RANS simulations, detailed flame structures are often not resolved, and combustion models are needed at subgrid scales (SGS) (Candel et al. [476]). Modeling of the SGS reaction rate terms using the Arrhenius law based on filtered quantities (i.e., no SGS combustion model) often under-predicts the global turbulent burning rate, since the unresolved flame is wrinkled at scales below the LES resolution, which typically increases the global reaction rate (Charlette et al. [479]), and thus may lead to unexpected flame blow-off (Boger et al. [480]). Since for both RANS and LES simulations, chemical reactions usually occur at unresolved scales, similar modeling techniques may apply for both cases. Many RANS combustion models thus have been adapted to LES simulations with slight modifications, such as the G-equation model and the flame surface density model.

Table 3 summarizes a variety of approaches that have recently been employed to perform LES of premixed turbulent combustion. These models can be broadly classified into two categories: flamelet and non-flamelet models. Flamelet models, such as the flame-surface density approach, flame-wrinkling model and level-set model, generally assume chemical reactions to be confined in a thin, sheet-like laminar flame structure whose inner layer is unaffected by turbulence, a situation that occurs in many combustion systems (Peters [468], Hawkes [481]). In the following, the combustion models listed in Table 3 are briefly reviewed.

Eddy-break-up (EBU) type models usually assume that the fuel reaction rate is controlled by a characteristic turbulent time scale (Candel et al. [476]), although a chemical time scale can be included (Furbey and Lofstrom [482], Furbey and Moller [483], Moller et al. [484]). The models often tend to over-estimate the reaction rate within the context of RANS. For LES, the model constants seem to be strongly dependent on flow conditions and numerical mesh size (Candel et al. [476], Furbey and Lofstrom [482]). The eddy-break-up type model may be improved through use of a fractal model for subgrid scale structures (Giacomazzi et al. [485]). In thickened flame models (Thibaut and Candel [486], Angelberger et al. [487], Charlette et al. [479], Colin et al. [488]), the flame is artificially broadened by increasing the thermal diffusivity, while keeping the flame propagation properties (i.e., flame speed) unchanged by reducing the reaction rate. The resultant thickened flame can thus be resolved on the LES grid using the Arrhenius law. Thickened

flame models are widely used because of their capability of treating complex chemistry and transient phenomena such as ignition, extinction, and flame–wall interaction. As indicated by Colin et al. [488], the Damkohler number (defined as the ratio of turbulent to chemical time scale) varies in this approach. The ensuing modification of the flame response to turbulent motions may introduce some unknown effects in the simulation of combustion dynamics. To overcome this deficiency, a flame wrinkle function (Nottin et al. [489]) and an approximate deconvolution model (Mathew [490]) were proposed to compensate for the modified turbulence/chemistry interactions of the thickened flame.

In the linear-eddy model (Chakravarthy and Menon [491,492]), the large-scale, resolvable scalar processes are simulated explicitly on the LES grid, while SGS turbulent processes and chemical reactions occurring within each numerical cell are treated using a one-dimensional model. This approach is complex and time-consuming, since the one-dimensional model is applied in each cell and the advection of scalars between LES cells requires additional treatment. In the flame surface density approach (Boger et al. [480], Hawkes and Cant [481,493]), similarity model (Knikker et al. [494]), flame-wrinkling model (Weller et al. [495]; Furbey [496]), and turbulent flame-speed closure model (Flohr and Pitsch [497]), a filtered progress variable is usually solved. The unclosed reaction source term is modeled by introducing an SGS flame surface density, an SGS flame-wrinkling factor (defined as the ratio of the SGS flame surface area to its projection in the propagation direction), or an SGS turbulent flame speed. The first two parameters can be obtained from either an algebraic expression (Charlette et al. [479,498]; Boger et al. [480]; Knikker et al. [494]) or a balance equation (Hawkes and Cant [493]), while the last parameter comes from existing theoretical and experimental data for turbulent flame speed. In general, modeling of these three terms is closely related to flame-wrinkling effects caused by unsolved turbulent motions.

The G-equation approach attempts to describe premixed turbulent combustion from a geometrical point of view. The flame front is represented by an arbitrary iso-surface G_0 in a scalar field G whose evolution is formulated using the so-called G-equation. Since the G-field outside the flame front is not uniquely defined, several approaches can be used. Menon and his colleagues (Menon and Jou [499]; Kim et al. [500]) regarded G as a progress variable (i.e., $G = 0$ and 1 for the fresh unburnt and burnt gases, respectively). The model is simple and easy to implement, but the numerical difficulties and grid resolution may incorrectly broaden the flame [499,500]. Peters [468], on the other hand, proposed a level-set approach that defines G as a distance function outside the flame front, where the flame front position is given by $G = 0$. The model requires the SGS flame thickness as an input, which can be obtained either from an analytical model or by solving the transport equation of G variance. This approach, along with a laminar flamelet library and a presumed PDF method, decouples the chemistry computationally from turbulence, and thus offers a realistic treatment of premixed turbulent flame dynamics. The level-set approach has been extensively explored by Peters in his monograph [468] and tested by Herrmann [501], Nilsson and Bai [502] and many others within the context of RANS. Its application to LES has recently received substantial attention (Pitsch and Duchamp de Lageneste [503], Huang et al. [199], Wang and Bai [504], Janicka and Sadiki [505]).

The probability density function (PDF) method provides an alternative way to overcome closure problems in turbulent reacting flow simulations [506]. In this approach, the statistical moments of any flow variable are directly determined from joint velocity-composition PDFs. There are two ways to construct PDFs: presumed and calculated PDF. In the former method, PDF shapes are obtained using empirical knowledge and its application is usually limited to relatively simple reaction systems, which can be described by one

Table 3
Survey of LES combustion models for premixed turbulent flame.

Model description	Application	References	Remarks
Eddy-break-up type model	Triangular-shaped bluff-body	Fureby and Lofstrom, 1994 [482]; Fureby and Moller, 1995 [483]; Moller et al., 1996 [484]	Filtered reaction rate determined by subgrid-scale mixing and chemical kinetics
Fractal model	Premixed bluff-body flame	Giacomazii et al., 2004 [485]	Eddy dissipation concept along with the fractal model; chemical reactions are assumed to take place only at the dissipative scales of turbulence
Thickened flame model	Backward-facing step; premixed dump combustor; Premixed flame in decaying isotropic turbulent flow	Thibaut and Candel, 1998 [486]; Angelberger et al., 2000 [487]; Charlette et al., 2002 [479,498]; Colin et al., 2000 [488]; Nottin et al., 2000 [489]	Arrhenius law used for artificially thickened flame
Approximate deconvolution model	Premixed triangular flame holder	Mathew, 2002 [490]	Effect of unresolved small scales turbulence on the reaction rate is assumed to be small; useful for thick or thickened flames
Linear-eddy model	Turbulent stagnation point premixed flame	Chakravarthy and Menson, 2000 [491], 2001 [492]	Small-scale turbulence and chemical process treated using a one-dimensional model
Flame surface-density approach	Freely propagating turbulent premixed flame	Boger et al., 1998 [480]; Hawkes and Cant, 2001 [481], 2000 [493]	Filtered reaction rate modeled by introducing flame surface density
Similarity model	Premixed triangular flame holder	Knikker et al., 2002 [494]	Flame front is assumed to behave like a fractal surface at scales larger than a cutoff scale
Flame-wrinkling model	Rearward-facing step; triangular-shaped bluff-body	Weller et al., 1998 [495]; Fureby, 2000 [496]	Filtered reaction rate estimated using flame-wrinkling factor
Turbulent flame-speed closure model	Backward-face step combustor	Flohr and Pitsch, 2000 [497]	Turbulent flame speed used to model filtered reaction term
G-equation model based on progress variable	Swirl-stabilized gas turbine combustors	Kim et al., 1999 [500]; 2000 [517]	Flame front evolution described using G-equation based on progress variable
Level-set approach	Turbulent Bunsen burner; Swirl-stabilized combustor	Duchamp de Lageneste and Pitsch, 2002 [503]; Huang et al., 2003 [199], 2004 [198]	Flame front evolution governed by a level-set equation

or two scalars. The latter method solves the transport PDF equations, and chemical reaction source terms appear in closed-form. An unclosed molecular-mixing term exists in transport PDF equations, however, and its modeling is very challenging. In addition, the dimensionality of equations increases with the number of species. The Monte Carlo technique is usually used to calculate transport PDF equations; it requires significant computer resources. The transport equations for subgrid scale PDF in the context of LES have been derived (Gao and O'Brien [507], Colucci et al. [508], Jaberi et al. [509]) and applied to study non-premixed combustion (Sheikhi et al. [510], Raman et al. [511]). This methodology has not yet been extensively tested in the LES study of premixed turbulent combustion. A recent review on large-eddy simulation of premixed turbulent combustion can be found in Ref. [512].

7.1.4. LES of premixed combustion dynamics in gas turbine engines

The literature on LES studies of lean-premixed combustion with gas-fueled swirl injectors up to 2000 was previously reviewed by Huang et al. [199]. More studies have appeared recently. Table 4 summarizes recently published three-dimensional simulations of gas turbine combustion using both gaseous and liquid fuels. Many two-dimensional LES studies can also be found in the literature [486,513,514,515]. These two-dimensional analyses, despite the lack of vortex-stretching mechanisms, have been shown to be able to capture some salient features of turbulent flowfields and unsteady flame propagation. Three-dimensional simulations are usually more desirable, however, for a proper and comprehensive description of unsteady turbulent flame evolution.

As Table 4 indicates, simulations have been performed for both laboratory-scale research combustors and industry test rigs including GE, Rolls-Royce, and Pratt & Whitney combustors. The combustor configurations in existing LES studies are usually confined to a single swirl injector, due to limitations of computer resources. The flow/flame coupling between injectors can only be partially simulated, if at all. Nonetheless, attempts have been made to model the flame dynamics in an array of injectors [516].

The majority of simulations have been carried out for gaseous fuels. As compared to gaseous fuels, liquid spray combustion involves an additional array of intricacies, such as atomization, droplet dispersion and evaporation, mixing, and combustion. All these processes must be considered for accurate prediction, but many of them have not yet been fully understood and well modeled for highly turbulent environments typical of gas turbine combustors. Thus, only a few LES studies of liquid-fueled swirl combustors have been reported [531,534,536,541]. Several three-dimensional simulations of non-premixed swirl combustors have recently appeared [528,530], and are also given in Table 4 for reference. Turbulent combustion models used in these LES studies of premixed or partially premixed gaseous flames include Arrhenius rate expression, thickened flame model, *G*-equation model based on progress variable, level-set *G*-equation model, and flame-wrinkling model. For gaseous non-premixed and liquid-fuel simulations, the Arrhenius rate expression [531,532] and linear-eddy model [540,541] were used. Almost all of the simulation results compare favorably with experimental data to some extent, although uncertainties still remain.

Substantial efforts have been applied to study the dynamic behavior of gas turbine combustion. Stone and Menon [520,521] investigated the effects of swirl and equivalence ratio on flame dynamics in a swirl combustor. Schluter [524] examined the role of large-scale vortices on combustion oscillations in a coaxial combustor with and without swirl. Roux et al. [118] treated a premixed swirl burner for both non-reacting and reacting cases. A strong precessing vortex core was observed in the nonreacting flows. This vortex, however, disappears when combustion occurs.

Selle et al. [117] reported similar observations in an industrial swirl burner. Grinstein and Fureby [526] simulated the flowfield in a swirl combustor, with emphasis on the effects of combustor confinement on the flow and flame evolution. Sommerer et al. [523] conducted an investigation of the flashback and blow-off in a lean partially premixed swirl burner. Duwing and Fuchs [527] studied the flame stabilization phenomena in a swirl combustor. Huang and Yang [198,199,522] examined the influences of inlet flow conditions on the combustion dynamics in a lean-premixed swirl-stabilized combustor. The flame bifurcation phenomenon and stability boundary were investigated as a function of burner operating conditions. Shinjo et al. [545] and Sengissen et al. [543] studied the secondary fuel injection and fuel modulation on unsteady combustion behavior in swirl-stabilized combustors, respectively. Pollutant emissions and temperature profile in swirl combustors were also predicted by Cannon et al. [519], Eggenspieler and Menon [525], Schmitt et al. [542], and Boudier et al. [544].

The aforementioned LES studies have generated an avalanche of information about the combustion dynamics and flow evolution in specific geometries of concern under well-defined operation conditions. A huge database has been established, which, however, may not lead to a corresponding enhancement of our knowledge if the numerical results are not effectively analyzed. The LES computations themselves represent meticulous exploratory numerical experiments, and it is important to be able to extract phenomenological information contributing to a deeper understanding and subsequent modeling of the processes of concern from these large quantities of detailed flow and combustion data. Huang et al. [244] attempted to establish a comprehensive and systematic methodology to explore the dynamic processes in gas turbine combustors and to identify the underlying mechanisms and key parameters dictating the combustion characteristics. Various data processing and analysis approaches were developed and implemented in the context of a time-resolved numerical database for an LPM swirl-stabilized combustor. These include triple decomposition of flow properties, vortex identification, spectral analysis, linear acoustic modal and hydrodynamic stability analyses, and proper orthogonal decomposition (POD).

These simulations have demonstrated the capabilities of LES techniques as a design tool for gas turbine combustion with complex geometries. In the next section, a recent example representing the state-of-the-art in LES of gas turbine combustion is presented.

7.1.5. LES study of LPM single-element swirl injector
7.1.5.1. Theoretical formulation, numerical method, and physical model.
LES was performed to study the combustion dynamics of an LPM swirl-stabilized combustor [199,244,522], simulating the experimental conditions reported in Refs. [195] and [196]. The formulation employs the Favre-filtered conservation equations of mass, momentum and energy in three dimensions. The subgrid-scale (SGS) terms are modeled using a compressible-flow version of the Smagorinsky model suggested by Erlebacher et al. [437]. The damping function of Van-Driest is used to take into account the flow inhomogeneities near the walls. A level-set flamelet library approach is applied to simulate premixed turbulent combustion.

Boundary conditions must be specified to complete the formulation. At the inlet boundary, the mass flow rate and temperature are specified. The pressure is obtained from a one-dimensional approximation to the axial momentum equation, i.e., $\partial p/\partial x = -\rho\partial u/\partial t - \rho u\partial u/\partial x$. The mean axial velocity distribution follows the one-seventh power law by assuming a fully developed turbulent pipe flow. The radial and azimuthal velocities are

Table 4
Survey of large-eddy simulations of gas turbine combustion since 2000.

Physical configuration	Turbulent combustion model	Grid resolution and numerical method	References	Remarks
General Electric LM6000 lean-premixed combustor with rectangular chamber	Flamelet G-equation model	0.5 Million structured grids; finite volume discretization; second-order explicit time integration	Kim et al., 1999 [500]; 2000 [517]	Mean and rms of velocity components
DOE-NETL lean-premixed swirl combustor with axisymmetric chamber	Arrhenius rate expression	0.796 Million unstructured cells; finite volume discretization; second-order implicit time integration	Cannon et al., 2001 [518]; 2003 [519]	Comparison of 3D RANS and LES simulation results
Lean partially premixed, swirl-stabilized combustor with axisymmetric chamber	Flamelet G-equation model along with mixture fraction Z equation	1.07 Million structured grids; finite volume discretization; predictor-corrector time integration	Stone and Menon, 2002 [520]; 2003 [521]	Control of combustion instabilities through swirl and equivalence ratio variations
General Electric DACRS combustor using liquid fuel	Arrhenius rate expression	0.86 Million grids; finite volume discretization; second-order explicit time integration	Sankaran and Menon, 2002 [531,532]	Velocity profiles and droplet distribution
Lean-premixed swirl-stabilized combustor with axisymmetric chamber	Flamelet level-set G-equation model	3.44 Million structured grids; finite volume discretization; four-stage Runge–Kutta time integration	Huang et al., 2003 [199], 2005 [522]; 2006 [244]	Flame bifurcation phenomenon and stability boundary
Siemens premixed swirl burner with rectangular chamber	Thickened flame model	2.38 Million unstructured cells; finite volume discretization; third-order explicit time integration	Selle et al., 2004 [117]; 2006 [538]	Precessing vortex core
Lean partially premixed swirl burner with axisymmetric chamber	Thickened flame model	0.7 Million hybrid grids; finite volume discretization; third-order explicit time integration	Sommerer et al., 2004 [523]	Flame flashback and lean blow-off
Premixed axisymmetric combustor with and without swirl	Flamelet G-equation model	1.6 Million grids; finite volume discretization	Schluter, 2004 [524]	Control of combustion oscillations by coaxial flows
DOE-HAT premixed swirl combustor with axisymmetric chamber	Flamelet G-equation model	1.8 Million grids; finite volume discretization; second-order explicit time integration	Eggenspieler and Menon, 2004 [525]	Pollutant emissions
Non-premixed coaxial jet combustor	Flamelet/progress variable model along with presumed PDF approach	2.45 Million grids; staggered space-time, conservative discretization; semi-implicit time integration.	Pierce and Moin, 2004 [528]	Velocity, temperature and concentration profiles
Non-premixed can-type combustor representative of the Rolls-Royce Tay gas turbine	Flamelet model along with presumed PDF approach	1.02 Million grids; finite difference discretization; fully implicit time integration.	Jones, 2002 [529]; Di Mare et al., 2004 [530]	Temperature and concentration profiles
Premixed swirl combustor	Thickened flame model	3.0 Million unstructured cells; finite volume discretization; third-order explicit time integration	Roux et al., 2005 [118]	Precessing vortex core
General Electric LM6000 lean-premixed combustor with rectangular or axisymmetric chamber	Flame-wrinkling model and Arrhenius rate expression	0.85 or 1.5 Million grids; finite volume discretization; predictor-corrector time integration	Grinstein and Fureby, 2005 [526]	Effect of combustor confinement geometry on flame dynamics
Premixed swirl-stabilized combustor with rectangular chamber	Flamelet formulation based on progress variable with flame-wrinkling treatment	1.8 Million grids; finite difference discretization; fully implicit time integration	Duwig and Fuchs, 2005 [527]	Flame stabilization; effect of inlet velocity and equivalence ratio profiles
Single-sector of an annul combustor	Eddy-breakup model	1.0 Million grids; finite volume discretization, structured grid; second-order backward difference time integration.	James et al., 2006 [533]	Mean exit mixture fraction profile
Pratt & Whitney combustor using liquid fuel	Flamelet/progress variable model along with PDF approach	1.9 Million grid points; Finite volume discretization; fully implicit second-order time integration	Moin, 2004 [535]; Mahesh et al., 2006 [536]; Moin and Apte, 2006 [537]	Validation of the numerical tool
Premixed staged swirl combustor	Thickened flame model	0.5 Million nodes; finite volume discretization; third-order explicit time integration	Martin et al., 2006 [539]	Flame/acoustics interactions
General Electric-2 sector combustor consisting of two cups using liquid fuel	Linear-eddy model	6.9 Million structured grids; finite volume discretization; second-order explicit time integration	Menon and Patel, 2006 [540]	Fuel/air mixedness and exit emission profile
Lean direct injection swirl combustor	Linear-eddy model	2.2 Million grids; finite volume discretization; second-order explicit time integration	Patel et al., 2007 [541]	Spary dispersion, fuel/air mixing and flame stabilization
Lean partially premixed cone-shaped swirl burner	Thickened flame model	3.0 Million tetrahedral cells; finite volume discretization; centred spatial scheme and explicit time integration	Schmitt et al., 2007 [542]	Heat transfer, nitric oxide emissions, and combustion instability
Partially premixed swirl burner	Thickened flame model	2.7 Million tetrahedral cells; finite volume discretization; third-order explicit time integration	Sengissen et al., 2007 [543]	Effect of fuel modulation on flame dynamics

Table 4 (*continued*)

Physical configuration	Turbulent combustion model	Grid resolution and numerical method	References	Remarks
Premixed annular combustor with multiple perforated plates and film cooling	Thickened flame model	1.55 Million tetrahedral cells; finite volume discretization; third-order explicit time integration	Boudier et al., 2007 [544]	Exit radial temperature distribution
Lean partially premixed swirl-stabilized combustor with rectangular chamber	Flamlet G-equation model along with mixture fraction Z equation	10.0 Million structured grids; finite volume discretization; multistage Runge–Kutta time integration	Shinjo et al., 2007 [545]	Effect of secondary fuel injection on flame dynamics

determined from the swirler vane angle. Turbulence properties at the inlet are specified by superimposing broadband disturbances with an intensity of 15% of the mean quantity onto the mean velocity profiles. In addition, the acoustic response to disturbances arising from downstream is modeled by means of an impedance function (Huang et al. [199]). At the outlet boundary, the characteristic conditions proposed by Poinsot and Lele [546] are applied, and a time-invariant back pressure is specified. Finally, the no-slip adiabatic conditions are enforced along all the solid walls.

The resultant governing equations and boundary conditions are solved numerically by means of a density-based, finite volume methodology. The spatial discretization employs a second-order, central-differencing method in generalized coordinates. Fourth-order matrix dissipation along with a total-variation-diminishing switch developed by Swanson and Turkel [547] and tested by Oefelein and Yang [548] is included to ensure computational stability and to prevent numerical oscillations in regions with steep gradients. Temporal discretization is obtained using a four-step Runge–Kutta integration scheme. A multi-block domain decomposition technique along with static load balance is used to facilitate the implementation of parallel computation with message passing interface at the domain boundaries. A more detailed description of the theoretical formulation and numerical methods can be found in Ref. [199].

The physical model considered was a single swirl injector with an axisymmetric chamber and a choked nozzle, as shown in Fig. 12. Gaseous methane was injected radially from the centerbody through ten holes immediately downstream of the swirler vanes. The fuel/air mixture was assumed to be perfectly premixed before entering the combustor. The chamber measurements were 45 mm in (diameter) and 235 mm in (length). The baseline condition includes an equivalence ratio of 0.573 and a chamber pressure of 0.463 MPa. The mass flow rates of the natural gas and air were 1.71 and 50.70 g/s, respectively. The inlet flow velocity of 86.6 m/s produced a Reynolds number of 35,000 based on the height of the inlet annulus. The inlet temperature of 660 K was chosen to match the case of unstable combustion reported in Refs. [195] and [196].

According to the experimental observations, the dominant acoustic motion in the axial direction corresponds to the first longitudinal mode. Since there exists an acoustic pressure node at the middle of the chamber, the computational domain included a portion of the inlet annulus downstream of the swirler vane and the upstream half of the chamber, with a time-invariant back pressure specified at the exit plane. To avoid the numerical singularity along the combustor centerline, a central-square grid system (consisting of a square grid near the centerline and a cylindrical grid in the outer region) was adopted. The entire grid system had approximately 3.44 million ($301 \times 141 \times 81$) points, which were clustered in the shear layers downstream of the dump plane and near the solid walls in order to resolve the steep flow gradients in these regions. The largest grid spacing (around 0.7 mm) fell in the inertial sub-range of the turbulent kinetic energy spectrum based on the inlet Reynolds number. The computational domain was divided into 72 blocks. All the calculations were conducted on

a distributed-memory parallel computer with each block calculated on a single processor.

7.1.5.2. Oscillatory flame structures. Three different swirl numbers, $S = 0.44$, 0.76 and 1.10, were investigated for oscillatory flame dynamics. For $S = 0.44$, there were three dominant modes at the frequencies of 1761, 10,367 and 17,618 Hz, corresponding to the first longitudinal (1L), first tangential (1T) and second tangential (2T) modes of acoustic motions in the chamber, respectively. For $S = 0.76$, the frequencies of these three modes shifted slightly to 1795, 10,970, and 17,356 Hz due to the change in the temperature field. For $S = 1.10$, the longitudinal wave disappeared, and the frequencies of the 1T and 2T modes changed to 10,795 and 18,133 Hz.

Fig. 74 shows snapshots of the vorticity magnitude and temperature fields on the $x - r$ and $r - \theta$ planes for swirl number $S = 0.44$. The temperature fields clearly exhibit enveloped flames anchored at the rim of the centerbody and the corner of the backward-facing step. Large vortical structures arise in the shear layers downstream of the dump plane. In addition to the swirl-induced vorticity, the volume dilation and baroclinic effects in the flame zone significantly contribute to the production of vorticity. These vortices are convected downstream, breakup into small-scale eddies, and are eventually dissipated by turbulent diffusion and viscous damping. The vortex shedding frequencies are close to that of the first tangential mode of the acoustic wave in the chamber. Flames are contorted and convoluted by these vortex structures, thus revealing the interactions between the local flow evolution and the flame dynamics.

Fig. 75 shows snapshots of the iso-vorticity surface at $\omega = 75,000$ 1/s. The flowfield in the region $r > 2$ cm is blanked to provide a clear picture of the vortex structures. For the low swirl number case with $S = 0.44$, a vortex spiral evolves from the shear layer originating at the backward-facing step, due to the Kelvin–Helmholtz instabilities in both the axial and azimuthal directions. This vortical structure gyrates around the centerline and persists for several turns before breaking up into small fragments. For the high swirl number case with $S = 1.10$, a spiral vortex structure can also be observed. The structure, however, is much more complex, due to the high centrifugal force. It spreads outward rapidly and soon breaks up into small-scale structures. The evolution of these spiral vortex structures can be regarded as a kind of vortex shedding process with well-defined frequencies, as indicated in Fig. 74. The acoustic oscillation in the combustor actually acts as a forced excitation to the system. The shear layers respond to the excitation by locking their shedding frequencies close to the forcing frequency.

Fig. 76 presents the temporal evolution of the isothermal surface at $T = 1700$ K over one cycle of the 1L mode of acoustic oscillation at $S = 0.44$. The phase angle θ is referenced to the 1L acoustic pressure at the chamber head-end. The entire process is dictated by the cold flow entrainment into, and mixing with, hot gases in the vortical structures in the flame zone. Fig. 77 shows the time histories of the pressure immediately downstream of the dump plane (top), the total flame surface area (middle) and the rate of heat release
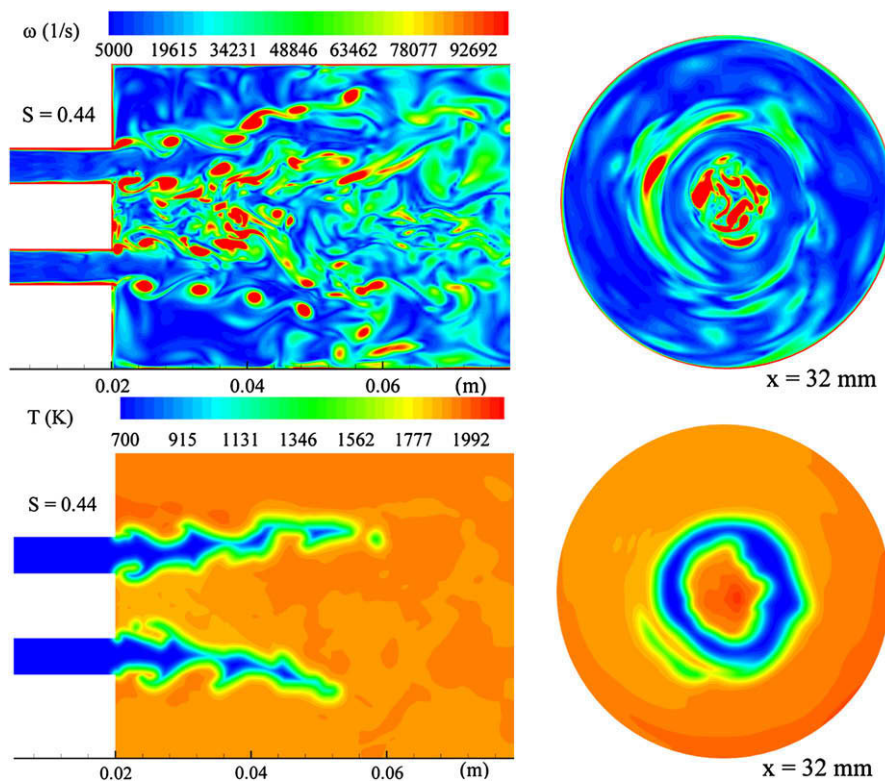
Fig. 74. Snapshots of vorticity magnitude and temperature fields on $x - r$ and $r - \theta$ planes for $S = 0.44$ (Huang et al. [244]).

(bottom). These signals involve a wide range of frequencies corresponding to turbulent flow and acoustic oscillations. The extracted 1L oscillations (denoted by the thick black lines) of these quantities are also plotted for clarity. The flame surface-area variation can be elucidated by considering its interaction with the local oscillatory flowfield. It lags behind the pressure oscillation by 76 degrees. Fig. 77 also indicates that the heat release and flame surface area fluctuations are nearly in-phase. The former only lags behind the flame surface-area oscillation by 4 degrees.

Fig. 78 presents the temporal evolution of the isothermal surface at $T = 1700$ K over one cycle of the 1T mode of acoustic oscillation for $S = 0.44$ and 1.10. For both swirl numbers, new vortices are produced at the edge of the backward-facing step and bulge the flame front. They continue to distort the flame or even produce

separated flame pockets when traveling downstream, although for the high swirl number case this process is less apparent, due to the reduced flame length. This kind of interaction between the vortex and the flame is also observed downstream of the centerbody. As the swirl number increases, the flame anchored by the center recirculating flow may propagate upstream periodically and cause flame flashback.

The combustion dynamics were further explored using the proper orthogonal decomposition (POD) technique. The POD method is an empirical mathematical technique, capable of extracting dynamically significant structures from the flowfield of concern in terms of POD mode [549–553]. The instantaneous flowfield can be reconstructed from the POD modes. Such a procedure permitted the examination of how the various POD modes
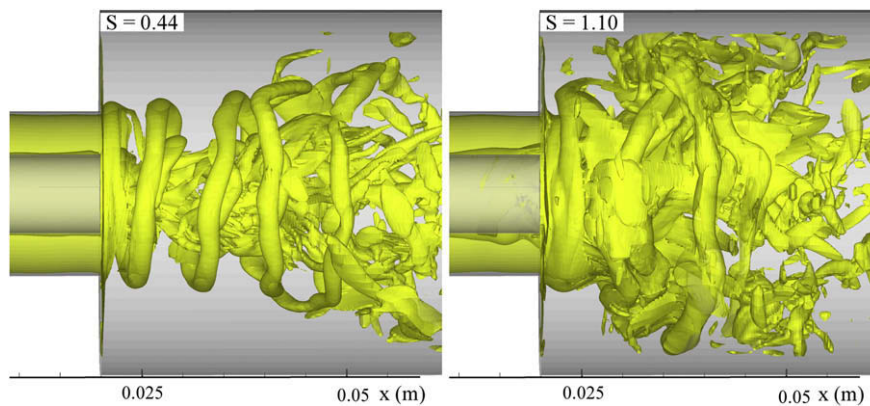
Fig. 75. Snapshots of iso-vorticity surface at $\omega = 75,000$ s^{-1} ($r > 0.02$ m is blanked) for $S = 0.44$ and 1.10 (Huang et al. [244]).
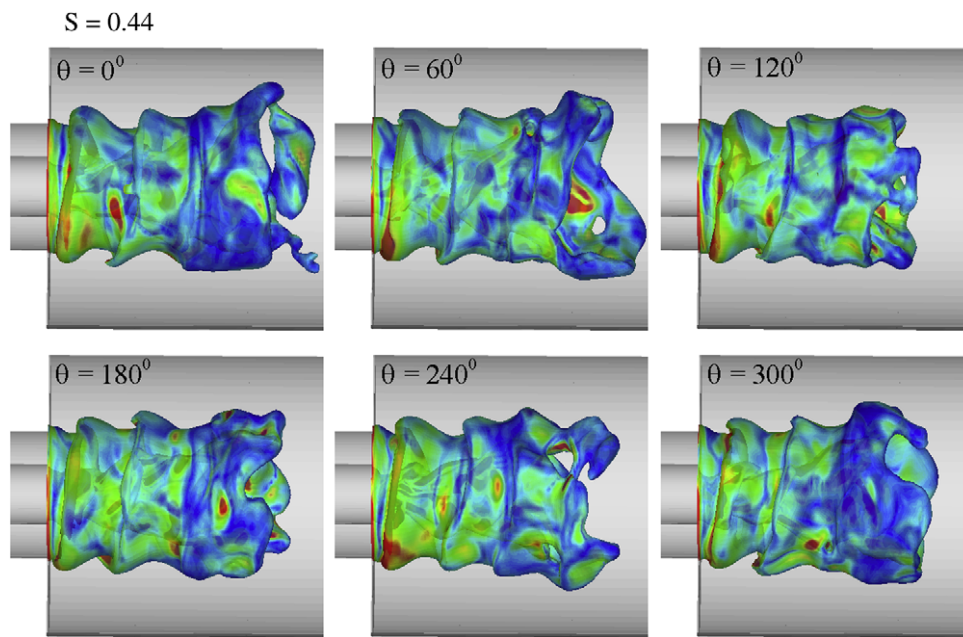
S = 0.44

Fig. 76. Temporal evolution of isothermal surface at $T = 1700$ K (colored by vorticity magnitude) over one cycle of 1L mode of oscillation for $S = 0.44$ (Huang et al. [244]).

contribute to the instantaneous events occurring in the chamber. The analysis indicates that, for both swirl number cases, the first two modes correspond to the 1T acoustic modes in the chamber. Fig. 79 shows the temporal evolution of the reconstructed pressure and heat release field based on the first two POD modes on a transverse plane ($x = 32$ mm) over one cycle of the 1T mode of oscillation for swirl number $S = 0.44$. The spinning 1T acoustic wave motions in the azimuthal direction which are related to the spatio-temporal symmetry of the system are clearly observed. This kind of behavior is encountered in many fluid dynamics problems [553–555]. The helical structures in the flame development are also evidenced in the shear layer region.

Fig. 80 shows the distributions of $Ra = \overline{p^a \dot{q}^a}(\gamma - 1)/\gamma\overline{p}$, $R_{\rho uu} = \overline{\rho u_i^a u_j^a}\partial \overline{u}_i/\partial x_j$, and $R_{pu} = \overline{p^a \partial u_j^a/\partial x_j}$ for the 1T acoustic oscillation on a longitudinal and a transverse plane for swirl number $S = 0.44$. Here the periodic components of the fluctuating

flowfield, p^a, $\dot{q}^a$ and u_i^a are 1T oscillations obtained using the POD method and triple decomposition technique (Huang et al. [244]). The Rayleigh parameter, Ra, represents the coupling between oscillatory heat release and pressure. It provides a qualitative measure of the extent to which unsteady heat release drives or suppresses flow oscillations. The acoustic motion is amplified if $Ra > 0$ or damped out if $Ra < 0$. A wavy distribution of Ra takes place along the flame front. The Rayleigh parameter has a positive value in much of the flame zone. The 1T acoustic oscillation is favorably correlated with the unsteady heat release and extracts energy from chemical reactions. The parameter $R_{\rho uu}$ characterizes the kinetic energy exchange between the mean and oscillatory flowfields. If $R_{\rho uu}$ is negative, energy is transferred from the mean to the oscillatory flowfield. A well-organized distribution of $R_{\rho uu}$ is observed in the shear layers downstream of the backward-facing step and the centerbody. These structures, aligned with regions with alternate positive and negative values, exhibit strong interactions between the mean and periodic flowfields. The parameter R_{pu} stands for the exchange between the kinetic and potential energies of flow oscillations. Such an energy exchange process was found to occur almost everywhere in the chamber, but much more vigorously in the flame zone and the central toroidal recirculation region.

7.2. Analytical modeling of combustion instabilities

Several analytical models (Hsiao et al. [556,557], Dowling and Stow [558], Paschereit et al. [559], You et al. [560]) have been developed to help understand, analyze, and predict combustion instabilities in gas turbine engines. Compared to numerical simulations, analytical analyses are able to deduce general rules and investigate theoretically the global behavior of a complicated system, thereby providing an efficient and compact practical tool for the treatment of gas turbine combustion instability.

7.2.1. Acoustic wave equation and approximate solutions

In analytical techniques, the formulation of the oscillatory flowfield is often expressed as a wave equation, and then solved using either the Green function or the Galerkin method. The former
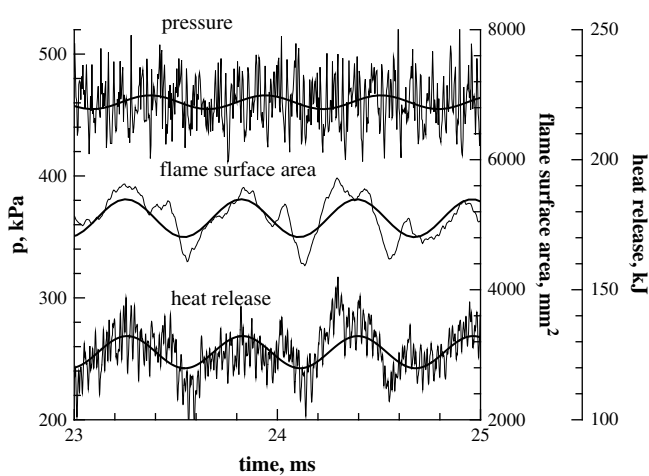
Fig. 77. Time histories of pressure immediately downstream of dump plane (top), heat release rate (middle), and flame surface-area (bottom) for $S = 0.44$, thick black lines represent the extracted 1L oscillations (Huang et al. [244]).

S = 0.44
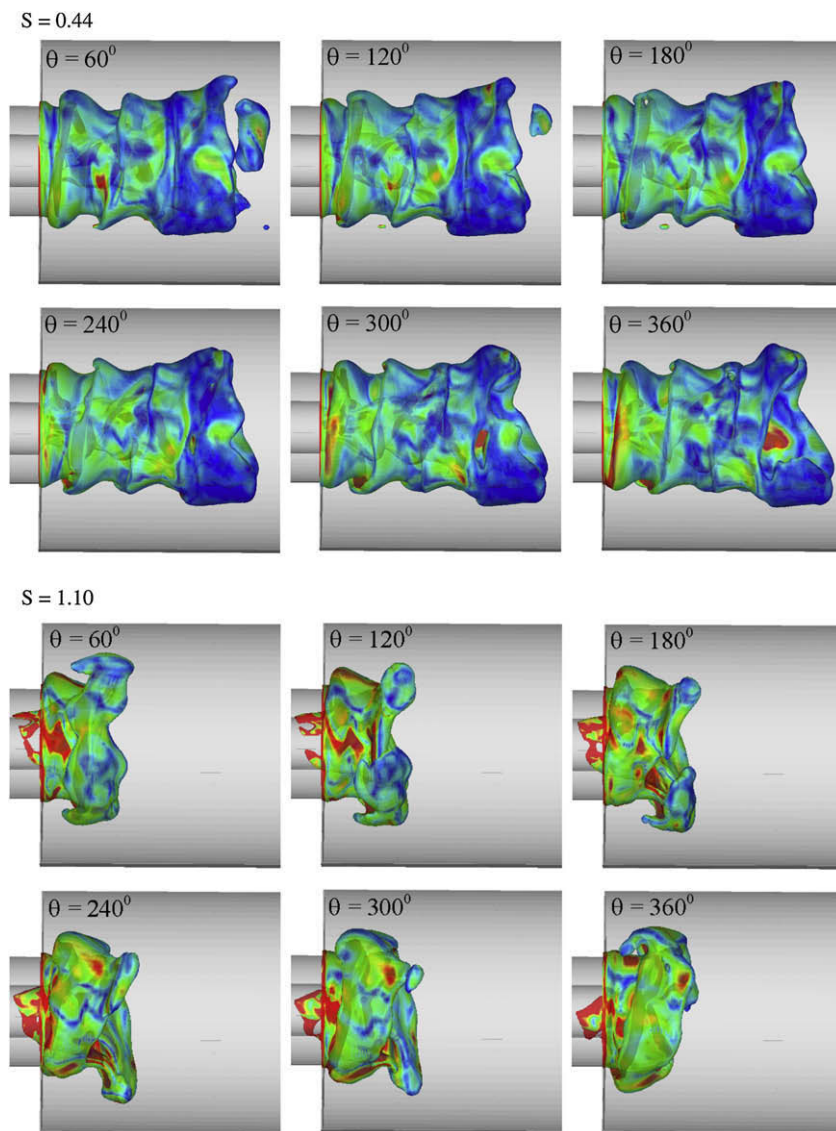
Fig. 78. Temporal evolution of isothermal surface at $T = 1700$ K (colored by vorticity magnitude) over one cycle of 1 T mode of oscillation for two different swirl numbers (Huang et al. [244]).

was first applied to the study of liquid rocket combustion instability by Culick [561]. Through the introduction of a Green's function of eigenfunction expansion, the governing equation was converted from a differential to an integral form, in which the boundary conditions and volumetric sources can be conveniently accommodated. The solutions were obtained by iteration using the classical acoustic modes as the initial eigenfunctions. For systems with strong mean flows, source terms, and boundary effects, initial values other than the classical modes should be carefully selected to achieve convergence (Mitchell [562]). The Green function technique is in general valid for linear stability analyses. A comprehensive review of this technique as applied to liquid rocket combustion stability analysis as of about 1970 is given in Chapter 4 of the volume compiled by Harrje and Reardon [8]. A more recent summary of progress in the area can be found by Mitchell [562].

The Galerkin method was first employed by Zinn and Powell [563] for the problem of nonlinear transverse oscillations in liquid rocket engines. With the application of the normal mode expansion, they were able to derive a system of second-order ordinary differential equations governing the time variation of each acoustic

mode, which was then solved numerically to predict the existence of limit cycles. The same approach was applied to the study of solid rocket combustion instabilities by Culick [564], and was later extended to incorporate a time-averaging technique (the Krylov–Bogoliubov–Mitropolski technique) for obtaining closed-form solutions for the wave evolution (Culick [565]). Details of the procedure can be found by Culick and Yang [14]. The overall approach has been employed to explore a variety of nonlinear stability phenomena, including limit cycle behavior (Awad and Culick [566]; Yang and Culick [567]) and pulse-triggered instability (Wicker et al. [190]).

The approximation of normal mode expansion in either the Green function or the Galerkin method is valid when the frequencies and spatial variations of oscillations deviate only slightly from the corresponding classical acoustic motions solved from the wave equation without source terms. This requirement is satisfied for such systems as solid and liquid rockets having small Mach number and mean flow variations (Culick and Yang [14,15]). For gas turbine combustors, however, the large Mach number and strong mean flow gradients prohibit the use of the standard

Pressure field
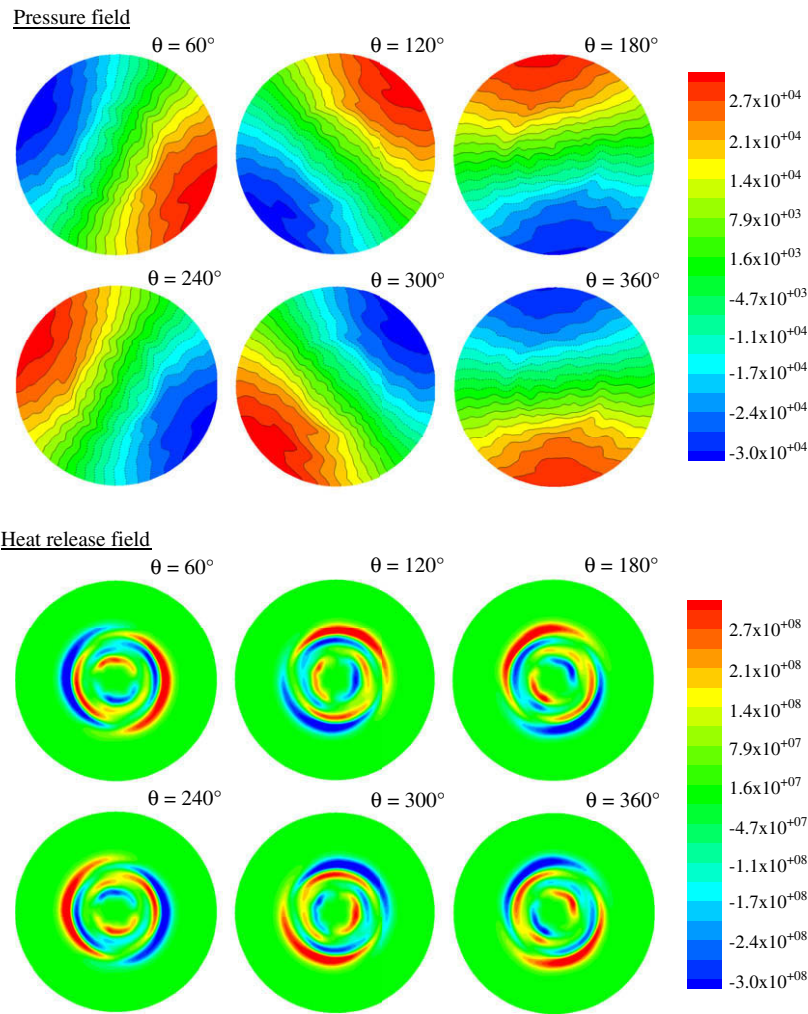
Heat release field

Fig. 79. Temporal evolution of pressure and heat release field reconstructed from first two POD modes on a transverse plane ($x = 32$ mm) over one cycle of 1 T mode of oscillation for $S = 0.44$ (Huang et al. [244]).

Galerkin method, due to the limitations of the underlying assumptions. You et al. [560] established a more general theory capable of treating both longitudinal and transverse acoustic oscillations, as well as their combinations, in complex geometries with non-uniform mean flowfields. The analysis provides a framework within which all known effects on the instability behavior can be assessed explicitly. In brief, it can be constructed in several steps. First, a generalized wave equation governing the oscillatory field in the chamber is derived,

$$\nabla^2 p' - \frac{1}{\bar{c}^2}\frac{\partial^2 p'}{\partial t^2} = h\left(\bar{u}, \bar{p}, u', p', \dot{Q}', etc.\right)$$ (7.3)

subject to $\mathbf{n} \cdot \nabla p' = -f$ along the boundary. The source terms h and f involve all the volumetric and surface effects. To account for spatial variations of the chamber geometry and mean flowfield, the combustor is discretized axially into a number of cells, as shown in Fig. 81, such that the mean axial flow properties within each cell can be taken to be uniform. Furthermore, the mean flow Mach number on the transverse plane is assumed to be small, as in most practical combustion systems. The acoustic field in each cell is synthesized as a Fourier-type series in terms of the eigenfunctions for the cross section, but allows for temporal and axial variations through the series coefficients. In cylindrical coordinates, this can be expressed as

$$p'(\mathbf{r}, t) = \sum_{n=0}^{\infty} \sum_{m=-\infty}^{\infty} [\psi_{mn}(\theta, r)\eta_{mn}(x, t)]$$ (7.4)

The eigenfunction ψ_{mn} can be well approximated by that of a classical acoustic field without source terms. It satisfies the Helmholtz equation for the transverse plane and is subject to the homogeneous boundary condition along the combustor wall. The subscripts m and n stand for mode indices in the circumferential and radial directions, respectively. After expansion, a spatial-averaging technique is applied to solve for the axial variation of the acoustic field.

For linear stability analysis, each fluctuating quantity can be decomposed to a spatial and a time-harmonic temporal part, i.e.,

$$\eta_{mn}(x, t) = \widehat{\eta}_{mn}(x) \cdot \exp(i\Omega t), \quad h(\mathbf{r}, t) = \widehat{h}(\mathbf{r}) \cdot \exp(i\Omega t), etc.$$ (7.5)

The overhat ^ denotes a complex function of spatial coordinates. The characteristic modal frequency Ω is also complex

$$\Omega = \Omega_r + i\Omega_i$$ (7.6)

The real part, Ω_r, represents the radian frequency of oscillation, and the imaginary part, Ω_i, is referred to as the damping coefficient, since its value determines the decay rate of a particular acoustic
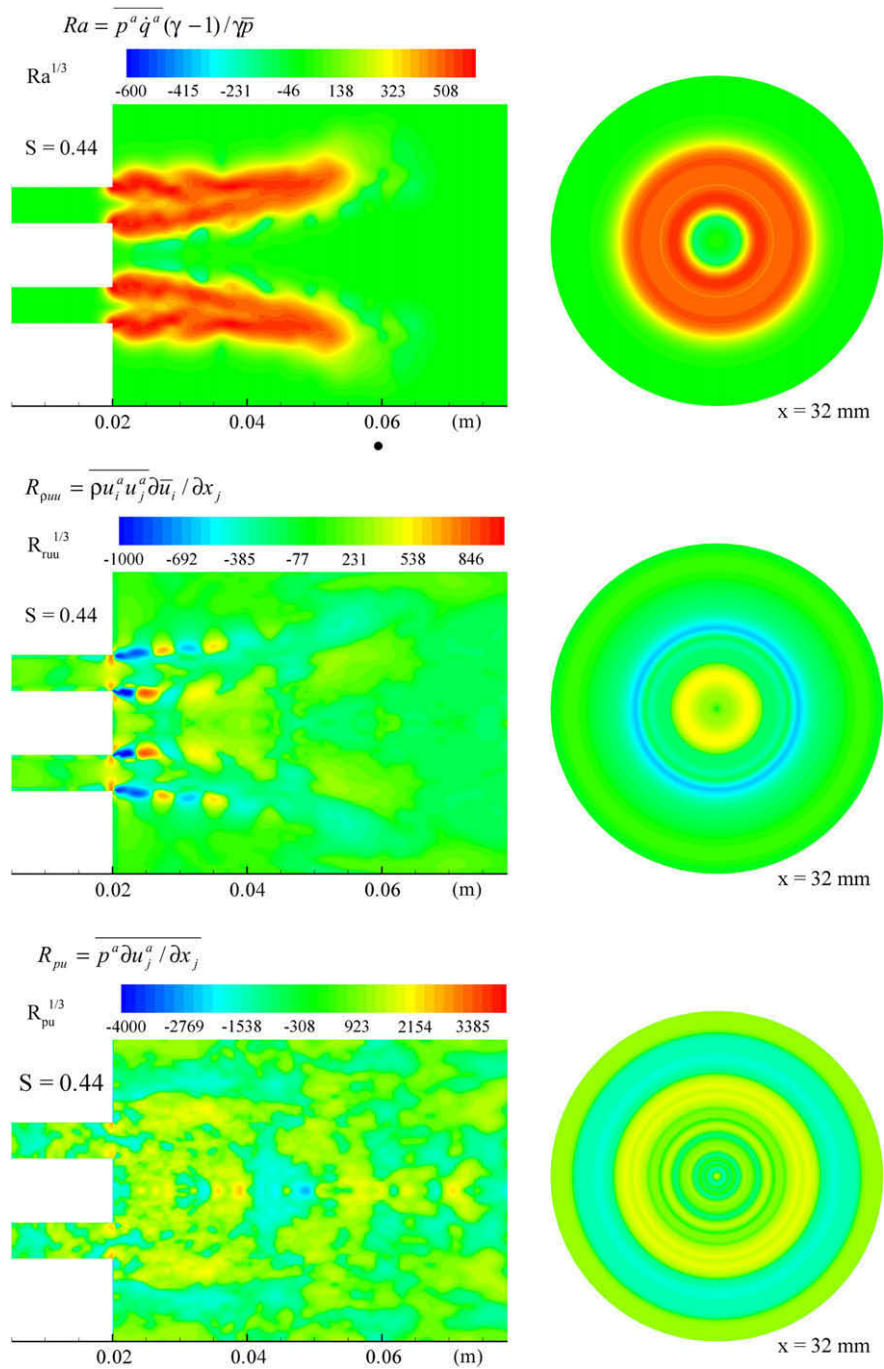
Fig. 80. Distributions of $Ra = \overline{p^a \dot{q}^a}(\gamma - 1)/\gamma\overline{p}$, $R_{\rho uu} = \overline{\rho u_i^a u_j^a \partial \overline{u}_i / \partial x_j}$, and $R_{pu} = \overline{p^a \partial u_j^a / \partial x_j}$ for 1 T mode of oscillation on $x - r$ and $r - \theta$ planes for $S = 0.44$ (Huang et al. [244]).

mode. The volumetric and boundary processes appearing on the right hand side of the wave equation must be modeled. To facilitate formulation, the coefficients C_h and C_f are introduced to represent these terms, as shown below.

$$\iint \psi_{mn} \widehat{h} ds = C_{h,mn} \widehat{\eta}_{mn}(x)$$
$$\oint \psi_{mn} \widehat{f} dl = C_{f,mn} \widehat{\eta}_{mn}(x) \tag{7.7}$$

The source term arising from oscillatory combustion can be written as

$$h = -i\Omega \dot{Q}'(\gamma - 1)/\overline{c}^2 \tag{7.8}$$

Substituting Eq. (7.8) into Eq. (7.7), and applying the response function derived, the coefficient $C_{h,mn}$ is obtained after modeling the various source terms in the wave equation. The acoustic pressure field in each cell can be solved in the following form.

$$p'(\mathbf{r}, t) = e^{i\Omega t} \sum_{n=0}^{\infty} \sum_{m=-\infty}^{\infty} \left[\psi_{mn}(\theta, r) \widehat{\eta}_{mn}(x) \right] \tag{7.9}$$

where

$$\widehat{\eta}_{mn}(x) = p_{mn}^+ \exp\left(i\alpha_{mn}^+ x\right) + p_{mn}^- \exp\left(i\alpha_{mn}^- x\right) \tag{7.10}$$

The axial wave number α_{mn} is given by
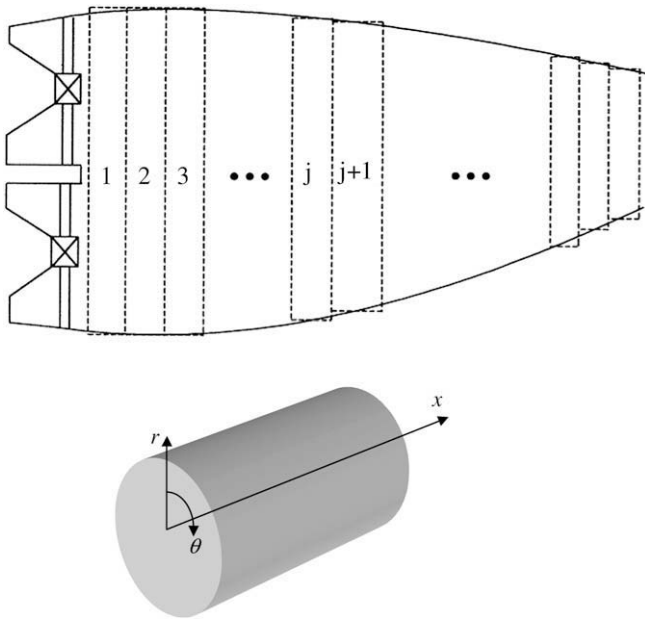
Fig. 81. Discretization of combustion chamber into cells in axial direction (You et al. [267,560]).

$$\alpha_{mn}^2 = \left(\Omega^2/\overline{c}^2\right) - k_{mn}^2 - C_{h,mn} - C_{f,mn} \tag{7.11}$$

where k_{mn} is the eigenvalue corresponding to the transverse eigenfunction ψ_{mn}.

The oscillatory flow properties in each cell are matched with those in the adjacent cells at the cell interfaces by enforcing the conservation laws. The procedure eventually leads to a system equation which determines the stability characteristics in terms of the complex frequency Ω, as well as the spatial structure of the acoustic waves in the entire system.

An alternative approach based on the wave expansion technique (Dowling and Stow [558]) was employed to study the acoustic pressure behavior governed by Eq. (7.3) within a combustion system. It assumes that combustion is concentrated in some compact planes. The wave equation outside these planes then becomes homogeneous, to allow for analytical solutions. This method uses a wave expansion rather than a mode expansion, as follows.

$$p'(x,t) = f(t - x/\overline{c}) + g(t + x/\overline{c}) \tag{7.12}$$

$$u'(x,t) = (1/\rho\overline{c})[f(t - x/\overline{c}) - g(t + x/\overline{c})] \tag{7.13}$$

By matching the flowfields across the combustion zones, all plane waves in a one-dimensional system can be determined from two unknowns, which are the wave strengths upstream and downstream of the combustion zone. The wave expansion approach provides a more accurate analysis of the shift in mode shape and nature frequency, due to the coupling between the unsteady flow and heat release. This approach is usually valid for longitudinal disturbances. In addition, restricting source terms at the matching interface could lead to inaccurate prediction of the instability characteristics. A more detailed description of this approach can be found in Ref. [558].

7.2.2. Combustion response

Unsteady heat release $\dot{Q}'$ in Eq. (7.3) is the most important source term providing the energy that drives combustion instability. For a lean-premixed combustion system, this term depends on a variety of physical processes, such as flame surface and equivalence ratio fluctuations, hydrodynamic instability, and liquid fuel atomization and droplet evaporation. None of these processes can be modeled in sufficient detail. Traditionally, the response of unsteady heat release $\dot{Q}'$ to acoustic excitation can be represented by a response function as defined below.

$$R_p = \frac{\dot{Q}'/\overline{\dot{Q}}}{p'/\overline{p}} \tag{7.14}$$

This parameter, which is a complex variable characterizing the magnitude and phase differences between pressure and heat release oscillations, must be determined for the specific problem and frequency in question. One of the commonly used combustion response models is the time lag model, which has been extensively employed to study combustion instabilities in liquid-propellant rocket engines (Crocco and Cheng [187]). The model globally describes the dynamic relationship between fuel injection and heat release, and can be briefly summarized as follows (Culick [11]).

Suppose that at time t, the pressure in the chamber suddenly decreases, causing an increase in the flow of fuel through the injector. The increased mass is convected downstream to the flame front and burns at some later time $t + \tau$, where τ is the time lag. The time scales that contribute to the time lag are the convection time needed to travel the distance from the fuel injection location to the flame front, the mixing time for fresh air and fuel to mix with hot product gases, and the chemical time corresponding to the ignition delay. If the pressure in the chamber is increasing when the added fuel burns, the energy release tends to encourage the increase in pressure. A quantitative expression relating the fuel burning rate $\dot{m}_b$ to the injection rate $\dot{m}_i$ can be derived as:

$$\dot{m}_b(t) = \dot{m}_i(t - \tau)(1 - \mathrm{d}\tau/\mathrm{d}t) \tag{7.15}$$

In the above equation, the mass-burning flow rate at time, t, can be given by the fuel mass flow rate injected at an earlier time, $t - \tau$. Assuming the time lag τ is constant and independent of local thermodynamic properties, Eq. (7.15) becomes:

$$\dot{m}_b(t) = \dot{m}_i(t - \tau) \tag{7.16}$$

The assumption that the time lag is constant is usually not valid. To derive an equation for the rate of change in the time lag, one usually considers the process of the conversion of fuel into combustion products. Many models assume that the time lag is only sensitive to the pressure and let $f(p)$ designate a function that globally describes this conversion process. Then an expression for $\mathrm{d}\tau/\mathrm{d}t$ can be obtained as:

$$1 - \mathrm{d}\tau/\mathrm{d}t = 1 + n[p'(t)/\overline{p} - p'(t - \tau)/\overline{p}] \tag{7.17}$$

where n is the interaction index given by $n = \partial(\ln f)/\partial(\ln p)$. After some manipulations, the basic result of the time lag theory can be obtained as:

$$\dot{m}_b'(t) = \overline{\dot{m}}_b n[p'(t)/\overline{p} - p'(t - \tau)/\overline{p}] \tag{7.18}$$

The heat release fluctuation can be expressed by a similar expression:

$$\dot{q}'(t) = \overline{\dot{q}} n[p'(t)/\overline{p} - p'(t - \tau)/\overline{p}] \tag{7.19}$$

Obviously, such a two-parameter (n, τ) representation is an enormous simplification of the real situation. The time lag model has many difficulties in explaining and predicting combustion instability phenomena associated with nonlinear processes. Even

with its shortcomings, however, the model can qualitatively explain the interaction between the fuel supply system and the combustion chamber. Recently, the time lag model was applied to the study of combustion dynamics in lean-premixed combustors by Richards and Janus [273,310], Lieuwen and Zinn [235,236] and You et al. [267]. Effects of fuel line length and inlet acoustical boundary conditions were incorporated into the development of these time lag models.

An alternative heat release response model was proposed by Fleifil et al. [261]. The model treats the equation of thin flame surface evolution, and heat release is determined from the flame surface area per volume and flame speed. Their results give the response of a laminar-premixed flame stabilized on the rim of a cylindrical duct to flow oscillations. After correlating with the time lag model, the relationship between unsteady heat release and velocity perturbation was acquired as a function of flame Strouhal number, a reduced frequency normalized by the flame speed and the duct radius $\omega R/S_L$. The time lag is maximum at high-frequency and smallest at low-frequency. The approach of Fleifil et al. [261] was later further developed by Dowling [262], Ducruix et al. [264], Schuller et al. [265], Lieuwen [268], and You et al. [267] for various flame configurations and flow conditions.

Peracchio and Proscia [568] summarized and extended the previously published studies, and proposed a more comprehensive heat release/acoustic model for a single nozzle rig, considering both equivalence ratio and flame surface area fluctuations as sources of heat release fluctuations. The effect of equivalence ratio was included using the time lag concept, and the dynamics of flame surface area were described using the model proposed by Fleifil et al. [261]. More recently, You et al. [267] developed a generalized model of acoustic response of turbulent premixed flame based on a flamelet model along and triple decomposition technique. All known factors affecting unsteady heat release were examined, including variations of heat of reaction, density, flame speed, and flame surface area. The model is also able to accommodate the effects of spatial variations in chamber geometry and mean flowfield. More detailed information will be presented in the next section.

7.2.3. Instability analysis of an LPM swirl-stabilized combustor

As an illustration, the linear instability analysis by You et al. [267] of an LPM swirl-stabilized combustor shown schematically in Fig. 82 is described here. Detailed information about the experimental observations can be found in the papers by Broda et al. [195] and Seo [196]. The flow and flame evolutions and underlying mechanisms for driving instabilities were also studied by Huang et al. [198,199] using large-eddy simulations, as discussed in Section 7.1.5. In the analysis of You et al. [267], a generalized model of the acoustic response of a turbulent premixed flame was first constructed. The resultant flame response was then incorporated into a three-dimensional instability analysis [560] to determine the stability characteristics of the combustor.

In gas turbine combustors, both random and periodic (coherent) motions exist. The intricate coupling between these flow motions and flame plays an important role in determining the characteristics of turbulent combustion. The effects of coherent structures on the propagation of premixed flames were investigated by Ulitsky and Collins [569]. Their results indicate that the turbulent burning rate is enhanced by coherent structures. Lieuwen [570] analyzed acoustic wave interactions with turbulent premixed flames, and found that with increased flame-wrinkling, the coherent field becomes increasingly independent of the temperature jump across the flame and response of the mass-burning rate. In addition, the flame-wrinkling damps the acoustic energy. The triple decomposition technique, which allows the random and periodic motions to be separated from each other, is employed here to investigate the

effects of acoustic oscillations and turbulence on the periodic behavior of a turbulent flame. Within the flamelet assumption, the rate of heat release per unit volume can be given as, $\dot{Q} = q\rho S_L A$. When the triple decomposition technique is applied, we can obtain following expression for heat release fluctuation (You et al. [267]),

$$\frac{\dot{Q}^a}{\dot{\bar{Q}}} = \frac{q^a}{\bar{q}} + \frac{\rho^a}{\bar{\rho}} + \frac{S_T^a}{\bar{S}_T} + \frac{A_{\xi^a}}{A_{\bar{\xi}}} \tag{7.20}$$

where S_T is turbulent flame speed, $A_{\bar{\xi}}$ the specific surface area at the long-time-averaged flame location, and A_{ξ^a} the area increase due to the periodic flame displacement. The superscript a denotes the periodic (coherent) component of a fluctuating quantity. Thus, the fluctuation of heat-release rate contains contributions from the fluctuations in heat of reaction, density, flame speed, and flame surface area. The fluctuation of heat of reaction is attributed to the changes in the mixture-equivalence ratio resulting from flow disturbances. The density fluctuation, mainly arising from pressure perturbation, has a negligible effect on unsteady heat release as compared to other three factors. The oscillation of flame speed, similar to that of heat of reaction, is caused by equivalence ratio fluctuation for a given chamber and flow condition. The mechanisms of flame surface-area fluctuation are relatively complicated and primarily dictated by local velocity perturbations.

To evaluate the flame response to an acoustic velocity perturbation, an analytic model, which can accommodate the effects of spatial variation in chamber geometry and mean flowfield, was derived by You et al. [267] and is discussed as follows. Under the flamelet assumption, the flame movement can be tracked using a field variable G and the location of the flame front is assigned to a particular level $G = G_0$. The flame surface propagates in the normal direction at a speed S_L relative to the unburnt mixture with the local velocity $\boldsymbol{u}$. The evolution of the flame surface can be described using the following transport equation, commonly known as the G-equation (Williams [466], Kerstein et al. [571]):

$$\frac{\partial G}{\partial t} + u_j \frac{\partial G}{\partial x_j} \nabla G - S_L |\nabla G| = 0 \tag{7.21}$$

with the application of the triple decomposition technique to Eq. (7.21), modeled equations for $\bar{G}$ and G^a can be derived as follows
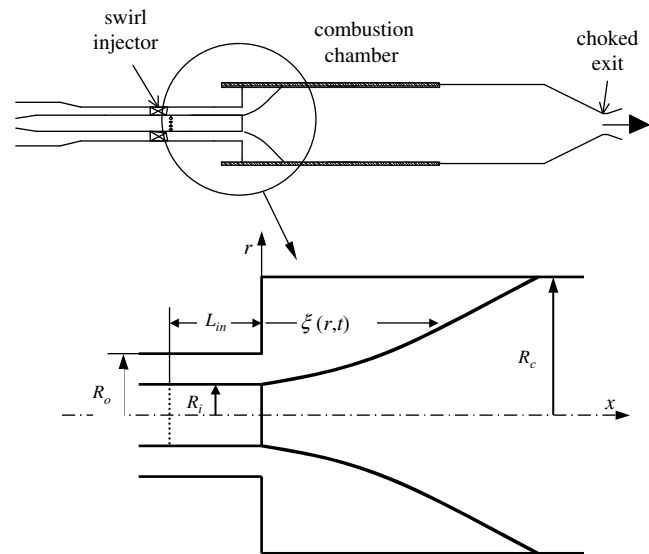
Fig. 82. Schematic of a swirl-stabilized combustor (You et al. [267]).

$$u_j \frac{\partial \overline{G}}{\partial x_j} + \overline{u_j^a \frac{\partial G^a}{\partial x_j}} = (\overline{S}_T + v_t \overline{k}) \frac{\nabla \overline{G}}{|\nabla \overline{G}|} \nabla \overline{G} \tag{7.22}$$

$$\frac{\partial G^a}{\partial t} + \overline{u}_j \frac{\partial G^a}{\partial x_j} + u_j^a \frac{\partial \overline{G}}{\partial x_j} + u_j^a \frac{\partial G^a}{\partial x_j} - \overline{u_j^a \frac{\partial G^a}{\partial x_j}} = (\overline{S}_T + v_t \overline{k}) \frac{\nabla \overline{G}}{|\nabla \overline{G}|} \nabla G^a \tag{7.23}$$

where $\overline{k}$ is the mean flame front curvature, $\overline{k} = \nabla \cdot \overline{\mathbf{n}}$, and $\overline{\mathbf{n}} = -\nabla \overline{G}/|\nabla \overline{G}|$.

To facilitate formulation of the flame response, we consider the axisymmetric configuration shown schematically in Fig. 82. Premixed combustible gases are delivered to a dump chamber, and the flame is stabilized in the wake of the centerbody. The variable G is expressed as

$$G(x, r, t) = x - \xi(r, t) \tag{7.24}$$

where $\xi(r,t)$ is the instantaneous axial displacement of the flame front. The above equation is valid only when $\xi(r,t)$ is a single-valued function of r. Accordingly, the time-averaged and periodical flame surfaces can be expressed as

$$\overline{G}(x, r, t) = x - \overline{\xi}(r) \quad and \quad G^a(x, r, t) = -\xi^a(r, t) \tag{7.25}$$

Substitution of Eq. (7.25) into Eqs. (7.22) and (7.23), and rearrangement of the results leads to the equations for the mean and periodically fluctuating components of the flame surface displacement in a cylindrical coordinate system. Both the nonlinear terms and the curvature terms are neglected to simplify the analysis.

$$\overline{u} - \overline{v} d\overline{\xi}/dr - \overline{S}_T \left[(d\overline{\xi}/dr)^2 + 1 \right]^{1/2} = 0 \tag{7.26}$$

$$\frac{\partial \xi^a}{\partial t} + \left\{ \overline{v} + \overline{S}_T \left[\left(\frac{d\overline{\xi}}{dr}\right)^2 + 1 \right]^{-1/2} \frac{d\overline{\xi}}{dr} \right\} \frac{\partial \xi^a}{\partial r} = \left(u^a - v^a \frac{d\overline{\xi}}{dr} \right) \tag{7.27}$$

The mean velocity components, $\overline{u}$ and $\overline{v}$, and flame displacement $\overline{\xi}(r)$ can be determined from a separate numerical analysis, which solves the complete conservation equations (e.g., Wang and Yang [572], Huang et al. [198,199]). The turbulent flame speed $\overline{S}_T$ can be deduced directly as follows.

$$\overline{S}_T = (\overline{u} - \overline{v} d\overline{\xi}/dr)/\left[(d\overline{\xi}/dr)^2 + 1 \right]^{1/2} \tag{7.28}$$

For linear perturbation with a radian frequency, Eq. (7.28) gives a first order ordinary differential equation for the periodic oscillation of the flame displacement

$$\left\{ \overline{v} + \overline{S}_T \left[(d\overline{\xi}/dr)^2 + 1 \right]^{-1/2} d\overline{\xi}/dr \right\} \frac{d\widehat{\xi}}{dr} + i\Omega\widehat{\xi} - \left(\widehat{u} - \widehat{v} d\overline{\xi}/dr \right) = 0 \tag{7.29}$$

An analytical solution exists if the flame-spreading angle and flow velocity remain fixed in the region of concern.

Consider the simple flame configuration shown in Fig. 82, with uniform mean flow velocity and constant flame spread angle α. After some straightforward algebraic manipulations, the fluctuating flame displacement can be derived as

$$\frac{\xi^a}{R_c - R_i} = \frac{1}{i\Omega_u} \left[\frac{u^a}{\overline{u}} + \frac{v^a}{\overline{v}} C_r \right] \left[1 - \exp\left(-i\Omega_f \frac{r - R_i}{R_c - R_i} \right) \right] \tag{7.30}$$

The normalized fluctuation of the flame displacement depends on three parameters: Ω_f, Ω_u, and C_r. The coefficient C_r is defined as

$C_r = \overline{S}_T/(\overline{u} \cos \alpha) - 1$. The flame Strouhal number, Ω_f, is associated with the flame speed in the radial direction: $\Omega_f = \Omega(R_c - R_i)/(\overline{v} + \overline{S}_T \sin \alpha)$. The flow Strouhal number, Ω_u, is defined based on the mean axial velocity $\Omega_u = \Omega(R_c - R_i)/\overline{u}$. Fig. 83 shows the temporal evolution of the instantaneous flame displacement within one cycle of oscillation for excitation frequencies of 1000 and 10,000 Hz, respectively. The mean flow properties include $\alpha = 60°$ and $\overline{S}_T/\overline{u} = 0.3$, and the acoustic velocity amplitudes are $\widehat{u}/\overline{u} = 0.5$ and $\widehat{v}/\overline{v} = 0$. At low frequencies of $f = 1000$ Hz, the surface wavelength is greater than the characteristic flame scale $R_c - R_i$. The flame deviates from its mean location monotonically without obvious wavy structure. The situation, however, becomes drastically different at the high-frequency $f = 10,000$ Hz. The flame exhibits periodic oscillations on its surface, and is more wrinkled with increasing frequency.

The total flame surface area is obtained by integrating the displacement over the flame surface.

$$A_{\langle \xi \rangle}^g = \int_{R_i}^{R_c} \left\{ 2\pi r \left[(\partial \langle \xi \rangle / \partial r)^2 + 1 \right]^{1/2} \right\} dr \tag{7.31}$$

where the superscript g denotes integration over the entire flame. $< \xi > = \overline{\xi} + \xi^a$ Represents the ensemble-averaged flame location. The fluctuation of the total flame surface area normalized by its quantity at the time-mean position can be obtained as

$$\frac{A_{\xi^a}^g}{A_{\overline{\xi}}^g} = \left[\frac{2}{(R_c^2 - R_i^2)} \int_{R_i}^{R_c} (r \cdot f) dr \right] - 1 \tag{7.32}$$

where

$$f = \left[1 + \left(\frac{2u_n^a \tan \alpha \cos^2 \alpha}{\overline{U}_\alpha} \right) e^{\frac{-i\Omega(r-R_i)}{\overline{U}_\alpha}} + \left(\frac{\cos \alpha u_n^a}{\overline{U}_\alpha} \right)^2 e^{\frac{-2i\Omega(r-R_i)}{\overline{U}_\alpha}} \right]^{1/2}$$

Equation (7.30) can be numerically integrated to obtain the overall flame response to acoustic disturbances, defined by

$$(R_u^g)_u = \frac{A_{\xi^a}^g/A_{\overline{\xi}}^g}{u^a/\overline{u}}, \quad (R_v^g)_u = \frac{A_{\xi^a}^g/A_{\overline{\xi}}^g}{v^a/\overline{v}} \tag{7.33}$$

where the subscript u denotes the velocity sensitivity of the response function. The above transfer functions between the disturbances in the overall flame surface area and flow velocity depend intimately on the flame Strouhal number Ω_f. Fig. 84 shows the results for three different excitation amplitudes. The transfer function has a magnitude of unity at zero frequency, and decays sinusoidally with increasing frequency. The flame undergoes a large excursion of oscillation at a low-frequency, although its surface is less wrinkled. Similar observations were previously made by Fleifil et al. [261] and Schuller et al. [265]. The magnitude of velocity fluctuation $\widehat{u}/\overline{u}$ exerts little influence on the flame response, except in the low-frequency range.

The generalized three-dimensional linear acoustic analysis outlined in Section 7.2.1 was employed to determine the stability characteristics of the combustor [267,560], using LES numerical results as a basis. The analysis is capable of treating both longitudinal and transverse waves as well as their combinations in complex configurations with non-uniform distributions of mean flow properties. Based on the experimental [195,196] and numerical results [198,199], two cases were investigated. Case 1 is associated with a stable operating condition with an inlet temperature of 600 K. The flame spreads from the corner of the centerbody to the chamber wall, which is regarded as a simple flame. Case 2 corresponds to an unstable situation with an inlet temperature of 660 K. The flame is anchored by both the corner- and the center
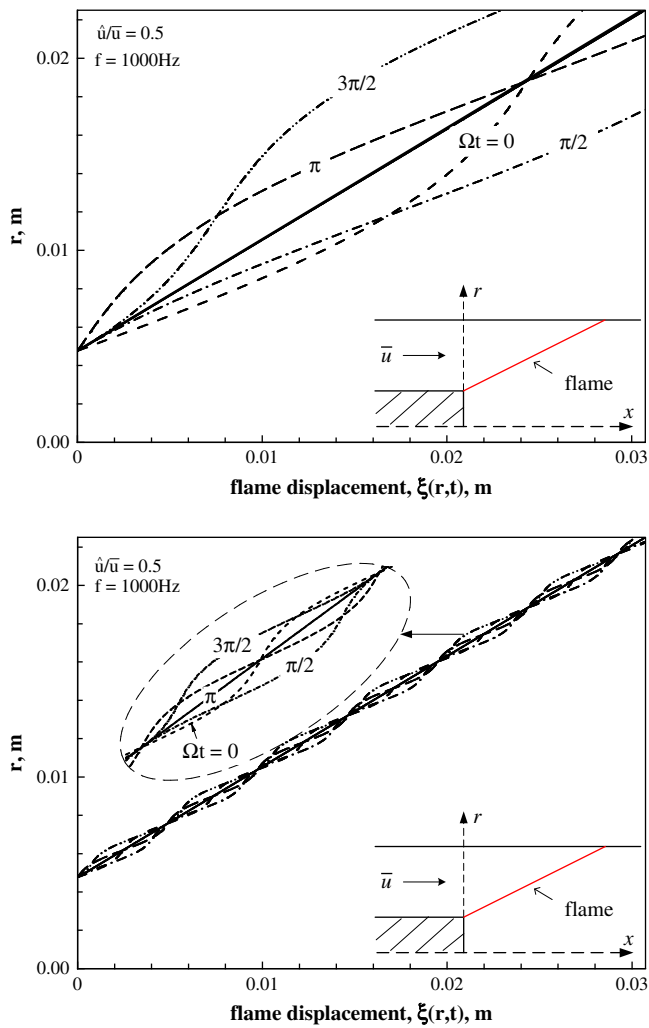
Fig. 83. Temporal evolution of flame displacement within one cycle of oscillation, $\hat{u}/\overline{u} = 0.5$, $\hat{v}/\overline{v} = 0$, $\overline{S}_T/\overline{u} = 0.3$ and $\alpha = 60°$. $f = 1000$ Hz (left), $f = 10,000$ Hz (right). Thick black line represents the mean flame location (You et al. [267]).
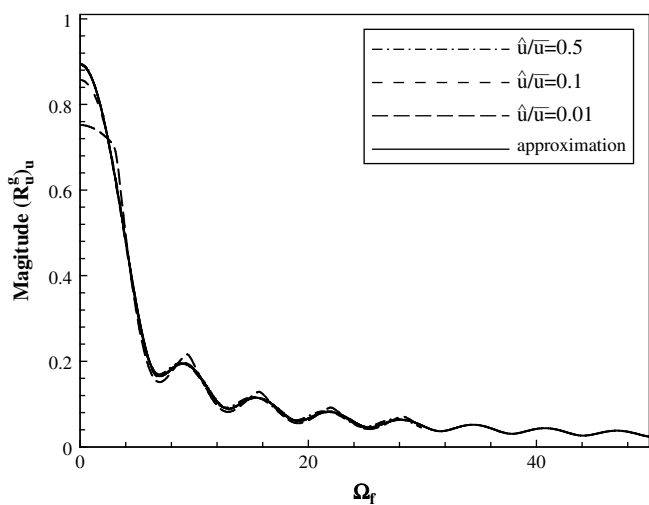
Fig. 84. Magnitude of transfer function between fluctuations of overall flame surface area and flow velocity as function of flame Strouhal number Ω_f ($\hat{v}/\overline{v} = 0$, $\overline{S}_T/\overline{u} = 0.3$, $\alpha = 60°$) (You et al. [267]).
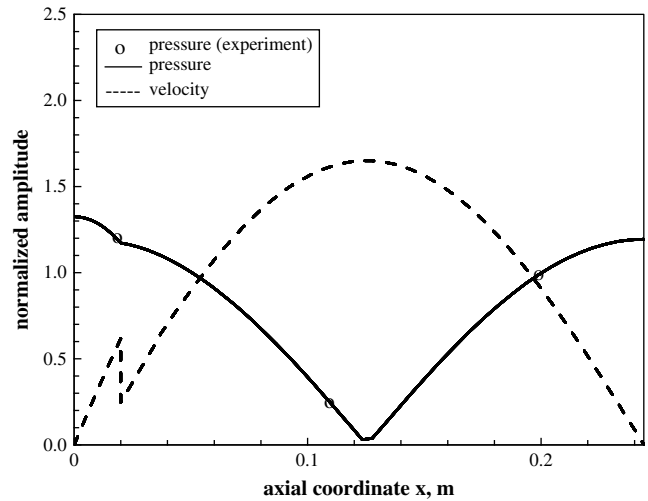
Fig. 85. Distributions of acoustic oscillations in swirl-stabilized combustor, first longitudinal mode (You et al. [267,560]).

recirculating flows and forms a compact enveloped configuration. The flame structures of both cases are shown in Fig. 31. The average flame-spreading angles can be estimated from the calculated mean temperature fields. These quantities, along with the mean flow properties, are used to determine the combustion response function in Eq. (7.21), which is then employed in the generalized acoustic analysis, to characterize the stability behavior of the combustor. The calculated acoustic frequencies of the first longitudinal mode are close to the experimental vales of 1750 Hz in both cases. For the stable flame (case 1), the damping coefficient is positive, but it becomes negative for the unstable flame (case 2). This is consistent with the experimental observation. The spatial distribution of the first longitudinal mode of unstable flame shown in Fig. 85 also demonstrates the validity of the acoustic analysis.

8. Conclusions

This paper provides an overview of the dynamics and stability of LPM swirl-stabilized combustion. Various dry-low-emission industry gas turbine combustion systems are described. Swirl injector configurations and related flow characteristics, including vortex breakdown, precessing vortex core, large-scale coherent structures, and atomization of sprays of liquid fuel, are discussed in detail. The effect of injector configuration on flow development, and the flow dynamic response of swirl injectors to external excitations, are also examined. Nonlinear behavior of combustion oscillations, such as limit cycle, bifurcation, and hysteresis, is described. In addition, the roles of fuel preparation, combustor geometry, and operating conditions on combustion characteristics in lean-premixed swirl-stabilized combustors are elaborated.

The Rayleigh criterion, which has been used in many qualitative descriptions of combustion instabilities, is revisited using a triple decomposition technique. It is found that an oscillating flow can acquire energy through several different pathways, including mean flows, chemical reactions, and background turbulent motions. When there are no chemical reactions, the major energy source for periodic motions is the mean flow. With combustion, heat release from chemical reactions is the major energy source for driving acoustic motions. The transfer of energy from chemical reactions to the periodic flowfield only takes place when heat release oscillations are in phase with pressure oscillations. It was then shown that the major driving mechanisms of combustion instabilities in

lean-premixed gas turbine engines are hydrodynamic instabilities, equivalence ratio fluctuations, flame surface variations, and oscillatory fuel atomization and vaporization.

Both passive and active control techniques have been adopted to attenuate combustion instabilities. Passive control methods include employment of Helmholtz resonators and quarter-wave tubes, fuel staging and pilot fuel, fuel injector geometry modification, equivalence ratio oscillation damping, and air-flow damping. Since combustion instabilities are often induced by a collection of mechanisms, a combination of the methods described tends to be more effective. The problems with passive approaches are that they are effective over only a limited range of operating conditions, and the changes of design involved are usually costly and time-consuming. A large number of active instability control (AIC) techniques have been developed and applied to laboratory-scale research combustors. Some full-scale implementations on industry gas turbine combustors have also been reported. In most AIC systems, control actions are achieved using mechanical acoustic actuation devices such as loudspeakers, or by modulation of the primary or secondary fuel flow. All full-scale implementations have employed auxiliary fuel modulation along with simple control algorithms, largely due to technological issues related to the control hardware, i.e., sensors and actuators.

Both numerical simulations and analytical approaches have been adopted for treating combustion instabilities. Numerical analyses solve the conservation equations and usually take into account finite-rate chemical reactions. Turbulence closure is often achieved by means of large-eddy simulation (LES) techniques. The reported simulations have demonstrated the capabilities of LES techniques as a research and predictive tool to study combustion dynamics in complex geometries, but this approach is still developing, and is far from mature. Improved models that incorporate liquid fuel combustion, pollutant chemistry, and radiation heat transfer are needed in the future. Further developments in boundary condition treatments are also desired. Compared to numerical simulations, analytical analyses are able to deduce general rules and investigate theoretically the global behavior of a complicated system. The analytical model can also serve as backbone for devising control techniques to modulate combustion processes. Modeling of the response of unsteady combustion to acoustic excitation, however, remains a major challenge.

Acknowledgements

References

[1] Bahr DW. Aircraft turbine engine NO_x emission abatement. Chapter 10. In: Culick FEC, Heitor MV, Whitelaw JH, editors. Unsteady combustion. the Netherlands: Kluwer Academic Publisher; 1996.

[2] Correa SM. A review of NO_x formation under gas-turbine combustion conditions. Combustion Science and Technology 1992;87:329–62.

[3] Lefebvre AH. The role of fuel preparation in low-emission combustion. Journal of Engineering for Gas Turbines and Power 1995;117:617–54.

[4] Correa SM. Power generation and aero-propulsion gas turbines: from combustion science to combustion technology. Proceedings of the Combustion Institute 1998;28:1793–807.

[5] Zeldovich J. The oxidation of nitrogen in combustion and explosions. Acta Physicochimica 1946;21(4):577–628.

[6] Lieuwen T, Yang V. Combustion instabilities in gas turbine engines: operational experience, fundamental mechanisms, and modeling. Progress in Astronautics and Aeronautics 2005;210.

[7] Goy CJ, James SR, Rea S. Monitoring combustion instabilities: E.ON UK's experience. Chapter 8. In: Lieuwen T, Yang V, editors. Combustion instabilities in gas turbine engines: operational experience, fundamental mechanisms, and modeling. Progress in Astronautics and Aeronautics 2005;210:163–75.

[8] Harrje DT, Reardon FH, editors. Liquid rocket combustion instability. NASA; 1972. SP-194.

[9] Yang V, Anderson W, editors. Liquid rocket engine combustion instability. Progress in Aeronautics and Astronautics, vol. 169. AIAA; 1995.

[10] De Luca L, Price EW, Summerfield M, editors. Nonsteady burning and combustion stability of solid propellants. Progress in astronautics and aeronautics, vol. 143. AIAA; 1992.

[11] Culick FEC. Combustion instabilities in liquid-fueled propulsion systems—an overview. AGARD Conference Proceedings 450. Belgium: NATO ASI Series Publication Coordination Office; 1989.

[12] Ma FH, Li J, Yang V, Lin KC, Jackson TA. Thermo-acoustic flow instability in a scramjet combustor. AIAA Paper 2005-3824; 2005.

[13] Putnam AA. Combustion-driven oscillations in industry. New York: Elsevier; 1971.

[14] Culick FEC, Yang V. Prediction of the stability of unsteady motions in solid propellant rocket motors. Chapter 18. In: DeLuca L, Summerfield M, editors. Nonsteady burning and combustion stability of solid propellants. Progress in Astronautics and Aeronautics 1992;143:719–79.

[15] Culick FEC, Yang V. Overview of combustion instabilities in liquid-propellant rocket engines. Chapter 1. In: Yang V, Anderson WE, editors. Liquid rocket engine combustion instability. Progress in Astronautics and Aeronautics 1995;169:3–37.

[16] Mongia HC, Held TJ, Hsiao GC, Pandalai RP. Challenges and progress in controlling dynamics in gas turbine combustors. Journal of Propulsion and Power 2003;19(5):822–9.

[17] Keller JJ. Thermoacoustic oscillations in combustion chambers of gas turbines. AIAA Journal 1995;33(12):2280–7.

[18] Pandalai RP, Mongia HC. Combustion instability characteristics of industrial engine dry low emission combustion systems. AIAA Paper 1998-3379; 1998.

[19] Lieuwen T, McManus K. Combustion dynamics in lean-premixed prevaporized gas turbine. Journal of Propulsion and Power 2003;19:721.

[20] Bluestein J. NO_x control for gas-fired industrial boilers and combustion equipment: a survey of current practices. GRI-9210374, Gas Research Institute Report; 1992.

[21] Leonard G, Stegmaier J. Development of an aero-derivative gas turbine dry low emissions combustion system. Journal of Engineering for Gas Turbines and Power 1994;116:542–6.

[22] Joshi ND, Epstein MJ, Durlak S, Marakovits S, Sabla PE. Development of a fuel air premixer for aeroderivative dry low emissions combustors. ASME Paper 1994-GT-0253.

[23] Joshi ND, Mongia HC, Leonard G, Stegmaier JW, Vickers EC. Dry low emissions combustors development. ASME Paper 1998-GT-0310; 1998.

[24] Lefebvre AH. Gas turbine combustion. Philadelphia, PA: Taylor & Francis; 1998.

[25] Rokke PE, Hustad JE, Rokke NA, Svendsgaard OB. Technology update on gas turbine duel fuel, dry low emission combustion systems. ASME Paper 2003-GT-38112; 2003.

[26] Scarinci T, Halpin JL. Industrial trent combustor-combustion noise characteristics. Journal of Engineering for Gas Turbines and Power 2000;122:280–6.

[27] Scarinci T, Halpin JL. Passive control of combustion instability in a low emissions aero-derivative gas turbine. ASME Paper 2004-GT-53767; 2004.

[28] Scarinci T. Combustion instability and its passive control: Rolls-Royce Trent 60 dry low emissions aero-derivative engine experience. Chapter 4. In: Lieuwen T, Yang V, editors. Combustion instabilities in gas turbine engines: operational experience, fundamental mechanisms, and modeling. Progress in Astronautics and Aeronautics 2005;210:65–88.

[29] Badeer GH. GE aero-derivative gas turbines-design and operating features. GE Reference Documents, GER-3695E; Oct 2000.

[30] Etheridge CJ. Mars SoLoNO$_x$—lean premixed combustion technology in production. ASME Paper 1994-GT-255; 1994.

[31] Rocha G, Saadatmand M, Bolander G. Development of the Taurus 70 industrial gas turbine. ASME Paper 1995-GT-411; 1995.

[32] Cowell LH, Rajput A, Rawlins DC. Developments of a dual-fuel injection system for lean premixed industrial gas turbines. ASME Paper 1996-GT-195; 1996.

[33] Steele RC, Cowell LH, Cannon SM, Smith CE. Passive control of combustion instability in lean-premixed combustors. Journal of Engineering for Gas Turbines and Power 2000;122:412–9.

[34] Smith KO, Blust J. Combustion instabilities in industrial gas turbines: solar turbines' experience. Chapter 2. In: Lieuwen T, Yang V, editors. Combustion instabilities in as turbines engines: operational experience, fundamental mechanisms, and modeling. Progress in Astronautics and Aeronautics 2005;210:29–42.

[35] Smith KO, Kurzynske FR, Angello LC. Experimental evaluation of fuel injection configurations for a lean-premixed low NO_x gas turbine combustor. ASME Paper 1987-GT-0141; 1987.

[36] Cowell LH, Smith KO. Development of a liquid-fueled lean-premixed gas turbine combustor. Journal of Engineering for Gas Turbines and Power 1993;115:554–62.

[37] Bauermeister KJ, Schetter B, Mohr KD. A 9.25 MW industrial gas turbine with extreme low dry NO$_x$ and CO emissions. ASME Paper 1993-GT-307; 1993.

[38] Streb H, Prade B, Hahner T, Hoffmann S. Advanced burner development for the VX4.3A gas turbines. ASME Paper 2001-GT-0077; 2001.

[39] Deuker E, Waldinger R, Rauh HU, Schade F. Multi fuel concept of the Siemens 3A-gas turbine series. ASME Paper 2001-GT-78; 2001.

[40] Hermsmeyer H, Prade B, Gruschka U, Schmitz U, Hoffmann S, Krebs W. V64.3A gas turbine natural gas burner development. ASME Paper 2002-GT-30106; 2002.

[41] Meisi J, Lauer G, Hoffmann S. Low NO$_x$ emission technology for the VX4.3A gas turbine series in fuel oil operation. ASME Paper 2002-GT-30104; 2002.

[42] Krebs W, Flohr P, Prade B, Hoffmann S. Thermo-acoustics stability chart for high-intensity gas turbine combustion systems. Combustion Science and Technology 2002;174(7):99–128.

[43] Prade B, Streb H, Meisl J. Burner development for flexible engine operation of the newest Siemens gas turbines. ASME Paper 2003-GT-38442; 2003.

[44] Krebs W, Bethke S, Lepers J, Johnson C, Sattinger S, Flohr P, et al. Thermoacoustic design tools and passive means applied by Siemens power generation. Chapter 5. In: Lieuwen T, Yang V, editors. Combustion instabilities in gas turbine engines: operational experience, fundamental mechanisms, and modeling. Progress in Astronautics and Aeronautics 2005:89–112.

[45] Lepers J, Prade B, Pollarolo G, Krebs W, Flohr P, Ferrante A. Investigation of thermoacoustic stability limits of an annular gas turbine combustor test-rig with and without Helmholtz-resonators. ASME Paper 2005-GT-68246; 2005.

[46] Hantschk C, Hermann J, Vortmeyer D. Active instability control with direct-drive servo valves in liquid-fuelled combustion systems. Proceedings of the Combustion Institute 1996;26:2835–41.

[47] Hermann J, Gleis S, Vortmeyer D. Active instability control (AIC) of spray combustors by modulation of the liquid fuel flow rate. Combustion Science and Technology 1996;118:1–25.

[48] Seume JR, Vortmeyer N, Krause W, Hermann J, Hantschk CC, Zangl P, et al. Application of active combustion instability control to a heavy duty gas turbine. Journal of Engineering for Gas Turbines and Power 1998;120:721–6.

[49] Berenbrink P, Hoffmann S. Suppression of dynamic combustion instabilities by passive and active means. ASME Paper 2000-GT-0079; 2000.

[50] Hermann J, Hoffmann S. Implementation of active control in a full-scale gas turbine combustor. Chapter 19. In: Lieuwen T, Yang V, editors. Combustion instabilities in gas turbine engines: operational experience, fundamental mechanisms, and modeling. Progress in Astronautics and Aeronautics 2005;210:611–34.

[51] Fox TG, Schlein BC. Full annular rig development of the FT8 gas turbine combustors. Journal of Engineering for Gas Turbines and Power 1992;114:27–32.

[52] McVey JB, Padget FC, Rosfjord TJ, Hu AS, Peracchio AA, Schlein B, et al. Evaluation of low-NO$_x$ combustor concepts for aero-derivative gas turbine engines. Journal of Engineering for Gas Turbines and Power 1993;115:581–7.

[53] Synder TS, Rosfjord TJ, McVey JB, Chiappetta LM. Comparison of liquid fuel/air mixing and NO$_x$ emissions for a tangential entry nozzle. ASME Paper 1994-GT-283; 1994.

[54] Snyder TS, Rosfjord TJ, McVey JB. Emission and performance of a lean-premixed gas fuel injection system for aero-derivative gas turbine engines. Journal of Engineering for Gas Turbines and Power 1996;118:38–45.

[55] Kendrick DW, Anderson TJ, Sowa WA, Snyder TS. Acoustic sensitivities of lean-premixed fuel injectors in a single nozzle rig. Journal of Engineering for Gas Turbines and Power 1999;121:429–35.

[56] Kendrick DW, Bhargava A, Colket MB, Sowa WA. NO$_x$ scaling characteristics for industrial gas turbine fuel injectors. ASME Paper 2000-GT-98; 2000.

[57] Schlein BC, Anderson DA, Beukenberg M, Mohr KD, Leiner HL, Traptau W. Development history and field experiences of the first FT8 gas turbine with dry low NO$_x$ combustion system. ASME Paper 1999-GT-241; 1999.

[58] Cohen JM, Rey NM, Jacobson CA, Anderson TJ. Active control of combustion instability in a liquid-fuelled low-NO$_x$ combustor. Journal of Engineering for Gas Turbines and Power 1999;121:281–4.

[59] Barooah P, Anderson TJ, Cohen JM. Active combustion instability control with spinning valve actuator. Journal of Engineering for Gas Turbines and Power 2003;125:925–32.

[60] Cohen JM, Stufflebeam JH, Proscia W. The effect of fuel/air mixing on actuation authority in an active combustion instability control system. Journal of Engineering for Gas Turbines and Power 2001;123:537–42.

[61] Cohen JM, Banaszuk A. Factors affecting the control of unstable combustors. Journal of Propulsion and Power 2003;19(5):811–21.

[62] Banaszuk A, Ariyur KB, Krstic M, Jacobson CA. An adaptive algorithm for control of combustion instability. Automatica 2004;40:1965–72.

[63] Hibshman JR, Cohen JM, Banaszuk A, Anderson TJ, Alholm HA. Active control of combustion instability in a liquid-fuelled sector combustor. ASME Paper 1999-GT-215; 1999.

[64] Sattelmayer T, Felchlin MP, Haumann J, Hellat J, Styner D. Second-generation low-emission combustors for ABB gas turbines: burner development test at atmospheric pressure. Journal of Engineering for Gas Turbines and Power 1992;114:118–25.

[65] Aigner M, Muller G. Second-generation low-emission combustors for ABB gas turbines: field measurements with GT11N-EV. Journal of Engineering for Gas Turbines and Power 1993;115:533–6.

[66] Joos F, Brunner P, Schulte-Werning B, Syed K, Eroglu A. Development of the sequential combustion system for the ABB GT24/GT26 gas turbine family. ASME Paper, 1996-GT-315; 1996.

[67] Joos F, Brunner P, Stalder M, Tschirren S. Field experience for the sequential combustion system for the GT24/GT26 gas turbine family. ASME Paper 1998-GT-220; 1998.

[68] Dobbeling K, Knopfel HP, Polifke W, Winkler D, Steinbach C, Sattelmayer T. Low-NO$_x$ premixed combustion of MBTu Fuels using the ABB double cone burner (EV burner). Journal of Engineering for Gas Turbines and Power 1996;118:46–53.

[69] Reiss F, Griffin T, Reyser K. The ALSTOM GT13E2 medium BTU gas turbine. ASME Paper 2002-GT-30108; 2002.

[70] Nord LO, Scoemaker DR, Andersen HG. A NO$_x$ reduction project for a GT11 type gas turbine. ASME Paper 2005-GT-68779; 2005.

[71] Dobbeling K, Hellat J, Koch H. 25 Years of BBS/ABB/ALSTOM lean premix combustion technologies. ASME Paper 2005-GT-68269; 2005.

[72] Bellucci V, Flohr P, Paschereit CO, Magni F. On the use of Helmholtz resonators for damping acoustic pulsations in industrial gas turbines. Journal of Engineering for Gas Turbines and Power 2004;126:271–5.

[73] Eroglu A, Dobbeling K, Joos F, Brunner P. Vortex generators in lean-premix combustion. Journal of Engineering for Gas Turbines and Power 2001;123:41–9.

[74] Paschereit CO, Flohr P, Knopfel H, Geng W, Steinbach C, Stuber P, Bengtsson K, et al. Combustion control by extended EV burner fuel lance. ASME Paper 2002-GT-30462.

[75] Paschereit CO, Gutmark E. Enhanced performance of a gas-turbine combustor using miniature vortex generators. Proceedings of the Combustion Institute 2002;29:123–9.

[76] Paschereit CO, Gutmark E. Passive combustion control for enhanced stability and reduced emissions in a swirl-stabilized burner. AIAA Paper 2003-1011; 2003.

[77] Paschereit CO, Gutmark E. The effectiveness of passive combustion control methods. ASME Paper 2004-GT-53587; 2004.

[78] Paschereit CO, Gutmark E. Control of combustion instability and emissions by burner's exit geometry modifications. AIAA Paper 2004-0636; 2004.

[79] Bazarov V, Yang V, Puri P. Design and dynamics of jet and swirl injectors. Chapter 2. In: Yang V, Habiballah M, Hulka J, Popp M, editors. Liquid rocket thrust chambers: aspects of modeling, analysis, and design. Progress in Astronautics and Aeronautics 2004;200:19–103.

[80] Beer JM, Chigier NA. Combustion aerodynamics. Krieger Publishing Company; 1983.

[81] Winterfeld G, Eickhoff HE, Depooter K. Fuel injectors. Chapter 3. In: Design of modern gas turbine combustors. San Diego, CA: Academic Press; 1990. p. 229–341.

[82] Mansour A. Gas turbine fuel injection technology. ASME Paper GT-2005-68173; 2005.

[83] Huang Y, Wang S, Yang V. Flow and flame dynamics of lean-premixed swirl injectors. Chapter 10. In: Lieuwen T, Yang V, editors. Combustion instabilities in gas turbine engines: operational experience, fundamental mechanisms, and modeling. Progress in Astronautics and Aeronautics 2005;210:213–76.

[84] Graves CB. Outer shear layer swirl mixer for a combustor. US Patent 5-603-211; 1997.

[85] Wang S, Hsieh SY, Yang V. Unsteady flow evolution in swirl injector with radial entry. I. Stationary conditions. Physics of Fluids 2005;17:045106.

[86] Gupta AK, Lilley DG, Syred N. Swirl flows. London: Abacus Press; 1984.

[87] Hall MG. Vortex breakdown. Annual Review of Fluid Mechanics 1972;4:195–218.

[88] Leibovich S. The structures of vortex breakdown. Annual Review of Fluid Mechanics 1978;10:221–46.

[89] Leibovich S. Vortex stability and breakdown: survey and extension. AIAA Journal 1984;22:1192–206.

[90] Lucca-Negro O, O'Doherty T. Vortex breakdown: a review. Progress in Energy and Combustion Science 2001;27:431–81.

[91] Sarpkaya T. On stationary and traveling vortex breakdown. Journal of Fluid Mechanics 1971;45:545–59.

[92] Sarpkaya T. Vortex breakdown in swirling conical flows. AIAA Journal 1971;9:1792–9.

[93] Faler J, Leibovich S. An experimental map of the internal structure of a vortex breakdown. Journal of Fluid Mechanics 1977;86:313–35.

[94] Faler J, Leibovich S. Disrupted states of vortex flow and vortex breakdown. Physics of Fluids 1977;20:1385–400.

[95] Grabowski WJ, Berger SA. Solution of the Navier–Stokes equation for vortex breakdown. Journal of Fluid Mechanics 1976;75:525–44.

[96] Spall RE. Transition from spiral- to bubble-type vortex breakdown. Physics of Fluids 1996;8:2301–3.

[97] Spall RE, Gatski TB. Computational study of the topology of vortex breakdown. Proceedings of the Royal Society of London, Series A 1991;435:321–37.

[98] Sarpkaya T. Turblent vortex breakdown. Physics of Fluids 1995;7:2301–3.

[99] Sarpkaya T, Novak F. Turbulent vortex breakdown experiments. In: Krause E, Gersten I, editors. IUTAM symposium on dynamics of slender vortices. Kluwer; 1998. p. 287–96.

[100] Squire HB. Analysis of vortex breakdown phenomenon, part 1. Aeronautics Department Report No. 102, Imperial College of Science and Technology; 1960.

[101] Benjamin TB. Theory of vortex breakdown phenomenon. Journal of Fluid Mechanics 1962;14:593–629.

[102] Ludwieg H. Vortex breakdown. Deutsche Luft-und Raumfahrt Report 70–40; 1970.

[103] Jones JP. On the explanation of vortex breakdown. IUTAM symposium on vortex motion, Ann Arbor (BSPA Conference 4984.500, Vol. 21, Part 1); 1964.

[104] Lessen, M., Singh, P.J., and Paillet, F., The stability of a trailing line vortex, part 1: inviscid theory, Journal of Fluid Mechanics, 63, 4, pp. 753–763.

[105] Leibovich S, Stewartson K. A sufficient condition for the instability of columnar vortices. Journal of Fluid Mechanics 1983;126:335–56.

[106] Hall MG. A new approach to vortex breakdown. In: Proceedings of the heat tranctions and fluid mechanics institute. San Diego, La Jolla: University of California; 1967. p. 319–40.

[107] Lu X, Wang S, Sung H, Hsieh S, Yang V. Large eddy simulations of turbulent swirling flows injected into a dump chamber. Journal of Fluid Mechanics 2005;527:171–95.

[108] Wang S, Hsieh SY, Yang V. Unsteady flow evolution in swirl injector with radial entry. II. External excitations. Physics of Fluids 2005;17:045107.

[109] Syred N, Beer J. The damping of precessing vortex cores by combustion in swirl generators. Asttonautica Acta 1972;17:783–801.

[110] Gupta AK, Beer JM, Swithenbank J. Concentric multi-annular swirl burner, stability limits and emission characteristics. Proceedings of the Combustion Institute 1977;14:79–91.

[111] Dellenback PA, Metzger DE, Neitzel GP. Measurements in turbulent swirling flow trough an abrupt axisymmetric expansion. AIAA Journal 1988;26(6):669–81.

[112] Froud D, O'Doherty T, Syred N. Phase averaging of the precessing vortex core in a swirl burner under piloted and premixed combustion conditions. Combustion and Flame 1995;100:407–12.

[113] Fick W, Syred N, Griffiths AJ, O'Doherty T. Phase-averaged temperature characterization in swirl burners. Journal of Power and Energy, Part A 1996;210:383–95.

[114] Syred N, Fick W, O'Doherty T, Griffiths AJ. The effect of the precessing vortex core on combustion in a swirl burner. Combustion Science and Technology 1997;125:139–57.

[115] Anacleto PM, Fernandes EC, Heitor MV, Shtork SI. Swirl flow structure and flame characteristics in a model lean premixed combustor. Combustion Science and Technology 2003;175:1369–88.

[116] Wang S, Yang V, Hsiao G, Mongia H. Large eddy simulation of gas turbine swirl injector flow dynamics. Journal of Fluid Mechanics 2007;583:99–122.

[117] Selle L, Lartigue G, Poinsot T, Koch R, Schildmacher KU, Krebs W, et al. Compressible large eddy simulation of turbulent combustion in complex geometry on unstructured meshes. Combustion and Flame 2004;137:489–505.

[118] Roux S, Lartigue G, Poinsot T, Meier U, Berat C. Studies of mean and unsteady flow in a swirled combustor using experiments, acoustic analysis, and large eddy simulations. Combustion and Flame 2005;141:40–54.

[119] Wang P, Bai XS, Wessman M, Klingmann J. Large eddy simulation and experimental studies of a confined turbulent swirling flow. Physics of Fluids 2004;16(9):3306–24.

[120] Guo B, Langrish TAG, Fletcher DF. Simulation of turbulent swirl flow in an axisymmetric sudden expansion. AIAA Journal 2001;39:96–102.

[121] Syred N. A review of oscillation mechanisms and the role of the precessing vortex core (PVC) in swirl combustion systems. Progress in Energy and Combustion Science 2006;32(2):93–161.

[122] Hussain AKMF. Coherent structures—reality and myth. Physics of Fluids 1983;26(10):2816–50.

[123] Ho CM, Huerre P. Perturbed free shear layer. Annual Review of Fluid Mechanics 1984;16:365–424.

[124] Huerre P, Monkewitz PA. Local and global instabilities in spatially developing flows. Annual Review of Fluid Mechanics 1990;22:473–537.

[125] Holmes P, Lumley JL, Berkooz C. Turbulence, coherent structures, dynamical systems and symmetry. United Kingdom: Cambridge University Press; 1996.

[126] Coats CM. Coherent structures in combustion. Progress in Energy and Combustion Science 1996;22:427–509.

[127] Ferziger JH. The physics and simulation of turbulence. In: Introduction to turbulence modeling IV. Von Karman Institute for Fluid Dynamics; 2002. Lecture Series, 2002-02.

[128] Panda J, McLaughlin DK. Experiments on the instabilities of a swirling jet. Physics of Fluids 1994;6:263–76.

[129] Billant P, Chomaz JM, Huerre P. Experimental study of vortex breakdown in swirling jets. Journal of Fluid Mechanics 1998;376:183–219.

[130] Loiseleux T, Chomaz JM. Breaking of rotational symmetry in a swirling jet experiments. Physics of Fluids 2003;15(2):511–22.

[131] Ivanic T, Foucault E, Pecheux J. Dynamics of swirling jet flow. Experiments in Fluids 2003;35:317–24.

[132] Gallaire F, Rott S, Chomaz JM. Experimental study of a free and forced swirling jet. Physics of Fluids 2004;16(8):2907–17.

[133] Liang H, Maxworthy T. An experimental investigation of swirling jets. Journal of Fluid Mechanics 2005;525:115–59.

[134] Wu C, Farokhi S, Taghavi R. Spatial instability of a swirling jet – theory and experiment. AIAA Journal 1992;30(6):1545–52.

[135] Khorrami MR. Stability of a compressible axisymmetric swirling jet. AIAA Journal 1995;33(4):650–8.

[136] Lim DW, Redekopp LG. Absolute instability conditions for variable density, swirling jet flows. European Journal of Mechanics, B/Fluids 1998;17(2):165–85.

[137] Loiseleux T, Chomaz JM, Huerre P. The effect of swirl on jet and wakes: linear instability of the Rankine vortex axial flow. Physics of Fluids 10(5):1120–34.

[138] Gallaire F, Chomza JM. Instability mechanism in swirling flows. Physics of Fluids 2003;15(9):2622–39.

[139] Martin JE, Meiburg E. Numerical investigation of three-dimensionally evolving jet subject to axisymmetric and azimuthal perturbation. Journal of Fluid Mechanics 1991;230:271–318.

[140] Martin JE, Meiburg E. Numerical investigation of three-dimensionally evolving jet under helical perturbations. Journal of Fluid Mechanics 1992;243:457–87.

[141] Martin JE, Meiburg E. Nonlinear axisymmetric and three dimensional vorticity dynamics in a swirling jet model. Physics of Fluids 1996;8:1917–28.

[142] Mcllwain S, Pollard A. Large eddy simulation of the effects of mild swirl on the near field of a round free jet. Physics of Fluids 2002;14(2):653–61.

[143] Ruith MR, Chen P, Meiburg E, Maxworthy T. Three-dimensional vortex breakdown in swirling jet and wakes: direct numerical simulation. Journal of Fluid Mechanics 2003;486:331–78.

[144] Szasz RZ, Fuchs L. Numerical study of the instabilities of swirling jets. AIAA Paper 2005-1258; 2005.

[145] Presser C, Gupta AK, Semerjian HG. Aerodynamic characteristics of swirling spray flames: pressure-jet atomizer. Combustion and Flame 1993;92:25–44.

[146] Presser C, Gupta AK, Semerjian HG, Avedisian CT. Droplet transport in a swirl-stabilized spray flames. Journal of Propulsion and Power 1994;10(5):631–8.

[147] Cohen JM, Rosfjord TJ. Spray patternation at high pressure. Journal of Propulsion and Power 1991;7(4):481–7.

[148] Cohen JM, Rosfjord TJ. Influences on the spray formed by high-shear fuel nozzle/swirler assemblies. Journal of Propulsion and Power 1993;9(1):16–27.

[149] Chin JS, Rizk NK, Razdan MK. Study of hybrid airblast atomization. Journal of Propulsion and Power 1999;15(2):241–7.

[150] Chin JS, Rizk NK, Razdan MK. Effect of inner and outer airflow characteristics on high liquid pressure prefilming airblast atomization. Journal of Propulsion and Power 2000;16(2):297–301.

[151] McDonell VG, Samuelsen S. Gas and drop behavior in reacting and non-reacting air-blast atomizer sprays. Journal of Propulsion and Power 1991;7(5):684–91.

[152] Wang HY, McDonell VG, Sowa WA, Samuelsen S. Scaling of the two phase flow downstream of a gas turbine combustor swirl cup: part I—mean quantities. Journal of Engineering for Gas Turbines and Power 1993;115:453–60.

[153] Wang HY, McDonell VG, Sowa WA, Samuelsen S. Experimental study of a model gas turbine combustor swirl cup, part I: two phase characterization. Journal of Propulsion and Power 1994;10(4):441–5.

[154] Wang HY, McDonell VG, Sowa WA, Samuelsen S. Experimental study of a model gas turbine combustor swirl cup, part II: droplet dynamics. Journal of Propulsion and Power 1994;10(4):446–52.

[155] Wang HY, McDonell VG, Samuelsen S. Influence of hardware design on the flow field structures and patterns of droplet dispersion: part I—mean quantities. Journal of Engineering for Gas Turbines and Power 1995;117:282–9.

[156] McDonell VG, Arellano L, Lee SW, Samuelsen GS. Effect of hardware alignment on fuel distribution and combustion performance for a production engine fuel injection assembly. Proceedings of the Combustion Institute 1996;26:2725–32.

[157] Fu Y, Caim J, Elkady M, Jeng SM, Mongia HC. Fuel and equivalence ratio effects on spray combustion of a counter-rotating swirler. AIAA Paper 2005-0354; 2005.

[158] Jeng SM, Flohre NM, Mongia HC. Air temperature effects on non-reacting spray characteristics issued from a counter-rotating swirler. AIAA Paper 2005-0355; 2005.

[159] Jeng SM, Flohre NM, Mongia HC. Fluid property effects on non-reacting spray characteristics issued from a counter-rotating swirler. AIAA Paper 2005-0356; 2005.

[160] Ibrahim AA, Jog MA, Jeng SM. Effect of liquid swirl-velocity profile on the instability of a swirling annular liquid sheet. Atomization and sprays 2006;16:237–63.

[161] Ateshkadi A, Mcdonell VG, Samuelsen GS. Lean blowout model for a spray-fired swirl-stabilized combustor. Proceedings of the Combustion Institute 2000;28:1281–8.

[162] Rizk NK, Chin JS, Razdan MK. Modeling of gas turbine fuel nozzle spray. Journal of Engineering for Gas Turbines and Power 1997;119:34–44.

[163] Zheng QP, Jasuja AK, Lefebvre AH. Structure of airblast spray under high ambient pressure conditions. Journal of Engineering for Gas Turbines and Power 1997;119:512–8.

[164] Clack HL, Kosbland CP, Lucas D, Sawyer RF. Development of an air-blast atomizer for independent control of droplet size and spray density. Atomization and Sprays 2004;14:265–88.

[165] Han YM, Seol WS, Lee DS, Yagodkin VI, Jeung IS. Effects of fuel nozzle displacement on prefilming airblast atomization. Journal of Engineering for Gas Turbines and Power 2001;123:33–40.

[166] Bachalo WD. Injection, dispersion, and combustion of liquid fuels. Proceeding of the Combustion Institute 1994;25:333–44.

[167] Benjamin MA. Fuel atomization for next-generation gas turbine combustors. Atomization and Sprays 2000;10:427–38.

[168] Etemad S, Forbes BC. CFD modeling of a gas turbine combustor air swirler effect, Computational fluid dynamics in aero-propulsion. In: Proceedings of the ASME international mechanical engineering congress and exposition; 1995. p. 193–7. San Francisco, CA.

[169] Ateshkadi A, McDonell VG, Samuelson GS. Effect of hardware geometry on gas and drop behavior in a radial mixer spray. Proceeding of the Combustion Institute 1998;27:1985–92.

[170] Merkle K, Haessler H, Buchner H, Zarzalis N. Effect of co- and counter-swirl on the isothermal flow- and mixture-field of an airblast atomizer nozzle. International Journal of Heat and Fluid Flow 2003;24:529–37.

[171] Li G, Gutmark EJ. Effect of swirler configurations on flow structures and combustion characteristics. ASME Paper 2004-GT-53674; 2004.

[172] Mehta JM, Shin HW, Wisler DC. Mean velocity and turbulent flow-field characteristics inside an advanced combustor swirl cup. AIAA Paper AIAA-1989-0215; 1989.

[173] Durbin MD, Ballal DR. Studies of lean blowout in a step swirl combustor. Journal of Engineering for Gas Turbines and Power 1996;118:72–7.

[174] Durbin MD, Vangsness MD, Ballal DR, Katta VR. Study of flame stability in a step swirl combustor. Journal of Engineering for Gas Turbines and Power 1996;118:308–15.

[175] Gupta AK, Lewis MJ, Daurer M. Swirl effects on combustion characteristics of premixed flames. Journal of Engineering for Gas Turbines and Power 2001;123:619–26.

[176] Longmire EK, Eaton JK. Active open-loop control of particle dispersion in round jets. AIAA Journal 1994;32:555–63.

[177] Swanson TR, Richards CD. The structures of an acoustically forced, droplet-laden jet. Atomization and Sprays 1997;7:561–79.

[178] Cerecedo L, Aisa L, Garcia J, Santolaya J. Changes in a coflowing jet structure caused by acoustic forcing. Experiments in Fluids 2004;36:867.

[179] Cohen J, Hibshman J. An experimental study of combustor air swirler acoustic and fluid dynamic sensitivities. Proceedings of Propulsion Engineering Research Center, Pennsylvania State University, University Park; October 1–2, 1997.

[180] Anderson TJ, Kendrick DW, Cohen JW. Measurement of spray/acoustic coupling in gas turbine fuel injectors. AIAA Paper 1998-0718; 1998.

[181] Haile E, Lacas P, Desrayaud C, Veynante D, Durox D. Characterization of a liquid fuel injector under continuous and modulated flow conditions. Particle and Particle Systems Characterization 1998;15:136–44.

[182] Haile E, Delabroy O, Lacas F, Veynante D, Candel S. Structures of an acoustically forced turbulent spray flame. Proceedings of the Combustion Institute 1996;26:1663–70.

[183] Chang H, Nelson D, Sipperley C, Edwards C. Development of a temporally modulated fuel injector with controlled spray dynamics. Journal of Engineering for Gas Turbines and Power 2002;125:284–91.

[184] Hassa C, Heinze J, Stursberg K. Investigation of the response an air blast atomizer combustion chamber configuration on forced modulation of air feed at realistic operating conditions. Journal of Engineering for Gas Turbines and Power 2002;125:872–8.

[185] Arana CA, Sekar B, Mawid MA, Graves CB. Determination of thermo-acoustic response in a demonstrator gas turbine engine. Journal of Engineering for Gas Turbines and Power 2002;124:46–57.

[186] Law CJ. The thermo-acoustic response of a premixed swirl burnerProceedings of the Institute of Mechanical Engineers, Part A. Journal of Power and Engineering 2000;214(Part A):333–54.

[187] Crocco L, Cheng SI. Theory of combustion instability in liquid propellant rocket motors. London: Butterworths Scientific Publications; 1956. AGAR-Dograph No.8.

[188] Weiss RR. An introduction to combustion instability in liquid propellant rocket engines. AFRPL-TR-66-150, Edwards, CA; 1966.

[189] Sutton GP, Biblarz O. Rocket propulsion elements. 7th ed. John Wiley and Sons; 2000.

[190] Wicker JM, Greene WD, Kim SI, Yang V. Triggering of longitudinal combustion instabilities in rockets motors: nonlinear combustion response. Journal of Propulsion and Power 1996;12(6):1148–58.

[191] Wang T. Modeling of combustion dynamics in gas turbine engines. Ph.D. Thesis, Department of Mechanical Engineering, The Pennsylvania State University, University Park, PA; 1997.

[192] Fernandes EC, Heitor MV, et al. Unsteady flames and the Rayleigh criterion. In: Culick FEC, editor. Unsteady combustion; 1996. p. 1–16.

[193] Mongia HC, Held TJ, Hsiao GC, Pandalai RP. Incorporation of combustion instability issues into design process: GE aero-derivative and aero engines experience. Chapter 3. In: Lieuwen T, Yang V, editors. Combustion instabilities in gas turbine engines: operational experience, fundamental mechanisms, and modeling. Progress in Astronautics and Aeronautics 2005;43–64.

[194] Sewell J, Sobieski P. Combustion instability monitoring experience at Calpine. Chapter 7. In: Lieuwen T, Yang V, editors. Combustion instabilities in gas turbine engines: operational experience, fundamental mechanisms, and modeling. Progress in Astronautics and Aeronautics 2005:147–62.

[195] Broda JC, Seo S, Santoro RJ, Shirhattikar G, Yang V. An experimental study of combustion dynamics of a premixed swirl injector. Proceedings of the Combustion Institute 1998;27:1849–56.

[196] Seo S. Parametric study of lean-premixed combustion instability in a pressurized model gas turbine combustor. Ph.D. Thesis, Department of Mechanical and Nuclear Engineering, The Pennsylvania State University, University Park, PA; 1999.

[197] Lee SY, Seo S, Broda JC, Pal S, Santoro RJ. An experimental estimation of mean reaction rate and flame structure during combustion instability in a lean premixed gas turbine combustor. Proceedings of the Combustion Institute 2000;28:775–82.

[198] Huang Y, Yang V. Bifurcation of flame structure in a lean-premixed swirl-stabilized combustor: transition from stable to unstable flame. Combustion and Flame 2004;136:383–9.

[199] Huang Y, Sung HG, Hsieh SY, Yang V. Large-eddy simulation of combustion dynamics of lean-premixed swirl-stabilized combustor. Journal of Propulsion and Power 2003;19(5):782–94.

[200] Venkataraman KK. An investigation of the acoustic instability mechanism in lean-premixed dump combustor. Ph.D. Thesis, Department of Mechanical Engineering, the Pennsylvania State University, University Park, PA; 2000.

[201] Knoop P, Culick FEC, Zukoski EE. Extension of the stability of motions in a combustion chamber by nonlinear active control based on hysteresis. Combustion Science and Technology 1997;123:363–76.

[202] Lieuwen T. Experimental investigation of limit-cycle oscillations in an unstable gas-turbine combustor. Journal of Propulsion and Power 2002;18:61–7.

[203] Sterling JD. Nonlinear analysis and modeling of combustion instabilities in a laboratory combustor. Combustion Science and Technology 1993;89:167–79.

[204] Jahnke CC, Culick FEC. Application of dynamical systems theory to nonlinear combustion instabilities. Journal of Propulsion and Power 1994;10(4):508–17.

[205] Ananthkrishnan N, Deo S, Culick FEC. Reduced-order modeling and dynamics of nonlinear acoustic waves in a combustion chamber. Combustion Science and Technology 2005;177:221–47.

[206] Di Benedetto A, Marra FS, Russo G. Spontaneous oscillations in lean-premixed combustion. Combustion Science and Technology 2002;174(10):1–18.

[207] Di Benedetto A, Marra FS, Russo G. Bifurcation analysis of lean-premixed combustion of hydrogen/propane mixtures. Combustion Science and Technology 2005;177:413–34.

[208] Ananthkrishnan N, Sudhakar K, Sudershan S, Agarwal A. Application of secondary bifurcations to large-amplitude limit cycles in mechanical systems. Journal of Sound and Vibration 1998;215(1):183–8.

[209] Ananthkrishnan N, Sudhakar K, Sudershan S, Agarwal A. Large-amplitude limit cycles in resonantly coupled oscillators. Journal of Sound and Vibration 2000;231(5):1377–82.

[210] Drazin PG. Nonlinear systems. London: Cambridge University Press; 1992.

[211] Strogatz SH. Nonlinear dynamics and chaos: with applications to physics, biology, chemistry, and engineering. MA: Addison-Wesley Publishing Company; 1994.

[212] Kuznetsv YA. Elements of applied bifurcation theory. 3rd ed. New York: Springer-Verlag; 2004.

[213] Khalil HK. Nonlinear systems. 3rd ed. New Jersey: Prentice Hall; 2002.

[214] Isella G, Seywert C, Culick FEC, Zukoski EE. A further note on active control of combustion instabilities based on hysteresis. Combustion Science and Technology 1997;126:381–8.

[215] Mordaunt C. Dual-fuel issues related to performance, emissions, and combustion instability in lean premixed gas turbine systems. Ph.D. Thesis, Department of Mechanical and Nuclear Engineering, The Pennsylvania State University, University Park, PA; 2005.

[216] Katsuki M, Whitelaw JH. The influence of duct geometry on unsteady premixed flames. Combustion and Flame 1986;63:87–94.

[217] Sivasegaram, Whitelaw JH. The influence of swirl on oscillations in ducted premixed flames. Combustion and Flame 1991;85:195–205.

[218] Gutmark EJ, Schadow KC, Nina MNR, Pita GPA. Suppression of combustion instability by geometrical design of the bluff-body stabilizer. Journal of Propulsion and Power 1995;11:456–63.

[219] Shadow KC, Gutmark EJ, Wilson KJ, Smith RA. Multistep dump combustor design to reduce combustion instabilities. Journal of Propulsion and Power 1990;6:407–11.

[220] Straub DL, Richards GA. Effect of fuel nozzle configuration on premixed combustion dynamics. ASME Paper 1998-GT-492; 1998.

[221] Straub DL, Richards GA. Effect of axial swirl vane location on combustion dynamics. ASME Paper 1999-GT-0109; 1999.

[222] Venkataraman KK, Preston LH, Simons DW, Lee BJ, Lee JG, Santavicca DA. Mechanisms of combustion instability in a lean premixed dump combustor. Journal of Propulsion and Power 1999;15(6):909–18.

[223] Li G, Gutmark EJ. Effect of nozzle geometry on combustion flow field and combustion characteristics. Proceedings of the Combustion Institute 2005;30:2893–901.

[224] Shih WP, Lee JG, Santavicca DA. Stability and emissions characteristics of a lean premixed gas turbine combustor. Proceedings of the Combustion Institute 1996;26:2771–8.

[225] Richards GA, McMillian MM, Gemmen RS, Rogers WA, Cully SR. Issues for low-emission, fuel-flexible power systems. Progress in Energy and Combustion Science 2001;27:141–69.

[226] Janus MC, Richards GA, Yip MJ, Robey EH. Effects of ambient conditions and fuel composition on combustion stability. ASME Paper 1997-GT-266; 1997.

[227] Lieuwen T, McDonell V, Petersen E, Santavicca DA. Fuel flexibility influences on premixed combustor blowout, flashback, auto-ignition, and stability. ASME Paper 2006-GT-90770; 2006.

[228] Ferguson D, Straub D, Richards G, Robey E. Impact of fuel variability on dynamic instabilities in gas turbine combustion. Fifth US combustion meeting; 2007.

[229] Figura L, Lee JG, Quay BD, Santavicca DA. The effects of fuel composition on flame structure and combustion dynamics in a lean premixed combustor. ASME Paper 2007-GT-27298; 2007.

[230] Kido H, Nakahara M, Nakashima K, Hashimoto J. Influence of local flame displacement velocity on turbulent burning velocity. Proceedings of the Combustion Institute 2002;29:1855–61.

[231] Mordaunt C, Brossard C, Lee SY, Santoro RJ. Combustion instability studies in a high-pressure lean-premixed model combustor under liquid fuel operation. In: Proceedings of the joint power generation conference; 2001. JPGC2001/Fact-19089.

[232] Nerd LO, Andersen HG. A study of parameters affecting the combustion stability and emissions behavior of ALSTOM heavy-duty gas turbines. ASME paper ASME GT2004-53228; 2004.

[233] Bernier D, Lacas F, Candel S. Instability mechanisms in a premixed pre-vaporized combustor. Journal of Propulsion and Power 2004;20(4).

[234] Archarya S, Murugappan S, O'Donnell M, Gutmark EJ. Characteristics and control of combustion instabilities in a swirl-stabilized spray combustor. Journal of Propulsion and Power 2002;19(3):484–96.

[235] Lieuwen T, Zinn BT. The role of equivalence ratio oscillation in driving combustion instabilities in low NO_x gas turbines. Proceedings of the Combustion Institute 1998;27:1809–16.

[236] Lieuwen T, Torres H, Johnson C, Zinn BT. Mechanisms of combustion instability in lean premixed gas turbine combustors. Journal of Engineering for Gas Turbines and Power 2001;123:182–9.

[237] Lee JG, Kim K, Santavicca DA. Measurement of equivalence ratio fluctuation and its effect on heat release during unstable combustion. Proceedings of the Combustion Institute 2000;28:415–21.

[238] Lee JG, Kim K, Santavicca. A study of the role of equivalence ratio fluctuations during unstable combustion in a lean-premixed combustor. AIAA Paper 2002-4015; 2002.

[239] Rayleigh JWS. The theory of sound, vol. II. New York: Dover; 1945.

[240] Chu BT. On the energy transfer to small disturbances in fluid flow, part I. Acta Mechanica 1965;1:215–34.

[241] Pierce AD. Acoustics: an introduction to its physical principles and applications. Acoustical Society of America; 1989.

[242] Candel S, Huynh C, Poinsot T. Some modeling methods of combustion instabilities, Chapter 5. In: Culick FEC, Heitor MV, Whitelaw JH, editors. Unsteady combustion. Netherlands: Kluwer Academic Publisher; 1996.

[243] Dowling AP. Combustion noise and active control. Von Karman Institute for Fluid Dynamics; 1997. Lecture Series, 1997-07.

[244] Huang Y, Wang S, Yang V. A systematic analysis of combustion dynamics in a lean-premixed swirl-stabilized combustor. AIAA Journal 2006;44(4):724–40.

[245] Apte S, Yang V. Unsteady flow evolution in porous chamber with surface mass injection, part 2: acoustic excitation. AIAA Journal 2002;40(2):244–53.

[246] Huang Y. Modeling and simulation of combustion dynamics in lean-premixed swirl-stabilized gas turbine engines. Ph.D. Thesis, Department of Mechanical and Nuclear Engineering, The Pennsylvania State University, University Park, PA; 2003.

[247] Swift G. Thermoacoustics. New York: Acoustical Society of America; 2002.

[248] Harrison RL. Shake, rattle and roll—where there's heat, there's probably vibration. Sound and Vibration 2003;37(5):8–9.

[249] Zinn BT, Lieuwen. Combustion instabilities: basic concepts. Chapter 1. In: Lieuwen T, Yang V, editors. Combustion instabilities in gas turbine engines: operational experience, fundamental mechanisms, and modeling. Progress in Astronautics and Aeronautics 2005;210:3–28.

[250] Ducruix S, Schuller T, Durox D, Candel S. Combustion dynamics and instabilities: elementary coupling and driving mechanisms. Journal of Propulsion and Power 2003;19(5):722–34.

[251] Culick FEC. Dynamics of combustion systems, fundamental, acoustics and control. In: Active control of engine dynamics. Von Karman Institute for Fluid Dynamics; May 14–18, 2001. Lecture Series.

[252] Landau L. On the theory of slow combustion. Acta Physicochim URSS 1944;19:77.

[253] Sivashinsky GI. Nonlinear analysis of hydrodynamic instability in laminar flames. I. derivation of basic equations. Acta Astronautica 1977;4:1177–206.

[254] Clavin P. Dynamic behavior of premixed flame front in laminar and turbulent flows. Progress in Energy and Combustion Science 1985;11:1–59.

[255] Buckmaster J. The structure and stability of laminar flames. Annual Review of Fluid Mechanics 1993;25:21–53.

[256] Law CK, Sung CJ. Structure, aerodynamics, and geometry of premixed flamelets. Progress in Energy and Combustion Science 2000;26:459–505.

[257] Marble FE, Candel S. An analytical study of the non-steady behavior of large combustor. Proceedings of the Combustion Institute 1978;17:761–9.

[258] Subbaiah MV. Non-steady flame spreading in two-dimensional ducts. AIAA Journal 1983;21(11):1557–64.

[259] Poinsot T, Candel SM. A nonlinear model for ducted flame combustion instabilities. Combustion Science and Technology 1988;61:121–51.

[260] Yang V, Culick FEC. Analysis of low frequency combustion instabilities in a laboratory ramjet combustor. Combustion Science and Technology 1986;45:1–25.

[261] Fleifil M, Annaswamy M, Ghoneim ZA, Ghoniem AF. Response of a laminar premixed flame to flow oscillations: a kinetic model and thermo-acoustic instability results. Combustion and Flame 1996;106:487–510.

[262] Dowling AP. A kinematic model of a ducted flame. Journal of Fluid Mechanics 1999;394:51–72.

[263] Bloxsidge GJ, Dowling AP, Langhorne PJ. Reheat buzz: an acoustically coupled combustion instability, part 2. Theory. Journal of Fluid Mechanics 1988;193:445–73.

[264] Ducruix S, Durox D, Candel S. Theoretical and experimental determinations of the transfer function of a laminar premixed flame. Proceedings of the Combustion Institute 2000;28:765–73.

[265] Schuller T, Durox D, Candel S. A unified model for the prediction of laminar flame transfer functions: comparisons between conical and V-flame dynamics. Combustion and Flame 2003;134:21–34.

[266] Mehta PG, Soteriou MC, Banaszuk A. Impact of exotermicity on steady and linearized response of a premixed ducted flame. Combustion and Flame 2005;141:392–405.

[267] You D, Huang Y, Yang V. A generalized model of acoustic response of turbulent premixed flame and its application to gas-turbine combustion instability analysis. Combustion Science and Technology 2005;117:1109–50.

[268] Lieuwen T. Modeling premixed combustion–acoustic wave interactions: a review. Journal of Propulsion and Power 2003;19(5):765–81.

[269] Lee JG, Santavicca DA. Experimental diagnostics for the study of combustion instabilities in lean premixed combustion. Journal of Propulsion and Power 2003;19(5):735–50.

[270] Reuter DM, Hegde UG, Zinn BT. Flowfield measurements in an unstable ramjet burner. Journal of Propulsion and Power 1990;6:680–9.

[271] Zukoski FE. Afterburners. Chapter 21. In: Oates G, editor. The aero-thermodynamics of aircraft gas turbine engines. Air Force Aero Propulsion Laboratory; 1978. AFAPL-TR-78-52.

[272] Lieuwen T, Neumeier Y, Zinn BT. The role of unmixedness and chemical kinetics in driving combustion instabilities in lean premixed combustor. Combustion Science and Technology 1998;135:193–211.

[273] Richards GA, Janus MC. Characterization of oscillations during premix gas turbine combustion. ASME Journal of Engineering for Gas Turbines and Power 1998;120:294–302.

[274] Richards GA, Janus M, Robey EH. Control of flame oscillations with equivalence ratio modulation. Journal of Propulsion and Power 1999;15(2):232–40.

[275] Fung YT, Yang V, Sinha A. Active control of combustion instabilities with distributed actuators. Combustion Science and Technology 1991;78:217–45.

[276] Scarinci T, Freeman C. The propagation of a fuel–air ratio disturbance in a simple premixer and its influence on pressure wave amplification. ASME Paper 2000-GT-0106; 2000.

[277] Sattlemayer T. Influence of the combustor aerodynamics on combustion instabilities from equivalence ratio fluctuations. ASME Paper 2000-Gt-0082; 2000.

[278] Kaskan WE, Noreen AE. High frequency oscillations of a flame held by a bluff body. ASME Journal of Engineering for Gas Turbines and Power 1955;77:885–95.

[279] Rogers DE, Marble FE. A mechanism for high frequency oscillations in ramjet combustors and afterburners. Jet Propulsion 1956:456–62.

[280] Smith DA, Zukoski EE. Combustion instability sustained by unsteady vortex combustion. AIAA Paper 1985-1248; 1985.

[281] Sterling JD, Zukoski EE. Longitudinal mode combustion instabilities in a dump combustor. AIAA Paper 1987-0220; 1987.

[282] Poinsot TJ, Trouve AC, Veynante DP, Candel S, Esposito E. Vortex-driving acoustically coupled combustion instabilities. Journal of Fluid Mechanics 1987;177:165–292.

[283] Hegde UG, Reuter D, Daniel BR, Zinn BT. Flame driving of longitudinal instabilities in dump type ramjet combustors. Combustion Science and Technology 1987;55:125–38.

[284] Schadow KC, Gutmark E. Combustion instability related to vortex shedding in dump combustor and their passive control. Progress in Energy and Combustion Science 1992;18:117–32.

[285] Kailasanath JH, Gardner JH, Boris JP, Oran ES. Acoustic–vortex interactions and low frequency oscillations in axisymmetric combustors. Journal of Propulsion and Power 1989;5:165–71.

[286] Kailasanath K, Gardner JH, Oran ES, Boris JP. Numerical simulations of unsteady reactive flows, in a combustion chamber. Combustion and Flame 1991;86:115–34.

[287] Najm HN, Ghoniem AF. Numerical simulation of the convective instability in a dump combustor. Journal of Propulsion and Power 1991;29(6):911–9.

[288] Najm HN, Ghoniem AF. Coupling between vorticity and pressure oscillations in combustion instabilities. Journal of Propulsion and Power 1994;10:769–76.

[289] Ghoniem AF, Annaswamy A, Wee D, Yi T, Park S. Shear flow-driven combustion instabilities: evidence, simulation, and modeling. Proceedings of the Combustion Institute 2002;29:53–60.

[290] Ghoniem AF, Park S, Wachsman A, Annaswamy A, Wee D, Murat Altay H. Mechanism of combustion dynamics in a backward-facing step stabilized premixed flame. Proceedings of the Combustion Institute 2005;30:1783–90.

[291] Kulsheimer C, Buchner H. Combustion dynamics of turbulent swirling flames. Combustion and Flame 2002;131:70–84.

[292] Li GQ, Gutmark EJ. Experimental study of large coherent structures in a swirl-dump combustor. AIAA Paper 2004-0133; 2004.

[293] Paschereit CO, Gutmark EJ, Weisenstein W. Structure and control of thermoacoustic instabilities in a gas-turbine combustor. Combustion Science and Technology 1998;138:213–32.

[294] Paschereit CO, Gutmark EJ, Weisenstein W. Control of thermo-acoustic instabilities and emission in an industrial-type gas-turbine combustor. Proceedings of the Combustion Institute 1998;27:1817–24.

[295] Sirignano WA. Liquid-propellant droplet vaporization: a rate-controlling process for combustion instability. Chapter 11. In: Yang V, Anderson WE,

editors. Liquid rocket engine combustion instability. Progress in Astronautics and Aeronautics 1995;169:307–44.

[296] Tong AY, Sirignano WA. Oscillatory vaporization of fuel droplets in an unstable combustor. Journal of Propulsion and Power 1989;5(3):257–61.

[297] Bhatia R, Sirignano WA. One dimensional analysis of liquid-fueled combustion instability. Journal of Propulsion and Power 1991;7(6):953–61.

[298] Chiang CH. Isolated and interacting vaporizing fuel droplets: field calculation with variable properties. Ph.D. Thesis, Department of Mechanical Engineering, University of California, Irvine, CA; 1990.

[299] Chiang CH, Raju MS, Sirignano WA. Numerical analysis of convecting, vaporizing fuel droplet with variable properties. International Journal of Heat and Mass Transfer 1992;35(5):1307–24.

[300] Delplanque JP, Sirignano WA. Transcritical liquid oxygen droplet vaporization: effect on rocket combustion instability. Journal of Propulsion and Power 1996;12(2):349–57.

[301] Duvvur A, Chiang CH, Sirignano WA. Oscillatory fuel droplet vaporization: driving mechanism for combustion instability. Journal of Propulsion and Power 1996;12(2):358–65.

[302] Vandsburger U, McManus K, Bowman C. Effect of fuel spray vaporization on the stability characteristics of a dump combustor. AIAA Paper 1989-2436; 1989.

[303] Anderson WE, Miller KL, Ryan HM, Pal S, Santoro RJ, Dressler JL. Effect of periodic atomization on combustion instability in liquid-fueled propulsion systems. Journal of Propulsion and Power 1998;14(5):8180–825.

[304] Chao CC, Heister SD. Contribution of atomization to F-1 engine combustion instabilities. Engineering Analysis with Boundary Elements 2004;28:1045–53.

[305] Tanabe M, Kuwahara T, Satoh K, Fujimori T, Sato J, Kono M. Droplet combustion in standing sound waves. Proceedings of the Combustion Institute 2005;30:1957–64.

[306] Conrad T, Bibik A, Shcherbik D, Lubarsky E, Zinn BT. "Slow" control of combustion instabilities by fuel spray modification using smart fuel injector. AIAA Paper 2004-1034; 2004.

[307] Conrad T, Bibik A, Shcherbik D, Lubarsky E, Zinn BT. Control of instabilities in liquid fueled combustor by modification of the reaction zone using smart fuel injector. AIAA Paper 2004-4029; 2004.

[308] Schadow K, Yang V, Culick F, Rosfjord T, Sturgess G, Zinn BT. Active combustion control for propulsion systems. AGARD Workshop Report; 1996.

[309] Yang V. Introductions: stability characteristics and control approach. In: Active control of engine dynamics. Von Karman Institute for Fluid Dynamics; May 14–18, 2001.

[310] Richards GA, Straub DL, Robey EH. Passive control of combustion dynamics in stationary gas turbines. Journal of Propulsion and Power 2003;19(5):795–810.

[311] Bellucci V, Schuermans B, Nowak D, Flohr P, Paschereit CO. Thermoacoustic modeling of a gas turbine combustor equipped with acoustic dampers. Journal of Engineering for Gas Turbines and Power 2005;127:372–8.

[312] Gysling DL, Copeland GS, McCormick DC, Proscia WM. Combustion system damping augmentation with Helmholtz resonators. Journal of Engineering for Gas Turbines and Power 2005;122:269–74.

[313] Dupere IDJ, Dowling AP. The use of Helmholtz resonators in a practical combustor. Journal of Engineering for Gas Turbines and Power 2005;127:268–75.

[314] Mastrovito M, Camporeale SM, Forte A, Fortunato B. Analysis of pressure oscillations data in gas turbine annular combustion chamber equipped with passive damper. ASME Paper 2005-GT-69056; 2005.

[315] James D. A solution for noise associated with a series staged DLE combustion systems. Proceedings of the fourth international pipeline conference. Paper IPC2002-27342; 2002.

[316] Reardon FH. Design factors affecting damping-available theory. SP-194. In: Harrje DT, Reardon FH, editors. Liquid propellant rocket combustion instability. NASA; 1972. p. 386–9.

[317] Combs LP, Oberg CL, Coultas TA, Evers WH. Liquid rocket engine combustion stabilization devices. SP-8113. NASA; 1974.

[318] Wicker JM, Yoon MW, Yang V. Linear and non-linear pressure oscillations in baffled combustion chambers. Journal of Sound and Vibration 1995;184(1):141–71.

[319] Male T, Kerslake WR. A method for prevention of screaming in rocket engines. NASA-RM-E54F28A; 1954.

[320] Kurtz AD, Chivers JWH, Ned AA. Sensor requirements for active gas turbine engine control. In: Active control technology for enhanced performance operational capabilities of military aircraft, land vehicles and sea vehicles; May 8–11, 2000. Braunschweig, Germany.

[321] Yu K. Active control of engine dynamics: fundamentals and fluid dynamics – experiments, active control of engine dynamics. VKI/RTO. Von Karman Institute for Fluid Dynamics; May 14–18, 2001.

[322] Nori V, Seitzman JM. Evaluation of chemiluminescence as a combustion diagnostic under varying operating conditions. AIAA-2008-953; 2008.

[323] Furlong ED, Baer DS, Hanson RK. Real-time adaptive combustion control using diode-laser absorption sensor. Proceedings of the Combustion Institute 1998;27:103–11.

[324] Furlong ED, Mihalcea RM, Webber ME, Baer DS, Hanson RK. Diode-laser sensors for real-time control of pulsed combustion systems. AIAA Journal 1999;37(6):732–7.

[325] Hanson R, Ma L, Mattison D, Sanders S. Diode laser sensors for combustion control. In: International colloquium on combustion and noise control. Cranfield, UK: Cranfield University Press; 2003.

[326] Docquire N, Candel S. Combustion control and sensors: a review. Progress in Energy and Combustion Science 2002;28:107–50.

[327] Lang W, Poinsot T, Candel S. Active control of combustion instability. Combustion and Flame 1987;70:281–9.

[328] Poinsot T, Bourienne F, Candel S, Esposito E, Lang W. Suppression of combustion instabilities by active control. Journal of Propulsion and Power 1989;5(1):14–20.

[329] Gulati A, Mani R. Active control of unsteady combustion induced oscillations. Journal of Propulsion and Power 1992;8(5):1109–15.

[330] Sivasegaram S, Tsai RF, Whitelaw JH. Control of combustion oscillations by forced oscillation of part of fuel supply. Combustion Science and Technology 1995;105:67–83.

[331] Vaudrey MA, Baumann WT, Saunders WR. Time-averaged gradient control of thermoacoustic instabilities. Journal of Propulsion and Power 2003;19(5):830–6.

[332] Bloxsidge GJ, Dowling AP, Hooper N, Langhorne PJ. Active control of reheat buzz. AIAA Journal 1988;26(7):783–90.

[333] Poinsot T, Yip B, Veynante D, Trouve A, Samaniego JM, Candel S. Active control: an investigation method for combustion instabilities. Journal De Physique, France 1992;2:1331–57.

[334] Schadow KC, Gutmark E, Wilson KJ. Active combustion control in a coaxial dump combustor. Combustion Science and Technology 1992;81:285–300.

[335] Gutmark E, Parr TP, Wilson KJ, Hanson-Parr DM, Schadow KC. Closed-loop control in a flame and a dump combustor. IEEE Control Systems Magazine April, 1993:73–8.

[336] Wilson KJ, Gutmark E, Schadow KC, Smiths RA. Feedback control of a dump combustor with fuel modulation. Journal of Propulsion and Power 1995;11(2):268–74.

[337] Padmanabhan KT, Bowman CT, Powell JD. An adaptive optimal combustion control strategy. Combustion and Flame 1995;100:101–10.

[338] Paschereit CO, Gutmark EJ, Weisenstein W. Coherent structures in swirling flows and their role in acoustic combustion control. Physics of Fluids 1999;11(9):2667–78.

[339] Paschereit CO, Gutmark EJ, Weisenstein W. Excitation of thermo-acoustic instabilities by interaction of acoustics and unstable swirling flow. AIAA Journal 2000;38(6):1025–34.

[340] Paschereit CO, Gutmark EJ. Proportional control of combustion instabilities in a simulated gas turbine combustor. Journal of Propulsion and Power 2002;18(6):1298–304.

[341] Langhorne PJ, Dowling AP, Hooper N. Practical active control system for combustion oscillations. Journal of Propulsion and Power 1990;6(3):324–33.

[342] Fleifil M, Hathout JP, Annaswamy AM, Ghoniem AF. The origin of secondary peaks with active control of thermo-acoustic instability. Combustion Science and Technology 1998;133:227–65.

[343] Fung YT, Yang V. Active control of nonlinear pressure oscillations in combustion chamber. Journal of Propulsion and Power 1992;8(6):1282–9.

[344] Yang V, Sinha A, Fung YT. State-feedback control of longitudinal combustion instabilities. Journal of Propulsion and Power 1992;8(1):66–73.

[345] Neumeier Y, Zinn BT. Experimental demonstration of active control of combustion instabilities using real-time modes observation and secondary fuel injection. Proceedings of the Combustion Institute 1996;26:2811–8.

[346] Bloxsidge GJ, Dowling AP, Hooper N, Langhorne PJ. Active control of an acoustically driven combustion instability. Journal of Theoretical and Applied Mechanics 1987;6(Suppl.):161–75.

[347] Doyle JC, Glover K, Pramod P, Francis BA. State-space solutions to standard H_2 and H_∞ control problems. IEEE Transactions on Automatic Control 1989;34:831–47.

[348] Packard A, Doyle JC. The complex structured singular value. Automatica 1993;29:71–109.

[349] Hong BS, Yang V, Ray A. Robust feedback control of combustion instability with model uncertainty. Combustion and Flame 2000;120:91–106.

[350] Chu YC, Glover K, Dowling AP. Control of combustion oscillations via H_∞ loop-shaping, μ-analysis and integral quadratic constraints. Automatica 2003;39:219–31.

[351] Safonov MG, Athans M. Gain and phase margin for multiloop LQG regulators. IEEE Transactions on Automatic Control 1977;22:1237–54.

[352] Doyle JC. Guaranteed margins in LQG regulators. IEEE Transactions on Automatic Control 1976;23:715–56.

[353] Hathout JP, Annaswamy AM, Fleifil M, Ghoniem AF. A model-based active control design for thermo-acoustic instability. Combustion Science and Technology 1998;132:99–138.

[354] Hathout JP, Fleifil M, Annaswamy AM, Ghoniem AF. Active control of combustion instability using fuel-injection in the presence of time-delays. Journal of Propulsion and Power 2002;18(2):390–9.

[355] Allgood S, Murugappan S, Acharya S, Gutmark E. Infrared measurements of thermoacoustic instabilities in a swirl-stabilized combustor. Combustion Science and Technology 2003;175:333–55.

[356] Murugappan S, Acharya S, Allgood DC, Park S, Annaswamy AM, Ghoniem AF. Optimal control of a swirl-stabilized spray combustor using system identification approach. Combustion Science and Technology 2003;175:55–81.

[357] Campos-Delgado DU, Zhou K, Allgood S, Acharya S. Active control of combustion instabilities using model-based controllers. Combustion Science and Technology 2003;175:27–53.

[358] Campos-Delgado DU, Schuermans BBH, Zhou K, Paschereit CO, Gallestey A, Poncet A. Thermoacoustic instabilities: modeling and control. IEEE Transactions on Control Systems Technology 2003;11(4):429–47.

[359] Gutmark E, Parr TP, Hanson-Parr DM, Schadow KC. Use of chemiluminescence and neural networks in active combustion control. Proceedings of the Combustion Institute 1990;23:1101–6.

[360] Allen MG, Butler CT, Johnson SA, Lo EY, Russo F. An imaging neural network combustion control system for utility boiler applications. Combustion and Flame 1993;94:205–14.

[361] Koshigoe S, Komatsuzaki T, Yang V. Adaptive control of combustion instability with on-line system identification. Journal of Propulsion and Power 1999;15(3):383–9.

[362] Evesque S, Dowling AP. LMS algorithm for adaptive control of combustion oscillations. Combustion Science and Technology 2001;164:65–93.

[363] Billoud G, Galland MA, Huynh Huu C, Candel S. Adaptive active control of combustion instabilities. Combustion Science and Technology 1992;81:257–83.

[364] Kemal A, Bowman CT. Real-time adaptive feedback control of combustion instability. Proceedings of the Combustion Institute 1996;26:2803–9.

[365] Blonbou B, Laverdant A, Zaleski S, Kuentzmann P. Active control of combustion instability on a Rijke tube using neural networks. Proceedings of the Combustion Institute 2000;28:747–55.

[366] Murugappan S, Gutmark EJ, Acharya S, Krstic M. Extremum-seeking adaptive controller for swirl-stabilized spray combustion. Proceedings of the Combustion Institute 2000;28:731–7.

[367] Menon S, Sun Y. Fuzzy logic control of reheat buzz. AIAA Paper 1996-2759; 1996.

[368] Krstic M, Krupadanam A, Jacobson C. Self-tuning control of a nonlinear model of combustion instabilities. IEEE Transactions on Control Systems Technology 1999;7(4):424–36.

[369] Annaswamy AM, El Rifal OM, Fleifil M, Hathout JP, Ghoniem AF. A model-based self-tuning controller for thermo-acoustic instability. Combustion Science and Technology 1998;135:213–40.

[370] Evesque S, Dowling AP, Annaswamy AM. Self-tuning regulators for combustion instabilities. Proceedings of the Royal Society's Journal: Mathematical, Physical and Engineering Sciences 2003;459(2035):1709–49.

[371] Evesque S, Park S, Riley AJ, Annaswamy AM, Dowling AP. Adaptive combustion instability control with saturation: theory and validation. Journal of Propulsion and Power 2004;20(6):1086–95.

[372] Hong BS, Yang V, Ray A. Wide-range robust control of combustion instability. Combustion and Flame 2002;128:242–58.

[373] Hong BS, Yang V, Ray A. Output feedback linear parameter varying (LPV) L_2-gain control. Journal of Dynamic Systems, Measurements, and Control 2003;125:485–9.

[374] Tsien HS. Servo-stabilization of combustion in rocket motors. ARS Journal 1952;22:256–63.

[375] Marble FE, Cox Jr DW. Servo-stabilization of low-frequency oscillations in a liquid bipropellant rocket motor. ARS Journal 1953;23:63–74.

[376] Lee YC, Gore MR, Ross CC. Stability and control of liquid propellant rocket systems. ARS Journal 1953;23:75–81.

[377] Ffowcs-Williams JE. Anti-sound. Proceedings of the Royal Society of London, Series A 1984;395:63–88.

[378] Dine PJ. Active control of flame noises. Ph.D. Thesis, Cambridge University, Cambridge, England; 1983.

[379] Heckl MA. Heat sources in acoustic resonators. Ph.D. Thesis, Cambridge University, Cambridge, England; 1985.

[380] Heckl MA. Active control of the noise from a Rijke tube. In: IUTAM symposium on aero- and hydro-acoustics, Lyon, 1985. Springer-Verlag; 1986. p. 211–6.

[381] Menon S. Active combustion control in a ramjet using large-eddy simulations. Combustion Science and Technology 1992;84:51–79.

[382] Shyy W, Thakur S, Udaykumar HS. A high accuracy sequential solver for simulation and active control of a longitudinal combustion instability. Computing Systems in Engineering 1993;4:27–41.

[383] Mohanraj R, Neumeier Y, Zinn BT. Combustor model for simulation of combustion instabilities and their active control. Journal of Propulsion and Power 2000;16(3):485–91.

[384] Candel SM. Combustion instabilities coupled by pressure waves and their active control. Proceedings of the Combustion Institute 1992;24:1277–96.

[385] Candel SM. Combustion dynamics and control. Proceedings of the Combustion Institute 2002;29:1–28.

[386] McManus KR, Poinsot T, Candel S. A review of active control of combustion instabilities. Progress in Energy and Combustion Science 1993;19:1–29.

[387] Hendricks EW, Schadow KC. Recent progress in the implementation of active combustion control, unsteady combustion. In: Culick F, Heitor MV, Whitelaw JH, editors. Unsteady combustion. The Netherlands: Kluwer Academic Publishers; 1993.

[388] Annaswamy AM, Ghoniem AF. Active control in combustion systems. IEEE Control System Magazine Dec 1995:49–63.

[389] Annaswamy AM, Ghoniem AF. Active control of combustion instability: theory and practice. IEEE Control System Magazine Dec 2002:37–54.

[390] Zinn BT, Neumeier Y. An overview of active control of combustion instabilities. AIAA Paper 1997-0461; 1997.

[391] Zinn BT. Smart combustors, just around the corner. ASME Paper 2005-GT-69138; 2005.

[392] Dowling AP, Morgans AS. Feedback control of combustion oscillations. Annual Review of Fluid Mechanics 2005;37:151–82.

[393] Brouwer J, Ault BA, Bobrow JE, Samuelsen GS. Active control for gas turbine combustors. Proceedings of the Combustion Institute 1990;23:1087–92.

[394] Miyasato MM, McDonell VG, Samuelsen GS. Active optimization of the performance of a gas turbine combustor. Combustion Science and Technology 2005;177:1725–45.

[395] Lubarsky E, Shcherbik D, Bibik A, Zinn BT. Active control of combustion oscillations by non-coherent fuel flow modulation. AIAA Paper 2003-3180; 2003.

[396] Lubarsky E, Shcherbik D, Bibik A, Zinn BT. Open-loop control of severe combustion instabilities by fuel flow modulation at non-resonant frequencies. AIAA Paper 2004-0634; 2004.

[397] Richards GA, Yip MJ, Robey EH, Cowell L, Rawlins D. Combustion oscillation control by cyclic fuel injection. Journal of Engineering for Gas Turbines and Power 1997;119:340–3.

[398] Uhm JH, Acharya S. Low-bandwidth open-loop control of combustion instability. Combustion and Flame 2005;142:348–63.

[399] McManus KR, Magill JC, Miller MF, Allen MG. Combustion instability suppression in liquid-fueled combustors. AIAA Paper AIAA-1998-0462; 1998.

[400] Magill J, Bachmann M, McManus K. Combustion dynamics and control in liquid-fuelled direct injection systems. AIAA Paper AIAA-2000-1022; 2000.

[401] Lee JG, Kim K, Santavicca DA. Effect of injection location on the effectiveness of an active control system using secondary fuel injection. Proceedings of the Combustion Institute 2000;28:739–46.

[402] Auer MP, Gebauer C, Mosl KG, Hirsch C, Sattelmayer T. Active instability control: feedback of combustion instabilities on the injection of gaseous fuel. Journal of Engineering for Gas Turbines and Power 2005;127:748–54.

[403] Choi GM, Tanahashi M, Miyauchi T. Control of oscillating combustion and noise based on local flame structure. Proceedings of the Combustion Institute 2005;30:1807–14.

[404] Bernier D, Ducruix S, Lacas F, Candel S. Transfer function measurements in a model combustor: application to adaptive instability control. Combustion Science and Technology 2003;175:993–1013.

[405] Riley AJ, Park S, Dowling AP, Evesque S, Annaswamy AM. Advanced closed-loop control on an atmospheric gaseous lean-premixed combustor. Journal of Engineering for Gas Turbines and Power 2004;126:708–16.

[406] Sattinger SS, Neumeier Y, Nabi A, Zinn BT, Amos DJ, Darling DD. Sub-scale demonstration of the active feedback control of gas turbine combustion instabilities. Journal of Engineering for Gas Turbines and Power 2000;122:262–8.

[407] Johnson CE, Neumeier Y, Neumaier M, Zinn BT. Demonstration of active control of combustion instabilities on a full-scale gas turbine combustor. ASME Paper 2001-GT-519; 2001.

[408] Richards GA, Thornton JD, Robey EH, Arellano L. Open-loop active control of combustion dynamics on a gas turbine engine. Journal of Engineering for Gas Turbines and Power January 2007;129(1):38–48.

[409] Moran AJ, Steele D, Dowling AP. Active control and its application. In: Proceedings of RTO AVT symposium on active control technology for enhanced performance operational capabilities military aircraft, land vehicles sea and vehicles; May 2000.

[410] Neumeier Y, Zinn BT. Active control of combustion instabilities with real-time observation of unstable combustor modes. AIAA Paper 1996-0758; 1996.

[411] McManus KR, Bowman CT. Effects of controlling vortex dynamics on the performance of a dump combustor. Proceedings of the Combustion Institute 1990;23:1093–9.

[412] McManus KR, Bowman CT. Combustor performance enhancement through direct shear layer excitation. Combustion and Flame 1990;82:75–92.

[413] De Zilwa SRN, Sivasegaram S, Whitelaw JH. Control of combustion oscillations close to stoichiometry. Flow, Turbulence and Combustion 1999;63:395–414.

[414] Emiris I, Whitelaw JH. Control of combustion oscillations. Combustion Science and Technology 2003;175:157–84.

[415] Parr TP, Gutmark E, Hanson-Parr DM, Schadow KC. Feedback control of an unstable ducted flame. Journal of Propulsion and Power 1993;9(4):529–35.

[416] Yu KH, Parr TP, Wilson KJ, Schadow KC, Gutmark EJ. Active control of liquid-fueled combustion using periodic vortex–droplet interaction. Proceedings of the Combustion Institute 1996;26:2843–50.

[417] Yu KH, Wilson KJ, Schadow KC. Liquid-fueled active instability suppression. Proceedings of the Combustion Institute 1998;27:2039–46.

[418] Yu KH, Wilson KJ. Scale-up experiments on liquid-fueled active combustion control. Journal of Propulsion and Power 2002;18(1):53–60.

[419] Neumeier Y, Nabi A, Arbel A, Vertzberger M, Zinn BT. Open-loop performance of a fast-response actively controlled fuel injector actuator. Journal of Propulsion and Power 1997;13(6):705–13.

[420] Jones CM, Lee JG, Santavicca DA. Closed-loop active control of combustion instabilities using subharmonic secondary fuel injection. Journal of Propulsion and Power 1999;15(4):584–90.

[421] Uhm JH, Acharya S. Control of combustion instability with a high-momentum air-jet. Combustion and Flame 2004;139:106–25.

[422] Lee JY, Lubarsky E, Zinn BT. "Slow" active control of combustion instabilities by modification of liquid fuel spray properties. Proceedings of the Combustion Institute 2005;30:1757–64.

[423] Tennekes II, Lumley JL. A first course in turbulence. Cambridge, MA: MIT Press; 1972.

[424] Pope SB. Turbulent flows. Cambridge, UK: Cambridge University Press; 2000.

[425] Mathieu J, Scott J. An introduction to turbulent flow. Cambridge, UK: Cambridge University Press; 2000.

[426] Givi P. Model-free simulation of turbulent reacting flows. Progress in Energy and Combustion Science 1989;15:1–107.

[427] Poinsot T, Candel S, Trouve A. Applications of direct numerical simulation to premixed turbulent combustion. Progress in Energy and Combustion Science 1996;21:531–76.

[428] Vervisch L, Poinsot T. Direct numerical simulation of non-premixed turbulent flames. Annual Review of Fluid Mechanics 1998;30:655–91.

[429] Brookes SJ, Cant RS, Dupere IDJ, Dowling AP. Computational modeling of self-excited combustion instabilities. Journal of Engineering for Gas Turbines and Power 2001;123:322–6.

[430] Zhu M, Dowling AP, Bray KNC. Self-excited oscillations in combustors with spray atomizers. Journal of Engineering for Gas Turbines and Power 2001;123:779–86.

[431] Zhu M, Dowling AP, Bray KNC. Forced oscillations in combustors with spray atomizers. Journal of Engineering for Gas Turbines and Power 2002;124:20–30.

[432] Zhu M, Dowling AP, Bray KNC. Transfer function calculations for aero-engine combustion oscillations. Journal of Engineering for Gas Turbines and Power 2005;127:18–26.

[433] Brewster BS, Cannon SM, Farmer JR, Meng F. Modeling of lean premixed combustion in stationary gas turbines. Progress in Energy and Combustion Science 1999;25:353–85.

[434] Piomelli U. Large-eddy simulation: achievements and challenges. Progress in Aerospace Science 1999;35:335–62.

[435] Smagorinsky J. General circulation experiments with the primitive equations. I. The basic experiment. Monthly Weather Review 1963;91:99.

[436] Lilly DK. The representation of small-scale turbulence in numerical simulation experiments. In: Proceedings of IBM scientific computing symposium on environmental science; 1967. p. 195–210. Yorktown Heights, N.Y.

[437] Erlebacher G, Hussaini MY, Speziale CG, Zang TA. Toward the large eddy simulation of compressible turbulent flows. Journal of Fluid Mechanics 1992;238:155–8.

[438] Germano M, Piomelli U, Moin P, Cabot W. A dynamic subgrid-scale eddy viscosity model. Physics of Fluids A 1991;3(7):1760–5.

[439] Ghosal S, Lund T, Moin P, Akselvoll K. A dynamic localization model for large eddy simulation for turbulent flows. Journal of Fluid Mechanics 1995;286:229–55.

[440] Moin P. Advances in large-eddy simulation methodology for complex flows. International Journal of Heat and Fluid Flow 2002;23:710–20.

[441] Da Silva CB, Pereira JCF. The effect of subgrid-scale models on the vortices computed from large-eddy simulations. Physics of Fluids 2004;16(12):4506–34.

[442] Schumann U. Subgrid scale model for finite difference simulations of turbulent flows in plane channels and annuli. Journal of Computational Physics 1975;18:376–404.

[443] Kraichnan RH. Eddy viscosity in two and three dimensions. Journal of Atmosphere Science 1976;33:1521–936.

[444] Chollet JP, Lesieur M. Parameterization of small scales of three-dimensional isotropic turbulence utilizing spectral closures. Journal of Atmosphere Science 1981;38:2747–57.

[445] Metais O, Lesieur M. Spectral large-eddy simulation of isotropic and stably-stratified turbulence. Journal of Fluid Mechanics 1992;239:157–94.

[446] Bardina J, Ferziger JH, Reynolds WC. Improved subgrid scale models for large-eddy simulation. AIAA Paper 1980-1357; 1980.

[447] Liu S, Menevea C, Katz J. On the properties of similarity subgrid-scale models as deduced from measurements in a turbulent jet. Journal of Fluid Mechanics 1994;275:83–119.

[448] Boris JP, Grinstein FF, Oran ES, Kolbe RL. New insights into large eddy simulation. Fluid Dynamics Research 1992;10:199–228.

[449] Domaradzki JA, Saiki EM. A subgrid-scale model based on the estimation of unresolved scales of turbulence. Physics of Fluids 1997;9:1–17.

[450] Domaradzki JA, Loh KC. The subgrid-scale estimation model in the physical space representation. Physics of Fluids 1999;11:2330–42.

[451] Stolz S, Adams NA. An approximate de-convolution procedure for large-eddy simulation. Physics of Fluids 1999;11(7):1699–701.

[452] Meneveau C, Katz J. Scale-invariance and turbulence models for large-eddy simulation. Annual Review of Fluid Mechanics 2000;32:1–32.

[453] Lesieur M, Metais O. New trends in large-eddy simulations of turbulence. Annual Review of Fluid Mechanics 1996;28:45–82.

[454] Mongia HC, Al-Roub M, Danis A, Elliott-Lewis D, Jeng SM, John A, et al. Swirl cup modeling, part I. AIAA Paper 2001-3576; 2001.

[455] Hsiao G, Mongia HC, Vij A. Swirl cup modeling part II: inlet boundary conditions. AIAA Paper 2001-1350; 2001.

[456] Hsiao G, Mongia HC. Swirl cup modeling part iii: grid independent solution with different turbulence models. AIAA Paper 2001-1349; 2001.

[457] Cai J, Fu Y, Jeng S, Mongia HC. Swirl cup modeling part IV: effect of confinement on flow characteristics. AIAA Paper 2003-0486; 2003.

[458] Giridharan MG, Mongia HC, Singh G. Swirl cup modeling part VI: dilution jet modeling. AIAA Paper 2003-1203; 2003.

[459] Stevens EJ, Held TJ, Mongia HC. Swirl cup modeling part VII: premixed laminar flamelet model validation and simulation of a single-cup combustor with gaseous N-Heptane. AIAA Paper 2003-0488; 2003.

[460] Giridharan, MG, Mongia HC, Jeng SM. Swirl cup modeling part VIII: spray combustion in CFM56 single cup flame tube. AIAA Paper 2003-0319; 2003.

[461] Jeng SM, Flohre NM, Mongia HC. Swirl cup modeling part IX: atomization. AIAA Paper 2004-0137; 2004.

[462] James S, Zhu J, Anand MS. Large-eddy simulation of gas turbine combustors. AIAA Paper 2004-0552; 2004.

[463] Kim WW, Syed S. Large-eddy simulation needs for gas turbine combustor design. AIAA Paper 2004-0331; 2004.

[464] Kim WW, Lienau JJ, Van Slooten PR, Colket MB, Malecki RE, Syed S. Towards modeling lean blow out in gas turbine flame holder applications. Journal of Engineering for Gas Turbines and Power 2006;128:40–8.

[465] Borghi R. Turbulent combustion modeling. Progress in Energy and Combustion Science 1988;14:245–92.

[466] Williams FA. Combustion theory. 2nd ed. California: Addison-Wesley Publishing Company; 1985. p. 411–5.

[467] Abdel-Gayed RG, Bradley D. Combustion regimes and the straining of turbulent premixed flames. Combustion and Flame 1989;76:213–8.

[468] Peters N. Turbulent combustion. Cambridge University Press; 2000.

[469] Poinsot T, Veynante D. Theoretical and numerical combustion. Philadelphia, PA: R.T. Edwards, Inc; 2005.

[470] Eggenspieler G, Menon S. Structure of locally quenched swirl stabilized turbulent premixed flames. AIAA Paper 2004-0979; 2004.

[471] Poinsot T, Veynante D, Candel S. Quenching process and premixed turbulent combustion diagram. Journal of Fluid Mechanics 1991;228:561.

[472] Linan A, Williams FA. Fundamental aspects of combustion. Oxford University Press; 1993.

[473] Driscoll J. Turbulent premixed combustion: flamelet structure and its effect on turbulent burning velocities. Progress in Energy and Combustion Science 2008;34(1):91–134.

[474] Pope SB. Computations of turbulent combustion: progress and challenges. Proceedings of the Combustion Institute 1990;23:591–612.

[475] Bray KN. The challenges of turbulent combustion. Proceedings of the Combustion Institute 1996;26:1–26.

[476] Candel S, Thevenin D, Darabiha N, Veynante D. Progress in numerical combustion. Combustion Science and Technology 1999;149:297–337.

[477] Veynante D, Vervisch L. Turbulent combustion model. Progress in Energy and Combustion Science 2002;28:193–266.

[478] Bilger RW, Pope SB, Bray KNC, Driscoll JF. Paradigms in turbulent combustion research. Proceedings of the Combustion Institute 2005;30:21–42.

[479] Charlette F, Meneveau C, Veynante D. A power-law flame wrinkling model for LES of premixed turbulent combustion. Part I: non-dynamic formulation and initial tests. Combustion and Flame 2002;131:159–80.

[480] Boger M, Veynante D, Boughanem H, Trouve A. Direct numerical simulation analysis of flame surface density concept for large eddy simulation of turbulent premixed combustion. Proceedings of the Combustion Institute 1998;27:917–25.

[481] Hawkes ER, Cant RS. Implications of a flame surface density approach to large eddy simulation of premixed turbulent combustion. Combustion and Flame 2001;126:1617–29.

[482] Fureby C, Lofstrom C. Large eddy simulation of bluff body stabilized flames. Proceedings of the Combustion Institute 1994;25:783–91.

[483] Fureby C, Moller SI. Large eddy simulation of reacting flows applied to bluff body stabilized flames. AIAA Journal 1995;33:2339–47.

[484] Moller SI, Lundgren E, Fureby C. Large eddy simulation of unsteady combustion. Proceedings of the Combustion Institute 1996;26:241–8.

[485] Giacomazzi E, Battaglia V, Bruno C. The coupling of turbulence and chemistry in a premixed bluff-body flame as studied by LES. Combustion and Flame 2004;138:320–35.

[486] Thibaut D, Candel S. Numerical study of unsteady turbulent premixed combustion: application to flashback simulation. Combustion and Flame 1998;113:53–65.

[487] Angelberger C, Veynante D, Egolfopoulos F. LES of chemical and acoustic forcing of a premixed dump combustor. Flow, Turbulence and Combustion 2000;65:205–22.

[488] Colin O, Ducros F, Veynante D, Poinsot T. A thickened flame model for large eddy simulation of turbulent premixed combustion. Physics of Fluids 2000;12:1843–63.

[489] Nottin C, Knikker R, Boger M, Veynante. Large-eddy simulation of an acoustically excited turbulent premixed flame. Proceedings of the Combustion Institute 2000;28:67–73.

[490] Mathew J. Large eddy simulation of a premixed flame with approximate de-convolution modeling. Proceedings of the Combustion Institute 2002;29:1995–2000.

[491] Chakravarthy VK, Menon S. Subgrid modeling of turbulent premixed flames in the flamelet regime. Flow, Turbulence and Combustion 2000;65:133–61.

[492] Chakravarthy VK, Menon S. Large-eddy simulation of turbulent premixed flames in the flamelet regime. Combustion Science and Technology 2001;162:175.

[493] Hawkes ER, Cant RS. A flame surface density approach to large eddy simulation of premixed turbulent combustion. Proceedings of the Combustion Institute 2000;28:51–8.

[494] Knikker R, Veynante D, Meneveau C. A priori testing of a similarity model for large eddy simulations of turbulent premixed combustion. Proceedings of the Combustion Institute 2002;29:2105–11.

[495] Weller H, Tabor G, Gosman AD, Fureby C. Application of a flame-wrinkling LES combustion model to a turbulent mixing layer. Proceedings of the Combustion Institute 1998;27:899–907.

[496] Fureby C. Large eddy simulation of combustion instabilities in a jet engine afterburner model. Combustion Science and Technology 2000;161: 213–43.

[497] Flohr P, Pitsch H. A turbulent flame speed closure model for LES of industrial burner flows. Proceedings of the summer program, Center for Turbulence Research, Stanford University; 2000.

[498] Charlette F, Meneveau C, Veynante D. A power-law flame wrinkling model for LES of premixed turbulent combustion. Part II: dynamic formulation. Combustion and Flame 2002;131:181–97.

[499] Menon S, Jou WH. Large-eddy simulation of combustion instability in an axisymmetric ramjet combustor. Combustion Science and Technology 1991;75:53–72.

[500] Kim WW, Menon S, Mongia HC. Large eddy simulation of a gas turbine combustor flow. Combustion Science and Technology 1999;143:25–62.

[501] Herrmann M. Numerical simulation of premixed turbulent combustion based on a level set flamelet model. Ph. D. Thesis, der Rheinisch-Westfalischen Technischen Hochschule Aachen; 2000.

[502] Nilsson P, Bai XS. Level-set flamelet library approach for premixed turbulent combustion. Experimental Thermal and Fluid Science 2001;21:87–98.

[503] Pitsch H, Duchamp de Lageneste L. Large eddy simulation of premixed turbulent combustion using a level-set approach. Proceedings of the Combustion Institute 2002;29:2001–8.

[504] Wang P, Bai XS. Large-eddy simulation of turbulent premixed flames using level-set G-equation. Proceedings of the Combustion Institute 2005;30: 583–91.

[505] Janicka J, Sadiki A. Large-eddy simulation of turbulent combustion systems. Proceedings of the Combustion Institute 2005;30:537–47.

[506] Pope SB. PDF methods for turbulent reactive flows. Progress in Energy and Combustion Science 1985;11:119–92.

[507] Gao F, O'Brien EE. A large-eddy simulation schemes for turbulent reacting flows. Physics of Fluids 1993;5(6):1282–4.

[508] Colucci PJ, Jaberi FA, Givi P, Pope SB. Filtered density function for large-eddy simulation of turbulent reacting flows. Physics of Fluids 10(2):499–515.

[509] Jaberi FA, Colucci PJ, James S, Givi P, Pope SB. Filtered density function for large-eddy simulation of turbulent reacting flows. Journal of Fluid Mechanics 1999;401:85–121.

[510] Sheikhi MRH, Drozda TG, Givi P, Jaberi FA, Pope SB. Large eddy simulation of a turbulent non-premixed piloted methane jet flame (Sandia Flame D). Proceedings of the Combustion Institute 2005;30:549–56.

[511] Raman V, Pitsch H, Fox RO. Hybrid large-eddy simulation/Lagrangian filtered-density-function approach for simulating turbulent combustion. Combustion and Flame 2005;143:56–78.

[512] Pitsch H. Large-eddy simulation of turbulent combustion. Annual Review of Fluid Mechanics 2006;38:453–82.

[513] Legier JP, Poinsot T, Veynante D. Dynamically thickened flame LES model for premixed and non-premixed turbulent combustion, Proceedings of the Summer Program. Center for Turbulence Research: Stanford University; 2000.

[514] Schonfeld T, Poinsot T. Influence of boundary conditions in LES of premixed combustion instabilities. Annual Research Briefs, Center for Turbulence Research, Stanford University; 1999.

[515] Fureby C. A computational study of combustion instabilities due to vortex shedding. Proceedings of the Combustion Institute 2000;28:783–91.

[516] Menon S. Acoustic–vortex–flame interactions in gas turbines. Chapter 11. In: Lieuwen T, Yang V, editors. Combustion instabilities in gas turbine engines: operational experience, fundamental mechanisms, and modeling. Progress in Astronautics and Aeronautics 2005;210:277–314.

[517] Kim WW, Menon S. Numerical modeling of turbulent premixed flames in the thin-reaction-zones regime. Combustion Science and Technology 2000;160:119–50.

[518] Cannon SM, Adumitroaie V, Smith CE. 3D LES modeling of combustion dynamics in lean-premixed combustors. ASME Paper 2001-GT-375; 2001.

[519] Cannon SM, Zuo BF, Smith CE. LES prediction of combustor emissions from a practical industrial fuel injector. ASME Paper 2003-GT-38200; 2003.

[520] Stone C, Menon S. Swirl control of combustion instabilities in a gas turbine combustor. Proceedings of the Combustion Institute 2002;29:155–60.

[521] Stone C, Menon S. Open-loop control of combustion instabilities in a model gas turbine combustor. Journal of Turbulence 2003;4:020.

[522] Huang Y, Yang V. Effect of swirl on combustion dynamics in a lean-premixed swirl-stabilized combustor. Proceedings of the Combustion Institute 2005;30:1775–82.

[523] Sommerer Y, Galley D, Poinsot T, Ducruix S, Lacas F, Veynante D. Large-eddy simulation and experimental study of flashback and blow-off in a lean partially premixed swirled burner. Journal of Turbulence 2004:037.

[524] Schluter JU. Static control of combustion oscillations by coaxial flows, a large-eddy simulations investigation. Journal of Propulsion and Power 2004;20(3):460–7.

[525] Eggenspieler G, Menon S. Large-eddy simulation of pollutant emission in a DOE-HAT combustor. Journal of Propulsion and Power 2004;20(6): 1076–85.

[526] Grinstein FF, Fureby C. LES studies of the flow in a swirl gas combustor. Proceedings of the Combustion Institute 2005;30:1791–8.

[527] Duwig C, Fuchs L. Study of flame stabilization in a swirling combustor using a new flamelet formulation. Combustion Science and Technology 2005;177:1485–510.

[528] Pierce M, Moin P. Progress-variable approach for large-eddy simulation of non-premixed turbulent combustion. Journal of Fluid Mechanics 2004;504:73–97.

[529] Jones WP. Large-eddy simulation of turbulent combustion process. Computer Physics Communications 2002;147:533–7.

[530] Di Mare F, Jones WP, Menzies KR. Large-eddy simulation of a model gas turbine combustor. Combustion and Flame 2004;137:278–94.

[531] Sankaran V, Menon S. LES of spray combustion in swirling flows. Journal of Turbulence 2002;3:011.

[532] Sankaran V, Menon S. Vorticity-scalar alignments, and small-scale structures in swirling spray combustion. Proceedings of the Combustion Institute 2002;29:577–84.

[533] James S, Zhu J, Anand MS. Large-eddy simulation as a design tool for gas turbine combustion systems. AIAA Journal 2006;44(4):674–86.

[534] Oefelein JC, Schefer RW, Barlow RS. Toward validation of large-eddy simulation for turbulent combustion. AIAA Journal 2006;44(3):418–33.

[535] Moin P. Large-eddy simulation of multi-phase turbulent flow in realistic combustors. Progress in Computational Fluid Dynamics 2004;4:237–40.

[536] Mahesh K, Constantinescu G, Apte S, Iaccarino G, Ham F, Moin P. Large-eddy simulation of reacting turbulent flows in complex geometries. Journal of Applied Mechanics 2006;73:374–81.

[537] Moin P, Apte SV. Large-eddy simulation of realistic gas turbine combustors. AIAA Journal 2006;44(4):698–708.

[538] Selle L, Benoit L, Poinsot T, Nicoud F, Krebs W. Joint use of compressible large-eddy simulation and Helmholtz solvers for the analysis of rotating modes in a industrial swirled burner. Combustion and Flame 2006;145:194–205.

[539] Martin CE, Benoit L, Sommerer Y, Nicoud F, Poinsot T. Large-eddy simulation and acoustic analysis of a swirled staged turbulent combustor. AIAA Journal 2006;44(4):741–9.

[540] Menon S, Patel N. Subgrid modeling for simulation of spray combustion in large-scale combustors. AIAA Journal 2006;44(4):709–23.

[541] Patel N, Kirtas M, Sankaran V, Menon S. Simulation of spray combustion in a lean-direct injection combustor. Proceedings of the Combustion Institute 2007;31:2327–34.

[542] Schmitt P, Poinsot T, Schuermans B, Geigle KP. Large-eddy simulation and experimental study of heat transfer, nitric oxide emissions and combustion instability in a swirled turbulent high-pressure burner. Journal of Fluid Mechanics 2007;570:17–46.

[543] Sengissen AX, Van Kampen JF, Huls RA, Stoffels GGM, Kok JBW, Poinsot TJ. LES and experimental studies of cold and reacting flow in a swirled partially premixed burner with and without fuel modulation. Combustion and Flame 2007;150:40–53.

[544] Boudier G, Gicquel LYM, Poinsot T, Bissieres D, Berat C. Comparison of LES, RANS and experiments in a aeronautical gas turbine combustion chamber. Proceedings of the Combustion Institute 2007;31:3075–82.

[545] Shinjo J, Matsuyama S, Mizobuchi Y, Ogawa S. Study on flame dynamics with secondary fuel injection control by large eddy simulation. Combustion and Flame 2007;150:277–91.

[546] Poinsot T, Lele S. Boundary conditions for direct simulation of compressible viscous flows. Journal of Computational Physics 1992;101:104–29.

[547] Swanson RC, Turkel E. On central difference and upwind schemes. Journal of Computational Physics 1992;101:292–306.

[548] Oefelein JC, Yang V. Modeling high-pressure mixing and combustion processes in liquid rocket engines. Journal of Propulsion and Power 1998;14:843–57.

[549] Sirvoich L, Kirby M, Winter M. An eigen-function approach to large scale transitional structures in jet flow. Physics of Fluids 1992;2(2):127–36.

[550] Sirovich L. Turbulence and the dynamics of coherent structures, part 1: coherent structures. Quarterly of Applied Mathematics 1987;45(3):561–71.

[551] Berkooz G, Holmes P, Lumley JL. The proper orthogonal decomposition in the analysis of turbulent flows. Annual Review of Fluid Mechanics 1993;25:539–75.

[552] Rowley CW, Colonius T, Murray RM. Model reduction for compressible flows using POD and Galerkin projection. Physica D 2004;189:115–29.

[553] Cordier L, Bergmann M. Proper orthogonal decomposition: an overview. In: Post-processing of experimental and numerical data. von Karman Institute for Fluid Dynamics; 2003. Lecture Series 2003-03.

[554] Rempfer D, Fasel HF. Evolution of three-dimensional coherent structures in a flat-plate boundary layer. Journal of Fluid Mechanics 1994;260:351–75.

[555] Graham WR, Peraire J, Tang KY. Optimal control of vortex shedding using low-order models, part 1: open-loop model development. International Journal for Numerical Methods in Engineering 1999;44:945–72.

[556] Hsiao GC, Pandalai RP, Hura HS, Mongia HC. Combustion dynamics modeling for gas turbine engines. AIAA Paper 1998-3380; 1998.

[557] Hsiao GC, Pandalai RP, Hura HS, Mongia HC. Investigation of combustion dynamics in dry-low-emission gas turbine engines. AIAA Paper 1998-3381; 1998.

[558] Dowling AP, Stow SR. Acoustic analysis of gas turbine combustors. Journal of Propulsion and Power 2003;19(5):751–64.

[559] Paschereit CO, Schuermans B, Bellucci V, Flohr P. Integrated analytical, numerical and experimental design process. Chapter 15. In: Lieuwen T, Yang V, editors. Combustion instabilities in gas turbine engines: operational experience, fundamental mechanisms, and modeling. Progress in Astronautics and Aeronautics 2005;210:445–80.

[560] You D, Yang V, Sun X. Three-dimensional linear stability analysis of gas turbine combustion dynamics. Chapter 14. In: Lieuwen T, Yang V, editors. Combustion instabilities in gas turbine engines: operational experience,

fundamental mechanisms, and modeling. Progress in Astronautics and Aeronautics 2005;210:415–44.

[561] Culick FEC. High frequency oscillations in liquid rockets. AIAA Journal 1963;1:1097–104.

[562] Mitchell CE. Analytical model for combustion instability. Chapter 15. In: Yang V, Anderson W, editors. Liquid rocket engine combustion instability. Progress in Astronautics and Aeronautics 1994;169:403–30.

[563] Zinn BT, Powell EA. Nonlinear combustion instability in liquid propellant rocket engines. Proceedings of the Combustion Institute 1971;13:491–503.

[564] Culick FEC. Nonlinear growth and limiting amplitude of acoustic oscillations in combustion chambers. Combustion Science and Technology 1971;3:1–16.

[565] Culick FEC. Nonlinear behavior of acoustic waves in combustion chambers—parts I and II. Acta Astronautica 1976;3:715–56.

[566] Awad E, Culick FEC. On the existence and stability of limit cycles for longitudinal acoustic modes in a combustion chamber. Combustion Science and Technology 1986;46:195–222.

[567] Yang V, Culick FEC. On the existence and stability of limit cycles for transverse acoustic oscillations in a cylindrical combustion chamber, 1: standing modes. Combustion Science and Technology 1990;72:37–65.

[568] Peracchio AA, Proscia WM. Nonlinear heat-release/acoustic model for thermo-acoustic instability in lean premixed combustors. Journal of Engineering for Gas Turbines and Power 1999;121:415–21.

[569] Ulitsky M, Collins LR. Relative importance of coherent structures vs. background turbulence in the propagation of a premixed flame. Combustion and Flame 1997;111:257–75.

[570] Lieuwen T. Analysis of acoustic wave interactions with turbulent premixed flames. Proceedings of the Combustion Institute 2002;29:1817–24.

[571] Kerstein AR, Ashurst WT, Williams FA. Field equation for interface propagation in an unsteady homogeneous flow field. Physics Review A 1988;37:2728–31.

[572] Wang TL, Yang V. Modeling of longitudinal combustion instability in a gas-turbine combustor. AIAA Paper 1997-0694; 1997.